HYDRO-MECHANICAL BEHAVIOR OF COMPACTED SAND – BENTONITE –FIBER COMPOSITE FOR LANDFILL APPLICATION

A Thesis

Submitted in Partial Fulfilment of the Requirements for the Degree of

DOCTOR OF PHILOSOPHY

by

Krishanu Mukherjee

Department of Civil Engineering

Indian Institute of Technology Guwahati

Guwahati -781039

January 2020

I dedicate this dissertation to

my Parents and

all my 'Teachers'

STATEMENT

I do hereby declare that the matter embodied in this thesis is the result of investigations carried out by me in the Department of Civil Engineering, Indian Institute of Technology Guwahati, Guwahati, Assam, India.

In keeping with the general practice of reporting scientific observations, due acknowledgements have been made wherever the work described is based on findings of other investigators.

Place: IIT Guwahati

Date: January 9th , 2020

Krishanu Mukherjee

CERTIFICATE

This is to certify that the thesis entitled "**Hydro-mechanical behavior of compacted sand – bentonite –fiber composite for landfill application**," submitted by Mr. Krishanu Mukherjee (Roll No.146104001), to the Indian Institute of Technology Guwahati, for the award of degree of Doctor of Philosophy in Civil Engineering, is a record of bonafide research work carried out by him under my supervision and guidance. The thesis work, in our opinion, has reached the requisite standard fulfilling the requirement for the degree of Doctor of Philosophy.

The results contained in this thesis have not been submitted in part or full to any other university or Institute for award of any degree or diploma.

Dr. A. K. Mishra
Associate Professor
Department of Civil Engineering
Indian Institute of Technology Guwahati
Guwahati -781039, India

ACKNOWLEDGEMENT

Firstly, I would like to express my gratitude to the ***IIT Guwahati, Department of Civil engineering,*** for providing funding, equipment and facilities that made this project possible.

The work reported in this thesis was carried out under the esteemed supervision and guidance of **Dr. Anil Kumar Mishra**. My special thanks to **Dr. Anil Kumar Mishra** for his constant guidance and supervision during my M.Tech research and, introducing me in the field of research. I remain deeply grateful to him for his guidance and constant encouragement throughout the course, but also for their invaluable advice and encouragement that enriched my doctoral study.

I would like to thank my doctoral committee members, **Prof. Sreedeep S**., **Dr. Arindam Dey** and **Prof. Subrata Majumder** for sparing their valuable time in reviewing my work. I extend my sincere thanks to the other faculty members of the ***Geotechnical Engineering Division of IIT Guwahati*** for their cooperation, whenever required. I gratefully acknowledge the unstinted help provided by **Mr.Hari Ram Upadhyaya**, during different phase of my research work. Furthermore, I would like to thank the office staff of Civil Engineering Department, for their support in administrative works.

I convey my special thanks to my friends: Mr.Chandrabhanu Gupt, Mr. Janarul Shaikh, Ms. Saswati Ray, Mr. Arya Anuj, Mr.Vinay K.Gadi, Ms.Chinumani, Ms.Purabi Das, Ms.Rohini C Kale, Mr.Chiranjib P.Sarma, Mr.Alok Chandra, Mr.Dharmendra Barman, Mr.Bharat Rattan, Mr. Osho Sagar, Mr. Shakti Singh, Mr.ManMohan , Mr.Atma Prakash, Mr.Prashant Kr.Jha, Mr.Balaji Mudaliyar, Mr.Ankit Gautam, Mr.Bipin Kumar Gautam and many others, who made my time enjoyable during my research at IIT Guwahati.

My special thanks to **Dr. Suchit Kumar Patel, Dr. Doordarshi Chaterjee, Dr. Yagom Gapak, Dr. Tanmoy Deb, Dr. Sondom Bali Reddy, Dr, V.Shrinkanth, and Dr. Jagori Dutta** for their valuable suggestion, moral support and encouraging interaction which helped me improving my skills.

My special thanks to **Dr.Bipin Kumar Gupta** (from waterloo, Canada) and **Dr.Achinta Sarkar (**From Mechanical Engg, IIT Guwahati**)** for their support and encouraging interaction, which helped me, improving my doctoral work.

My special thanks to **Chandra Bhanu Gupt** and **Syantan Chakraborty (**Senior Ph.D Student from IIT Bombay**)** for their help and advice during my project work.

My special thanks to elder brother **Kuntal Mukherjee** (Master of Arts in English literature, Writer, Senor Teacher in English literature at Govt. School.WB) for his valuable suggestion during my project work.

I am grateful to Late Emeritus **Prof. Ramaranjan Mukherji**, Prof. **B.T.Ghosal** (former Dean of NIT Durgapur), **Dr.Bhabes Bhattacharya** (Director of BIET Suri) and **Santanu Saha** for their help and advice at the initial stages.

I would like to thank my special friends, **Barsha Saha** (Master of Arts in Bengali literature) for her support, encouragement, and enthusiasm, without which this project could not have been possible.

I am thankful to **Mr. Sumit Rajon Kanjilal** (B.Tech sir) and **Subhasish Karmakar** (WBJEE sir) for their valuable suggestion during my project work.

Lastly, but most importantly, I want to acknowledge the greatest supports, love, and encouragements received from my Mom (**Sipra Mukherjee**), Dad (**Monaj Mukherjee**), elder sister (**Kakoli Chatterjee**), **Molay Chatterjee**, **Tania Chatterjee** and **E*r*. Sayantan Chatterjee (**Mechanical Eng.) without whom it never be possible.

Krishanu Mukherjee

ABSTRACT:

Compacted sand-bentonite mixtures are generally placed at the waste disposal sites as a means of preventing contaminant movement to reduce or remove the potential for the groundwater pollution. The barrier essentially sustains a high level of usefulness over a longer phase of time. Generally, a compacted sand-bentonite mixture is used as a landfill liner material. However, at low stress, desiccation induced moisture variations can affect the reduction in plastic deformability and forms shrinkage cracks, which can increase the uncontrolled migration of leachates, particularly around the tensile failure. Also, if the strength of the base material is not enough, e.g. on steep slopes in bottom liners, capping systems and landfill stability, then the effective operation of the total liner system may be threatened. Therefore, the objective of this study was to examine the possibility of adding the waste fiber as a reinforcement material to sand-bentonite mixtures to improve the stability of the liner without significantly increasing its hydraulic conductivity. In this purpose, consolidated undrained triaxial (CU) and oedometer and shrinkage tests were performed on sand -bentonite mixtures mixed in the proportion of 90:10; 80:20 and 70:30 and reinforced with different type of the fiber. Two types of fibres i.e. glass fiber and waste tire fiber, used for the present study. Glass fiber of 0.5, 1 and 1.5% concentration with an aspect ratio of 40, 80 and 120 and tire fiber of 5, 10 and 15% concentration were added to the sand-bentonite mixtures.

Test result suggested that consolidation and strength behavior changed significantly with the addition of tire fiber. The swelling tendency of the SB30 and SB20 mixture was reduced radically with the presence of tire fiber. Reduction of the swelling pressure was observed to be a function of tire fiber content. A similar trend was obtained for swelling potential. The maximum swelling potential was predicted by the rectangular hyperbola method and indicated that the slope of the t/ε vs. ε plot was increased as the percentage of the tire fiber increased indicating a reduction in the

swelling potential. Compaction test result indicated that maximum dry density was reduced sharply with the increase in the tire content. Consolidation test result specified that coefficient of consolidation (c_v) was reduced with increase in consolidating pressure, but increased with increase in tire fiber content. The hydraulic conductivity (k) for the composite also followed a similar trend as observed for the c_v . From the unconfined compressive strength result, it was observed that axial stress of the composite was increased with tire fiber. The SB30 composite with 10% tire fiber content produced maximum axial stress among all the composite. The results from the triaxial test suggested that stiffness and load carrying capacity of the composite was improved substantially with the inclusion of tire fiber reinforcement. For SB10 and SB20 composite, the deviatoric stress at failure was increased due to the inclusion of tire fiber. The deviatoric stress at failure was improved up to 10% tire fiber content for the mixture of SB30 composite and then decreased slightly with the further addition of tire fiber. SB10 and SB20 exhibited composite, strain-softening behavior, whereas, SB30 exhibited strain hardening behavior. It was found that deviatoric stress continuously reduced as the percentage of bentonite content increased. Strain at failure, post-peak drop, elastic modulus (i.e. initial tangent and secant modulus) and energy absorption capacity were improved with the inclusion of tire fiber. For SB10 and SB20 composite, peak strength and residual strength both were improved with the presence of tire fiber, whereas, shear strength of the SB30 composite was increased up to 10% tire fiber addition. Positive excess pore water pressure (EPP) was increased with tire fiber content and reduced with increase in bentonite content. The negative EPP was reduced as the percentage of tire fiber increased for the mixture of SB10 and SB20. For SB30 mixture, EPP was reduced significantly with increase in tire fiber content. Based on the experimental result, multiple regression model was developed using fiber content, aspect ratio and confining pressure as an input parameter for predicting the effective major principle stress at failure. The critical state model parameter and yield surface were affected significantly with the

inclusion of tire fiber. Yield surface of the composite was increased sharply by the inclusion of tire fiber. Volumetric shrinkage of the SB30 and SB20 composite was reduced significantly due to the inclusion of tire fiber. Desiccation induced crack was expressed in the form of CDF and CIF and both were found to decrease significantly with the increase in the percentage of tire fiber.

From the experimental investigation, it was observed that the hydro-mechanical behavior of the sand–bentonite–glass fiber composite gets affected significantly due to the inclusion of glass fiber. Test result showed that OMC of the composite was reduced with fiber concentration, whereas, MDD was almost remained the same. The effect of aspect ratio on the OMC of the composite was marginal in comparison to fiber concentration. The initial degree of saturation of the composite was found to reduce significantly due to the inclusion of fiber. The swelling tendency of the composite was decreased due to the inclusion of glass fiber. The slope of the t/ε vs. ε was increased by the inclusion of fiber aspect ratio and fiber content, indicating a significant reduction in the swelling potential. From the void ratio-pressure response, it was observed that the reduction of void ratio was the function of fiber content and fiber aspect ratio. The compression index of the composite was reduced upto 1% of fiber content and then increased slightly, whereas, the swelling index was increased with an increase in fiber content. Coefficient of consolidation of the composite was reduced with increase in consolidating pressure, but it increased initially with the inclusion of the fiber. However, the c_v decreased, when the concentration and aspect ratio of the fiber was increased. A similar trend was obtained for the hydraulic conductivity of the composite. The axial stress of the composite was found to increase with fiber concentration and fiber aspect ratio for the mixture of SB10 and SB20 composite. There was no optimum fiber concentration and fiber aspect ratio was found in this case. However, axial stress of the SB30 composite was improved up to 1% fiber content and then dropped with the further addition of fiber content. The fiber aspect ratio was more effective in comparison to fiber concentration. The maximum unconfined compressive

strength of the composite was obtained for 1% fiber content with an aspect ratio of 120 for the mixture of SB30. UCS was increased with increased in bentonite fraction. Triaxial test result suggested that deviatoric stress at failure was increased with increased in fiber concentration and aspect ratio, but the improvement of the composite was noticed more by the inclusion of fiber aspect ratio in comparison to fiber concentration for any blend. Energy absorption capacity and elastic modulus of the composite were enhanced by the inclusion of glass fiber. Effective share strength parameter of the composite was increased by the inclusion of fiber. For SB10 and SB20 composite, peak strength parameter and residual strength parameter both were enhanced by the inclusion of fiber. Internal friction angle of the composite was improved more in comparison to the cohesion component. Cohesion component was improved up to the aspect ratio of 80; thereafter; cohesion component was almost constant with further increase in aspect ratio for any fiber concentration. No peak was observed for the mixture of SB30 composite; the pattern of stress-strain response was different from SB10 and SB20. However, Shear strength of the composite was reduced gradually when bentonite content was increased in the mixture. Positive EPP of the SB10 and SB20 composite was increased with increased in fiber concentration, aspect ratio and bentonite content. The negative EPP of SB10 composite was increased with an aspect ratio of 40, but negative EPP was reduced with an increase in aspect ratio. This pattern was followed for the composite of SB20. However, SB30 exhibited a different trend; in this case, excess pore water pressure was positive at the end of sharing. Positive excess pore water pressure was increased with increased in fiber concentration. With an aspect ratio of 80, positive EPP was reduced significantly in comparison to unreinforced soil for the composite of SB30 composite. Critical state parameter was altered significantly with the inclusion of fiber. Based on the experimental result, a mathematical model was developed to predict the effective major principal stress and experimental as well as predicted value are showing a good agreement for effective major principal stress at

failure. Volumetric shrinkage of SB30 strain was found to decrease with an aspect ratio of 40, 80, and 120 and SB20 composite had followed the same trend, which was similar to SB30 composite. Surface crack and shrinkage crack developed in the mixture after desiccation gets reduced with the addition of the glass fiber. The reduction of CDF and CIF was the function of fiber content and fiber aspect ratio. The complete evaluation of results has presented that sand bentonite fiber soil composite exhibited good potential and a candidate for the construction of a liner.

Keyword: Sand, bentonite, glass fiber, tire fiber, desiccation crack, residual strength, hydraulic conductivity, landfill liner, excess pore water pressure, Energy absorption capacity, Initial tangent modulus, Swelling pressure, Swelling potential, coefficient of consolidation

Table of Contents

List of the Figure

Tables

CHAPTER 1
INTRODUCTION

1.1 General

Landfill engineering is a relatively new branch of Civil engineering and therefore many uncertainties still exit concerning the construction of liner systems. Hoornweg and Bhada (2012) reported that the global urban municipal solid waste (MSW) had been forecasted to rise from 1.3 billion tons in 2010 to 2.2 billion tons in 2025. Landfilling is a suitable and suggested technique for the dumping of MSW in several countries across the world (Rowe et al.1995; Qian et al.2002). Generally, a combination of sand and bentonite compacted to a particular density is widely used as a barrier material at landfills. Bentonite leads an important role in reducing the movement of contaminants to the adjacent geo-environment and groundwater because of its contaminant adsorption ability and lower hydraulic conductivity (Chapuis 1990; Mishra et al. 2017). However, bentonite suffers a large interlayer shrinkage when exposed to chemicals resulting in the formation of crack (Quigley 1993), which leads to an increase in its hydraulic conductivity. Miller and Mishra (1989) observed desiccation cracks during their field investigation of landfill liners. The cracks exceeded 10 mm in width and penetrated the entire depth (0.30 m) of the compacted clay layer. Montgomery and Parsons (1989) observed desiccation cracking at test plots simulating covers constructed at a landfill in Wisconsin. Bosscher and Connell (1988) reported that jointing in desiccated clay has substantial effects on the hydraulic conductivity, shear strength, compressibility, and slope stability of the soil. Yong and Warkentin (1975) stated that cracking occurred at locations with low cohesion, which can correspond to the wettest spots in the soil.

Contrary to theoretical consideration, tensile stress may cause the shrinkage of the soil even at low pore water pressure. Shrinkage potential is additionally enhanced when the material previously experienced swelling by wetting due to a rise in the water table, precipitation during basal liner construction, geomembraine leakage, or rehydration at placement. The extent to which multi-lift liner placement is improved by dynamic vibration result in the earthen material being homogenized. Soil water under excess pore water pressure is strongly mobilized and so earthen material eventually return to its normal state of shrinkage (Horn et al 1997). Deformations of landfill material were initiated by settlement (Maher and Ho 1994; Scalia et al. 2017) in a landfill due to external and self-loading, which may produce tensile cracks, depending on stress levels and materials reliability. The study of the literature suggests that the landfill liner material generally possess a very low value of shear strength (Graham et al.1989; Wan et al. 1990 and Jones and Dixon 2003). Leung and Vipulanandan (1995) examined the influence of soil additives such as lime, cement, and sand on the hydraulic conductivity and volumetric shrinkage of soil and observed a decrease in shrinkage and increase in the hydraulic conductivity. They also found a reduction in the soil plasticity, which raised the potential of compacted soil to crack due to shear forces.

In addition to the different chemical additives, fibers can also be used to improve soil performance as a hydraulic barrier. The idea of reinforcing soil masses by containing some kind of fiber was experienced by early civilizations, which used soil, mixed with straw or other available fiber to improve durability and strength of the dried brick used as building materials and they observed that fibrous soil works better than natural soil (Miller and Rifai 2004).

Due to the rapid rise in the economy, the total number of discarded tires has been projected to grow up to 1.2 billion per year by 2030 (Thomas and Gupta 2016). Because most discarded tires are illegally disposed of, stored, or crammed into landfills, they can cause a major fire and health risks.

Hence, it is quite essential to reuse waste tires in order to decrease their adverse impact on the environmental and health. Tire fibers contain a compound combination of elastomers, polyisoprene, polybutadiene, and styrene-butadiene (Trouzine et al.2012). The tire fiber used in this study is a byproduct of the tire retread process and can be easily used as waste reinforcement material.

The glass waste in the form of broken glasses, bottles, glass sheets, and windowpanes can cause serious environmental problems (López et al.2012). The glass fiber, obtained from waste glass, possess a high strength, and heat resistance. Their non-biodegradable nature and ready availability have encouraged their use in the fibrous form and soil reinforcement in the geo-environmental application.

Cover liner system is subjected to low stress conditions and affected by the atmospheric condition (Shrinkage, desiccation etc. issue), on the other hand, side bottom linear system is subjected to high stresses and expected to be exposed to leachate for long –term conditions. Nevertheless, the hydraulic conductivity, shear strength, compressibility, and slope stability are critical issues to address both cover and side/bottom liner systems. Fibers are intended to be added to improvise these properties of sand –bentonite of sand-bentonite mix and it will be the more economical and eco-friendly solution for the purpose of environmental assessment.

ORGANISATION OF THE THESIS

The thesis has been categorized into six chapters. **Chapter 1** presents a general overview of the thesis, motivation behind this research work, and their importance. **Chapter 2** reviews the literature comprehensively on background research and identifies the gap areas. The objective and scope of the study are addressed based on the research gap. **Chapter 3** presents the details of the materials and methodology adopted in the study to meet the research objectives. The basic

characteristics of the individual material have been discussed in this chapter also. **Chapter 4** analyzes the effect of glass fiber (i.e. different fiber content and fiber aspect ratio) on hydro-mechanical behavior of various sand bentonite mixtures have been studied and discussed. **Chapter 5** investigates the impact of tire fiber on the hydro-mechanical behavior of sand bentonite mixtures have been analyzed and presented. Finally, **chapter 6** summarizes the major findings and conclusions of the study. Future work of this study has been reported in the final section of chapter 6.

CHAPTER 2
LITERATURE REVIEW

2.1 General

The amount of waste produced by urbanized and developing countries are increasing continuously due to an improvement in the living standard. Amount of waste produced in the cities has appeared as a major concern over the past years. The overall quantity of waste produced annually worldwide is about 4 billion tons and has been rising significantly (Hoornweg and Bhada-Tata 2012). Global urban municipal solid waste (MSW) production has been expected to increase by two times from 2010 to 2025 (Hoornweg and Bhada-Tata 2012). The waste can be categorized into two types as the municipal solid waste (MSW) and industrial waste. Burnt residue, sewage, waste oils, waste acid, waste alkali, waste plastics, waste paper, wood waste, waste textile, animal and plant residues, animal solid deadwood, waste metal, concrete and pottery waste, slag, debris, animal feces and urine, dead animal, ash dust, and wastes are categorized as nineteen different kinds of industrial waste. MSW specifies the waste other than industrial waste and is generated mainly from home, which also includes the wastes from business activities generated from the offices and restaurants. The waste having the possibility of inflicting damage on human health or life environment such as being explosive, toxic and infectious among these wastes are classified with "specially controlled MSW" or "specially controlled industrial wastes" and they are strictly controlled in all processes from collection to disposal. In developing countries, the per capita waste generation rate ranges from 0.4 to 1.1 kg per day, reaching in some urban areas 2.4 kg per day and more in tourist areas. The estimated quantity of MSW generated worldwide is 1.7 – 1.9 billion

metric tons (UNEP, 2010). The United States is the country that produces the largest amount of MSW in the world as it accumulates on a yearly basis of around 387 million tonnes of MSW (UNEP 2010). According to the Central Pollution Control Board report (2016), India produces about 52 million tonnes of waste each year, or approximately 0.144 million tons per day.

Landfilling is a suitable and suggested technique for the dumping of MSW in several countries across the world (Rowe et al. 1997; Qian et al. 2002). More than 50 % of the collected waste is often disposed of through uncontrolled landfilling and about 15 % processed through unsafe and informal recycling (Chalmin and Gaillochet 2009).

2.2 The major component of engineering Barrier system or landfill

The major key components of barrier materials and other additional components used in landfill engineering have been well documented and explained below.

2.2.1 Engineered cover

A cover placed over landfills, as shown in Fig.2.1 (a), are typically multicomponent cover system that is constructed directly on the top of the waste shortly after a specific unit or cell has been filled to capacity. Koerner and Daniel (1997) reported that the waste may be hazardous, non-hazardous industrial waste and construction /demolition waste. Modern waste management units so-called landfill are almost constructed with a bottom liner that includes leachate collection layer. Leachate is the contaminated liquid that drains from the waste material. The final cover is intended to (a) control infiltration of water into the landfill thus minimizing the leachate, (b) control the release of gasses from the landfill, and (c) provided for a physical separation between the waste and environment for protection for public health. Regulations for liner systems in the United States (including closer and poste closer regulations) fall into two broad categories:

a) New waste containment facilities (both hazardous and nonhazardous), which are regulated at the federal level under the resource conservation and recovery Act (RCRA).

b) Abandoned dumps and other contaminated sites that require corrective action and are regulated under the comprehensive Environmental response, Compensation, and liability Act (CERCLA), commonly known as Superfund.

RCRA and CERCLA regulation are very different from one another. The RCRA regulations are generally much more specific and detailed, and some case offers little flexibility to the designer. CERCLA regulations, in contrast, offer little specificity and instead simply state general goals and objectives for final cover systems.

Under RCRA, hazardous and nonhazardous solid waste landfills are regulated differently. Hazardous waste landfills are regulated under subtitle C, and nonhazardous waste landfills are regulated under subtitle D. Furthermore, regulated nonhazardous solid waste can be two types: industrial waste and municipal solid waste (MSW). Municipal solid wastes are regulated under subtitle D of RCRA; hence, MSW landfills are known as RCRA subtitle D and presented in Fig. 2.1(b) and Fig.2.1(c). Barrier-type covers commonly include five layers above the waste. A more complete discussion of these covers may be found in Koerner and Daniel (1997), McBean et al. (1995), Kreith (1994), and Tchobanoglous et al. (1993). The regulation of non-hazardous industrial waste is ambiguous at the federal level and appears to fall somewhere between subtitle C and subtitle D wastes. The regulation dealing with final covers for municipal solid waste landfills in the United States are found in title 40, part 258, Subpart F (closer and post closer care) of the Code of Federal Regulations (CFR). The citation for the applicable regulations is thus 40 CFR 258. The basic requirement as outlined in 258.60 (a), states that:

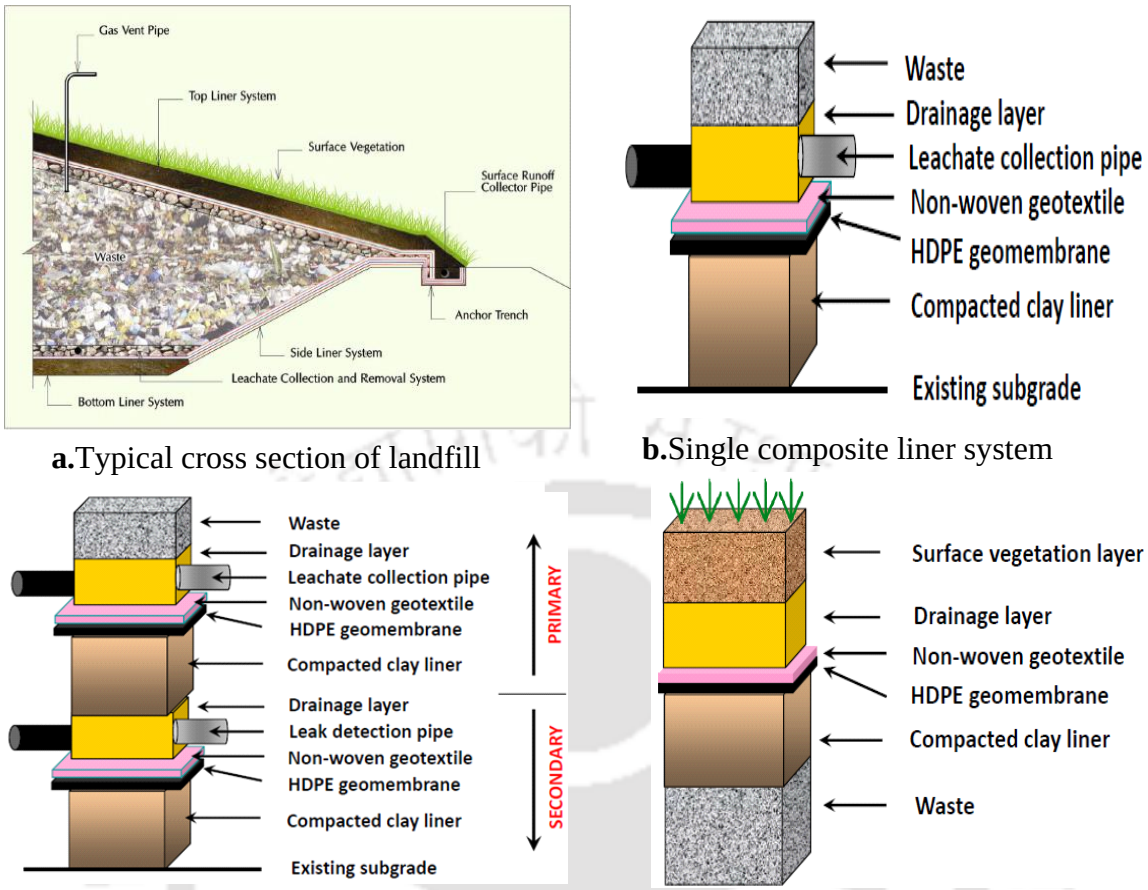

a.Typical cross section of landfill

b.Single composite liner system

c. Double composite liner system

d.Top liner system

Figure 2.1 Typical liner systems (Hughes et al. 2007)

"Owners or operators of all MSW landfill units must install a final cover system that is designed to minimize infiltration and erosion. The final cover system must be designed and constructed to:

i. Have a permeability less than or equal to the permeability of any bottom liner system or natural subsoil present, or a permeability no greater than **$1x10^{-5}$ cm/sec**, whichever is less, and

ii. Minimize infiltration through the closed MSW landfill by the use of an infiltration layer that contains a minimum 450 mm of earthen material, and

iii. Minimum erosion of the final cover by the use of erosion layer that contains a minimum 150 mm of earthen material that is capable of sustaining native plant growth".

Oppositely, the Subtitle D cover has four drawbacks: (1) the topsoil layer has limited water-holding capacity; (2) there is no drainage layer; (3) few roots can grow in the compacted barrier layer to remove water; and (4) soil freezing and root activity may increase the hydraulic conductivity value of the barrier soil layer over time. As a result, even though it has gained regulatory and public acceptance, the Subtitle D cover cannot ensure long-term protection against infiltration of water into the waste as reported by Hauser et al. (2001) and shown in Fig.2.1(d).

2.2.2 Landfill liner:

The design of waste disposal facilities typically involves some form of barrier, which separates the waste from the groundwater. This barrier is intended to minimize the migration of contaminants from the facility; thus the environmental impact of the facility is intimately related to its design and long-term performance. Generally compacted clayey liners and composite liner system with geomembranes are used at the waste disposal site (Fig.2.1 b & c). Landfilling employs an engineered method of disposing MSW on land in a manner that minimizes any environmental hazards. A landfill liner is relatively a thick structure of compacted natural clayey soil or manufactured material (i.e. geomembrane or geosynthetic clay liners) which serves as a barrier between leachate and groundwater to control the movement of leachate that reaches or mixes with the groundwater. Figure 2.1 shows the cross-section of a typical waste disposal site. Clay liners are frequently installed at waste disposal sites to prevent pollutant migration and to minimize or eliminate the risk for groundwater contamination due to low hydraulic conductivity and adsorption capability of the liner material. The liner may be required for one or two reasons; firstly, if the natural soil is fractured clayey soil then the liner may be required to retard movements of contaminant along the fractures, secondly, if the surrounding natural soil does not have a low

enough hydraulic conductivity to provide an adequate barrier, a liner is provided. There are some situations where the conceptual designs may not provide sufficient confidence that there will be a negligible effect on groundwater quality. Under these circumstances, an additional level of engineering in the form of a secondary leachate collection system or hydraulic control layer may be provided.

In the late 1980's the European commission began to draft the Council Directive on the landfill of waste. The directive went through much iteration until it was finally agreed in 1999 and proposed that landfill liners should satisfy at least one of the hydraulic conductivity and thickness requirements for the protection of soil, groundwater, and surface water:

Landfill for hazardous waste:

Hydraulic conductivity (k) < $1x10^{-9}$ m/sec; thickness > 5m

Landfill for non-hazardous waste:

Hydraulic conductivity (k) < $1x10^{-9}$ m/sec; thickness > 1m

Landfill for inert waste:

Hydraulic conductivity (k) < $1x10^{-7}$ m/sec; thickness > 1m

The thickness and hydraulic conductivity criteria of the mineral barrier used in liners vary from country to country and are shown in Fig.2.2 and Fig.2.3. The thickness of the barrier to be used should be less than 0.6 m and 1 m for USA and UK respectively and the hydraulic conductivity (k) should be less than 10^{-9} m/sec. For Japan, the thickness of the barrier should be less than 5 m and k should be less than 10^{-9} m/sec.

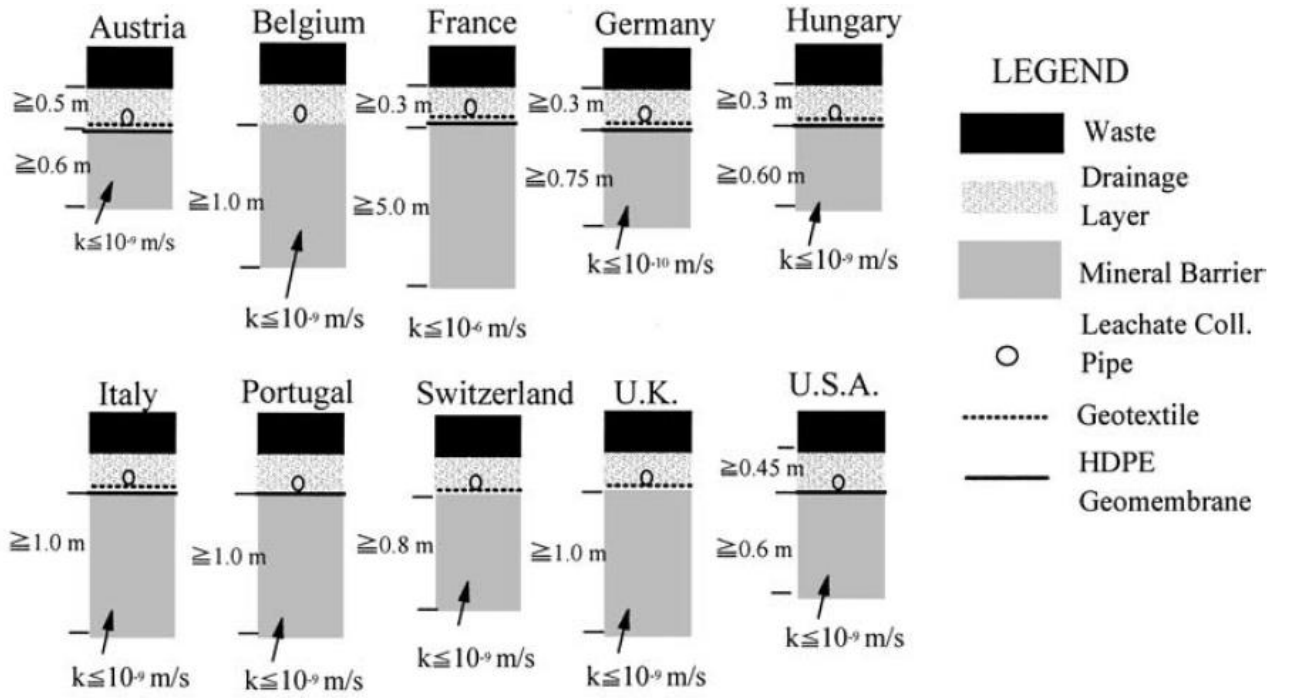

Figure 2.2 Liner systems specified in Europe and America (Chai and Miura 2002)

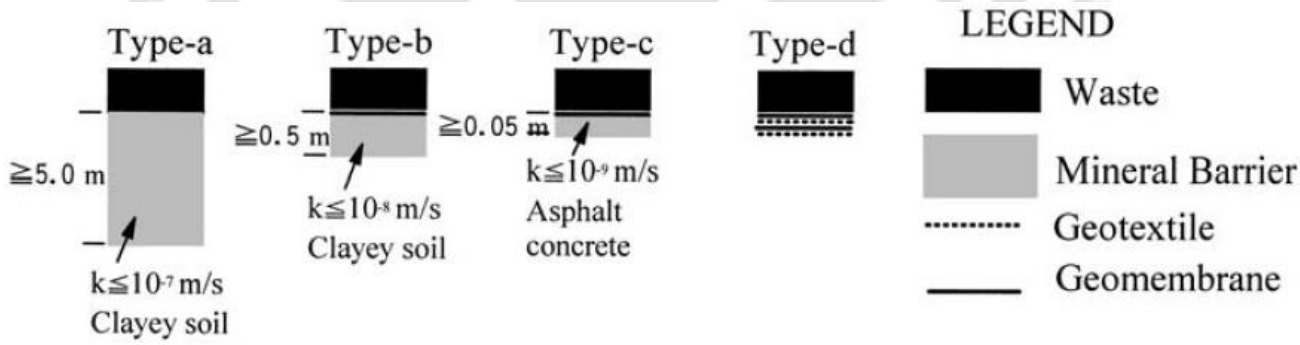

Figure 2.3 Japanese liner systems (Chai and Miura 2002)

2.3 Major factor and problem of engineering Barrier system

The factor and problem of the engineering barrier have been discussed below.

2.3.1 Hydraulic conductivity

Hydraulic conductivity of the soil is one of the most essential conditions, which must be satisfied in the order it to be used as a liner and cover material at the landfill. Many environmental agencies and researchers (USEPA 1988; Koerner and Daniel 1997; Hauser et al. 2001) have suggested that the landfill liner and cover material should have at least a hydraulic conductivity value of 10^{-9} m/sec and 10^{-7} m/sec or less, respectively. Komine (2004) performed experimental studies on sand-bentonite mixtures to assess their suitability as backfill material in a nuclear waste disposal facility. Studies were conducted on the mixtures with 5, 10, 20, 30 and 50% bentonite by dry weight. All the mixtures were tested using standard compaction test and the results indicated that 30% bentonite mix provide the highest dry density of all the other mixes. It was also observed that the mixes containing 5 to 30% bentonite content behaved more like a sandy soil than a clayey soil probably due to their relatively lower bentonite content; while, the mixture with 50% or higher bentonite content showed the characteristics of a clayey soil owing to its relatively high bentonite content. The mixes were tested for hydraulic conductivity, and the observed that the hydraulic conductivity decreases as the dry density and bentonite content increases. The decrease in the hydraulic conductivity was particularly noticeable for bentonite contents of 5 to 20% where the hydraulic conductivity decreased from 2.66×10^{-10} m/s to 4.85×10^{-12} m/s; whereas, mixtures with bentonite content in the range of 30 to 50% exhibited hydraulic conductivities in the range of 6.87×10^{-12} m/s to 1.21×10^{-12} m/s. The reduction in mixes with higher bentonite content was less as there were almost no voids left for the swollen bentonite to fill. Another notable observation

was that for mixtures with bentonite content less than 20%, when in contact with water there was not enough bentonite to fill all the voids in those mixtures.

The hydraulic properties of such soil-based structures can be compromised by the formation of desiccation cracks, which can result in the loss of effectiveness of the containment system as an impermeable barrier. Cracks increase the matrix hydraulic conductivity while also reducing the strength of the soil. Contaminated fluids migrate through the cracks at a much greater rate than the surrounding matrix (Miller and Rifai 2004). On the other hand, bentonite clay minerals may undergo large interlayer shrinkage in contact with certain chemicals. This is accompanied by an enormous loss in double-layer volume, potential cracking and increase in hydraulic conductivity value unless consolidation at the in-situ field stresses compensates for the chemically induced changes (Quigley 1993). Evans and Quigley (1992) showed that municipal solid waste leachate causes volumetric reduction and decrease in hydraulic conductivity of sand-bentonite mixtures.

2.3.2 Settlement

The settlement is one of the important factors that cause of the poor performance of final covers. Koerner and Daniel (1997) studied that all solid waste will settle over time, causing subsidence of the upper surface and with it the engineered cover. Design estimates of both total settlement and differential estimate are required in order to analyze the long term functioning and stability of the final cover. In general, the upper surface of the solid waste mass will have a layer of soil placed over it acting as a foundation layer for the eventual placement of the cover material. The final grade of the foundation layer must take into account the estimated total settlement after cover placement. As seen in Table 2-1, this can amount to from 10 to 20% thickness of the waste for MSW solid waste landfills. Because of the uncertainties of estimating total settlement or

differential settlement, a post-closure monitoring and maintenance plan for repair is strongly recommended.

Table 2-1 Impact of liquids Management Practice on Cover Settlement at Municipal Solid Waste Landfills (Koerner and Daniel 1997)

Leachate Management Practice	Total Settlement		Deferential Settlement	
	Amount	Time	Amount	Time
Standard Leachate withdrawal	10-20%	≤ 30yrs.	Little to Moderate	≤ 20yrs
Leachate Recirculation				
None, e.g., at abandoned Landfills or dump	10-20% UP to 30%	≤ 15Yrs > 30yrs	Moderate to major Unknown	≤ 10 > 20

There are many issues concerning the differential settlement of solid waste. In the situation where differential settlement is likely to occur and the localized depressions cannot be eliminated by suitable grading, the choices are (a) continuously grading and maintaining the site, or (b) reinforcement of the cover system as suggested by Koerner and Daniel (1997). Normally, clayey soils in conjunction with synthetic materials (geomembranes, geotextiles, etc.) are used for the construction of landfill liners and covers. The non-uniform settlement of waste materials in landfills may cause excessive deformation and cracking in the cover and undermine the long-term performance of the landfill system. Differential settlement of compacted clay liners, caused by compaction over weak ground or over soft spots in an underlying drainage (or leak detection) layer, may result in the release of leachate into the surrounding soil/groundwater system (Maher and Ho 1994). Scalia et al. (2017) studied the differential settlement of the barrier system after 14 years of service, as shown in Fig.2.4 (a).

2.3.3 Slope Instability

Final covers are almost always sloped to maximize waste volume and to promote runoff. Sometimes, slopes are very steep, approaching grades of 50%. The "grade" is defined as the vertical distance divided by horizontal distance and is numerically equal to the tangent of the slope angle. In case of the liner, the introduction of a geomembrane, geosynthetic clay liner, and/or compacted clay liner on a landfill cover slope steeper than a grade of 5 to 10% must be done with the utmost care. Generally, a factor of safety of at least 1.5 is recommended as the minimum value for static loading of final covers as suggested by Koerner and Daniel (1997).

Gnojna Grora landfill in Poland, Istanbul Landfill in Turkey, Hiriya landfill in Israel and Payatas landfill in Philippines was failed due to slope instability and shown in Fig.2.4(b). Landfill lining systems are comprised of multiple geosynthetic and mineral layers. The interfaces between these materials can form preferential slip surfaces. The majority of failures reported in the literature are controlled by slippage at interfaces between lining components. Seed et al. (1990) studied the failure of the Kettleman Hills Waste Landfill slope and reported that failure was developed by sliding along interfaces within the composite geosynthetic-compacted-clay liner system beneath the waste fill. After 2-D and 3-D numerical analysis, they reported that the 2-D stability analyses gave factors of safety of 1.2-1.25 and 1.1-1.15 for the minimum wetting case and the full base wetting case, respectively, while the 3-D analyses yielded values of 1.08 and 1.01 for these two cases. Koerner and Soong (2000) back-analyzed 10 large landfill failures and demonstrated that assessment of stability was most sensitive to shear strength parameters defined for the critical slip surface.

2.3.4 Shear strength

Catastrophic slope failure of MSW landfill was responsible due to the low shear strength of landfill material as shown in Figure 2.4(c). Maher and Ho (1994) stated that clayey soils in conjunction with synthetic materials (geomembranes, geotextiles, etc.) could be used for the construction of landfill liners and covers. The non-uniform settlement of waste materials in landfills may cause excessive deformation and cracking in the cover and undermine the long-term performance of the landfill system. Therefore, it is required that the compacted clay liners (CCLs) must have an adequate internal shear strength to maintain the stability of landfill liner. Daniel and Wu (1993) suggested a minimum unconfined compressive strength of 200 kPa, which was arbitrarily selected for stiff clay. Giroud and Beech (1989) described that lining structures inclined in the range of 14°–22° are more prone to uncertainty. Benson and Othman (1993) stated that the hydraulic barrier should also be physically stable in order for it to be used as landfill material, and it should have acceptable shear strength to avoid sliding on the slope. Singh and Sun (1995) stated that sliding surface can also occur at points where there is high pore water pressure that result in leachate accumulation along with the interface.

2.3.5 Desiccation cracking:

The stability of clay slopes and liners is connected intimately to desiccation cracking. Khire et al. (1997) have shown that compacted clay barriers in earthen covers undergo seasonal changes in water content, even at significant depth, due to seasonal variations in precipitation and evapotranspiration. Field studies (Fig.2.4d) have also shown that desiccation can induce severe cracking of unprotected clay barriers (Benson 1997; Benson and Khire 1997). Compacted soil liner systems may also suffer damage from desiccation if they are left exposed prior to placement of a geomembrane and if the geomembrane is not maintained in intimate contact with the clay via surcharge (Basnett and Bruner 1993). Lachenbruch (1963) stated that desiccation cracks are

characteristics of a somewhat nonhomogeneous or plastic media in which the stress builds up gradually with cracks forming first at loci of low strength or high-stress concentration. **Sharma et al. (2004)** have discussed problem and major aspect of the landfill in detail.

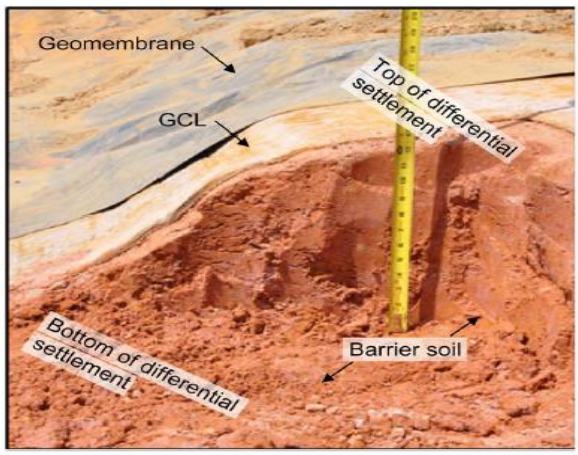

a. Differential settlement of barrier system (Scalia et al.2017)

b.Tension cracks on top of landfill and steep backscarp in MSW after slope failure (Kocasoy and Curi 1995)

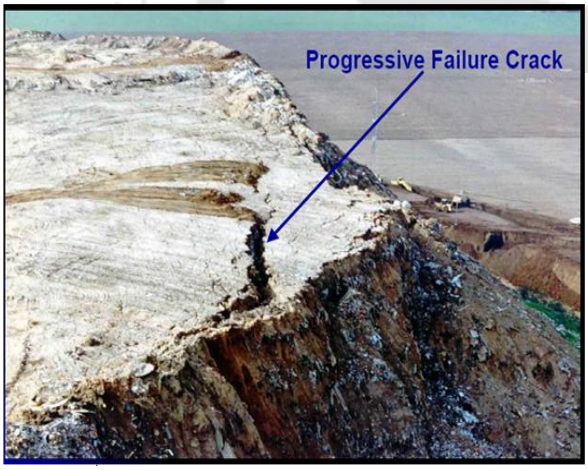

c. 1997 Hiriya landfill slope failure (Isenberg 2003)

d. A close-up view of the desiccation crack at the hydraulic fill site in Los Angeles (Mitchell 1986)

Figure 2.4 Differential settlement, slope failure, and desiccation cracking of barrier system

2.4 Bentonite

Bentonite is widely used as a backfill material during the construction of slurry trench walls, as a soil admixture for the construction of seepage barriers, as a grout material, as a sealant for piezometer installations and for various other civil engineering construction techniques. Bentonite

is an absorbent aluminum phyllosilicate, essentially impure clay, formed as a deposit of volcanic ashes at shallow wet sites in various location of the world (Grim & Guven 1978). These deposits are variable, depending on the nature of the volcanic ashes and the salinity of the water into which they were deposited. Since the bentonite is a natural material, it's mineral composition, chemical state, and grain size distribution varies considerably from one source to another. Different parameters such as mineralogical composition (i.e., amount and type of montmorillonite), type of exchangeable cations, surface area and the surface charge density affect the behavior of bentonite considerably.

Bentonite is primarily composed of the smectite group of minerals, most common among which is montmorillonite (Mitchell and Soga 2005). The behavior of bentonite primarily is governed by montmorillonite which has characteristics like a large specific surface area (as high as 800 m^2/g), high charge deficiency (0.5-1.2 per unit cell), high cation exchange capacity (80-150 $cmol_c/kg$), and the ability for interlayer swelling. These factors contribute to the high swelling, low hydraulic conductivity, and contaminants adsorption ability of the bentonite.

2.4.1 Structure of Montmorillonite

Phyllosilicates as its main mineralogical components of the mineral montmorillonite. These phyllosilicates are made of silica (SiO_2) tetrahedral sheets and Aluminium (Al^{3+}) or Magnesium (Mg^{2+}) oxides octahedral sheets. Montmorillonite has a prototype structure similar to that of pyrophyllite consisting of an octahedral sheet sandwiched between two tetrahedral sheets (2:1 mineral) and diagrammatically in three dimensions (Fig. 2.5a). The silica and gibbsite sheets are combined in such a way that the tips of the tetrahedron of each silica sheet and one of the hydroxyl layers of octahedral sheet form a common layer and all the tips of the tetrahedral point toward the center of the unit cell. The oxygen forming the tips of the tetrahedral is shared with the octahedral

sheet as well. The anions in the octahedral sheet that fall directly above and below the hexagonal holes formed by the bases of the silica tetrahedral are hydroxyls. Bonding between successive layers is by van der Waal's forces and by cations that balance charge deficiencies in the structure. These bonds are weak and water or other polar liquids can easily enter between the layers, causing them to expand significantly. It has a lateral dimension of 1000 to 5000 A^0 and thickness 10 to 50 A^0.

The layers formed in this way are continuous in 'a' and 'b' directions and stacked one above the other in the 'c' direction. Bonding between successive layers is by van der Waal's forces and by cations that balance the charge deficiencies in the structure. These bonds are weak and easily separated by cleavage or adsorption of water or other polar liquids. The basal spacing in the c direction, d(001), is variable, ranging from about 0.96 nm (1nm = 10^{-6} mm) to complete separation.

The montmorillonite is the primary mineral of bentonite. In the dry state, a particle of montmorillonite (Fig.2.5a) resembles a closed book composed of many thin crystalline sheets held together by weak van der Waal's forces and by cations. Each sheet has charge deficiencies within its crystal structure and is neutralized by the presence of cations held loosely to the surface of the sheets. When the dry bentonite and water are mixed, water is drawn into the montmorillonite particles to hydrate the surface of the elemental sheets and the cations. For the combination of sodium montmorillonite and freshwater, the fluid that enters the particles forms thick, viscous diffuse ionic layers around the layer, causing the montmorillonite particles to swell, possibly to the extent of complete separation of the sheets. The fabric of freshwater, low salt, sodium bentonite resembles a pile of crumpled paper. For the combination of dry sodium bentonite and a saline solution, less fluid is required to neutralize the negatively charged sheets, and if the ion concentration is large or the valence of the cations are large, the separation distance between sheets

will remain small and the montmorillonite particles will remain in the form of closed books. The fabric of bentonite, in this case, will consist of swollen but intact montmorillonite particles surrounded by thin, viscous diffuse ionic layers, in an arrangement resembling a pile of fallen books. A third case is that of calcium bentonite, an example of bentonite in which dominant exchangeable cations is polyvalent. The calcium cation is very effective in holding together the montmorillonite sheets, and therefore calcium bentonite has a small potential to swell, even when mixed with fresh water. Calcium bentonite behaves similarly to sodium bentonite in a high salt state and its permeability properties are about same.

2.4.2 Swelling behavior of bentonite

The swelling of bentonite takes place in two stages, inner-crystalline swelling and osmotic swelling (Norrish and Quirk 1954).

2.4.2.1 Inner-crystalline swelling

In inner-crystalline swelling, water molecules enter the interlayer region of the montmorillonite to hydrate the exchangeable cations located there. The cations upon contact with water order themselves on a plane halfway between the clay layers, which lead to a widening of the spacing between the layers. The volume of montmorillonite can double in the process of inner-crystalline swelling. The polarity of the water molecule is an important factor in the inner-crystalline swelling of clay. When cations hydrate, the water molecules orient their negative dipoles towards the cation and thus weaken the electrostatic interaction between the negatively charged layers and the interlayer cations. Inner-crystalline swelling, which has also been referred to as Type I swelling, is a process whereby expandable 2:1 phyllosilicates sequentially intercalate one, two, three or four discrete layers of H_2O molecules between the mineral interlayers (Norrish 1954). In this process, the swelling occurs prior to osmotic (Type II) swelling, which is associated with longer range

electrical diffuse double layer effects. Figure 2.5b and Figure 2.5c shows inner-crystalline swelling of sodium montmorillonite. In inner-crystalline swelling, there is a balance between attractive and repulsive forces operating between adjacent interlayer surfaces (Norrish, 1954; Vanolphen 1965; Kittrick, 1969). Electrostatic attraction between the exchange cations and the basal surfaces of the clay dominates the net potential energy of interaction (Laird 1996 and 2006). The positively charged cations provide links or are like charge bridges between adjacent negatively charged clay layers. On the other hand, the hydration energy of the exchange cations dominates the net potential energy of repulsion. Net forces of attraction are dominant for unsaturated conditions or saturated conditions with high electrolyte concentrations, while net forces of repulsion are dominant in case of fully saturated conditions of low electrolyte concentration.

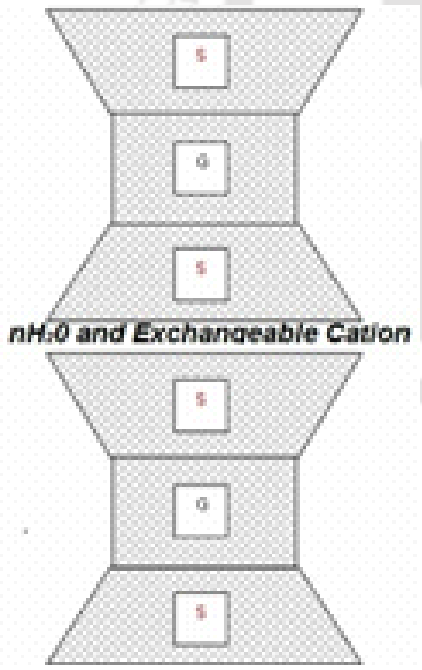

a. Structure of montmorillonite (Mitchell and Soga 2005)

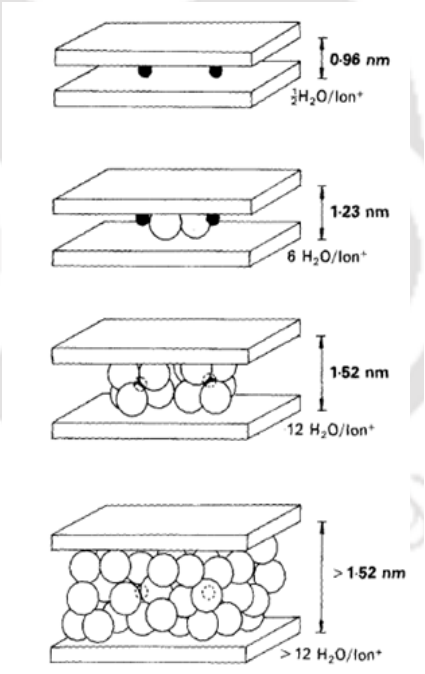

b. Inner-crystalline swelling of sodium montmorillonite.Given are the layer distances and the maximum number of water molecules per sodium ion (Kraehenbuehl et al.1987)

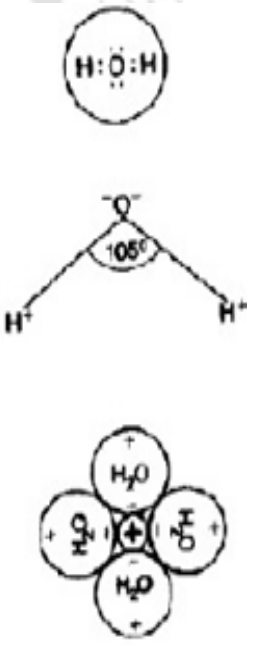

c.Structure of water molecule (Mitchell and Soga 2005)

Figure 2.5 Structure and crystalline behavior of Montmorillonite

2.4.2.2 Osmotic swelling

The osmotic phase of swelling follows the hydration phase but occurs only when the exchange sites contain monovalent cations (McBride 1994; Prost et al.1998). The interlayer region retains numerous layers of water molecules during the osmotic phase. The number of layers of water molecules at equilibrium is proportional to the cation concentration in the bulk water (Onikata et al. 1999). Accordingly, when the bulk water contains a low concentration of monovalent cations and monovalent cations occupy the exchange sites, a larger fraction of the total water is bound and less mobile water is available for flow resulting in a lower value of hydraulic conductivity. This condition is commonly observed when sodium montmorillonite are hydrated and/or permeated with DI water (Shackelford et al. 2000). When polyvalent cations occupy the exchange sites, only the hydration phase occurs. The interlayer expands until it contains four monolayers of water and then expands no further (Prost et al. 1998). There are several explanations for the lack of additional interlayer swelling when polyvalent cations occupy the exchange sites, but consensus does not exist regarding which explanation is correct (McBride 1994). Nevertheless, the absence of the osmotic phase is well documented experimentally in the literature (Prost et al. 1998). Lack of an osmotic phase is evident in the free swelling of calcium montmorillonite (i.e., bentonites where the exchange sites are occupied by Ca^{2+} cations), which typically is about 3 mL/2g even when DI water is the hydrating liquid. In contrast, the free swelling of sodium- montmorillonite typically exceeds 30 mL/2g in dilute monovalent solutions or DI water (Lin and Benson 2000).

In sodium-montmorillonite, the swelling can result in the complete separation of the layers. The driving force for the osmotic swelling is the large difference in concentration between the ions electrostatically held close to the clay surface and the ions in the pore water of the rock (Figure 2.6a). Irregularities in the crystal lattice are manifested by an excess negative charge, which must be compensated by positive ions close to the surface of the clay. The concentration of positive ions

close to the surface is thus extremely high, while that of negative ions is very small. The positive ion concentration decreases with increasing distance from the surface, whereas the concentration of negative ions increases. The negatively charged clay surface and the cloud of ions form the diffuse electric double layer (Fig.2.6b). A high negative potential exists directly at the surface of the clay layer. The value of this potential is reduced, with increasing distance from the surface and reaches zero in the pore water. When two such negative potential fields overlap, they repel each other and cause the observed swelling in clay. The profile of the potential curves, and therefore the repulsion at a given distance vary with the valence and the radius of the counter-ions in the double layer and with the concentration of electrolytes in the pore water. A transformation of sodium montmorillonite into its calcium form or an increase in the electrolyte concentration in the pore water results in the decrease in the double layer thickness and a reduction in the swelling stress.

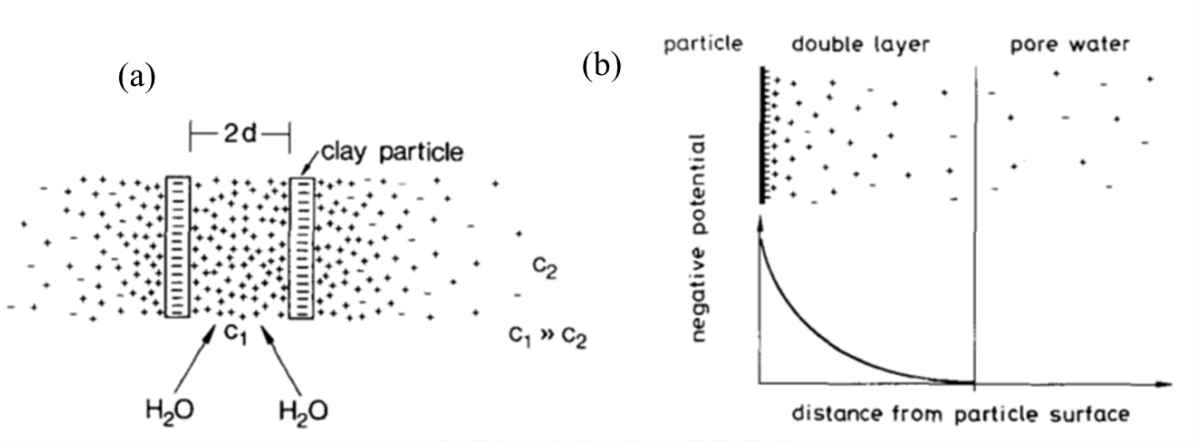

Figure 2.6 Osmotic swelling of bentonite (Madsen and Vonmoos 1989)

a). Two negatively charged clay layers with ion cloud. The ion concentration C1 between the layers is much higher than the ion concentration C2 in the pore water. An equilibration of the concentration can only be reached through the penetration of water into the space between clay layers, since the interlayer cations are fixed electrostatically by the negative charge of the layers (osmotic swelling)

b). Negatively charged clay surface, ions in the diffuse double layer and ions in the pore water. The distribution of the negative potential changes with the valence and the radius of the ions in the double layer and with the electrolyte concentration in the pore water

2.5 Use of bentonite for the engineering barrier system

Compacted soil liners had been utilized for several years as engineered hydraulic barriers for waste dumping landfills and this compacted soil liner was made from naturally occurring soils that hold a substantial amount of clay. Moreover, the compacted soil liners were normally used together with geomembranes to form a composite liner, which generally contains a geomembrane, placed directly on the surface of compacted clay (USEPA 1995). Alternatively, compacted sand–bentonite mixtures have also been treated as a good substitute hydraulic barrier material to compacted clays when clayey soils were not accessible on or near sites. According to Akgun (2006), the sand component of a compacted bentonite-sand mixture contributes to the strength; whereas, the bentonite component fills the pore space between the sand grains in order to decrease the hydraulic conductivity. However, Quigley (1993) reported that bentonite suffered a large interlayer shrinkage when exposed to chemicals resulting in the formation of crack, which led to an increase in hydraulic conductivity. Dutta and Mishra (2015) investigated the influence of salt concentration on bentonites to study the physico-chemical characteristics and indicated that the hydraulic conductivity gets affected prominently for high swelling bentonite in comparison to low swelling bentonite. Desiccation induced moisture variations on the compacted sand-bentonite mixture with a low stress can affect the reduction in plastic deformability (Morris et al. 1992; Rodatz and Oltmanns 1997) and produce shrinkage cracks (Miller and Rifai 2004 and Rayhani et al. 2008). Yesiller et al. (2000) observed that the highest amount of cracking of the soil was directly controlled with the maximum amount of fines fraction and the minimum amount of cracking of soil was noticed with the minimum amount of fines fraction. Even, a number of engineered barrier materials have been proposed, including bentonite clays and bentonite–sand mixtures. Engineered barriers will be subjected to a number of non-typical environmental stresses including high temperature, changing groundwater conditions, changing groundwater chemistry, and varying

stresses (Blatz et al.2002). Graham et al. (1989) conducted the triaxial and one-dimensional swelling tests on the compacted sand-bentonite mixture at pressures up to 3 MPa due to potential use for containing nuclear and other toxic wastes. The result suggested that the material expanded in a low stress range up to 0.6 MPa, with the volumetric expansion depending on the confining pressure and the duration of the tests and swelling is inhibited by confining pressures in excess of 0.8 MPa. They reported that effective cohesion and effective internal frictional angle of saturated compacted sand-bentonite mixture were measured around 40 kPa and 14˚ under an undrained condition, respectively. Wan et al. (1990) performed the triaxial test on the compacted sand-bentonite mixture to investigate the strength and constitutive behavior of the mixture and reported the shear strength parameters of c'= 0 kPa and ϕ' = 14° in a pressure range of 0 to 1.5 MPa. Mollins et al. (1999) stated that the shear strength of sand-bentonite mixture strongly related to relative density and frictional angle of sand. Chen and Meehan (2011) performed an unconsolidated undrained triaxial test to determine the shear strength of bentonite-sand blends having clay substances of 15, 25 and 50% by dry weight of the mixture, reported that undrained shear strength reduced with adding water content, and enhancing with increasing bentonite content. Sun et al. (2016) performed a triaxial test on sand-bentonite mixture (70:30) to study the hydro-mechanical characteristics under the undrained condition and observed that inflated volumetric deformation alters to contractive volumetric deformation due to rise in the confining pressure. The study of the literature concludes that the landfill liner material generally possesses a very low value of shear strength (Graham et al.1989; Wan et al. 1990; Blatz et al.2002; Jones and Dixon 2005). In addition, Bosscher and Connell (1988) observed that jointing in desiccated clay has important impact on the hydraulic conductivity, shear strength, compressibility, and slope stability of these soils.

Major Problem of the landfill found from earlier study and landfill failure case

1. Higher bentonite content was used to maintain the hydraulic conductivity

2. Desiccation –induced crack was related to higher bentonite content

3. Landfill liner settlement was increased with increase in bentonite content

4. Stress-strain response of the landfill material was highly related to bentonite content. At saturated state, stress–strain response was significantly low. Landfill liner underwent large settlement due to overburden pressure

5. Shear strength of the landfill liner material was also low. Most of the landfill failure was occurred due to low shear strength of the landfill material

6. Slope instability was the function of shear strength. Most of the liner slope was failed by the poor shear strength. Compacted clay and bentonite-enhanced soils (BES) can experience large strains, particularly on steep side slopes.

7. Large interlayer shrinkage was higher with higher bentonite content. Volumetric shrinkage was increased with increase in bentonite content.

8. Continuous reinforcements may not be a viable option in low permeability barrier layers as they could provide a preferential flow path for the migration of fluids and gasses

Therefore, the attention of using fibers has arisen to well improve clay performance as hydraulic barriers without altering the physical properties of the soil. Fiber-reinforced soil is a mixture of soil and fibers. Fibers can be natural or synthetics. Natural fibers can be obtained from the plants, animals other natural source. Jute, cotton, silk are some examples of natural fibers. Petrochemicals

are the major source of synthetic fibers. Polypropylene, polyester, polyamide etc. are examples of such type of synthetic fiber. The high strength, high heat resistance, non-biodegradable and readily availability of glass fiber (i.e. obtained from waste glass) have encouraged their use, in the fibrous form, as soil reinforcement in the geo-environmental application. Glass is an amorphous material, properties of glass fibers are uniform in all direction, and main constituent of the glass fiber is silica. Advantage of synthetic fibers over the natural fibers is less degradation, and therefore is widely being used in geotechnical applications (Consoli et.1998; and Patel and Singh 2017).

On the other hand, the use of several materials in soil reinforcement can be modified the rheology of soil, therefore, it is compulsory to know all generated reactions in the soil structure to analyze system. One of the materials can be used to reinforce the soils is scrapped tire rubber and this waste material can implement as a stabilizer as well. Furthermore, the use of the rubber can be an alternative to comfort pressure on rubber waste landfill. Furthermore, the life of the rubber is very long and enhances structural capacity of soils. Details study of waste fibers (i.e. glass and tire) have been discussed below.

2.5.1 Previous study on tire fiber

2.5.1.1 Back ground

The term "rubber" was invented by John Priestly in 1770 when he found that the material could erase pencil marks. Natural rubber, also called India rubber or caoutchouc, as initially produced, consists of polymers of the organic compound isoprene, with minor impurities of other organic compounds, plus water (Greve 2000). Rubber is obtained from latex that exudes from the bark of the Hevea tree (Fig 2.6) when it is cut. Latex is an aqueous dispersion of rubber, containing 25-40% rubber hydrocarbon, stabilized by a small amount of protein material and fatty acids. The latex is gathered, coagulated, washed and dried. Raw rubber is soft at high temperature and is too

brittle at low temperature. The tensile strength is very low. To improve the properties of rubber, it is compounded with some chemicals like Sulphur, hydrogen sulphide, benzoyl chloride etc. The most important is the addition of sulphur (i.e. the heating of raw rubber with sulphur to 100-140˚C). The extent of the stiffness of vulcanized rubber depends on the amount of sulphur added.

Figure 2.7 Rubber tree and Rubber latex (https://en.wikipedia.org/wiki/Natural_rubber)

A tire rubber may contain 3 to 5% sulphur, but a battery case rubber may contain as much as 30% sulphur. Vulcanized rubber has good tensile strength and can bear a load of 2000 kg/cm^2 before it breaks (Paladhi 2012).

2.5.2 Impact of tire on geotechnical technical properties of soil

The amount of waste tire is being devolved annually due to the increase in the number of automobiles both in developed and in developing countries. The amount of waste tire has further increased because of quick financial growth in some emerging countries such as China and India

where the demand for automobiles has been increasing significantly. Although, it is expected that 13.5 million tons of Tire (the United States, 4.4 million tons; European Union (EU), 3.4 million tons; and the rest of the world, 5.7 million tons) are expunged each year (Genan Business and Development A/S 2012). About 89% (by weight) of waste tire produced in the Unites States were recovered in 2007, whereas only 11% (on a per-tire basis) was recovered in 1990 (Rubber Manufacturer Association 2009). This is mostly because of state efforts to decrease stockpiled tires, develop sustainable waste fairs, and impose current tire laws and guidelines. In the year of 2009, major European countries recovered around 90% of their yearly waste tire (European Tire and Rubber Manufacturers' Association 2010). In spite of that,128 million waste tire (about 2.1 million tons) continued in stockpiles in the United States at the end of 2007, and 5.5 million tons persisted in the EU in 2010 (1.73 times the amount of scrap tire generated in 2009). The rescue rate of the waste tire in other areas, however, is not remarkable. Stockpiling of the waste tire is extremely objectionable, as it not only causes environmental pollution but also carriages fire and health threats. Therefore, there is a critical requirement for environmentally friendly ways to reutilize and recycle waste tire. In current ages, investigation in the use of waste tire for civil engineering application has improved. The use of waste tire (pure tire pieces or whole tire) in civil engineering application includes soil reinforcement in, ground erosion control, road construction, vibration isolation, slope stabilization, nonstructural sound barrier fills, aggregates in leach beds of landfills, lightweight materials for backfilling of retaining structures, additive materials to asphalt, and low-strength but ductile concrete (Sheikh et al. 2012). The use of pure tire shreds in civil engineering application practiced significant scrutiny because of its possible to progress exothermic reactions (Humphrey 1996; Gacke et al. 1997). According to this fact, the study is directed towards compacted clay or sand-bentonite mixture reinforced with waste tire fiber for

finding a suitable landfill material due to the environmental problem as well as environmental assessment.

Al-Tabbaa et al. (1997) investigated the influence of different sizes of shredded tires on compaction characteristics of kaolin soil and observed that the maximum dry density decreased by the inclusion shredded tire; whereas, the optimum moisture content (OMC) remained almost constant. Test result suggested that hydraulic conductivity of the composite was reduced by the inclusion of shredded tire.

Al-Tabbaa and Aravinthan (1998) examined the paraffin-treated rubber tire in clayey soil and estimated hydraulic conductivity of clay–tire mixtures using distilled water, acidic water, and paraffin. The rise in the permeability of clay–tire mixtures was observed to be insignificant when distilled water was used as permeant because of good bonding, which prohibited the formation of pores and cracks. The use of distilled water as permeant of clay–tire mixtures resulted in high permeability because of the flocculation facilitated by the acidic environment and a substantial drop in hydraulic conductivity by the use of paraffin as permeant was noticed. The hydraulic conductivity of clay incorporated with 15% tires of 4–8 mm size was reported to be reduced by 50 times when paraffin was used as permeant.

Cokca and Yilmaz (2004) conducted oedometer tests on rubber mixed with bentonite added fly ash to evaluate the compressibility behavior of the composite and observed a decrease in the initial void ratio with the increase in the rubber percentage. They also observed that the unconfined compression strength of the composite was decreased with an increase in rubber fiber. Test result suggested that swelling pressure of the composites reduced with the increase in the rubber fraction in the mixture. They found that hydraulic conductivity of the flay ash increased with rubber fraction and decreased with bentonite fraction.

Ozkul and Baykal (2006) studied the strength and deformation behavior of kaolinite clay reinforced with tire buffing under drained and undrained conditions. They reported that drained shear strength of the clay was essentially unchanged by the introduction of rubber buffings or by an increase in the level of compaction energy employed. Result also suggested that undrained strength was also not changed when standard compaction energy was used, but decreased slightly, showing a more ductile failure, when modified energy was employed. The result suggested that peak strength was slightly altered in comparison to clay at unconsolidated undrained condition at standard compactive effort. However, failure strain or reinforced specimen was much higher in compression to unreinforced specimen at modified compactive effort. Under a consolidated undrained condition, the strength of the reinforced specimen was slightly low in comparison to the unreinforced specimen for considering both energies. They recommended that effective frictional of 33° would be considered for designing the earth structures.

Cetin et al. (2006) investigated the impact of fine-grained (particle size below 0.425 mm) and coarse-grained (particle size between 2 and 4.75 mm) tire chips on Atterberg limits of the clayey soil. Clayey soil mixed with tire chips at level of 0, 10, 20, 30, 40, and 50%, by weight and reported that Atterberg limits of clayey soil significantly decreased with the increase in the percentage of tire chips. They observed that the combination of coarse tire chips (up to 30%) did not affect the liquid limit of clayey soil significantly. It was reported that decrease in liquid limit was almost 9.5% and 23.8% with the addition of 40 and 50% tire chips, respectively. Plastic limit of the clay was reduced by 12, 16, 24, and 20% with the addition of 20, 30, 40, and 50% of coarse tire chips, respectively. The decrease in the MDD of the clay due to the addition of fine-grained tire chips was higher in comparison to coarse-grained tire chips. However, the OMC was increased due to the addition of fine-grained tire chips but decreased with coarse-grained tire chips. They also reported that hydraulic conductivity values increased with tire chips, but with a decrease in normal

pressure, hydraulic conductivity increased again. Hydraulic conductivity was found to decrease with coarse-grained tire chips in comparison to fine-grained tire chip under a normal pressure of 100 kPa to 350 kPa. The test result specified that the shear strengths increase up to 30% for fine and 20% for coarse tire chip mixtures and shear strength increased with increase in normal pressure. Cohesion increased as the tire-chips content increase up to 40% for both fine and coarse mixtures while the angle of internal friction decreased. After 40%, the cohesion decreased and the angle of internal friction increased.

Ozkul and Baykal (2007) studied the pre-shear and post-shear hydraulic conductivity of clay specimens holding with 10% tire buffings of 4–15 mm length. Result suggested that pre-shear hydraulic conductivity did not altered with the inclusion of tire buffings but post shear hydraulic conductivity was slightly higher in comparison to post shear hydraulic conductivity. They found that pre-shear hydraulic conductivity did not alter with the inclusion of tire buffings but post shear hydraulic conductivity was slightly higher in comparison to post shear hydraulic conductivity. Result indicated that tire buffings exhibited slightly higher peak in comparison to unreinforced specimen at all range of confining pressure except 300 kPa.The reinforced specimen exhibited initial contraction over a wide range of strain and greater loss of post peak strength was noticed at 300 kPa confining pressure. The cohesion value of the reinforced specimen was increased from 34 to 64 kPa but internal frictional angle was decreased from 29.3° to 27.6°. They also reported that peak pore water pressure was increased with tire buffings and barrel type failure was observed for reinforced specimen after shearing.

Mokhtar and Chan (2007) performed the UCS of clayey soil mixed with 5% cement, 5, 10, and 15% tire chips of 2 mm size, and they observed that the addition of tire chips led to an increase in strength of cemented clayey soil associated to unrubberized cemented clay. It was also reported

that elasticity and strain softening behavior was increased; when tire chips mixed with cemented clay. Seda et al. (2007) investigated the index properties of expansive soil mixed with 20% granulated rubber (by weight) of size smaller than 6.7 mm and reported a negligible change in Atterberg limits and plasticity index of expansive soil with the inclusion of rubber.

Sarvade and Shet (2012) investigated the influence of crumb rubber (smaller than 1.18 mm size) as well as cement and lime on Atterberg limits of clay. The fraction additions of crumb rubber and cement and lime were 5, 10, 15, 20, and 25% and 1, 3, and 5% (by weight), respectively. They observed a drop of 7.60, 19.23, 14.61, 25.86, and 28.07% in the liquid limit of clayey soil combined with 5, 10, 15, 20, and 25% crumb rubber powder, respectively. A similar trend was observed for plastic and shrinkage limit. However, a reduction of 32.69 and 11.9% in liquid limit was noticed for rubberized clay (5% crumb rubber) with 5% cement and lime, respectively. The plastic limit of the rubberized clay with 5% cement and lime was found to be decreased to 19.21 and 7.83%, respectively.

Patil et al. (2011) studied the influence of silica sand and granulated tire rubber independently on the performance of expansive soil, which was used in study, comprises of 25% of Wyoming sodium bentonite and 75% of clean silica sand with poor gradation. The result suggested that swelling strain was reduced with the content as the silica and granulated tire fiber increased. The decrease in swell strain was related to non-expansive characteristics of additives.

Marefat and Soltani-Jigheh (2010) investigated the effect of three different sizes, namely 1.28, 3.56, and 5.53 mm (average size), and percentages (10, 20, and 30%, by weight) of tire chips on strength properties of clay through consolidated undrained triaxial tests under a confining stresses of 100, 200, and 300 kPa. The result suggested that the addition of tire chips of 20-30% to the cohesive soil did not produce any significant effect on the shear strength of the soil. On the other

side, the frictional angle decreased due to the addition of more than 10% of tire chips. It was also observed that secant deformation modulus and excess pore water pressure of clay was decreased with tire chips content.

Trouzine et al. (2012) examined the effect of rubber fibers (average length of 7 mm) on consistency limit of clay of low- and high-plasticity and observed a reduction in the liquid limit with the increase in fiber content. They reported that the addition of rubber fiber beyond 10% led to the gradual rise in the plastic limit of both the soils. The result suggested that compressibility parameter of low and high plastic clay composite was increased with an increase in fiber content. They observed that swelling pressure and swelling potential were decreased continuously with increased tire fiber. Kim and Kang (2013) presented the idea of composite geomaterial (CGM) prepared with dredged clay, rubber particles, cement, and bottom ash and noted a decrease in MDD from 13.7 to 10.9 kN/m^3 and from 14.8 to 12.2 kN/m^3.

Asadzadeh and Ersizad (2013) studied the consolidation characteristic of low-plasticity clay combined with 10, 20, and 30% tire chips of 1.275 mm size and observed that as the tire chips content increased the compression index reduced and in swelling index increased. They also reported an increase in the cohesion and decrease in the internal frictional with the increase in the tire chips fraction.

Kalkan (2013) investigated the swelling pressure of clay altered with silica fume and rubber fibers. The experiments were run with the rubber fibers (5–10 mm length, 0.25–0.50 mm thickness, 0.25–1.25 mm width) varying from 1 to 4% in a step of 1% and silica fume varying from 10 to 20%. The result suggested that swelling pressure was decreased from 230 kPa to 33 and 17 kPa, respectively due to the addition of 10 and 20% of silica fume. They reported that hydraulic conductivity of the clay was reduced with silica fume and increased sharply with increased in

rubber fiber. They noticed that clay containing 20% silica fume showed a maximum rise in unconfined compressive strength. The calcium silicates hydrate gel formed by the reaction between active silica fume and Ca^{2+} and OH^- ions of clayey soils produced this improve in strength but the behavior of the composite was more in brittle tendency. The unconfined compressive strength of mixture improved more with the increase in the content of rubber fiber up to 2% but beyond 2% led to the drop in strength. The enhanced strengths were credited to skin friction developed between clay–silica fume mixture and surface of the fiber. Prasad et al. (2014) studied the influence of crumb rubber (425–600 μm) on the compaction parameters of two types of clayey soils and reported that MDD and OMC decreased for both types of clay with the addition of rubber fiber.

Srivastava et al. (2014) performed the impact of fine (passing 2.00 and 0.075 mm retaining)- and coarse (passing 4.75 and 2.00 mm retaining)-sized shredded tire on index properties of expansive soil. The result indicated that in both the cases with the percentage increase in shredded tire waste, the values of liquid limit and plastic limit decreased and it was happened due to the reduction in percentage clay content in the soil tire waste mix. It was noticed that the plasticity index of clay–the coarse-sized shredded tire was stated to remain constant up to 20% presence of coarse-sized shredded tires, but the plasticity index remains almost unchanged with a fine-sized shredded tire. They also observed that shrinkage limit increased and the shrinkage ratio values decreased with different percentage of shredded tire waste. Finally, they concluded that the addition of coarser category size shredded tire waste was more advantageous for controlling the shrinkage behavior of black cotton soils. They also reported that increasing the shredded tire fractions lead to a reduction in swelling pressure of the expansive soil. The result suggested that undrained cohesion value of clay soil was improved with the inclusion of 5% coarse sized shredded tire but beyond the 5% led to significant loss of undrained cohesion. They reported that 5.92, 42.68, and 44.66%

decreased in undrained cohesion value for expansive soil containing 10, 15, and 20% coarse-sized shredded tires, while a continuous reduction of 41.63, 62.66, 67.8, and 84.18% in undrained cohesion value with the addition of 5, 10, 15, and 20% fine-sized shredded tires were noticed. Sellaf et al. (2014) carried out the influence of rubber fibers (7 mm average length) on consistency limits of Fergoug dam sediment and Tizi Tuff of Algeria. Rubber fiber of 10, 20, 25, and 50% were selected for this investigation and they reported that liquid limit and plastic limit of both types of soil gradually reduced as the percentage of rubber fiber increased but susceptibility of rubber fibers was found to be less for Tizi Tuff soil in comparison to Fergoug dam sediments due to its low plasticity.

Dunham-Friel and Carraro (2014) Performed isotopically consolidated undrained triaxial and compaction test on expansive soil reinforced with waste glass and granulated rubber fiber. Test result reported that MDD of the composite decreased with the inclusion of rubber fiber, whereas, OMC was almost unchanged. They observed that MDD of the composite was decreased, whereas, OMC of the composite was decreased with the addition of waste glass. Triaxial test result suggested that peak and critical state friction angle were increased with granulated rubber fiber. With the inclusion of waste glass, peak frictional angle was reduced in comparison to unreinforced soil, but critical state frictional angle was improved significantly.

Cabalar et al. (2014) investigated the effect of tire buffing on clayey soil and observed a reduction of 26.3, 58.5, and 69.6% decrease in UCS value due to the addition of 5, 10 and 15% of tire buffings. Daud et al. (2015) examined the influence of shredded tires of 1–5 mm size on Atterberg limit of peat and clayey soil and noticed an increase in the liquid limit and plastic limit due to the inclusion of shredded tires up to 20% to the clayey soil. However, a decreasing trend in liquid limit and plastic limit was detected for peat soil.

Razali et al. (2015) investigated unconfined compressive strength on low-plasticity clayey silt mixed with 5% cement and mixed with fly ash and rubber chip in various fractions (5, 10, and 15%) separately in both unsoaked and soaked conditions. The result suggested that the cemented soil specimens with 15% fly ash and with 10% rubber chips showed maximum increment in unconfined compressive strength. The cement-stabilized clay treated with fly ash in comparison to rubber chips exhibited larger strain due to its stiffness. Xin et al. (2015) carried out isotropic compression, and consolidated undrained triaxial tests on 28-days cured specimens of clay containing a different composition of cement and reported a decrease in the pore pressure and increase in shear strength with the increase in the tire chips percentage in the mixture. Signes et al. (2016) investigated the impact of crumb rubber on the compressibility of the clayey soil and reported an increase in the swelling index due to the addition of crumb rubber, whereas, compression index remained unchanged. Ravichandran et al. (2016) studied the hydraulic conductivity of two clayey soils holding with 5, 10, 15, and 20% crumb rubber and reported that hydraulic conductivity of the clay soil increased with the fraction of crumb rubber due to the increase of flow channel in between soil-bentonite mixture.

Rahgozar and Saberian (2016) investigated the effect of shredded tire chips on unconfined compressive strength of peat soil added with 5, 10, 15, and 20% tire chips and observed a maximum unconfined compressive strength with the 10% tire chips. Similarly, the highest modulus of elasticity of 3.5 MPa was measured with the same fraction of tire chips. Tajdini et al. (2016) conducted unconsolidated undrained and drained triaxial test on kaolinite clay mixed with crumb rubber in the proportion of 5, 10 and 15% by dry weight and observed that peak shear stress of clayey soil with 10% crumb rubber was less in undrained loading as compared to drained loading.

Yadav and Tiwari (2017) reported a decrease in the swelling pressure and unconfined compression strength (UCS) of clay due to the inclusion of rubber fiber. Yadav and Tiwari (2018) studied the compaction and strength characteristics of clayey soil mixed with waste crumb rubber and cement for its sustainable use in the geotechnical application. Test result indicated that MDD and OMC were decreased with the inclusion of tire fiber. The unconfined compressive strength of the composite was increased up to 5% tire fiber and then decreased with further addition of tire fiber. Soltani et al. (2018) performed the oedometer and desiccation shrinkage on expansive soil reinforced with crumb rubber and reported that swelling tendency of the composite reduced with increased in crumb rubber. Desiccation–the induced crack was decreased with increased in crumb rubber. MDD of the composite was decreased significantly with crumb rubber.

Saberian et al. (2019) reported that the maximum dry density and unconfined compression strength were reduced with the addition of waste crumb rubber. They also observed that a decrease in the unsoaked CBR with the inclusion of waste crumb rubber. Soltani et al. (2019) studied the rubber's capacity to improve the swell–shrink potential of expansive clays and reported a reduction in the void ratio due to the inclusion of tire fiber.

A detailed summary of the literature has been presented in Table 2-2.

Table 2-2 Summary of the literature (soil tire fiber mix)

References	Type of tire fiber	Amount of fiber used as reinforcement	Soil type	Major findings
Al-Tabbaa et al. (1997); Al-Tabbaa and Aravinthan (1998)	Shredded tire	6% (1–4, 4–8, and 8–12 mm)	Kaolin and Natural over consolidated fissured clay	**1.** MDD decreased and OMC almost remained constant **2.** Swelling decreased (when water was permeant) and increased (when paraffin works were paraffin)
Cokca and Yilmaz (2004)	Rubber fiber	10% by weight	Bentonite and Fly ash	**1.** MDD decreased **2.** *k* increased **3.** UCS decreased **4.**Compressibility parameter not affected
Ozkul and Baykal (2006)	Tire buffings	10% (4–15 mm length)	Kaolin clay	**1.** MDD decreased **2.** Peak strength increased **3.** Failure strain increased
Cetin et al. (2006)	Fine-grained and Coarse-grained	10, 20, 30, 40, and 50%, by weight	Cohesive clay (CL)	**1.** MDD decreased for both **2.** OMC increased with fine-grained tire chips **3.** *k* decreased with coarse-grained and increased with fine grain **4.** *c'* increased up to 40% tire chips for both. **5.** ϕ' increased above the 40% tire chips for both.

References	Type of tire fiber	Amount of fiber used as reinforcement	Soil type	Major findings
Ozkul and Baykal (2007)	Tire buffings	10% (4–15 mm length)	Kaolin clay	**1.** *k* decreased during pre-shear and increased during post shear **2.** Shear strength increased upto confining pressure of 300 kPa
Mokhtar and Chan (2007)	Tire chips	5, 10, and 15% (2mm in size)	Inorganic silt of high compressibility	UCS increased up to 10% of fiber
Seda et al. (2007)	Tire Shreds	20% granulated rubber (<6.7mm)	Tire rubber	**1.** MDD reduced **2.** Swelling potential reduced **3.** Swelling pressure reduced
Patil et al. (2011)	Rubber fiber	0.2, and 0.36 (by volume of solid) 0.6–0.1 mm	Active clay	1.Swelling decreased
Marefat and Soltani Jigheh (2011)	Tire chips	10, 20, and 30%, by weight with 1.28,3.56 and 5.53 mm in size	Lean clay	1. c' value increased 2. Excess pore water increased
Sarvade and Shet (2012)	Tire crumb	5%, 10, 15. 20 and 25%	Good clay and Problem Clay	**1.** Plasticity index decreased **2**.UCS increased up to 5%
Trouzine et al. (2012)	Rubber fibers	10, 20, 25, and 50%, by weight	Active clay	**1.**Compression and recompression index increased **2.**Swelling reduced
Kim and Kang (2013)	Rubber particles	25,50,75,100% by weight (0.1–2 mm)	Clay (CL)	1.MDD decreased 2.UCS decreased
Kalkan (2013)	Rubber fiber	Rubber fibers (1, 2, 3, and 4%, by weight)	Clay (LL=72%)	**1.** Swelling reduced **2.**UCS increased up to 2% of fiber **3.** *k* value increased

Reference	Type of fiber	Amount of fiber used as reinforcement	Soil type	Major findings
Asadzadeh and Ersizad (2013)	Tire chips	10, 20 and 30%	low-plasticity clay	**1.** Compression Increased **2.** Swelling index increased
Srivastava et al. (2014)	Fine-sized & shredded tires	5, 10, 15, and 20%, by weight (passing 4.75–2.00 mm retaining)	Expansive soil	**1.** UCS increased up to 5% **2.** MDD decreased **3.** Swelling decreased **4.** *k* value increased
Cabalar et al. (2014)	Tire buffings	5, 10, and 15%	Clay (LL=49.5)	**1.**Swelling decreased 2.MDD decreased 3.UCS decreased
Prasad et al. (2014)	Crumb rubber	0 to 20% in a step of 5% (425–600 µm)	Soil-1(LL=74%) and Soil-2 (LL=56%)	**1.** MDD decreased **2.**UCS increased up to 15% tire crumb
Sellaf et al. (2014)	Tire rubber	0 to 50%	Soil-A(LL=38%) and Soil-B (LL=28%)	**1.** LL decreased **2.** ϕ value decreased 3.c value increased
Dunham-Friel and Carraro (2014)	Granulated rubber	20% by weight	Expansive soil	**1.**MDD decreased **2.**ϕ_p' and ϕ_{cs} increased
Ramirez et al. (2015)	Granular rubber	5, 10, and 20% granular rubber (0.2 and 2.0mm)	Clay soil (LL=53%)	**1.**MDD decreased **2.** Shear strength increased **3.**Composite suggested for the landfill
Razali et al. (2015)	Rubber chips	5, 10, and 15% by weight	Soil (LL=26.70)	**1.** UCS increased up to 5% fiber inclusion
Daud et al. (2015)	Shredded tire	10, 20, and 30%, by weight	Peat (MH)	**1.** MDD decreased **2.** c' value increased **3.** ϕ value decreased

References	Type of fiber	Amount of fiber used as reinforcement	Soil type	Major findings
Xin et al. (2015)	Tire chips	0–120% by weight	Clay	**1.** Shear strength improved
Signes et al. (2016)	Crumb rubber	0, 2.5, 5, 10, 15, 20, and 25%, by weight	Clay (LL=52.2%)	**1.**Compression index not affected but swelling index increased 2.Swelling reduced
Saberian and Rahgozar (2016)	Tire chips	5%, 10, 15 and 20% tire chips (by dry weight)	Peat soil	**1.**UCS increased **2.** Shear strength improved
Tajdini et al. (2016)	Tire crumb	5%,10, 15 and 20%	Kaolinite	**1.** Shear strength improved **2.** Undrained strength less in comparison to drained strength
Yadav and Tiwari (2017)	Tire crumb	2.5, 5, 7.5, and 10%, by weight	Expansive soil	**1.** MDD reduced **2.** OMC reduced **3.**Swelling reduced
Yadav and Tiwari (2018)	Tire crumb	2.5, 5, 7.5, and 10%, by weight	Expansive soil	**1.**UCS increased up to 5% tire crumb **2.** Swelling pressure reduced **3.** Compression index reduced
Soltani et al.(2018)	Rubber powder	10%,20 and 30%	Expansive soil	**1.** Desiccation crack reduced **2.**Swelling reduced **3.**MDD reduced

References	Type of fiber	Amount of fiber used as reinforcement	Soil type	Major findings
Saberian et al.(2019a)	Crumb rubber	1% by dry mass	Unbound granular waste Aggregates (LL=30%)	1. Ductility increased 2.MDD reduced 3.Unsoked CBR increased
Soltani et al.(2019b)	Tire Rubbers	10% by mass	Expansive soil	1. Shrinkage and swelling potential reduced 2. Void ratio-water content curve reduced with tire rubber

LL=liquid limit, MDD=maximum dry density, OMC=Optimum moisture content, UCS=Unconfined compressive strength, CBR=California bearing ratio

2.6 A previous study on glass fiber

Glass fibers are the most common of all the reinforcing fibers for polymer matrix composites. The principal advantages of glass fibers are the low cost, high strength, hardness, resistance to chemical attack, stability, and stiffness (Wallenberger 2000). Glass fibers are amorphous solids and chemically composed primarily of a silica (SiO_2) backbone in the form of $(-SiO_4-)_n$ tetrahedra. Modifier ions are added for their contribution to glass properties and manufacturing capability. For structural composites, the two commonly used types of glass fiber are general-purpose fibers and premium special purpose. These fibers are known by the designation E-glass (Table 2-3) and are subject to ASTM specifications (D578-98). The remaining glass fibers are premium special-purpose products. Many, like E-glass, have letter designations implying special properties (Gupta 1988). Some have trade names, but not all are subject to ASTM specifications. Specifically:

Table 2-3 Type of glass fiber based on Wallenberger (2000)

Letter designation	Property or characteristics
E, electrical	Low electrical conductivity
S, strength	High strength
C, chemical	High chemical durability
M, modulus	High stiffness
A, alkali	High alkali or Soda lime glass
D, dielectric	Low dielectric constant

Agarwal et al. (2006) described that two forms of fiberglass can be produced-continuous fiber and staple (discontinuous) fiber. Both forms are made by the same production method up to the fiber-drawing stage. Ingredients such as sand, limestone, and alumina are dry-mixed and melted in a refractory furnace. The temperature of the melt varies for each glass composition but generally is about 1260°C. The molten glass flows directly into the fiber-drawing furnace in the direct-melt process or flows into a marble-making machine in the (Marble process). The marbles are subsequently remelted and drawn into fibers. Most fiber glasses are currently produced by the direct-melt process, illustrated schematically in

Fig.2.8. Continuous fibers are produced by introducing molten glass into a platinum bushing, where the molten glass is gravity-fed through a multiplicity of holes in the base of the bushing. The molten glass exits from each orifice and is gathered together and attenuated mechanically to the proper dimensions, passed through a light water spray (quench), and then traversed over a belt that applie's a protective and lubricating binder or size to the individual fibers. These fibers then are gathered together into a bundle of fibers called a strand or end. The fiberglass strand, typically consisting of 204 filaments, is then wound onto a receiving package (spool) at speeds of up to 50 mis. This "cake" is then conditioned or dried prior to further processing into other textile forms.

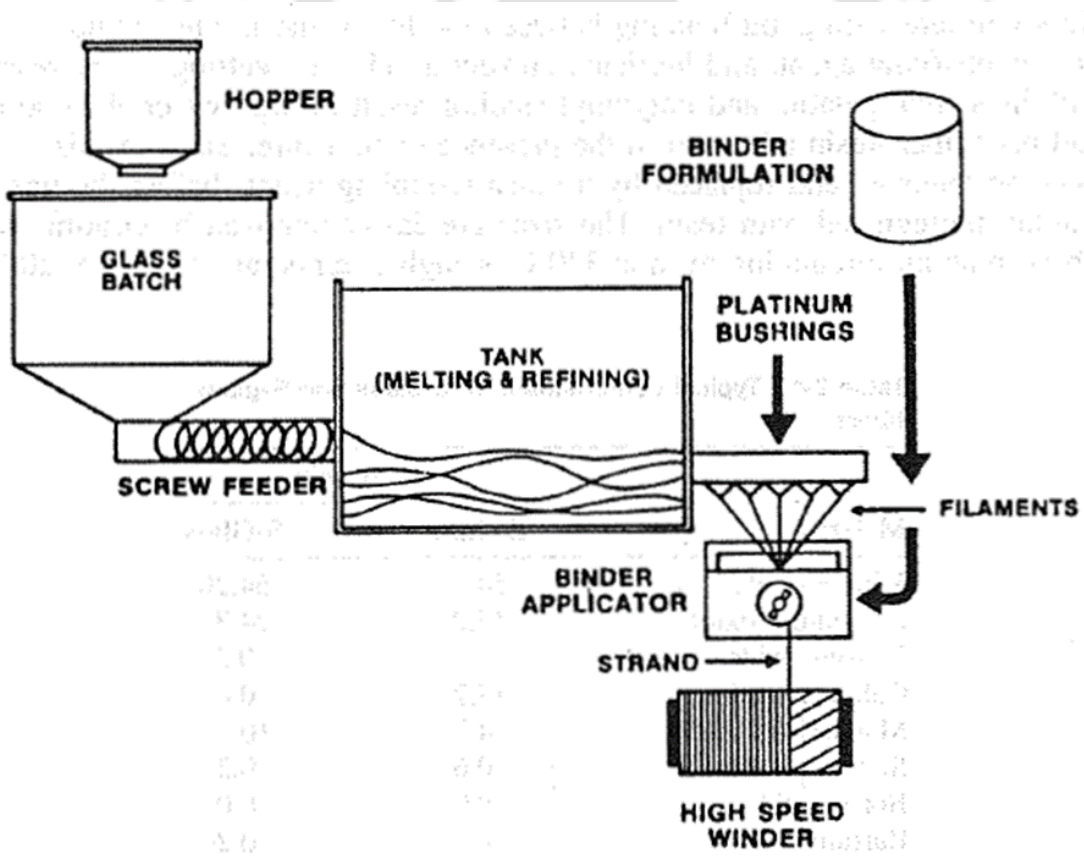

Figure 2.8 Glass-fiber production process (Agarwal et al. 2006)

2.6.1 Glass fiber recycling from waste glass:

The key incentive of using recycled glass fibers geomaterial stems from the fact that glass fibers are justifiable and also their unique property which is non-biodegradable in nature, thus providing their long

life span. The amount of glass waste disposed as mixed municipal solid waste (MSW). Most of this MSW would be in the form of broken glasses and bottles and broken glass sheets and windowpanes. Therefore, this arises serious environmental problems due to this kind of wastes are usually non-biodegradable and very bulky (López et al.2012). Ahmad (2012) stated that sustainable material derived from waste glass such as the recycled glass fibers (Fig.2.9 a and b) is desired from an environmental perspective because they are lightweight while having the ability to maintain internal stable structure, thus explaining their ability to withstand higher loading as compared to conventional steel reinforcements. These characteristics enable them to become practical solution to ground improvement technology especially in soft soil condition where low bearing capacity and long-term performance of the reinforcements are expected.

2.6.2 Influence of glass fiber on the geotechnical properties

Gray and Al-Refeai (1986) carried out triaxial compression tests to compare the stress-strain response of a dry sand reinforced with randomly distributed discrete fiber as opposed to continuous, oriented fabric layers. Natural reed fiber and glass fiber were considered for this study. The presence of fiber up to 2% by dry weight of soil was found to enhance the strength of the sand, expressed as the major principal stress at failure. The strength improvement was related to the fiber aspect ratio, and the fiber roughness was more effective than the stiffness property in increasing strength. Fiber-reinforced sand failed along a classic planar shear plane, whereas fabric-reinforced sand failed by bulging between layers. The existence of critical confining stress was common to both types of reinforcement.

Maher and Gray (1990) performed triaxial compression tests to determine the static stress-strain response of dry sands reinforced with discrete, randomly distributed fiber (rubber fiber, natural fiber and glass fiber), and noticed the influence of various fiber properties, soil properties, and test variables. The increase of stiffness and ultimate strength due to the fiber inclusions was found to be a function of sand granulometry (gradation, particle size and shape) and fiber properties (weight fraction, aspect ratio

and modulus). The reinforced sands had either a curved linear or a bilinear failure envelope, with the break occurring at critical confining stress. In addition to the experimental program, a model was developed, based on statistical theory of strength for composites, to predict the fiber contribution to strength under static loads. The predicted strength increases from fiber reinforcement using the theoretical model agreed reasonably well with measured values.

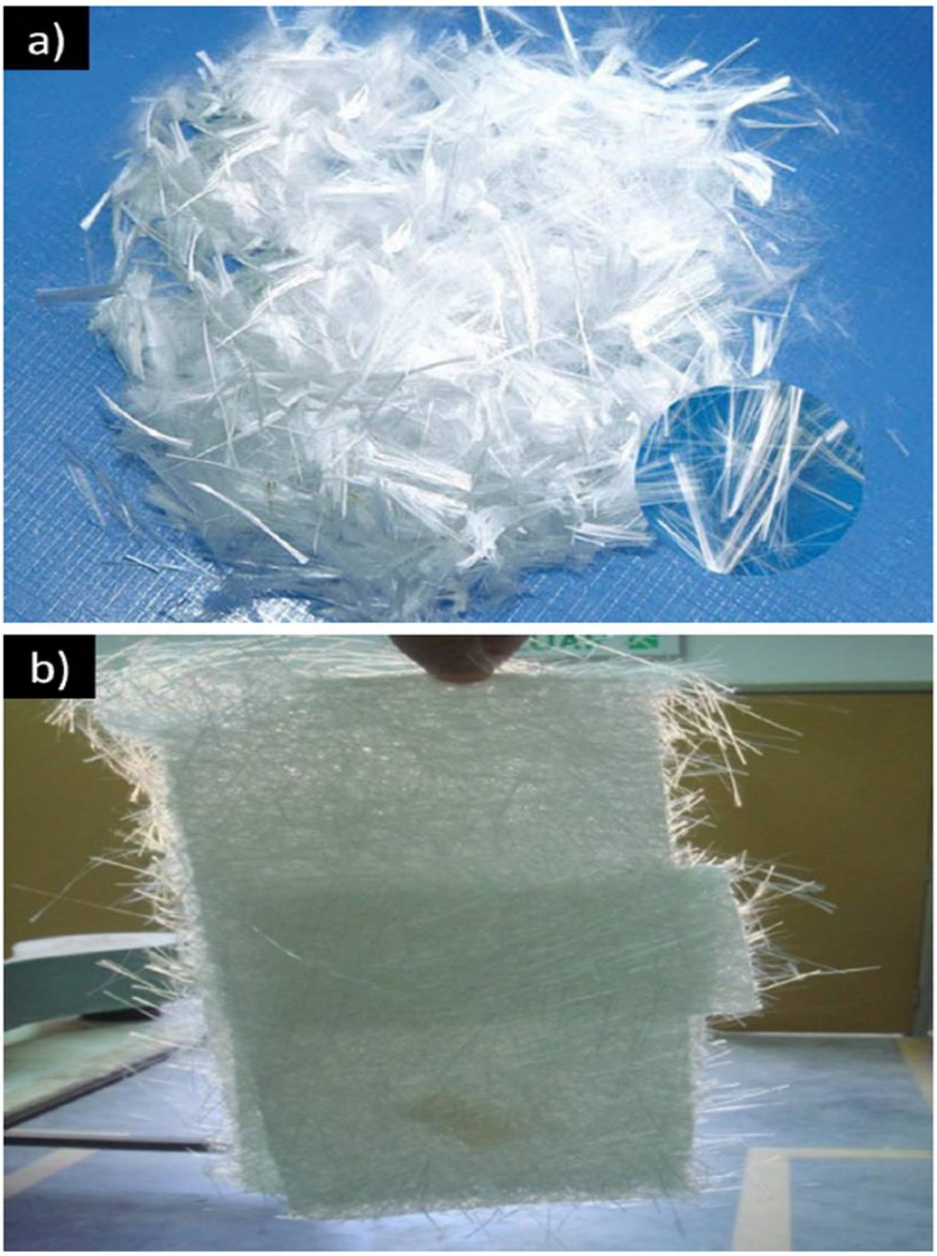

Figure 2.9 Polymeric fiber strands (a); recycled glass fiber sheet (b) (Mujah et al. 2013)

Al-Refeai (1991) conducted triaxial tests on fine sand with subrounded particles and medium sand with subangular particles reinforced with glass fibers. Three different fiber concentration (i.e. 0.5%, 1 and 2%, by weight) and five aspect ratio (i.e. 10, 25, 50,75 100) was used for this study. The results showed that; (1) load capacity of the sand was improved by fiber inclusion; (2) shorter fibers required a great confining stress to stop bond failure irrespective of size or shape of sand particles;(3) soil-inclusion friction interaction related mainly on the extensibility of the inclusion rather than the mechanical properties of the sand; (4) fine sand with subrounded particles showed a more favorable response to fiber reinforcement than medium sand with subangular particles; (5) the percentage increases in principal stress and secant modulus from the inclusion of glass fibers are directly proportional to fiber length, for a constant fiber concentration and short fiber inclusion decreased the stiffness of medium sand. From a series of unconfined-compression tests on kaolinite-glass fiber composite, Maher and Ho (1994) observed that the peak compressive strength and ductility of the composite increases with the fiber concentration. They also noticed a reduction in the peak compressive strength and decrease in energy absorption capacity with an increase in fiber length. They also observed that hydraulic conductivity of the composite increases with the increase in the fiber concentration and length.

Rodatz and Oltmanns (1997) performed direct shear, hydraulic conductivity, and unconsolidated undrained triaxial test on plastic clay reinforced with glass fiber. The result showed that the compressive strength increases about two to three-fold due to the inclusion of short fiber. The mechanical property of the fiber-reinforced specimen was improved significantly; whereas, the hydraulic conductivity decreased in comparison to the unreinforced specimens. They observed that cracks were developed in the shear zone when the specimen was sheared up to 15% strain.

Consoli et al. (1998) performed the triaxial test to assess the effect due to the inclusion of randomly distributed fiber and cement. Test results showed that the addition of cement to soil enhances stiffness,

brittleness, and peak strength. The fiber reinforcement improved both the peak and residual triaxial strength, decreased the stiffness, and changed the cemented soil's brittle behavior to a more ductile one. The peak strength increased due to fiber inclusion and was more effective for uncemented soil. However, the increase in residual strength was more fruitful when fiber was added to cemented soil. Due to the fiber reinforcement, the friction angle was increased from 35° to 46°, whereas, the residual angle increased from 34˚ to 43˚.

Gosavi et al. (2004) performed the compaction test on black cotton soil reinforced with glass fiber and observed an increase in the OMC. However, the MDD was decreased due to the inclusion of glass fiber up to 2% fiber content and then increased with a further increase in fiber content. Casagrande et al. (2006) performed ring shear test on bentonite reinforced with polypropylene fiber under the normal stress of 20 and 400 kPa. The result suggested that peak strength increases with an increase in fiber content and fiber length. However, they noticed that residual strength was not improved with the addition of fiber.

Abdi et al. (2008) performed the oedometer and volumetric shrinkage test to determine the shrinkage, swelling, and settlement behavior of the kaolinite and montmorillonite mixed in a proportion of 75:25. It was observed that the swelling tendency was decreased with an increase in the fiber content. The shrinkage test result suggested that shrinkage limit increases from 21to 33% by the inclusion of glass fiber and the fiber-reinforced specimen experienced less volumetric changes due to desiccation. The hydraulic conductivity increased 2.5 times with fiber concentration and different length of the fiber.

Consoli et al. (2009) carried out a drained triaxial test to determine the effects of three different randomly distributed fiber (polyester, polypropylene and glass fiber) and rapid hardening Portland cement on the engineering behavior of uniform fine sand. For this study, 0.5% fiber concentration (by weight) of 36 mm fiber length was used. Different initial mean effective stress (i.e. 20, 60 and 100

kN/m^2) and cement content (from 0% to 7% by weight) were used to improve the engineering behavior of soil. The result suggested that the ultimate frictional angle of cemented sand was increased significantly. No impact of glass fiber on ultimate cohesion was observed; whereas, both friction angle and cohesion intercept were increased with the inclusion of polypropylene fiber.

Benessalah et al. (2015) investigated the effect of glass-fibers content of medium and high density on the shear strength behavior of Chlef sandy soil. Test result suggested that the mechanical characteristics were increased in the presence of glass-fibers, especially for wet specimens. The test concluded that 0.3% of fiber content is a critical value for fiber contribution to improve the mechanical characteristics. The addition of fibers not only increased the shear strength of soil but also offer diversity in the resistance against the deformations under the imposed load, which could be established by a reduction in the soil dilatancy noticed by a minimization of the vertical displacement. For the dry case, the reinforcement with fiber had a negative effect on the residual strength especially for average dense samples, which might be explained probably by the low specific weight of geosynthetics materials.

Baruah (2015) performed the compaction and unconfined compression test on red soil reinforced with glass fiber and reported an increase in the OMC and decrease in the MDD with the increase in the concentration of the glass fiber. They also noticed that the mechanical behavior of the composite was improved significantly with the inclusion of fiber. Kalita et al. (2016) performed the unconfined compression test to study the stress-strain behavior of red soil reinforced with different type of fiber (glass, coir and waste cement bag fiber) and reported that all the three types of reinforcement had effectively led to an increase in UCS of the soil with increase in the fiber content. Ateş (2016) performed the direct shear and unconfined compression test on sand-glass-Portland cement composite to investigate the stress-strain performance of the composite specimen. The result showed a significant increase in strength of the specimens containing 1, 2, 3 and 4% glass fiber. Additions of 2% and 3% of

glass fiber and 5, 10, 15 and 20% of cement increased the strength from 1787 to 2467 kPa. The maximum compressive strength was achieved at the rate of 4% glass fiber and 20% cement content. From the direct shear test, normal stress and shear stress were affected by the inclusion of glass fiber. Test result suggested that internal frictional angle was increased with the inclusion of glass fiber, whereas, cohesion component was increased with the addition of cement.

Patel and Singh (2017) conducted drained triaxial test to determine the impact of glass fiber on shear strength behavior of sand. They reported that the effect of fiber reinforcement was significant at higher strain level and the peak stress increased with fiber content up to 3% for 10 mm fiber and up to 4% for 20 and 30 mm fiber. The deviator stress of reinforced specimens further increased with either increasing relative density or confining pressure keeping the other constant. The inclusion of fibers within sand inhibited the dilatancy and the dilation of specimen decreased either with increasing fiber content or fiber length or confining pressure and increased with increasing relative density.

Patel and Singh (2018) performed a consolidated undrained triaxial test to investigate the effect of glass fiber on shear strength properties of red soil. The result suggested that deviatoric stress at failure was increased only up to limiting magnitudes of fiber content or fiber length at any molding dry unit weight and confining pressure. Positive pore water pressure was found to increase with fiber content and different fiber length for any range of confining stress for the same dry unit weight. Maximum reduction of pore water pressure was observed with 30 mm length of the glass fiber and maximum positive pore water pressure was noticed with 20 mm glass fiber under confining pressure of 100 kPa at 0.75% fiber concentration, while dry density of the composite was 16.8kN/m^3. Maximum cohesion component was obtained around 67 kPa with 30 mm long glass fiber at 0.75% fiber concentration while dry density was 16.8 kPa. Remaining the same configuration, maximum effective internal friction angle was achieved around 35.2°. Detailed of the literature study has been summarized in Table 2-4.

Table 2-4 Summary of the earlier study (Glass fiber)

Reference	Fiber type	Amount of fiber used as reinforcement	Soil type	Major findings
Gray and Ohashi (1983)	Natural and synthetic fibers (including glass fiber)	0.21, 0.5, 1 and 2%, by weight	Dry sand	**1.**Shear strength improved **2.** Internal friction unaffected with fiber inclusion
Gray and Al-Refeai (1986)	Glass	0.21, 0.5, 1 and 2%, (by weight) glass with 13, 25 and 38 mm	Dry sand	**1.**Sheat strength increased
Maher and Gray (1990)	Glass	Different aspect ratio (60, 80 and 125) of glass fiber (3% by weight)	Saturated-Sand	**1.** Shear strength increased **2.**Stress-strain response increased **3.**Principal stress at
Al-Refeai (1991)	Glass	0.5%, 1 and 2%, (by weight) with five aspect ratio (i.e. 10, 25, 50, 75 100)	Dry Sand	**1.**Shear strength increased **2.**Load-deformation behavior improved 3.Interaction between
Maher and Ho (1994)	Glass	Glass fiber (0.5% to 4% fiber concentration (by weight), with 6.4 mm to 25.4 mm in length	Kaolinite clay	**1.**UCS increased **2.***k* value increased **3.**EAC increased

Reference	Fiber type	Amount of fiber used as reinforcement	Soil type	Major findings
Rodatz and Oltmanns (1997)	Glass	0-5%, 1, 1-5, 2 and 3% (by mass of dry soil)	Clay (CH), loam (CL/ML) and sand	**1.** *k* value reduced **2.** Shear strength increased
Consoli et al. (1998)	Glass	1% fiber by dry weight	Sand cement mixture	**1.** Large improvement of stress-strain **2.** Peak strength increased **3.** Residual strength
Gosavi et al. (2004)	Glass	3% glass fiber	Black cotton soil	**1.** MDD decreased but OMC increased up to 2%
Casagrande et al. (2006)	Polypropylene fiber	3% by dry weight	Bentonite	**1**.Residual strength unaffected **2**. Peak strength improved
Abdi et al. (2008)	Glass	Glass fiber with 1, 2, 4 and 8%, (by weight) concentration as well as 5, 10 and 15mm in	Kaolinite (i.e.75%) montmorillonite (i.e.25%)	**1.** *k* value increased **2.** Settlement reduced **3.** Shrinkage reduced **4.** Swelling reduced
Consoli et al. (2009)	Glass	(0.01% and 0.1%) Polyester and glass fibers respectively	Saturated sand	**1.** Failure plane was well-defined **2.** Material behavior improved
Benessalah et al.(2015)	Glass	0.1, 0.3 and 0.5% as a fiber volumetric content	Chlef sandy soil	**1**. Shear strength increased upto 0.3% of the fiber

Reference	Fiber type	Amount of fiber used as reinforcement	Soil type	Major findings
Baruah. H (2015)	Glass	0.5,1 and 1.5% glass fiber	Red soil	**1**. MDD decreased and OMC increased **2**. UCS increased
Ateş (2016)	Glass	Sandy soils with cement ratios (5, 10, 15 and 20% by weight of dry sandy soil)	Glass fiber ratios (1, 2, 3 and 4% by weight)	**1.** OMC increased upto 3% of the glass fiber **2.** UCS increased **3.** Shear strength increased
Patel and Singh (2017)	Glass	0 to 1% by weight	Saturated red soil	**1**. UCS increased **2**. EAC increased **3**. Mode of failure changed
Patel and Singh (2018)	Glass	0 to 1% by weight	Saturated red soil	**1**. MDD and OMC unaffected **2**. EPP increased fiber content, fiber length and confining pressure **3**. Shear strength enhanced

LL=liquid limit, MDD=maximum dry density, OMC=Optimum moisture content, UCS=Unconfined compressive strength, CBR=California bearing ratio

2.7 Critical review of the literature

A mixture of sand-bentonite is commonly used as a landfill material at the waste disposal site. At low stress, desiccation-induced moisture variations may cause a reduction in the plastic deformability and shrinkage cracking of bentonite, which can increase the uncontrolled migration of leachates. In addition, landfill barriers may be subjected to loading from waste material and multilayer capping. This overburden pressure gradually increases up to the end of the closure cap. Throughout this process, soft compressible soil is subjected to excessive stress under high overburden pressure. Under this circumstance, soft compressible soil undergoes high plastic strain; resulting in a differential settlement which may cause a migration of leachate into the surrounding soil/groundwater system. Due to this, the effective purpose of the liner system may be threatened. Low hydraulic conductivity liners are required in many containment applications. Geosynthetic liners can be used in a range of situations, including on steep side slopes, where the use of mineral liners can be problematic. Continuous reinforcements may not be a viable option in low hydraulic barrier layers as they could provide a preferential flow path for the migration of fluids and gasses (Fowmeset al 2006).

Waste materials continue to be a major environmental concern for all around the world. Fibers derived from these waste material, such as glass and tire, can be used as a reinforcing material at the waste disposal site to reduce the desiccation shrinkage. However, the addition of fibers to the landfill material may adversely affect its hydraulic-mechanical behavior. From the earlier study, several investigators reported a change in the MDD and OMC of non-active clay with the addition of tire fiber. Moreover, a study on bentonite added with tire fiber was very limited. It was also observed that waste tire chips controlled swelling pressure and most of the research had been focused on expansive soil. It was noticed that hydraulic conductivity was increased with tire fiber

but some researchers were also reported that hydraulic conductivity decreases with tire fiber. It has come to know that the inclusion of tire enhanced the unconfined compressive strength of clay but some study showed that unconfined compression strength of expansive clay dropped with the addition of tire fiber. It has been found that the inclusion of waste tire fiber increased the shear strength but some researcher obtained the decrease in shear strength with waste tire fiber. Very limited study was found with non-active clay mixed with tire fiber. However, no studies have been performed to investigate the impact of tire fiber on sand-bentonite mixtures, which is generally used a landfill material.

A review of the literature on the inclusion of the glass fiber indicated that the MDD of the soil does not gets affected, whereas, some researchers reported a definite effect on MDD of the soil. Similarly, some researchers reported an increase in the hydraulic conductivity, whereas, some researchers found a reduction in the hydraulic conductivity due to the inclusion of glass fiber.The shear strength behavior of sandy soil reinforced with fiber was studied well, but no study was observed on active clay with glass fiber.

The literature reviews concluded that there is some inconsistency in the hydro-mechanical behavior of soil in the presence of fiber. Furthermore, no literature has been found in the study the impact of glass fiber on the behavior of sand-bentonite mixture. Since, compacted sand-bentonite mixtures can be threatened material inconsistency, low shear strength, and excessive settlement because of tensile cracks developed due to environmental factors. Therefore, a composite material, that is, sand-bentonite reinforced with waste fiber, might be beneficial for designing compacted layers that will be more suitable and a sustainable solution for the purpose of environmental assessment.

2.8 Objective and Scope of the present study

A review of the literature suggests that the studies on the hydro-mechanical response of compacted sand-bentonite-fiber soil composite are relatively scanty. The broad objective of the present study is to evaluate the impact of the inclusion of waste fiber on the hydro-mechanical behavior of the compacted sand–bentonite (SB) mixture mixed in the proportion of 90:10; 80:20 and 70:30.

To achieve this objective, the detailed scopes of the present study are:

1. To investigate the effect of fiber (i.e. tire and glass individually) on the compaction characteristics sand-bentonite (SB) mixtures added in different proportions;

2. To analyze the effect of fiber (i.e. tire and glass individually) on the swelling, hydraulic and consolidation characteristic of the sand-bentonite mixtures;

3. To study the impact of fiber (i.e. tire and glass separately) on stress-strain response, excess pore water pressure, effective shear strength parameter, failure modes, and energy absorption capacity of the various sand-bentonite mixtures;

4. To analyze the effect of fiber (i.e. tire and glass separately) on the shrinkage of the various sand-bentonite mixture

CHAPTER 3
MATERIAL AND METHODS

3.1 Introduction

The details of the different materials and the testing procedure have been discussed and presented in this chapter. Planning of experiments, preparation of samples, and details of test procedures are presented and discussed.

3.2 Materials

Description of individual material has been shown below.

3.2.1 Bentonite

Bentonite used in this study was procured from the Rajasthan state of India and was in powdered form. The soil was light brown in color of smooth texture. The soil was mixed thoroughly and sieved through 425 micron sieves and stored in a drum for testing. The clay content of the bentonite was determined according to ASTM D422 (2002). The specific surface area (SSA) of the bentonite was determined as suggested by Cerato and Lutenegger (2002). Atterberg limits were determined according to ASTM D4318 (2000). Properties of bentonite has been shown in Table 3-1.

Table 3-1 Basic properties of bentonite clay

Bentonite clay	Values
Liquid limit (%)	286
Plastic limit (%)	44
Shrinkage limit (%)	24
Clay content (%)	46.6
Specific surface area (m^2/g)	347
Specific gravity	2.76
USCS classification	CH

3.2.2 Sand

Air-dried Brahmaputra river sand passing through 2 mm sieve was used for this study. Particle-size distribution of sand was determined per ASTM, D422-63 (ASTM 2002). The properties of sand have been listed in Table 3-2.

Table 3-2 Basic Properties of sand

Sand	Values
D_{60} (mm)	0.5
D_{30} (mm)	0.29
D_{10} (mm)	0.17
Coefficient of uniformity(Cu)	2.94<6
Coefficient of curvature (C_c)	0.98<1 to 3
Specific gravity	2.68
Classification of sand (USCS)	SP

3.2.3 Tire fiber

Shredded waste tire fiber passing through 4.75 mm and retained on 2 mm sieve (Fig.3.1a) were considered for the current study. The water absorption capacity of the tire fiber was determined as per as ASTM D6270 (1998) and found out to be 3.78%. The specific gravity of the tire fiber was determined to be 1.14. Field Emission scanning electron microscope (FESEM) and Energy-dispersive X-ray spectroscopy (EDX) was performed to understand the surface texture and elemental composition of the tire fiber. The surface of single tire fiber has been presented in Fig.3.1 (b) to show an optical appreciation of the surface texture of the tire fiber. The figures showed that the surface of the tire fiber was irregular and rough. Due to the rough surface the tire fibers are attached to the soil and their tensile strength mobilized to create the tire fiber-soil composite ductile. Due to this rough surface, the surface area of the fiber is to produce a larger interaction between tire and soil (Baykal 2007).

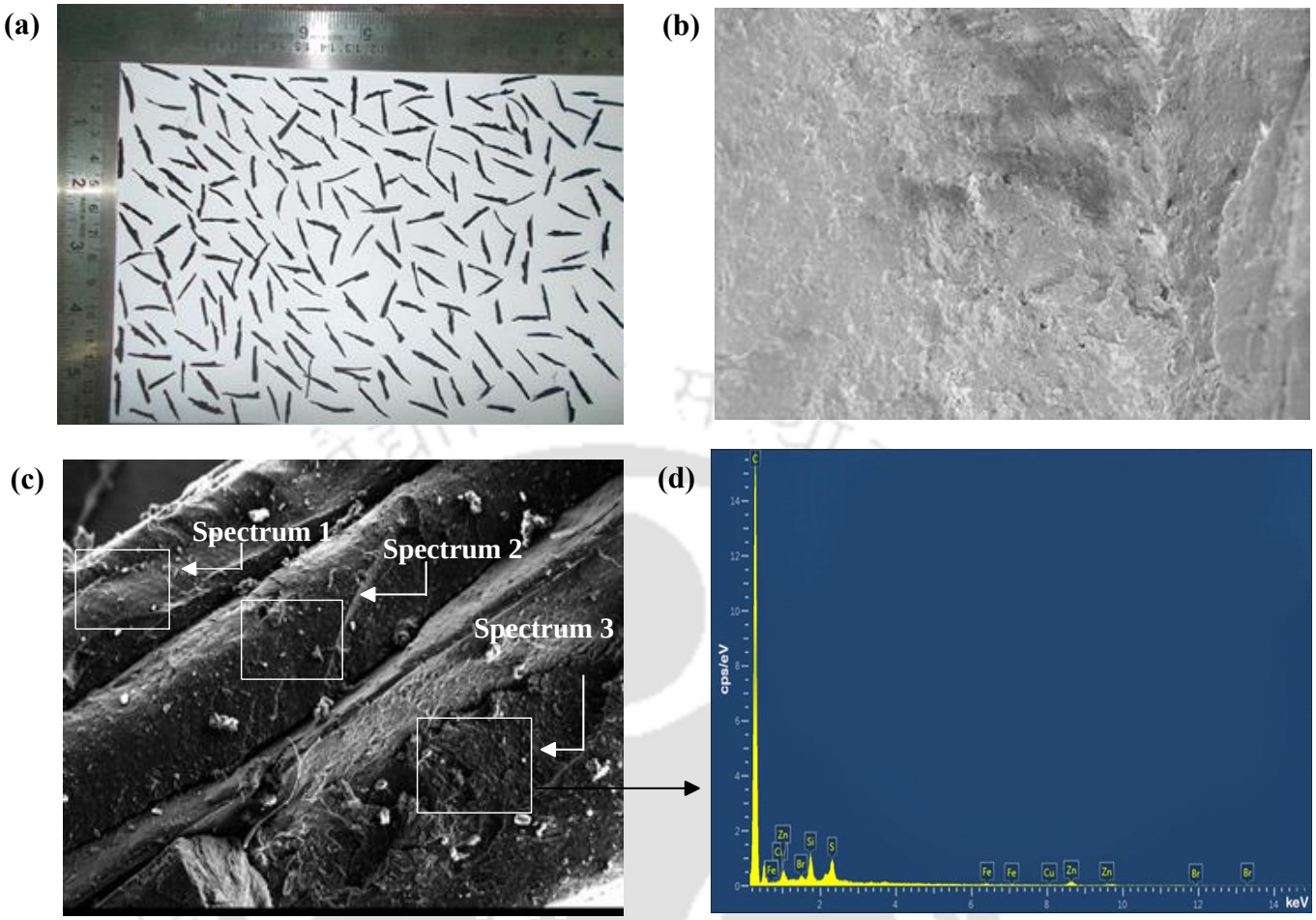

Figure 3.1 Tire fiber (a) passing through 4.75 mm and retained on 2 mm, used in this study; (b) surface of single tire fiber at 500 times magnification by field emission scanning electron microscope (FESEM); (c) EDX image of tire fiber;(d) EDX spectrum for waste tire fiber

3.2.4 Glass Fiber

Glass fiber mat was purchased from the West Bengal state of India. The glass fiber strands of average diameter (*d*) of 0.15 mm were extracted from glass fiber mat and then cut into three different lengths (*l* = 0.6, 1.2 and 1.8 cm) to produce an aspect ratio (i.e. *l*/d) of 40, 80 and 120. The surface texture of fasciculus type and single of glass fiber have been shown in Fig.3.2 (a and b) via FESEM. The specific gravity of the glass fiber determined as per as ASTM D792 (2013) and found out to be 2.59. The tensile properties of the yarn were determined by the single-strand

method as per the ASTM D2256 (2015) and the ultimate tensile strength and elongation at break of the fiber were found to be 1.51 GN/m^2 and 1.78%, respectively. The modulus of elasticity of the glass yarn was determined using the tangent method as suggested in the ASTM-D2256 (2015) and was found to be 112 GN/m^2. Water absorption capability of the glass fiber was found out to be zero.

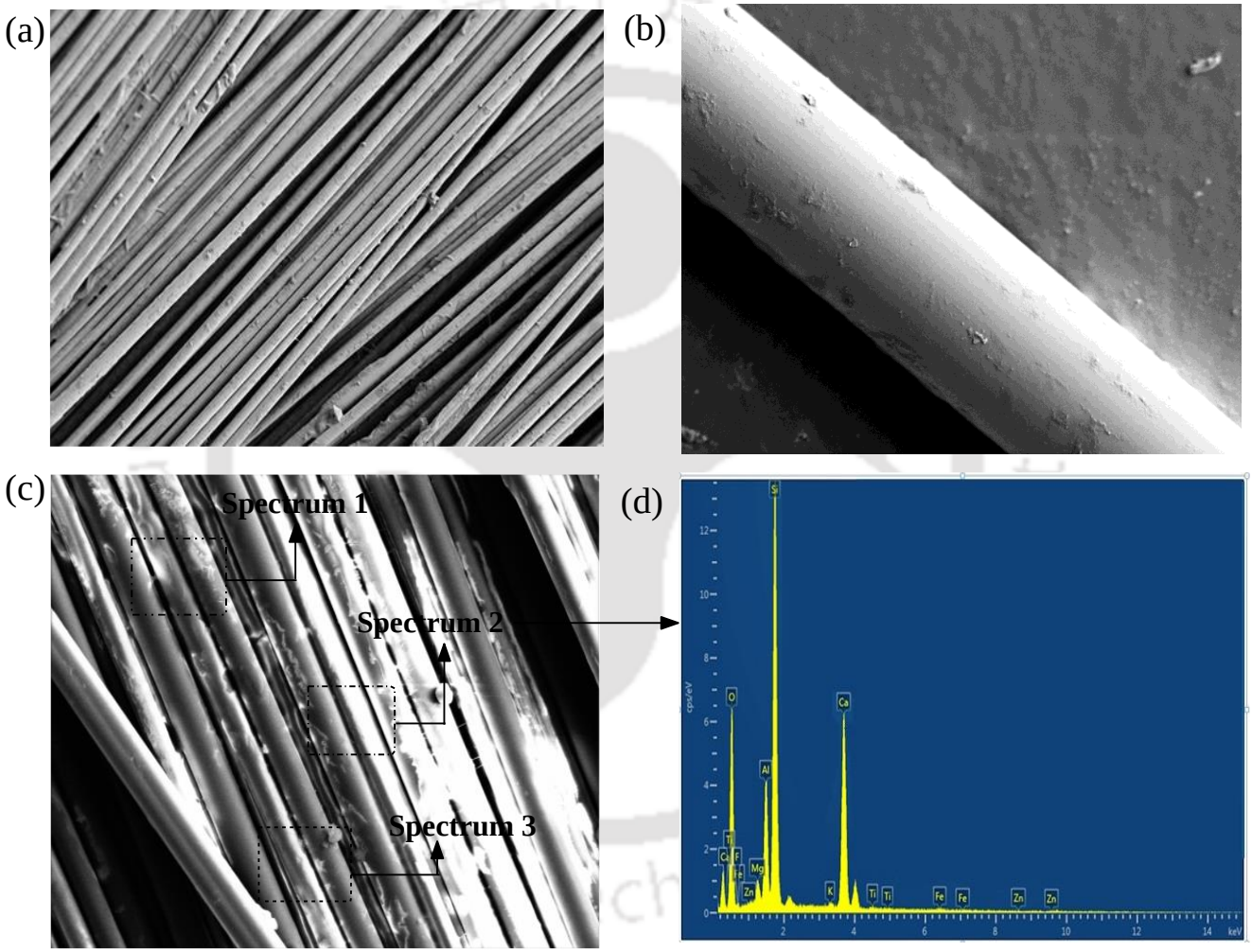

Figure 3.2 (a) Fasciculus type glass fiber used in this study from FESEM study under 300 times magnifications;(b) Surface texture of single glass fiber from FESEM study under 700 times magnifications (c) EDX image of fasciculus type glass fiber (d) EDX spectrum for glass fiber

3.3 Preparation of sand-bentonite tire fiber composite

Sand-bentonite mixture mixed in a proportion of 90:10 (SB10), 80:20 (SB20) and 70:30 (SB30) by their dry weight and reinforced with 5, 10 and 15 % of tire fiber has been used for this investigation. The tire fiber dosage was chosen based on the research conducted by other researchers (Ho et al.2010; Dunham-Friel and Carraro 2011; Tajdini et al. 2016). Tire fibers contain a compound combination of elastomers, polyisoprene, polybutadiene, and styrene-butadiene (Trouzine et al. 2012). The tire fiber used in this study is the by-product of the tire retread process and can be easily used as a waste reinforcement material.

Oven-dried bentonite and sand were mixed in a proposition of 10:90, 20:80 and 30:70 to prepare SB10 SB20 and SB30 mixtures, respectively. Then tire fibers in a proposition of 5, 10, and 15% of the total dry weight of the sample were added to the SB10, SB20, and SB30 mixtures. Since the tire fiber tangles together; considerable attention was given to develop a uniform distribution of the tire fiber in the mixtures. After that, samples were prepared by adding different amount of deionized (DI) water to the sand-bentonite–fiber mixtures and then kept for a period of 24 hours inside a humidity-controlled desiccator for moisture equilibrium (Booth 1976; Estabragh et al. 2015). After the moisture equilibrium, the maximum dry density (MDD) and optimum moisture content (OMC) of the mixture were determined using a standard Proctor test according to ASTM D698 (2012). Sand bentonite-tire fiber composite has been shown in Fig.3.3.

3.4 Preparation of sand-bentonite-glass fiber composite

Sand-bentonite mixture mixed in a proportion of 90:10, 80:20 and 70:30 to prepare SB10, SB20 and SB30 mixtures and reinforced with glass fiber (0.5%, 1 and 1.5%) with an aspect ratio of 40, 80 and 120, was adopted for this present study. Fiber dosage and aspect ratio were chosen based

on the source of research work conducted by other researchers (Rodatz and Oltmanns 1997; Abdi et al. 2008). Glass fiber has high stiffness, low dielectric constant, high chemical durability, readily availability (Wallenberger et al. 2000) high heat resistance capacity (Vejmelkova et al. 2010) and non-degradable material, which can be easily used as reinforcing the material. Since the glass fiber tangles together, considerable attention and time were consumed to develop the approximately uniform distribution of the glass fiber into the mixtures. Thereafter, different sand-bentonite–fiber mixtures were prepared by adding different amount of deionized (DI) water and then the samples were kept for a period of 24 hours for moisture equilibrium. After the moisture equilibrium, the MDD and OMC of the mixture were determined using a standard Proctor test according to ASTM D698 (2012). Sand–bentonite–glass fiber soil composite (before mixing) has been exhibited in Fig.3.4. Preparation of randomly distributed fiber reinforced soils mimics the conventional/traditional soil stabilization techniques, which uses the admixture, such as lime cement, fly ash, etc. Hence, the field application or construction procedure may be similar to that adopted for conventional soil stabilization techniques (Shukla 2017).

Figure 3.3 Sand-bentonite tire fiber composite

Figure 3.4 Sand–bentonite–fiber composite before mixing

3.5 Testing Methodology

This section deals with the methodology adopted to conduct the consolidation, triaxial and shrinkage test. This section specially focused on the specimen preparation technique, consolidation process, triaxial test, and shrinkage test adopted for the present study.

3.5.1 Standard Proctor compaction test

Compaction tests were performed as per as ASTM D 698 (2012) to determine the MDD and OMC for sand-bentonite mixes (SB) and sand-bentonite mixture reinforced with fiber (SBF). The compaction parameters obtained were used to prepare specimens for other tests like consolidation test, triaxial test and unconfined compression test to determine the engineering properties.

3.5.2 Determination of consolidation properties

Consolidation properties of the unreinforced and reinforced sand-bentonite mixture were determined by conducting one-dimensional consolidation test according to ASTM D2435 (1996). Deionized (DI) water was added to the mixture to bring the initial water content corresponding to the OMC and then stored in humidity-controlled desiccators for 24 hours to achieve the moisture

equilibrium. Thereafter, the sample was compacted to their MDD into an oedometer ring to achieve a sample diameter of 60 mm and a thickness of 15 mm. Then complete setup was mounted on a consolidation-loading frame and then flooded with DI water under nominal pressure of 5 kPa and permitted to swell. After the end of swelling, the surcharge pressure was gradually increased from 5 to 800 kPa, increasing stepwise by adding 5, 10, 20 kPa etc. at each step of loading. Change in the thickness of the soil sample was noted after application of incremental stress. Subsequently, the reduction in the void ratio was calculated under an incremental consolidating stress as;

$$\Delta e = \frac{\Delta H}{H} \times (1 + e_0) \tag{3.1}$$

Where,

ΔH = Reduction in the thickness of the sample by applying pressure

H = Initial thickness of the sample

e_0 = Initial void ratio

From the oedometer test result, a time-settlement curve was obtained for every stress increment. The coefficient of consolidation (c_v) was found using Taylor's square root time ($\sqrt{T}$) method (Taylor, 1948).

The coefficient of volume change (m_v) was estimated as,

$$m_v = -\frac{\Delta e}{\Delta \sigma (1 + e_0)} \tag{3.2}$$

Where,

$\Delta \sigma$ = Change in pressure

Δe = Change in void ratio

Coefficient of consolidation (c_v) evaluated by the square root of time fitting method specified by Taylor (1948) as,

$$c_v = \frac{D^2 T_v}{t_{90}} \tag{3.3}$$

(3)

Where,

t_{90} = Time for 90% degree of consolidation

T_v = Time factor

The hydraulic conductivity (k) calculated by fitting Terzaghi's theory of consolidation (1943) for different pressure increments using the c_v and m_v as,

$$k = c_v . m_v . \gamma_w \tag{3.4}$$

Where γ_w is the unit weight of the DI water

The compression index (C_c) is determined as the slope of the straight-line portion of the virgin void ratio (e) - pressure (P) curve as;

$$C_c = -\frac{e_i - e_j}{\log \frac{P_i}{P_j}} \tag{3.5}$$

Where,

e_i and e_j are the void ratio conforming to the consolidation pressure of P_i and P_j at i^{th} and j^{th} steps of loading, respectively.

Similarly, swelling index (C_s) was determined as the slope of the unloading portion of void ratio (e)- pressure (P) curve (Mitchell and Soga 2005). Swelling pressure of the samples was evaluated from the oedometer test set according to Sridharan and Gurtug (2004).

3.5.3 Determination of shear strength properties

Consolidated undrained (CU) tests were performed on a triaxial testing machine according to ASTM D4767 (2000) to determine the shear strength parameter. Cylindrical unreinforced and a

reinforced sample having a height-diameter ratio of 2:1 was used for the testing. A soil sample of diameter (*d*) of 38 mm and height (*h*) of 76 mm was positioned in a triaxial cell with pore pressure transducers and cell pressure, backpressure, and drainage outlets and shown in Fig. 3.5. The prepared specimen was then subjected to subsequent saturation, which was achieved from the complete dissolution of the air present in the sample by passing de-aired water through the application of suitable back pressure (BP). The amount of BP required to dissolve the air depends upon the initial degree of saturation of the specimen. During the BP saturation methodology, the Skemption's pore water pressure (B value) was checked to measure the degree of saturation at each increment of cell pressure (CP). The B value is expressed as the ratio of the increase of pore water pressure (Δu) to the cell pressure increment ($\Delta\sigma_c$). To determine the B value, a cell pressure increment was applied while keeping the drainage valve closed (undrained condition) and the corresponding increment in the pore pressure is measured. When the increment of pore water pressure attains an equilibrium state, the B value is calculated. B value greater than or equal to 0.93 is an indication of the degree of saturation nearly equal to 100% (Consoli et al.1998). The B value and corresponding degree of saturation is affected by the compressibility, soil texture hydraulic conductivity, density and compactness of packing of the soil (Karg and Haegeman 2009). Skempton's pore water pressure parameter B was measured for every increment of cell pressure. The specimen was saturated by applying a back pressure up to 480 kPa, 565 and 725 kPa to attain a minimum B value of 0.93 for SB10, SB20, and SB30 composite respectively. Specimen of SB10, SB20, and SB30 composite took 12, 17, and 21 days to attain their minimum B value and became saturated, respectively. After the end of the saturation stage, the specimen was isotropically consolidated to a desired effective confining pressure (i.e. 50, 100 and 150 kPa) by increasing the cell pressure while maintaining a constant back pressure. Once the pore pressure

becomes constant (i.e. residual pore water pressure should become almost equal to BP) during consolidation stage, the strain-controlled shearing of the specimen was carried out at a strain rate of 0.08%/min to secure the equilibrium of pore water pressure throughout the specimen during the experiment as proposed by Bishop and Henkel (1969). All the specimens sheared up to 20% axial strain deformation. Schematic diagram of a triaxial testing machine has been shown in Fig.3.5. The cell pressure, excess pore pressure, load, and displacement during the tests were recorded using an electronic data acquisition system. Deionized water was utilized in the triaxial chamber and in all pressure lines that were suited with air bladders, which imparts a partition between air and liquid phases. Based on their experimental data set, the Mohr circle was drawn based on peak and residual stress and Mohr-Coulomb failure criteria were used to determine the effective strength parameter of the composite.

3.5.4 Determination of volumetric shrinkage and desiccation cracking of sand-bentonite-fiber composite

Unreinforced and reinforced soil samples were prepared using a cylindrical mould of 7.0 cm diameter and 3.0 cm in length. Each specimen was prepared to their respective MDD and OMC condition and air dried under room temperature (25°±2° C). The process of drying was continued for a period of around 17 days.

Height and the diameter of the specimens were measured periodically and the corresponding value of the reduction in the volume was determined. The volumetric shrinkage was determined as the reduction in the volume of the specimen (ΔV) due to shrinkage to the initial volume (V) of the sample, i.e.

$$\text{Volumetric shrinkage (\%)} = \frac{\Delta V}{V} \times 100 \qquad (3.6)$$

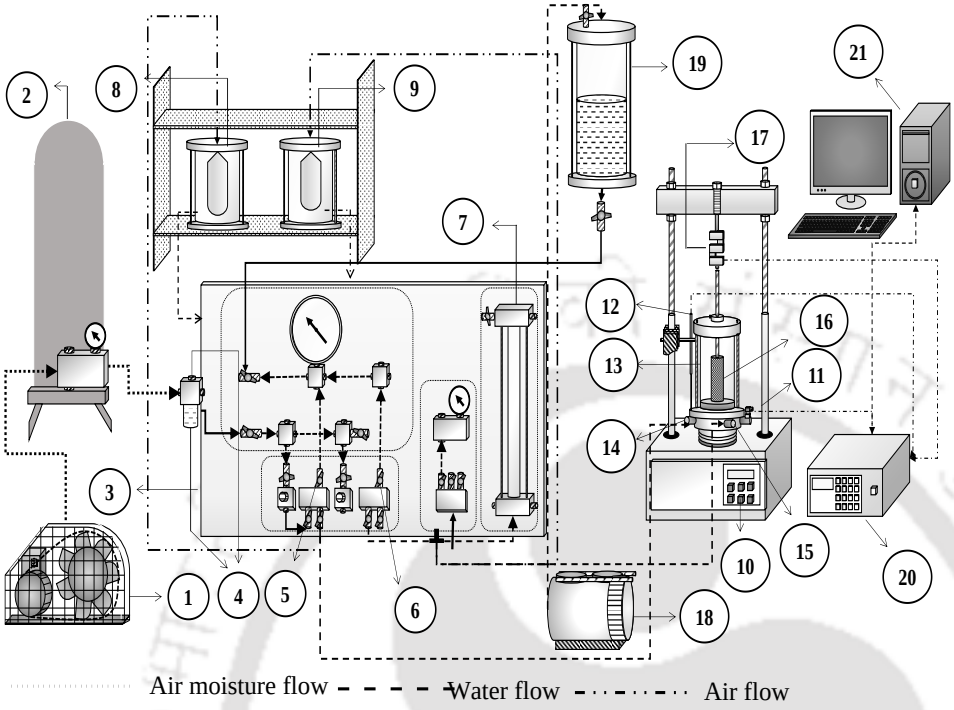

1: Air compressor
2: Air-moisture chamber
3: Air/water control panel
4: Moisture separator
5: Cell pressure controller
6: Back pressure controller
7: Twin-burette volume change
8: Air/water cell used for cell pressure
9: Air/water cell used for back pressure
10: Variable speed stepper motor drive unit
11: Pore pressure transducer
12: LVDT for measuring axial displacement of specimen
13: Cell body
14 and **15**: Cell and Back pressure line
16: Soil specimen
17: Load cell
18: Vertical pump
19: Water reserver
20: Data acquisition system
21: Computer assembly

Figure 3.5 Schematic diagram of triaxial testing machine

The cracking features of the compacted specimens was monitored during the tests. Thereafter, surface crack and specimen shrinkage were taken by a digital camera from 30 cm fixed height from the specimen. The analysis of the image was carried out by ImageJ 1.51j8 (Java 1.8.0 -112, 64-bit) as described by Burger and Burge (2016). ImageJ is a tool for studying cracking behavior of material and to determine surficial topographies of crack (Singh et al. 2018). In this process, the compacted sample with surficial crack was considered first and imports to ImageJ. Thereafter, the image was calibrated and divided in into equal grid in such a way that every grid measures 42547 square pixels. After gridding, the image was first converted into grayscale and then to the binary image and finally, the cracks of soil composite were located. In order to calculate the areas, initial specimen area (I_a), reduced specimen (R_s), cracked area (A_c), shrinkage area (S_a) and combined

crack area ($C_{ca} = A_c + S_a$) were calculated to get cracked intensity factor (CIF) and cracked density factor (CDF) for analyzing the desiccation crack developed in the soil. The CIF and CDF are defined as:

$$CIF = \frac{A_c \text{ in square Pixel}}{R_s \text{ in square Pixel}} \times 100\% \quad (3.7)$$

$$CDF = \frac{C_{ca}(i.e. A_c + S_a) \text{ in square Pixel}}{I_a \text{ in square Pixel}} \times 100\% \quad (3.8)$$

3.5.5 Microstructural study

The Field emission scanning electron microscope (FESEM) and Energy Dispersive X-ray analysis (EDX) were employed to study the micro-structural characteristics in the of the fiber used in the current study. Fiber was taken out from the failed triaxial specimens and was dried completely (after shearing). The dried specimen was mounted in a phenolic resin base with the help of a mounting device. The mounted sample was coated with a thin layer of gold palladium to provide surface conductivity. Polaron sputter coater, operating under a vacuum of 10^{-2} bar and 4mA current, was used for this purpose. The coated specimens were mounted in a commercial FESEM-EDX instrument (LEO, 1430VP). Both spot and overall EDX analysis were performed on the samples. The FESEM and EDX were operated with an acceleration potential of 15 kV and each spectrum was collected for about 100s (acquisition time). The photomicrographs were taken at different magnifications and their execution has been shown differently in Fig.3.1 and Fig.3.2.

EDX was conducted to find out the elemental composition of the tire fiber and EDX image of tire fiber presented in Fig.3.1 (c and d). EDX study of the tire fiber provides the estimate of atomic percentage as well as the percentage by weight of the elements present in the sample. Fig.3.1(c and d) shows an elemental composition of the tire fiber corresponding to spectrum 3.

lists the element observed in tire fiber based on three EDX observation (marked with white square box) and result suggested that a high percentage of carbon is predominate in the tire fiber.

Table 3-3 Elemental composition of tire fiber

Elemental	Symbol	Percentage (%)
Carbon	C	95.7
Zinc	Zn	1.7
Sulphur	S	1.1
Silicon	Si	1.0
Bromine	Br	0.3
Iron	Fe	0.1
Copper	Cu	0.1

Similarly, EDX analysis of the glass fiber had been conducted to study the elemental composition and exhibited in Fig.3.2 (c and d). From the EDX analysis, glass fiber delivers the estimate of atomic percentage as well as the percentage by weight of the elements present in the specimen. Fig.3.2 (c and d) depicted an elemental composition of the glass fiber corresponding to spectrum 2. Table 3-4 lists the element observed in glass fiber based on 3 EDX observations (marked with white square box) and result showed that a high percentage of silicon (S_i) was predominate in the glass fiber.

3.5.6 Unconfined compression test

Cylindrical samples of 38 mm diameter and 76 mm height were used to estimate the unconfined compressive strength (UCS) of the unreinforced and reinforced sample according to ASTM D2166 (2016). The sample of SB-glass fiber mixes was made to their corresponding MDD and OMC. Unreinforced soils were used as a reference for associating and measuring the performance enhancement due to the reinforcements i.e. compacted sand-bentonite, compacted sand-bentonite

reinforced with glass fiber. Unconfined compressive strength (σ_c) was performed according to ASTM D2166 (2016) under a constant strain rate of 1.25 mm/min to simulate the un-drained condition during the testing. The unconfined compressive strength of the unreinforced and reinforced sample was estimated from the relation:

Table 3-4 Elemental composition of glass fiber

Elemental Composition	Symbol	Percentage (%)
Oxygen(0)	O	54.0
Silicon (Si)	Si	21.2
Calcium (Ca)	Ca	15.9
Aluminum (Al)	Al	6.6
Magnesium	Mg	1.5
Titanium (Ti)	Ti	0.3
Iron (Fe)	Fe	0.2
Copper (Cu)	Cu	0.2
Manganese	Mn	0.1

Cylindrical samples of 38 mm diameter and 76 mm height were used to estimate the unconfined compressive strength (UCS) of the unreinforced and reinforced sample according to ASTM D2166 (2016). The sample of (Sand-bentonite –fiber) SBF mixes was made to their corresponding MDD and OMC. Unreinforced soils were used as a reference for associating and measuring the performance enhancement due to the reinforcements i.e. compacted sand-bentonite, compacted sand-bentonite reinforced with fiber. Unconfined compressive strength (σ_c) was performed according to ASTM D2166 (2016) under a constant strain rate of 1.25 mm/min to simulate the un-drained condition during the testing. Generally, CU and CD test on saturated composite is time consuming, but exact measurement of shear strength parameter, CU test was performed throughout the investigation process. However, UC test result was cross-validated with CU test result in the form of deviatoric stress and axial stress and it has been discussed individually in this chapter. The

unconfined compressive strength of the unreinforced and reinforced sample was estimated from the relation:

$$\sigma_c = \frac{p}{A} \tag{3.9}$$

Where,

σ_c = Unconfined compressive strength (kPa),

P = Applied load (kN)

A = Corresponding average cross-sectional area (mm^2)

$$A = \frac{A^o}{(1-\varepsilon)} \tag{3.10}$$

A^o = Initial average cross-sectional area of the specimen (mm^2)

Axial strain (%), $\varepsilon = \frac{\Delta l}{l} x100$

Δl = Change in length of the specimen (mm)

l = The initial length of the specimen (mm)

CHAPTER 4
Result and discussion
(Glass Fiber Composite)

4.1 Compaction behavior of fiber soil composite

In this chapter, the compaction properties of sand-bentonite mixtures amended with fiber are carried out. Subsequently, the impact of glass fiber on compaction properties of various sand–bentonite mixtures have been studied.

4.1.1 Compaction characteristics

Compaction tests were performed to determine the moisture content –dry density relationships for different sand–bentonite mixtures by following the procedure in section 3.5.1. The moisture content–dry density relationships for sand-bentonite mixture and composite soils are shown in Fig.4.1 and Fig.4.9. These plots clearly bring out the influence of glass fiber on the compaction characteristics of the different sand-bentonite mixture.

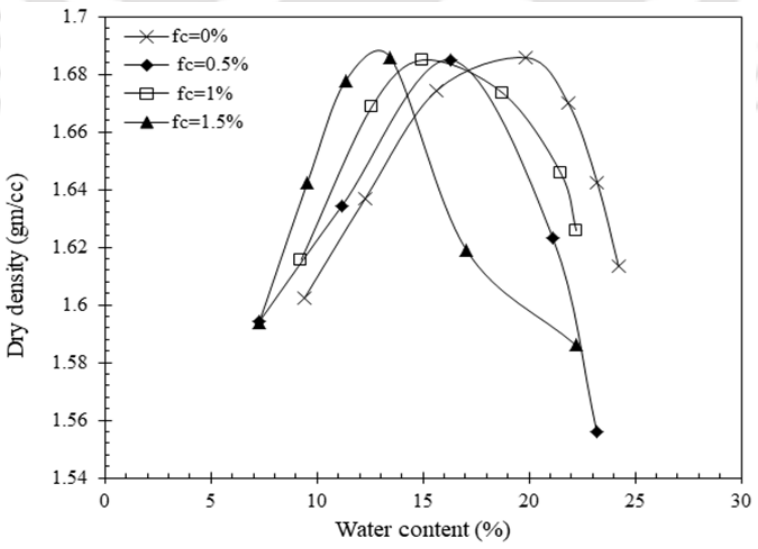

Figure 4.1 Compaction curves for SB30-glass fiber composite with an aspect ratio of 40

The addition of fiber to the unreinforced soil did not change the compaction behavior drastically in terms of the shape of the compaction curve but it did alter the compaction characteristics in terms of the maximum dry density (MDD) and optimum moisture content (OMC). The compaction behavior of three different composites differs in several ways:

a) OMC decreased with increase in fiber inclusion due to the non-porous tendency of the glass fiber,

b) Rate of decreases of OMC of the composite decreased with increase in sand content,

c) The saturation level at peak reduced with the addition of glass fiber.

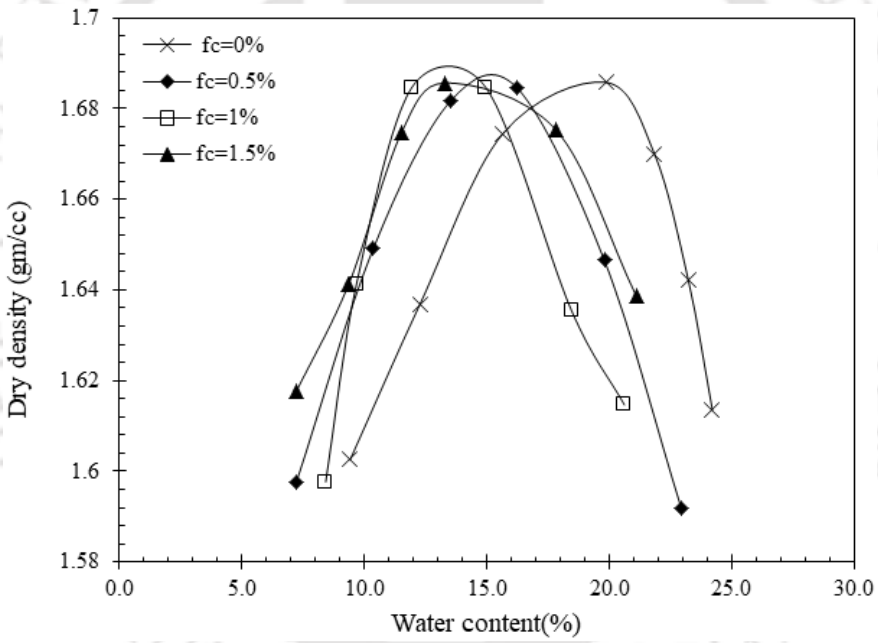

Figure 4.2 Compaction curves for SB30-glass fiber composite with an aspect ratio of 80

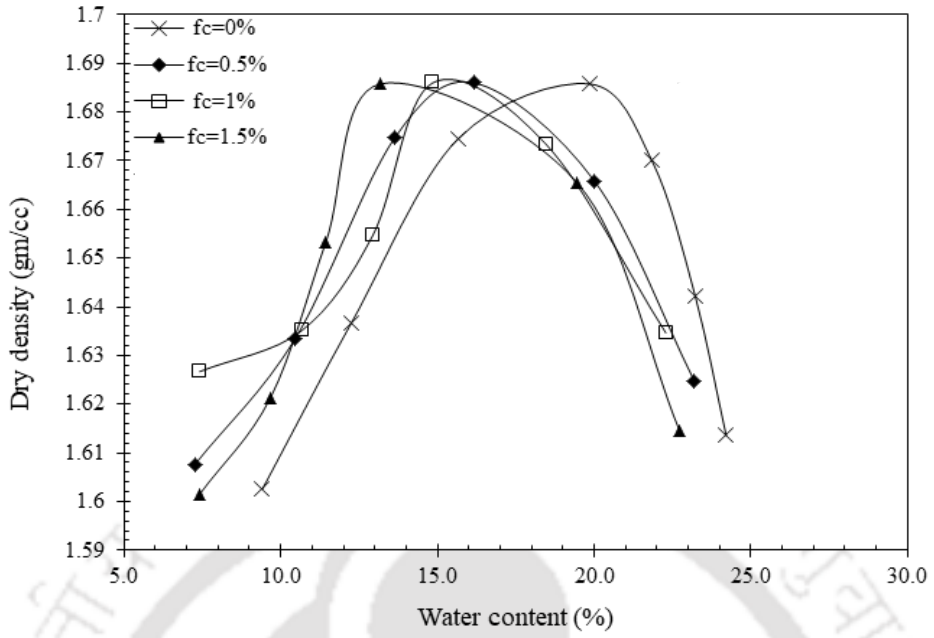

Figure 4.3 Compaction curves for SB30-glass fiber of aspect ratio 120

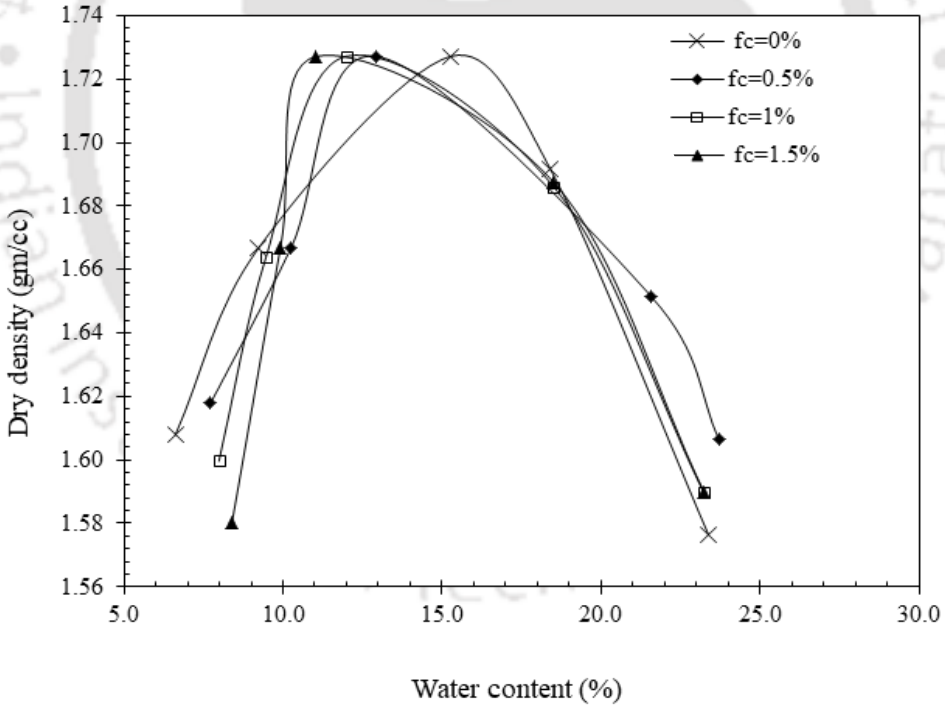

Figure 4.4 Compaction curves for SB20-glass fiber of aspect ratio 40

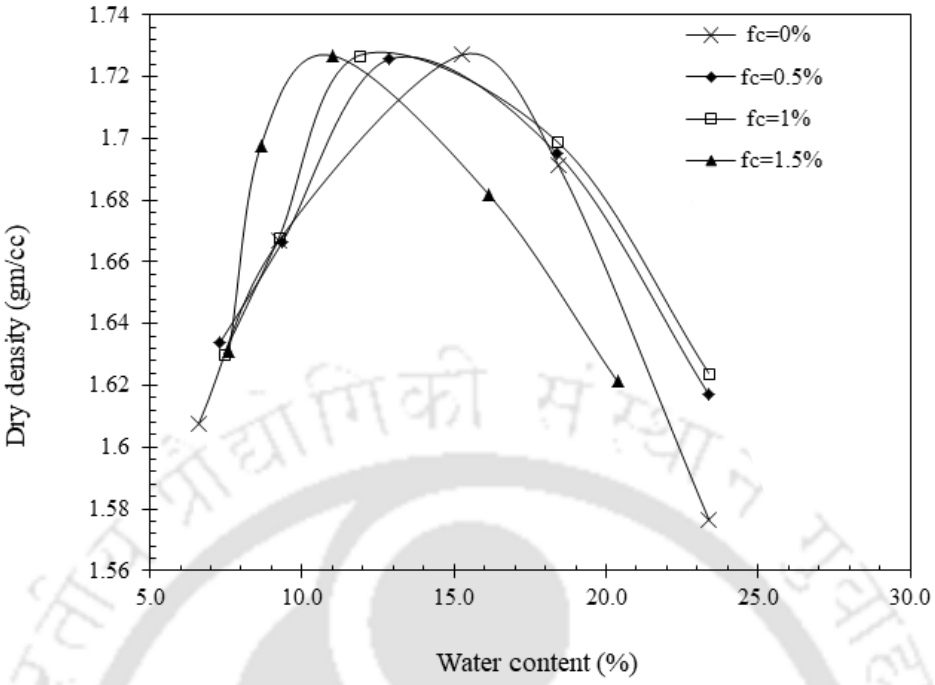

Figure 4.5 Compaction curves for SB20-glass fiber of aspect ratio 80

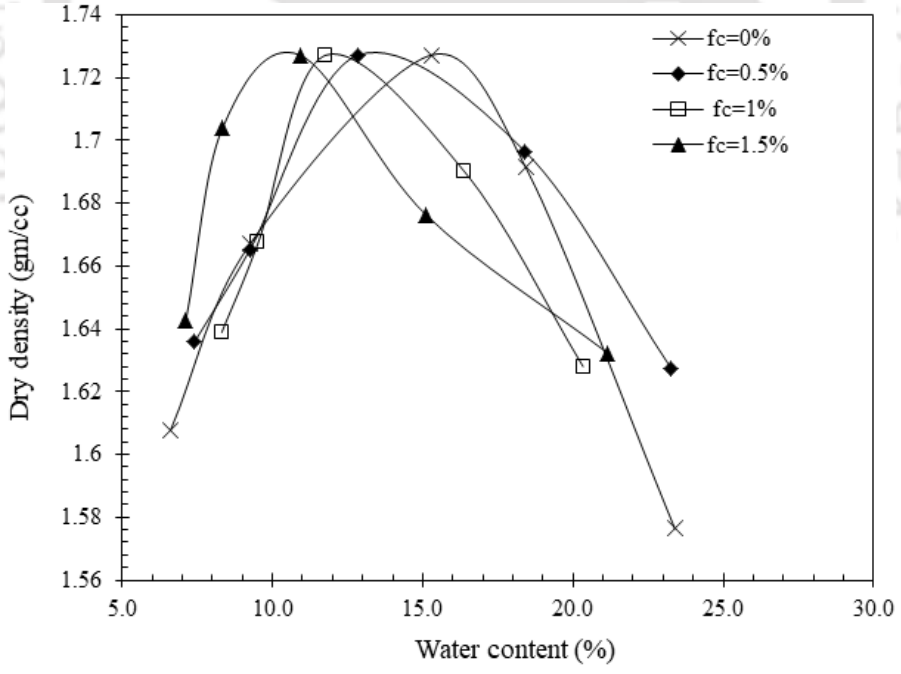

Figure 4.6 Compaction curves for SB20-glass fiber of aspect ratio 120

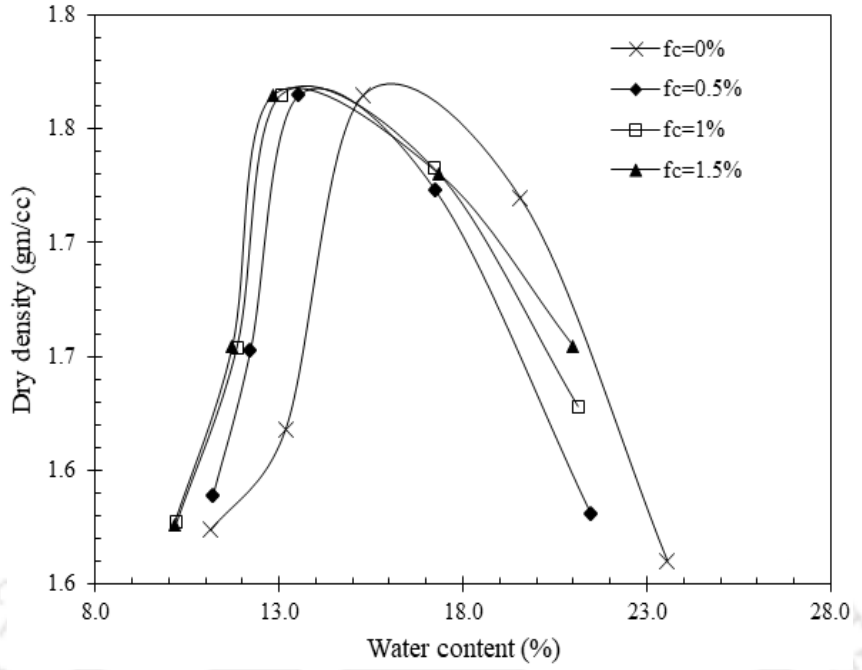

Figure 4.7 Compaction curves for SB10-glass fiber of aspect ratio 40

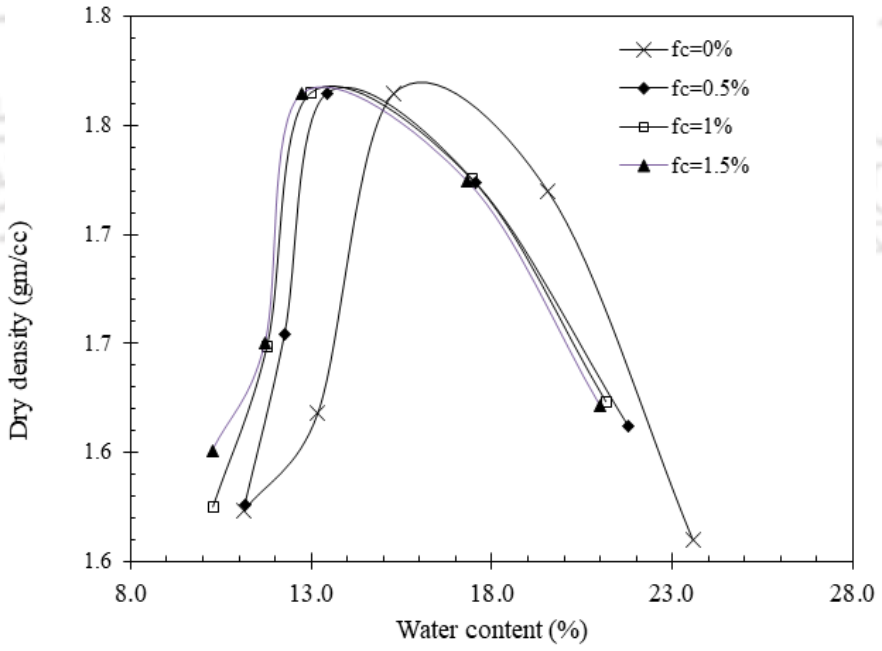

Figure 4.8 Compaction curves for SB10-glass fiber of aspect ratio 80

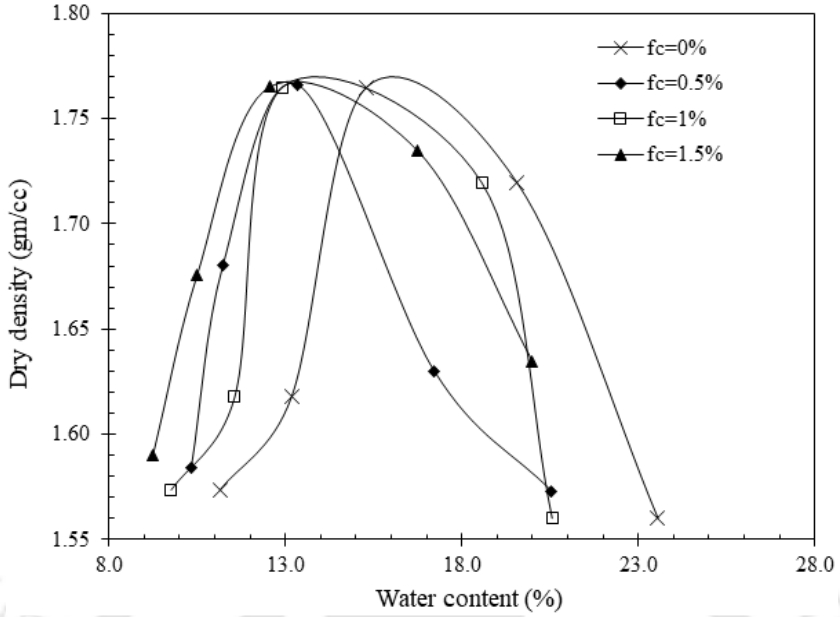

Figure 4.9 Compaction curves for SB10-glass fiber of aspect ratio 120

The OMC was found to decrease with the addition of glass fiber and this trend was followed by all the composite, whereas, MDD remained constant. This phenomenon was more affected by fiber concentration in comparison to the aspect ratio. For example, OMC of SB30 composite was decreased from 19.86% to 16.30, 14.98 and 13.44% due to the addition of 0.5, 1 and 1.5% fiber concentration of aspect ratio 40, respectively. With the increase in aspect ratio from 40 to 80, the OMC was reduced from 19.86% to 16.21, 14.95 and 13.28% with 0.5, 1 and 1.5% fiber concentration, respectively. However, due to an increase in the aspect ratio from 80 to 120, the OMC was reduced from 19.86% to 16.17, 14.84 and 13.17% at 0.5,1 and 1.5% fiber concentration, respectively. The maximum reduction of the OMC was around 6.69% for SB30 composite with 1.5% fiber concentration with the aspect ratio of 120. This mechanism was affected to an initial degree of saturation (IDS). The IDS of the SB30 composite was reduced from 87.01% to 73.11, 65.56 and 60.72% due to the inclusion of 0.5, 1 and 1.5% of fiber concentration of aspect ratio of 40, respectively. Similarly, for an aspect ratio of 80 the IDS was decreased from 87.01% to 72.64,

67.01 and 59.59% due to the inclusion of 0.5, 1 and 1.5% of fiber concentration, respectively. With a further increase in the aspect ratio from 80 to 120, the IDS was reduced slightly from 87.01% to 72.61, 66.34 and 59.45% for the same amount of fiber content.

For SB20 composite, the presence of higher amount of sand (or lower amount of bentonite) played a significant role in compaction parameters. The OMC was reduced from 15.28% to 12.94, 11.98, and 11.05% at 0.5, 1 and 1.5% fiber concentration with an aspect ratio of 40, respectively. At same fiber concentration, OMC further reduced from 15.28%, 12.87, 11.89, and 10.98% for aspect ratio 80. However, at the same fiber concentration, OMC was again reduced from 15.28% to 12.85, 11.77 and 10.92% with an aspect ratio of 120. For the same composite, the IDS was reduced from 73.7% to 62.39, 57.77 and 53.25% at 0.5,1 and 1.5% fiber concentration of an aspect ratio of 40, respectively. However, for the same fiber concentration, the IDS decreased from 73.71% to 61.86, 57.38 and 53.08% with an aspect ratio of 80. For a further increase in the aspect ratio from 80 to 120, the IDS was reduced from 73.71% to 61.78, 56.63 and 52.49%. A maximum reduction of OMC was observed around 4.36% for SB20 with an aspect ratio of 120 with 1.5% fiber concentration. The SB10 exhibited a similar trend as observed for SB30 and SB20. It can be noticed that the compaction curve was slightly altered and the peak point of SB10 composite moved left side slightly in comparison to unreinforced SB10. OMC of the composite was found to reduce maximally from 15.31% to 12.56 % for SB10 at 1.5% fiber concentration with an aspect ratio of 120 and the IDS decreased from 78.51% to 64.45%. Hence, the result suggested that the effect of fiber concentration is more in comparison to fiber aspect ratio on OMC of the composites. It can also be observed that the OMC reduces maximally from 6.69%, 4.36 and 2.74% for SB30, SB20, and SB10 composite at 1.5% fiber concentration with an aspect ratio of 120.

4.2 Swelling behavior of glass fiber soil composite

Bentonite undergoes significant volumetric changes with change in moisture content. The resulting heave and settlement cause damage to the structure founded on such soil. Swelling of bentonite has been mainly attributed to the electrical double layer. The exchangeable cations in the bentonite–water system remain at some distance from the particle surface. The cations are attracted towards the clay surface because of the negative charge on the clay surface, but their thermal energy and concentration gradient make them diffuse away from the surface. This attraction and thermal diffusion create a diffused layer of cations with its concentration highest adjacent to the surface. The concentration gradually decreases with an increase in distance from the clay surface (Sridharan et al.1986). The interaction of diffuse ion layers of adjacent particle explains the properties of swelling. To eliminate or reduce the effect of active clay, researchers suggested many methods to improve the mechanical performance by using the inward material, flay ash, lime and residual soil, etc. Among the proposed mechanical stabilization techniques, glass fiber-reinforcement seem to be the most economic and eco-friendly ones; yet they have received less attention, particularly in field landfill applications. Experiments were conducted to examine the reduction in swelling of the sand-bentonite mixture due to the inclusion of glass fiber. The purpose of this study was to investigate the impact of the addition of glass fiber of different aspect ratios on the swelling properties of sand –bentonite mixtures.

4.2.1 Effect of glass fiber on swell-time behavior

The effect of glass fiber on the swelling behavior of SB30 and SB20 are presented in Fig.4.10 and Fig.4.11. From the plots, it was observed that the increase in swelling with time started rapidly and then move towards an asymptotic value. However, this trend of swelling was significantly affected due to the addition of fiber. For example, the swelling height of SB20 mixture was decreased from

0.58 mm to 0.44, 0.38 and 0.36 mm due to the inclusion of 0.5, 1 and 1.5% fiber concentration of aspect ratio 40 under vertical stress of 5 kPa. However, under the same vertical stress, the swelling height was decreased from 0.58 mm to 0.42, 0.36 and 0.32 mm for similar fiber concentration of the aspect ratio 80. With a further increase in the aspect ratio from 80 to 120, the swelling height was reduced from 0.58 mm to 0.39, 0.32 and 0.28 mm with 0.5, 1 and 1.5% fiber concentration under the same vertical stress. In case of SB30 composite with an aspect ratio of 40, the swelling height was reduced from 1.44 mm to 1.06, 0.84 and 0.64 mm for the fiber concentration of 0.5,1 and 1.5% under the vertical stress of 5 kPa, respectively. With increase the aspect ratio from 40 to 80, the swelling was decreased from 1.43 mm to 0.69, 0.61 and 0.52 mm at different fiber concentration. However, the swelling height was further reduced from 1.06 mm to 0.533, 0.42 and 0.28 mm with the inclusion of 0.5%, 1 and 1.5% fiber of aspect ratio of 120, respectively. Hence, it can be concluded from this study that the swelling height is significantly controlled by fiber concentration and aspect ratio. Data also suggested that mixes with bentonite proportion of 10% were relatively incapable of swelling implying that bentonite content available was not sufficient for filling all the voids created by the sand skeleton. The role of glass fibers in reducing the effect of swelling can be due to the interlocking and the friction produced by presenting high stiffness glass fiber.

4.2.2 Effect of glass fiber on swelling pressure

Swelling pressure is defined as the pressure required to compress the specimen, which has been soaked and completed swelling under a pressure of 5 kPa, back to its original volume (Sridharan et al. 1986a). It is also defined as the pressure required for maintaining a constant volume of an unsaturated soil specimen during the hydration process (Sridharan et al. 1986a).

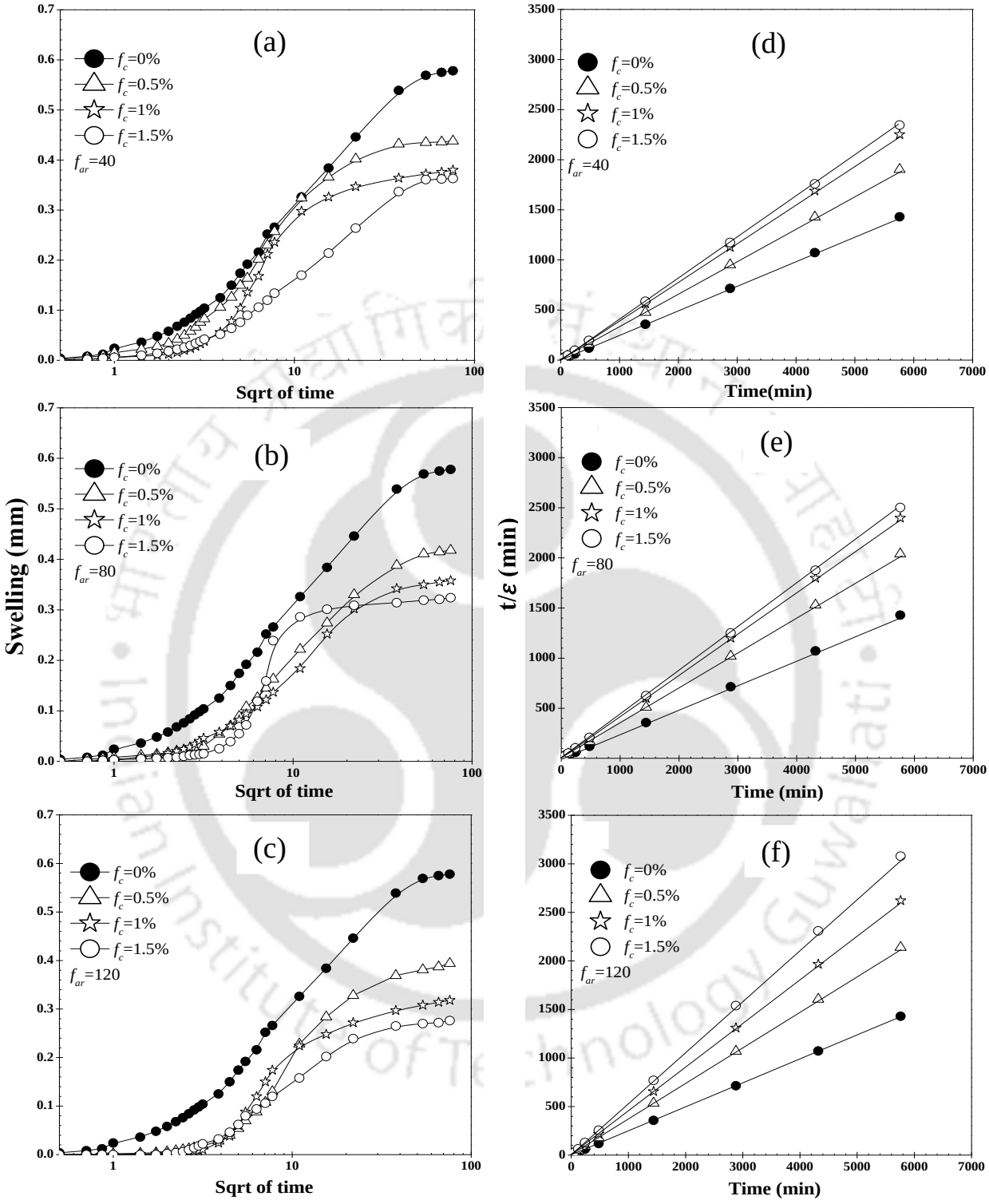

Figure 4.10 Time-swelling relationships for SB20 with different fiber concentration; (a) aspect ratio of 40;(b) aspect ratio of 80;(c) aspect ratio of 120; Linearized illustration of swelling data at different fiber concentration for SB20;(d) aspect ratio of 40;(e) aspect ratio of 80;(f) aspect ratio of 120

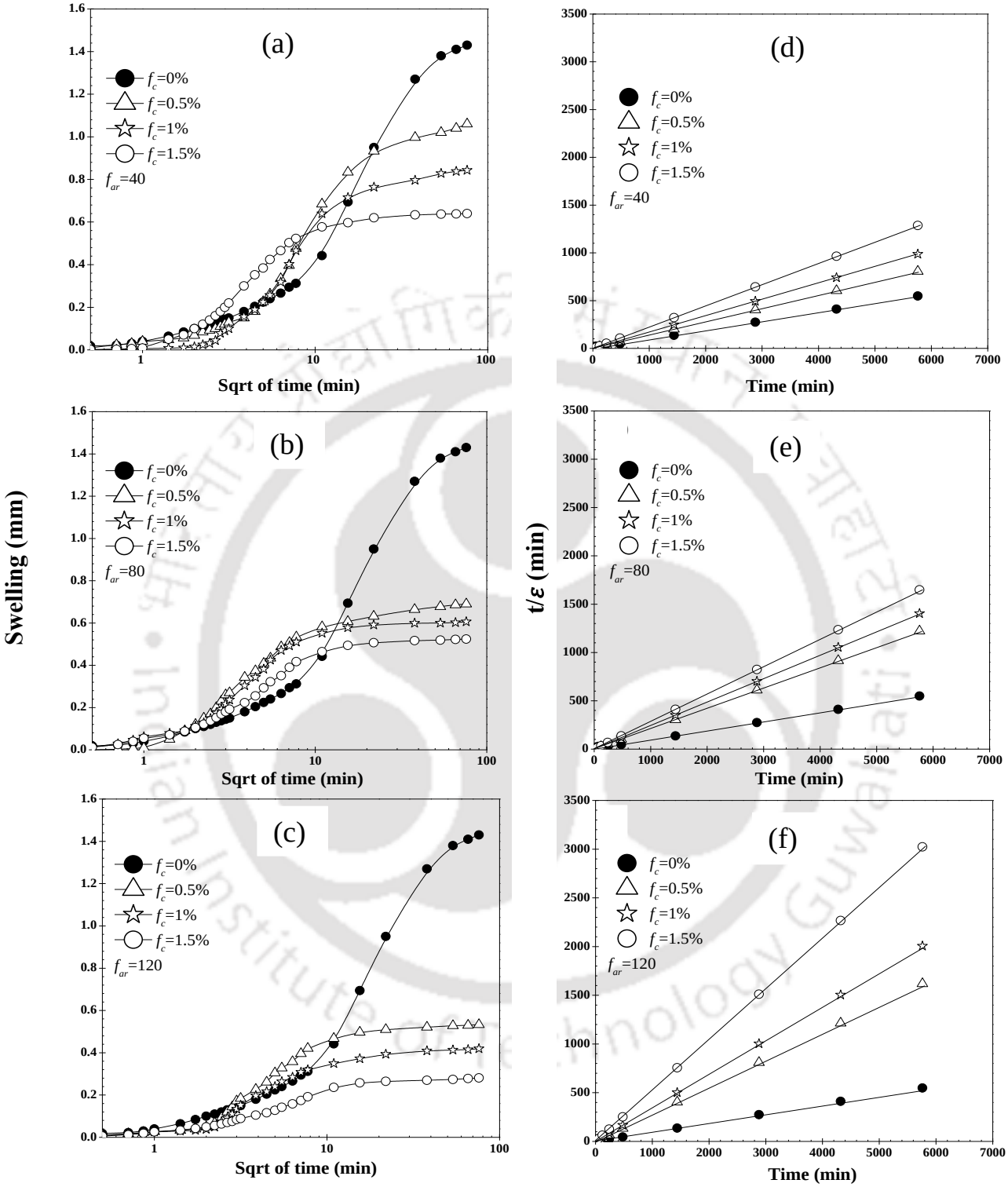

Figure 4.11Swelling-time relationships for SB30 with different fiber concentration; (a) aspect ratio of 40;(b) aspect ratio of 80;(c) aspect ratio of 120; Linearized illustration of swelling data at different fiber concentration for SB30;(d) aspect ratio of 40;(e) aspect ratio of 80;(f) aspect ratio of 120

The result shows that the swelling pressure of SB composite was decreased continuously with the fiber concentration and fiber aspect ratio. For example, swelling pressure of SB30 decreased substantially from 46 kPa to 40, 38 and 35 kPa at 0.5%, 1 and 1.5% fiber concentration with an aspect ratio of 40, respectively. Similarly, with increase the aspect from 40 to 80, swelling pressure was further reduced from 46 kPa to 35, 29, and 25 kPa at the same fiber concentrations. However, with increase the aspect ratio from 80 to 120, the swelling pressure was reduced again from 46 kPa to 28, 22, 16 kPa at 0.5%, 1 and 1.5% fiber concentrations. Identical observations were observed for SB20 mixture with different fiber content.

4.2.3 Effect of glass fiber on swelling potential

The swelling potential has been tabulated in Table 4-1 for all SB composite. The data in Table 4-1 indicates that swelling potential for the composite depends upon the fiber concentration and fiber aspect ratio. For example, the swelling potential was reduced from 9.53% to 7.07, 5.62 and 4.27% due to the increase in the fiber concentration from 0 to 0.5%, 1 and 1.5% of the aspect ratio 40. At same fiber concentrations, the swelling potential was reduced from 9.53% to 4.6, 4.04, and 3.49% for the aspect ratio of 80. With the increase in the aspect ratio from 80 to 120, the swelling potential was further decreased from 9.53% to 3.55, 2.79 and 1.87 % at 0.5, 1 and 1.5% fiber concentration, respectively. However, it was noticed that SB20 exhibits the almost similar trend. The shape of swelling curves can be considered similar to that of a rectangular hyperbola (Dakshanamurthy 1978) and defined as;

$$\frac{x}{y} = b + ax \qquad (4.1)$$

Where x and y are the variables, b is the intercept, and a is the slope of the linear portion. The non-linear stress-strain relations of soils are linearized by the method of rectangular hyperbola using

Eq. (4.1) as suggested by Kondner (1963) and Stark et al. (1994). The maximum swelling can be predicted using the hyperbolic model (Eq. 4.2) and calculated by Eq. (4.3).

$$S_p(\%) = \frac{t}{(b + at)} \tag{4.2}$$

$$S_{p\max}(\%) = \lim_{t\to\infty}\left(\frac{1}{\frac{(b+at)}{t}}\right) \cong \frac{1}{a} \tag{4.3}$$

Where,

t = time, since the sample is submerged with water

S (%) = vertical swelling at time (t)

a and b = constant, which was evaluated by fitting procedures

Since long testing time is required to achieve equilibrium swelling potential for unreinforced and reinforced composite, the swelling potential for different composite was predicted using the above equations. The linear portion of swelling data after the preliminary swelling was considered [Fig.4.10 (d to f) and Fig.4.11 (d to f)] for predicting the maximum swelling potential. The preliminary swelling may be illustrated by noticing the deviation from the initial swelling data. All the data points considered to determine the equation constants b and a in Eq. 4.2. The linear equations were considered using the equation constants and were used to predict maximum swelling potential. However, after infinite time, the importance of parameter b is absolute; therefore, reciprocal of parameter "a" will give the maximum swelling potential. Generally, The slope, a, of the linier equation increased with increasing time but the slope, a, is also increased with fiber concentration and fiber aspect ratio for any SB composite; which has been depicted in the Figure 4.10 (d to f) and Fig.4.11(d to f) for SB30 and SB20 composite. The observed and

predicted data have been tabulated in Table 4-1. The data indicates that the prediction was satisfactory and useful for obtaining maximum swelling potential for all SB composite from the early stage of swelling data.

4.2.4 Compressibility behaviour of glass-fiber soil composite

Compressibility of soil is determined by conducting one–dimensional consolidation test. Consolidation is a time-dependent process where the voids present in the soil decreases due to the expulsion of water. The main objective of this study is to investigate the impact of glass fiber concentrations of three different aspect ratios (l/d) on the consolidation behavior of different sand–bentonite mixture.

4.2.4.1 Volume change and compressibility performance of SB-glass fiber composite

The typical void ratio-pressure response of the different sand bentonite mixture is depicted in Fig.4.12. The data presented in the figures show that the unreinforced SB mixture specimen achieved the highest equilibrium void ratio (i.e. after the end of swelling), Additionally, as the fiber content in the sample increases the equilibrium void ratio decreases further. It was also noticed that under the same consolidating pressure, void ratio reduced further with the increase in aspect ratio. For example, void ratio of SB30 composite was reduced from 0.602 to 0.489, 0.477 and 0.471 at 0.5%, 1 and 1.5% of fiber concentration of aspect ratio of 80 under a consolidating pressure of 100 kPa. Under the same consolidating pressure, the void ratio was reduced from 0.602 to 0.459, 0.442 and 0.439 with increase the aspect ratio from 80 to 120 for the composite with 0.5, 1 and 1.5 % of fiber composition, respectively. SB20 composite depicted similar trend like SB30 composite. Hence, the study concludes that the fiber concentration and fiber aspect ratio have a certain impact to control the compressibility behavior under vertical pressure.

Table 4-1 Comparison of measured and predicted the maximum swelling potential for SB20 and SB30 at different fiber concentration with the different aspect ratio

Composite Name	**a**	b	Measured swell (%)	Max. Swell Predicted (%)
SB20, f_c=0%, f_{ar}=0	0.2482	0.0708	3.853	4.03
SB20, f_c=0.5%, f_{ar}=40	0.3303	0.0637	2.921	3.02
SB20, f_c=1%, f_{ar}=40	0.391	0.352	2.533	2.56
SB20, f_c=1.5%, f_{ar}=40	0.4072	0.0711	2.42	2.46
SB20, f_c=0.5%, f_{ar}=80	0.3541	0.0266	2.787	2.82
SB20, f_c=1%, f_{ar}=80	0.4162	0.9470	2.387	2.40
SB20, f_c=1.5%, f_{ar}=80	0.4345	0.0626	2.16	2.30
SB20, f_c=0.5%, f_{ar}=120	0.3715	0.087	2.63	2.69
SB20, f_c=1%, f_{ar}=120	0.455	0.0291	2.12	2.19
SB20, f_c=1.5%, f_{ar}=120	0.5344	0.095	1.84	1.87
SB30, f_c=0, f_{ar}=0	0.0953	0.0239	9.53	10.49
SB30, f_c=0.5%, f_{ar}=40	0.1401	0.0716	7.07	7.14
SB30, f_c=1%, f_{ar}=40	0.1714	0.0105	5.62	5.83
SB30, f_c=1.5%, f_{ar}=40	0.2234	0.0279	4.27	4.47
SB30, f_c=0.5%, f_{ar}=80	0.2121	0.035	4.6	4.71
SB30, f_c=1%, f_{ar}=80	0.2437	0.0637	4.04	4.10
SB30, f_c=1.5%, f_{ar}=80	0.2861	0.0254	3.49	3.50
SB30, f_c=0.5%, f_{ar}=120	0.2811	0.0365	3.55	3.58
SB30, f_c=1%, f_{ar}=120	0.3482	0.0429	2.79	2.87
SB30, f_c=1.5%, f_{ar}=120	0.5248	0.0735	1.87	1.90

f_c = fiber content; f_{ar} = fiber aspect ratio

A study on the effect of inclusion of fiber on compression index (C_c) shows that it decreased continuously with the increase in fiber concentration and aspect ratio and presented in Fig.4.13 to Fig.4.15 for the mixture of SB30 composite. For example, C_c for SB30 composite was reduced from 0.33 to 0.27, 0.23 and 0.25 at 0.5%, 1 and 1.5% of fiber concentration of an aspect ratio of 40, respectively. Similarly, at the same fiber concentration, C_c was dropped from 0.33 to 0.2, 0.19 and 0.24 of aspect ratio 80. Similarly, with an increase in fiber aspect ratio from 80 to 120, the C_c was reduced from 0.33 to 0.18, 0.14, and 0.2 with for the fiber concentration of 0.5, 1 and 1.5%, respectively. The results indicated that initially the C_c reduced with the increase in the fiber concentration up to 1%, with a further increase in the fiber concentration from 1 to 1.5% the C_c was increased. From the unloading portion of the void ratio-pressure curve (Fig.4.12), it was

noted that the void ratio increased more for reinforced composite in comparison to unreinforced composite upon removal of load. From the figure, it was observed that a rise in the void ratio of 1.414% occurred for unreinforced soil in comparison to 2.005, 2.24 and 2.452% rise for the composite with 0.5, 1 and 1.5% of fiber of aspect ratio of 40 due to the removal of 400 kPa of pressure for the composite of SB30. This trend was followed by other composites also.

The plot in Fig.4.13 to Fig.4.15. shows that the swelling index altered drastically by the fiber concentration. However, a marginal effect due to the increase in the fiber aspect ratio was observed. For example, the swelling index (C_s) of SB30 composite was increased from 0.018 to 0.029, 0.041, and 0.05 with 0.5%, 1 and 1.5% fiber concentration with an aspect ratio of 40, respectively. With increase the aspect ratio from 40 to 80, the C_s was changed from 0.018 to 0.03, 0.04 and 0.051 for the same fiber concentration. At same fiber configuration, C_s was changed from 0.018 to 0.03, 0.042 and 0.051 with an aspect ratio of 120. Hence, it has been observed that the increment of the swelling index was the function of fiber concentration mainly in comparison to fiber aspect ratio. A similar trend was followed by other SB composite also.

4.2.5 Consolidation and hydraulic behavior of glass fiber-soil composite

Performance of landfill structure is seriously affected by the high compressible nature of the soil (i.e. sand-bentonite mixture or bentonite clay). Very few studies have been carried out for developing the techniques to control the compressibility (Babu and Vasudevan 2008) and hydraulic conductivity when soil is mixed with fiber. In the current study, one-dimensional consolidation tests were performed on different sand-bentonite mixture reinforced with glass fiber to study the consolidation and hydraulic behavior of fiber soil composite.

4.2.5.1 Effect of glass fiber on the coefficient of consolidation (c_v) different SB mixes

The coefficient of consolidation (c_v) defines the rate at which a saturated soil sample undergoes one-dimensional consolidation when subjected to an increase in the consolidation pressure, which in turn directly depends on the hydraulic conductivity of the soil medium undergoing compression (Terzaghi 1943). To determine the rate of settlement of soils as well as hydraulic conductivity, it is essential to know the c_v value. A higher value of c_v indicates a faster rate of consolidation and vice versa. Figure 4.16 to Fig.4.18 exhibits that the c_v decreased with increasing consolidating pressure indicating a slower rate of consolidation at higher consolidation pressure, however, this trend was significantly changed with the inclusion of glass fiber.

Under any consolidating pressure, the coefficient of consolidation was increased initially with fiber and then decreased as the fiber concentration and fiber aspect ratio increased. However, a comparison of the c_v values for the three composites (i.e. SB30, SB20, and SB10) at different fiber concentration and aspect ratio for any given consolidation pressure, the c_v increased with increase in the fiber concentration and aspect ratio, indicating a faster rate of consolidation in the presence of fiber inclusion. Under the consolidating pressure of 400 kPa, the coefficient of consolidation of SB30 was found to be 5.19×10^{-4} cm^2/sec but it increased to 3.8×10^{-3} cm^2/sec (7.32 times) with the addition of 0.5% fiber. However, a further increase in the fiber concentration to 1 and 1.5% the c_v decreased to 3.2×10^{-3} (6.17 times) and 2.67×10^{-3} cm^2/sec (5.14 times) at 1 and 1.5% fiber concentration of aspect ratio of 40. Similar kind of trend was observed with the aspect ratio of 80 and 120 as well. At same consolidating pressure, comparing with SB30, the c_v of SB20 was determined to be 2.32×10^{-3} cm^2/sec, and it increased to 6.13×10^{-3}, 5.20×10^{-3} and 4.71×10^{-3} cm^2/sec at 0.5, 1 and 1.5% fiber concentration with an aspect ratio of 40, respectively. A similar trend was maintained by other SB20 composites also.

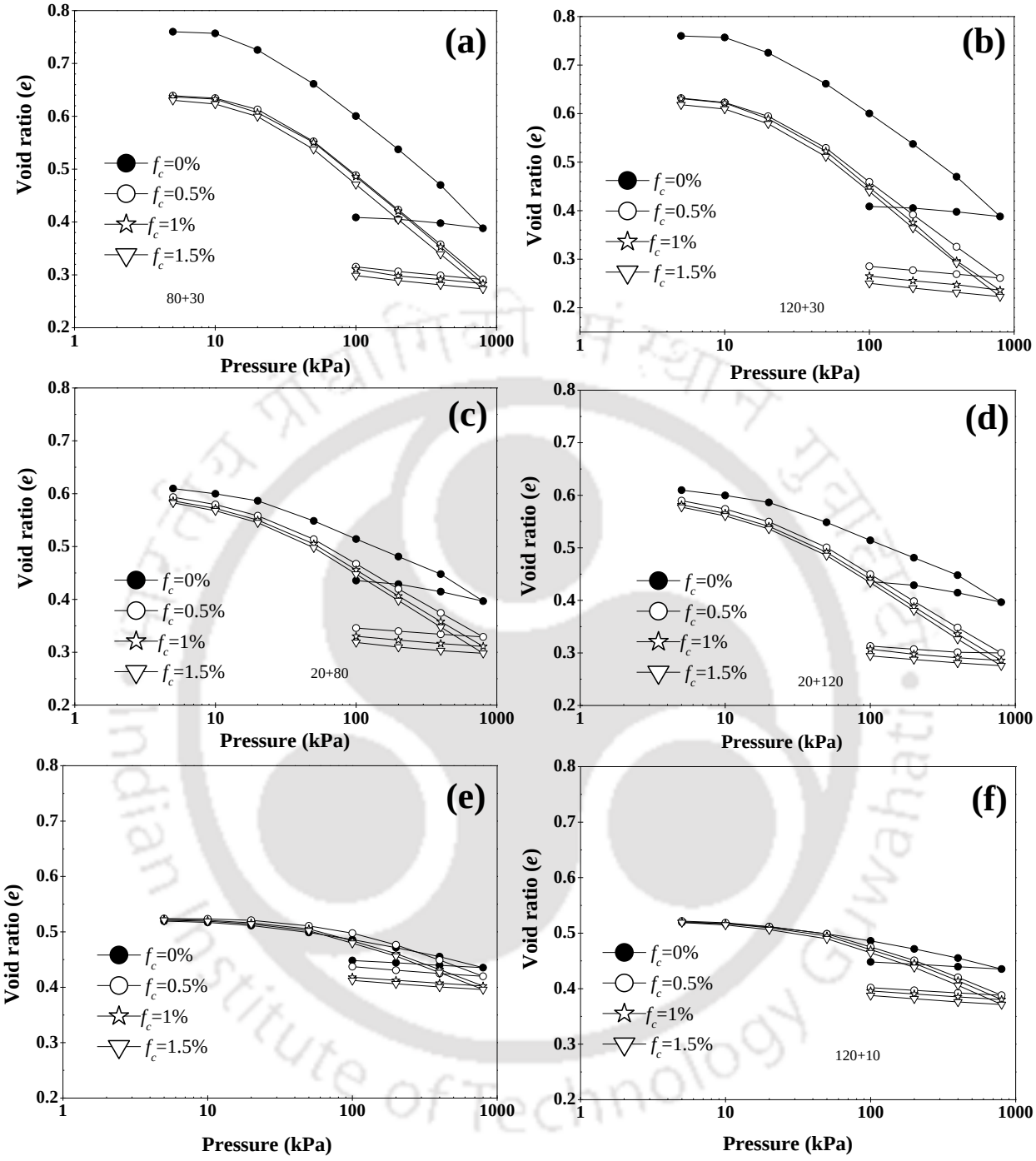

Figure 4.12 volume change behavior of SB-glass fiber composite; (a) SB30 with an aspect ratio of 80;(b) SB30 with an aspect ratio of 80;(c) SB20 with an aspect ratio of 80;(d) SB20 with an aspect ratio of 120;(e) SB10 with an aspect ratio of 80;(f) SB10 with an aspect ratio of 120

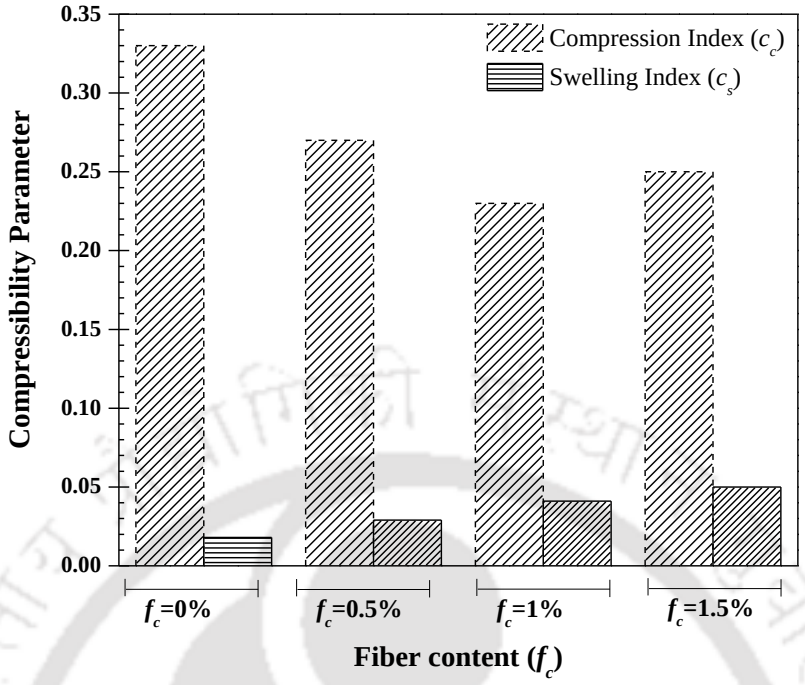

Figure 4.13 Compressibility parameter of SB30 with an aspect ratio of 40

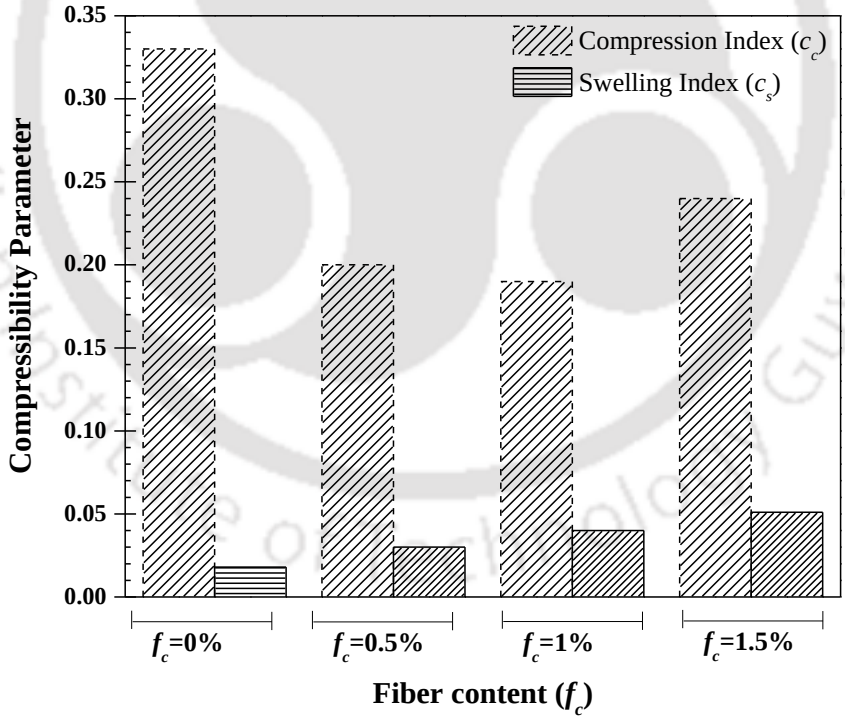

Figure 4.14 Compressibility parameter of SB30 with an aspect ratio of 80

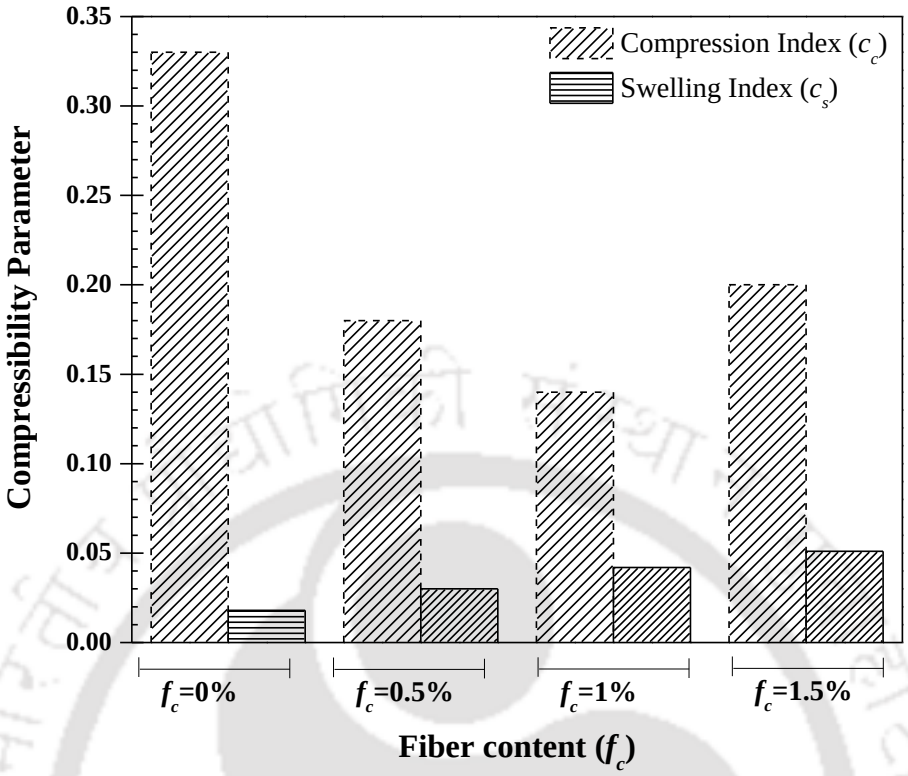

Figure 4.15 Compressibility parameter of SB30 with an aspect ratio of 120

Under a consolidating pressure of 400 kPa, coefficient of consolidation of SB10 was obtained to be 3.23 $\times 10^{-3}$ cm^2/sec and it increased to 7.81×10^{-3} cm^2/sec (2.42 times) at 0.5% fiber concentration, thereafter, it starts to decrease to 6.30×10^{-3} cm^2/sec (1.95 times) and 5.30×10^{-3} cm^2/sec (1.64 times) at 1 and 1.5% fiber concentration with an aspect ratio of 40, respectively. Similar kind of pattern was followed by SB10 composite with other aspect ratios. Hence, it can be concluded from this study that the coefficient of consolidation is not only controlled by the bentonite fraction but also by the fiber.

The result also showed that the increment rate of c_v is more prominent at higher clay content. Under a consolidating pressure of 400 kPa, the c_v for SB10 composite was found to be increased from 3.23×10^{-3} cm^2/sec to 5.5×10^{-3} cm^2/sec to 4.7×10^{-3} and 3.9×10^{-3} cm^2/sec at 1.5% fiber concentration

of aspect ratio of 40, 80 and 120, respectively. However, for the similar consolidation pressure the c_v for SB20 composite was increased from 2.32 × 10^{-3} cm^2/sec to 4.8×10^{-3} cm^2/sec, 4.3×10-3 cm^2/sec and 2.8×10^{-3} cm^2/sec at 1.5% fiber concentration with as aspect ratio of 40, 80 and 120, respectively. Similarly, for SB30 composite the c_v was found to be 5.19×10^{-4} cm^2/sec to 1.7×10-3 cm^2/sec, 7.99×10^{-4} and 7.81 × 10^{-4} cm^2/sec with an aspect ratio of 0, 40 and 80 and 120, respectively. This trend also concludes that the fiber aspect ratio also controls the c_v of the composite.

4.2.6 Effect of glass fiber on the hydraulic behavior of different SB mixes

Hydraulic characteristics are perhaps the most required after parameters while dealing with geotechnical barrier materials. Hydraulic conductivity of the material is one of the essential criteria, which must be satisfied in order to use as liner and cover material at the landfill. Many environmental agencies (USEPA 1988; Hauser et al.2001) have suggested that the landfill liner and cover material should have at least a hydraulic conductivity (k) value of 10^{-7} cm/sec and 10^{-5} cm/sec or less, respectively. The effect of glass fiber on hydraulic conductivity was exhibited in Fig.4.16 and Fig.4.18 for the different sand-bentonite mixture. From the figure it can be seen that at any given void ratio, the hydraulic conductivity was increased initially with the inclusion of fiber; however a further increase in the fiber concentration the hydraulic conductivity of the composite decreased. For example, hydraulic conductivity of the SB30 was measured to be 3.16×10^{-9} cm/sec at 0.49 void ratio. At same void ratio, hydraulic conductivity was increased from 3.16×10^{-9} cm/sec to 4.07×10^{-8} cm/sec at 0.5% fiber concentration with an aspect ratio of 120. A similar trend was also found by Maher and Ho (1994) for kaolinite clay reinforced with glass fiber.

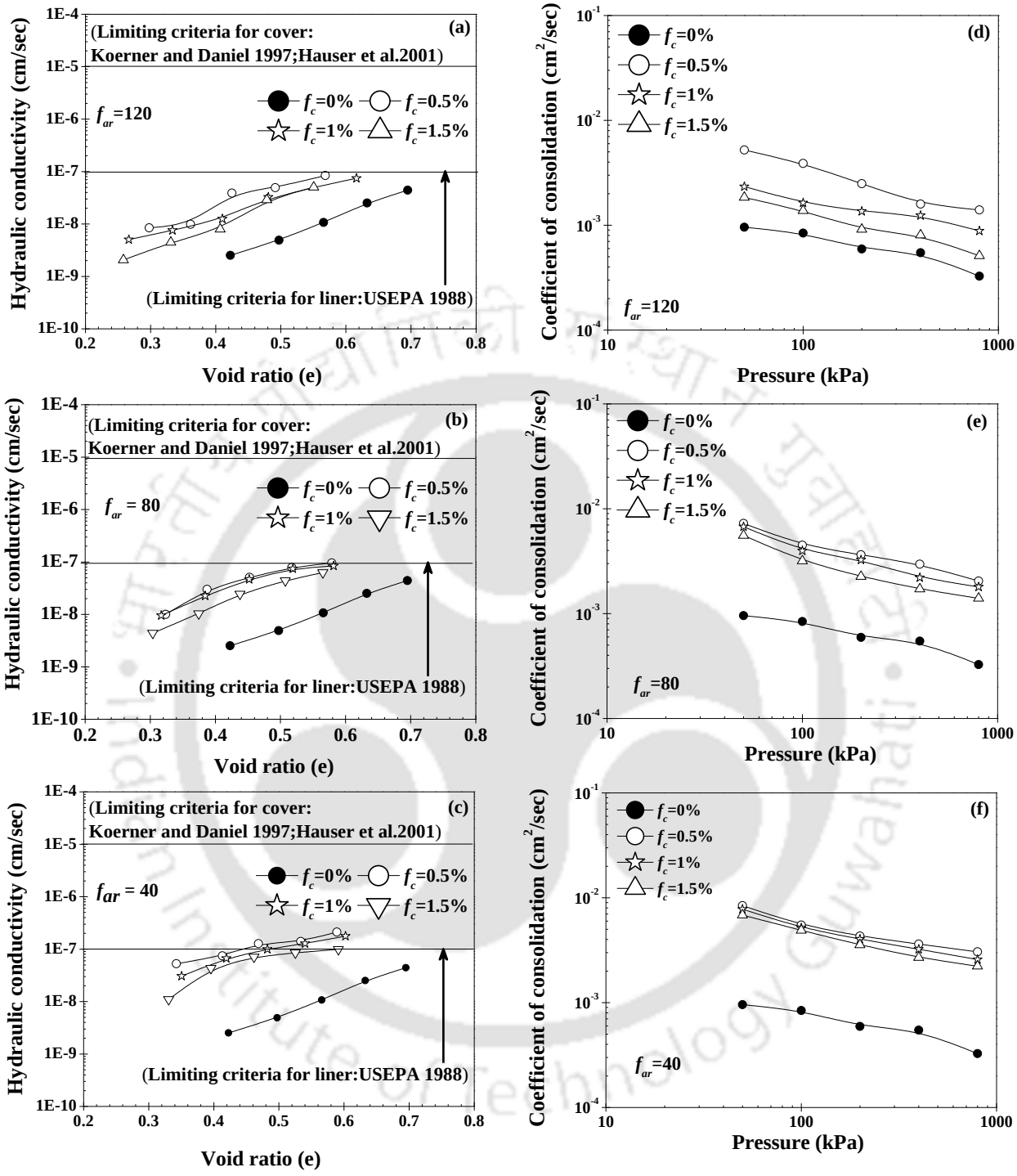

Figure 4.16 Hydraulic conductivity-void ratio (a) SB30 with an aspect ratio of 120; (b) SB30 with an aspect ratio of 80; (c) SB30 with an aspect ratio of 40; Coefficient of consolidation (cv)-pressure of different sand bentonite mixture with different fiber content; (d) SB30 with an aspect ratio of 120; (e) SB30 with an aspect ratio of 80; (f) SB30 with an aspect ratio of 40

However, with an increase in the fiber concentration from 0.5 to 1 and 1.5%, the hydraulic conductivity was decreased from 4.07×10^{-8} cm/sec to 2.02×10^{-8} and 1.54×10^{-8} cm/sec at 1 and 1.5% fiber concentration with an aspect ratio of 120. Rodatz and Oltmanns (1997) obtained a lower hydraulic conductivity for reinforced soil in comparison to unreinforced soil for the plastic clay reinforced with glass fiber. With an aspect ratio of 80, the hydraulic conductivity of SB30 was increased from 3.16×10^{-9} cm/sec to 4.15×10^{-8} cm/sec at 0.5% fiber concentration, after that, it decreased to 3.48×10^{-8} and 2.05×10^{-8} cm/sec at 1 and 1.5% fiber concentration, respectively. With a decrease in aspect ratio from 80 to 40, the hydraulic conductivity raised from 3.16×10^{-9} cm/sec to 8.70×10^{-8} cm/sec at 0.5% fiber concentration; whereas, at 1 and 1.5% fiber concentration it decreased from 8.70×10^{-8} cm /sec to 6.67×10^{-8} cm/sec and 5.59×10^{-8} cm/sec, respectively. The data presented in the figures show that the unreinforced SB20 mixture specimen achieved the higher hydraulic conductivity in comparison to SB30 mixture. However, after the inclusion of the glass fiber, the hydraulic behavior was changed drastically. For example, hydraulic conductivity of SB20 composite was increased initially from 4.49×10^{-9} cm/sec to 6.91×10^{-8} cm/sec due to the inclusion of 0.5% fiber concentration of aspect ratio 120 at a void ratio of 0.45, thereafter, it decreased to 5.30×10^{-8}, and 3.41×10^{-8} cm/sec with the further inclusion of 1 and 1.5% of fiber. However, at the same void ratio, the hydraulic conductivity was increased from 4.49×10^{-9} cm/sec to 8.58×10^{-8} cm/sec and then decreased to 6.03×10^{-8} and 4.63×10-8 cm/sec due to the inclusion of fiber of 0.5, 1 and 1.5% of the aspect ratio of 80. With a decrease in aspect ratio from 80 to 40, the hydraulic conductivity was increased from 4.49×10^{-9} cm/sec to 3.64×10^{-7} cm/sec at 0.5% fiber concentration, but a further increase in the fiber concentration to 1 and 1.5% the hydraulic conductivity reduced to 2.56×10^{-7} (57.02 times) and 1.06×10^{-7} cm/sec (23.61 times) at 1% and 1.5% fiber concentration with an aspect ratio of 40, respectively.

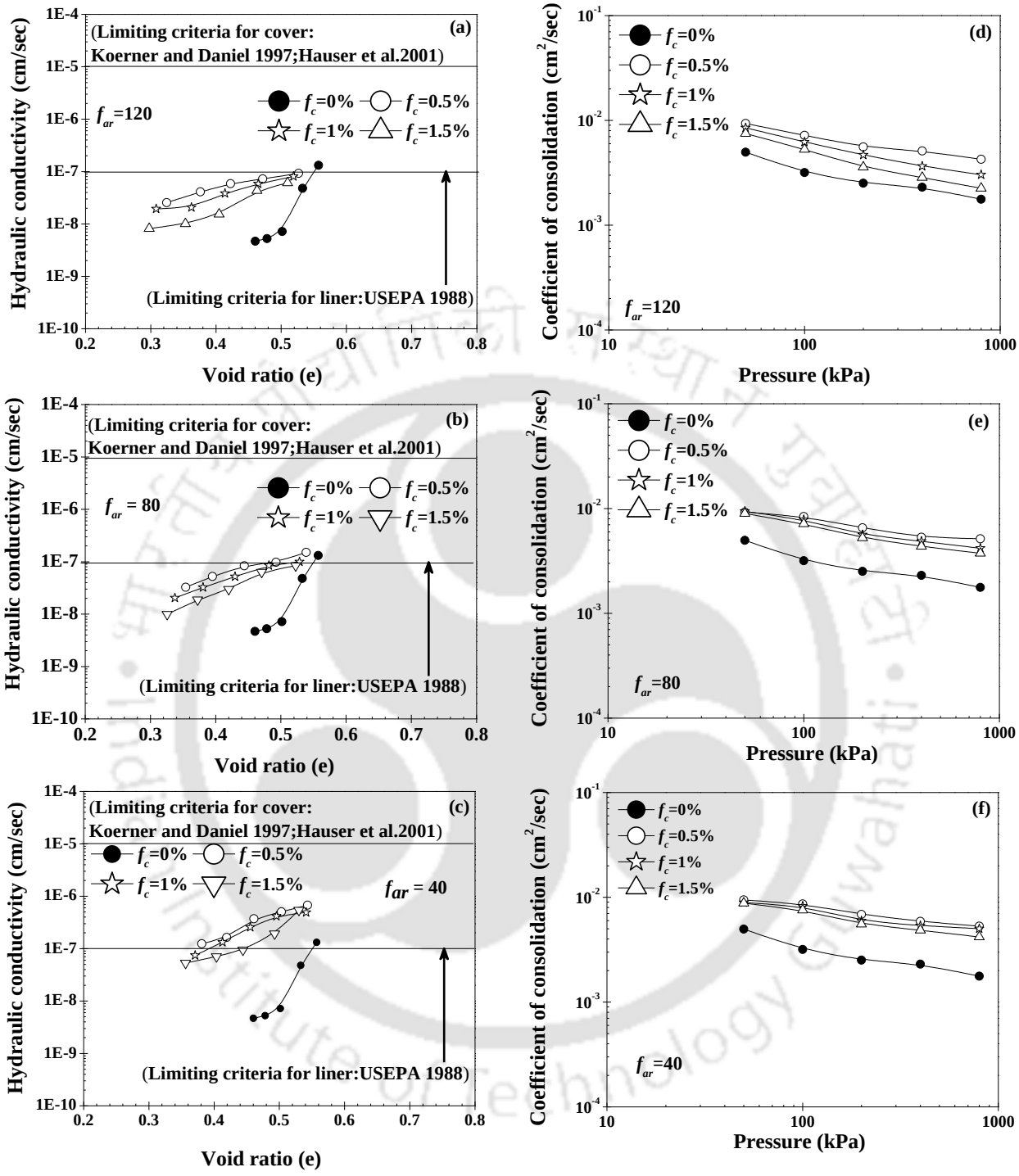

Figure 4.17 Hydraulic conductivity-void ratio (a) SB20 with an aspect ratio of 120; (b) SB20 with an aspect ratio of 80; (c) SB20 with an aspect ratio of 40; Coefficient of consolidation (cv)-pressure of different sand bentonite mixture with different fiber content; (d) SB20 with an aspect ratio of 120; (e) SB20 with an aspect ratio of 80; (f) SB20 with an aspect ratio of 40

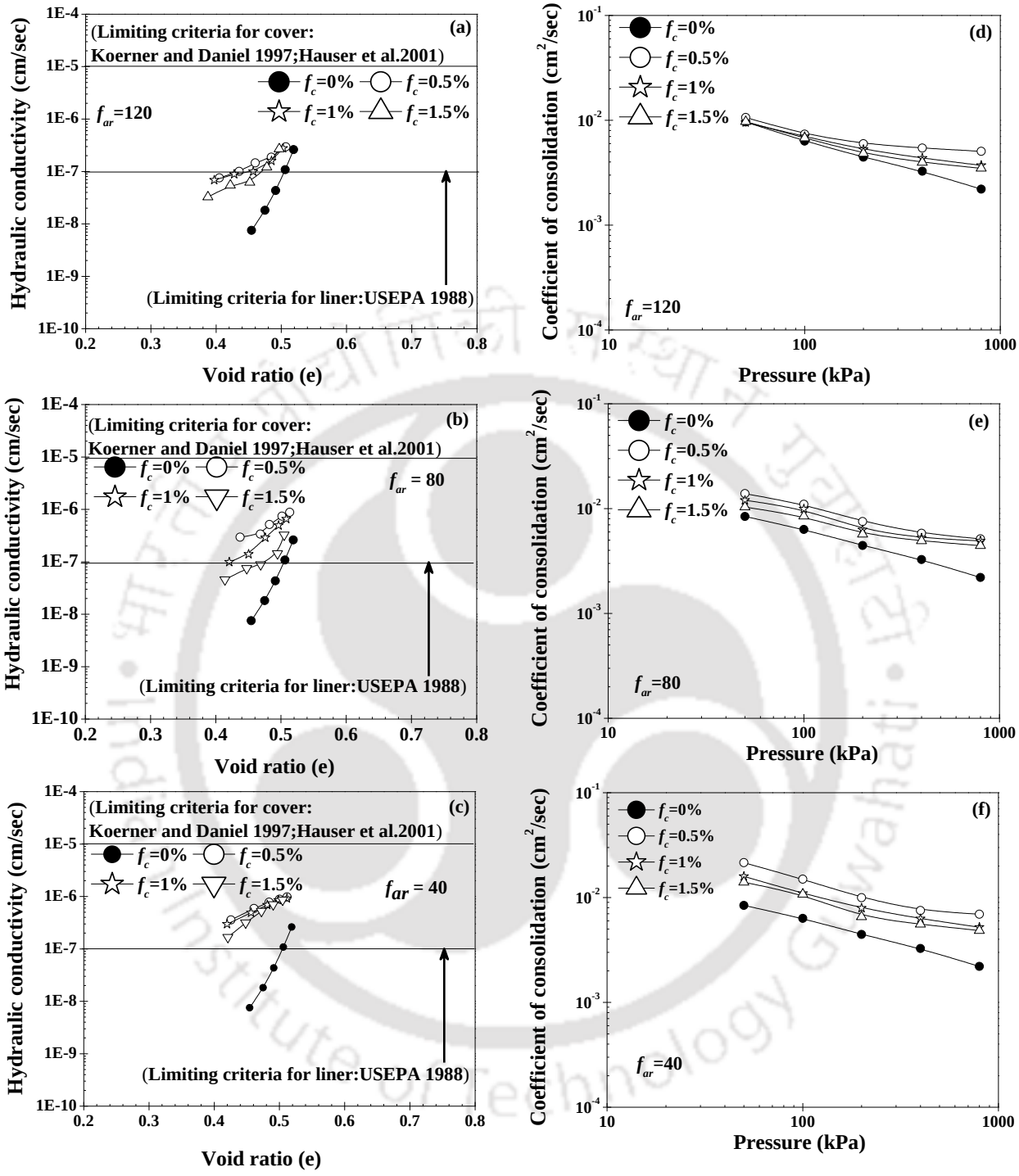

Figure 4.18 Hydraulic conductivity-void ratio (a) SB10 with an aspect ratio of 120; (b) SB10 with an aspect ratio of 80; (c) SB10 with an aspect ratio of 40; Coefficient of consolidation (c_v)- pressure of different sand bentonite mixture with different fiber content; (d) SB10 with an aspect ratio of 120; (e) SB10 with an aspect ratio of 80; (f) SB10 with an aspect ratio of 40

The SB10 reinforced with glass fiber also followed a similar trend as obtained for SB30 and SB20 composite. For example, at 0.45 void ratio, the hydraulic conductivity of the SB10 composite was measured as 7.17 $\times 10^{-9}$ cm/sec, but the hydraulic conductivity was increased significantly from 7.17×10^{-9} cm/sec to 1.32×10^{-7} cm/sec due to the inclusion of 0.5% fiber concentration of aspect ratio 120. At the same aspect ratio, *k* started to decrease from 1.32×10^{-7} cm/sec to 1.01×10^{-7} cm/sec and 5.95×10^{-8} cm/sec with an increase in the concentration from 0.5 to 1 and 1.5% fiber concentration. With the decrease in aspect ratio from 120 to 80, the hydraulic conductivity at the same void ratio was further increased from 7.17×10^{-9} cm/sec to 3.05×10^{-7} cm/sec at 0.5% fiber concentration, but it decreased from 3.05×10^{-7} cm/sec to 1.38×10^{-7} cm/sec and 7.45 $\times10^{-8}$ cm/sec at 1 and 1.5% fiber concentration. Similarly, at same fiber concentration, the hydraulic conductivity was raised from 7.17×10^{-9} cm/sec to 5.32×10^{-7} cm/sec and then dropped to 4.46×10^{7} and 3.14 $\times10^{-7}$ cm/sec with an aspect ratio of 40. A comparison for the hydraulic conductivity at 1.5% of fiber concentration of the aspect ratio 120, 80 and 40 shows that the hydraulic conductivity was enhanced from 7.17×10^{-9} to 3.14 $\times10^{-7}$ cm/sec, 7.45 $\times10^{-8}$ cm/sec and 5.95×10^{-9} cm/sec at respectively. This pattern was also followed by SB20 and SB30 composite.

The result also shows that with the inclusion of glass fiber, the hydraulic conductivity obtained was higher than the limiting value for a landfill liner (i.e.10^{-7}cm/sec), however, lower than the limiting value that for a landfill cover material (i.e. 10^{-5} cm/sec). Hence, it could be recommended to be used for landfill liner and landfill cover.

4.3 Stress-strain behavior of glass fiber soil composite

Landfill engineering structures founded on weak soils are prone to damage as these soils owing to their poor strength and high compressibility undergo bearing capacity failure and a large settlement. The problem is more severe in case of active soils (such as bentonite clay and sand-

bentonite mixture) which undergo a further reduction in shear strength upon increased void ratio due to swelling. The study of the literature suggests that the landfill liner material generally possess a very low value of shear strength (Graham et al.1989; Wan et al.1990 and Jones and Dixon 2005). Therefore, the interest of using fibers has arisen to better improve the landfill material performance as hydraulic barriers. Therefore, a series of consolidated undrained (CU) tests were performed in triaxial apparatus for SB10, SB20 and SB30 mixtures added with 0.5, 1 and 1.5% fiber content of an aspect ratio of 40, 80 and 120 under the confining pressure of 50, 100 and 150 kPa. The results of the stress-strain and pore water responses at the confining pressure of 150 kPa have been discussed below.

4.3.1 Stress-Strain behavior of fiber-reinforced SB10 and SB20 composite

Giroud and Beech (1989) described that the lining structures inclined in the range of 14° to 22° are more prone to uncertainty. Benson and Othman (1993) stated that the hydraulic barrier should also be physically stable in the order it to be used as a landfill material and should have the acceptable shear strength to avoid sliding on the slope. The sliding surface can also occur at points where there is high pore water pressure that result from leachate accumulation along with the interface (Singh and Sun 1995).

The impact of glass fiber on stress-strain behavior is depicted in Fig.4.19 and Fig.4.21 for the different sand-bentonite mixture. It was observed that the behavior of the stress-strain relationship was significantly different with respect to the bentonite fraction. For SB10 composite, plots depicted that the fiber-reinforced specimen exhibited a peak with large strength improvement for all range of confining pressure. It was observed that the deviatoric stress was increased when the fiber content, fiber aspect ratio, and confining pressure increased. Under a confining pressure of 150 kPa, deviatoric stress was increased from 490.1 kPa to 692.1, 922.1, and 1115.3 kPa at 0.5%,1

and 1.5% of an aspect ratio of 40, respectively. At a similar confining pressure, the deviatoric stress was enhanced from 490.1 kPa to 885.3, 1075.0, and 1284.5 kPa at 0.5, 1 and 1.5% fiber concentration with an aspect ratio of 80, respectively. For the aspect ratio of 120, the deviatoric stress was further increased from 490.1 kPa to 1065.0, 1249.7 and 1470.5 kPa, respectively. It was found that deviatoric stress was enhanced maximally from 490.1 kPa to 1115.2, 1284.5 and 1470.5 kPa with an aspect ratio of 40, 80 and 120 at 1.5% fiber concentration, respectively.

Similarly, for SB20 composite the deviatoric stress was increased from 355 kPa to 452.9, 636.0, and 747.0 kPa at 0.5, 1 and 1.5% fiber content with an aspect ratio of 40 under the confining pressure of 150 kPa, respectively. With a further increase in the aspect ratio from 40 to 80, the deviatoric stress was again enhanced from 355.0 kPa to 543.5, 727.5, and 1003.45 kPa. A subsequent increase in the aspect ratio from 80 to 120, the deviatoric stress was increased from 355 kPa to 820.9, 912.9, and 1023.3 kPa. Reinforcing action of the fiber is primarily occurs through local stretching between fiber and adjacent soil particle; as a result, the friction of fiber soil composite was mobilized.

Fiber overcame the limited resistance and thereby it undergoes pullout failure by breakage of fiber, due to tensile stress develops between fiber and soil particle. The breakage of fiber was captured by FESEM study (under 1500 times magnifications) by comparing the fiber before and after the shear (Fig.4.21). It was found that SB10 and SB20 composites were exhibited strain-softening behavior with a sharp peak, however, their load caring capacity was significantly different. SB10 composite was exhibited higher deviatoric stress in comparison to SB20 composite for all aspect ratio. For example, deviatoric stress was decreased from 692.1 kPa to 452.9 kPa at 0.5% fiber content with an aspect ratio of 40 for SB10 and SB20 composite, respectively.

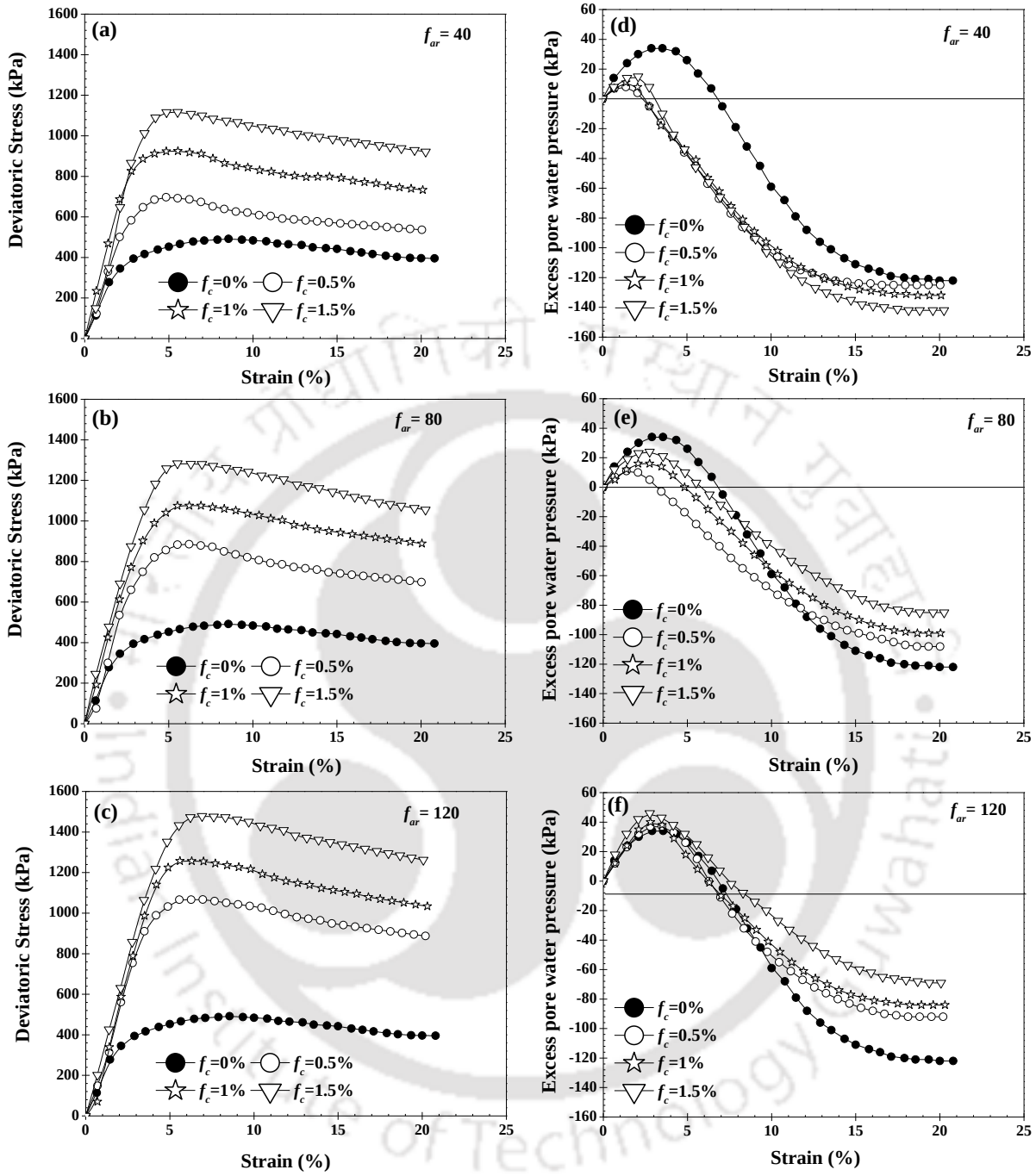

Figure 4.19 Deviatoric stress-strain response of different fiber content under a confining pressure of 150 kPa (a) SB10 composite with an aspect ratio of 40; (b) SB10 composite with an aspect ratio of 80; (c) SB10 composite with an aspect ratio of 120; Excess pore water pressure of different fiber content under a confining pressure of 150 kPa;(d) SB10 composite with an aspect ratio of 40; (e) SB10 composite with an aspect ratio of 80; (f) SB10 composite with an aspect ratio of 120

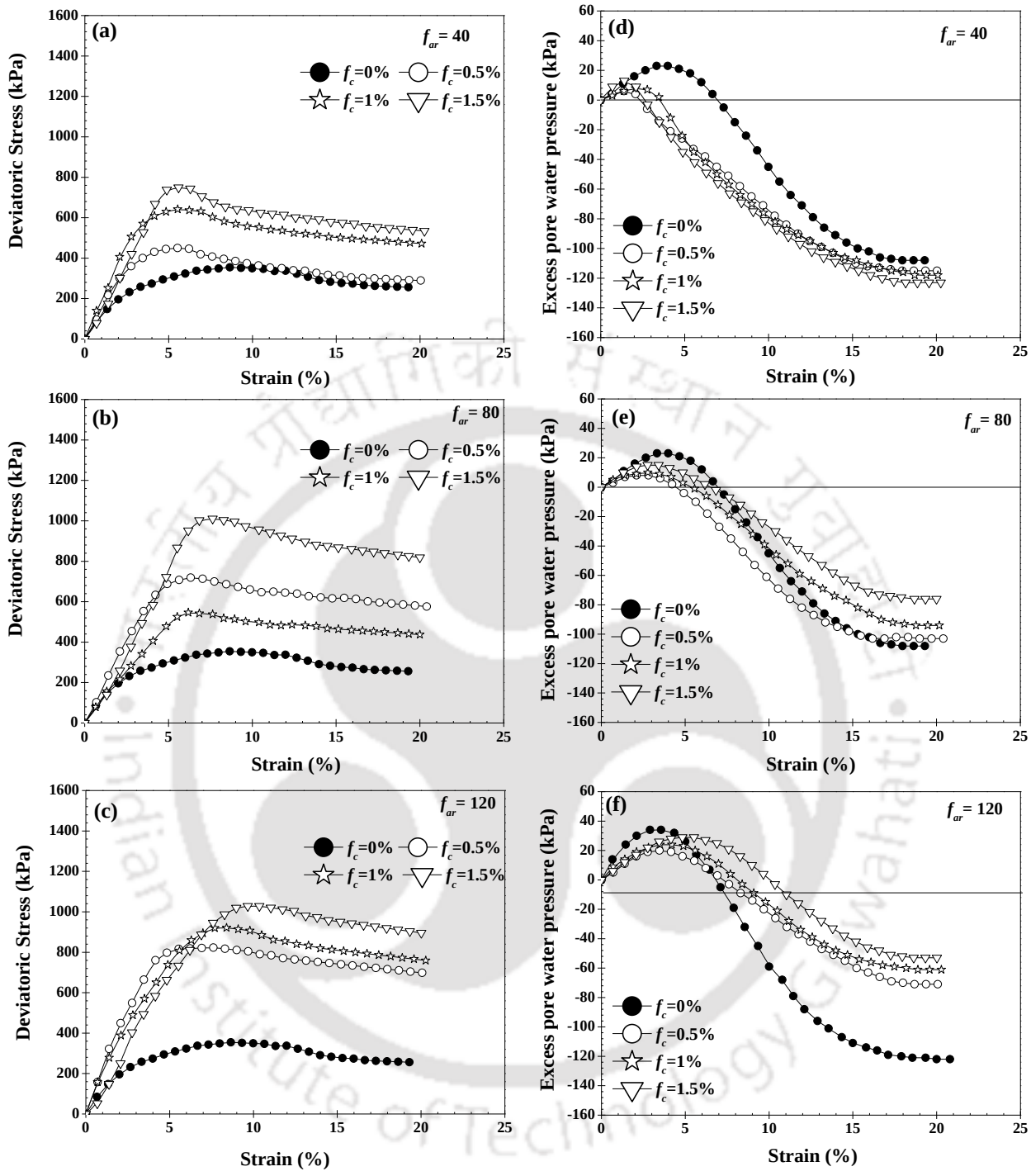

Figure 4.20 Deviatoric stress-strain response of different fiber content under a confining pressure of 150 kPa (a) SB20 composite with an aspect ratio of 40; (b) SB20 composite with an aspect ratio of 80; (c) SB20 composite with an aspect ratio of 120; Excess pore water pressure of different fiber content under a confining pressure of 150 kPa; (d) SB20 composite with an aspect ratio of 40; (e) SB20 composite with an aspect ratio of 80; (f) SB20 composite with an aspect ratio of 120

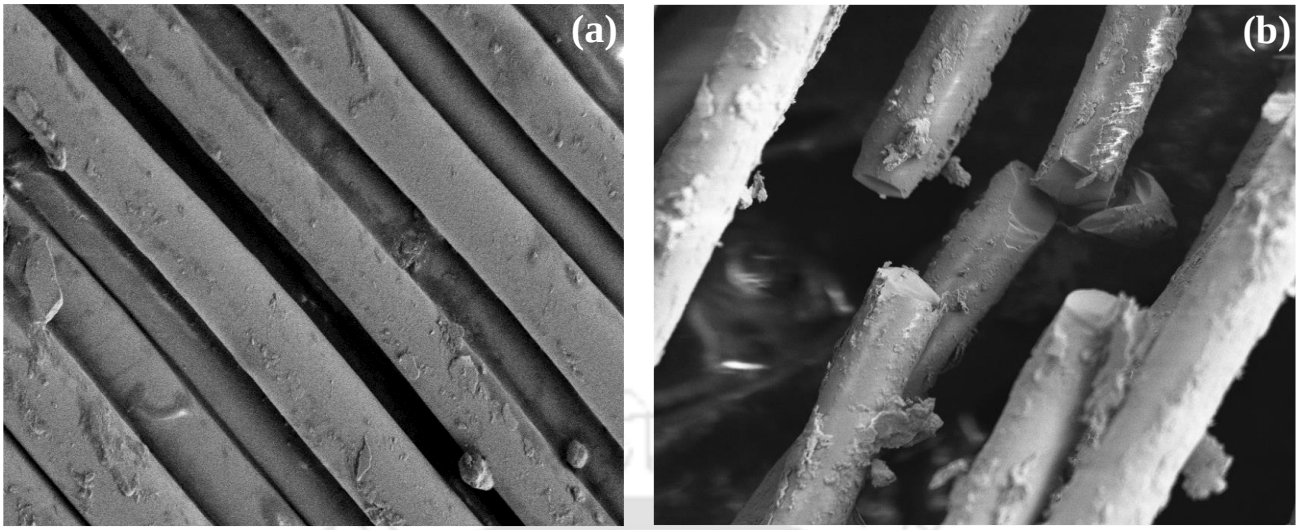

Figure 4.21 Tearing of fiber; (a) fiber before shearing; (b) fiber after shearing

On the other hand, with increase the aspect ratio from 40 to 80, the deviatoric stress was increased from 692.1 to 885.3 kPa at 0.5% fiber content for SB10, whereas, at the same configuration, deviatoric stress was decreased 452.9 to 543.5 kPa for SB20 composite. Hence, it can be concluded that the stress-strain behavior of SB composite was strongly controlled by the percentage of bentonite clay. In this context, bentonite clay did not act as a binder material under the saturated condition and it is likely to be noticed that bentonite is responsible to reduce that load carrying capacity of the SB composite.

4.3.2 Impact of glass fiber on post-peak behavior

It has been found that the post-failure deviatoric stress (at a strain level of 20%) of the fiber-reinforced soil was much higher than that of the unreinforced soil. This uniform trend was followed by the SB10 and SB20 composite. For example, under the confining pressure of 150 kPa, the deviatoric stress of SB10 composite was increased from 354.0 kPa to 538.5, 731.7, and 915.7 kPa at 0.5%, 1 and 1.5% fiber content of aspect ratio of 40, respectively. Under the same confining pressure, the deviatoric stress was increased from 354.0 kPa to 710.5 to 911.8, and 1091.7 kPa at 0.5%, 1 and 1.5% fiber content with the aspect ratio of 80, respectively. Under the same fiber content and confining pressure, post-failure deviatoric stress was enhanced from 354 to 881.0, 1037.4 and 1258.0 kPa with an increase in aspect ratio from 80 to 120.

In a similar manner, comparing to SB20 composite, post-failure deviatoric was found to increase from 256.3 kPa to 291.5, 466.3 and 530.7 kPa at 0.5, 1 and 1.5% fiber content of an aspect ratio 40 under a confining pressure of 150 kPa. Under the same configuration, post-failure deviatoric stress was enhanced from 256.3 kPa to 443.1, 580.9 and 811.3 kPa with an increase the aspect ratio from 40 to 80. However, with increase the aspect ratio from 80 to 120, the post-failure deviatoric stress was improved from 256.3 kPa to 697.0, 761.43 and 890.2 kPa. Hence, it may be concluded that fibers provided the more effective interlocking in the soil-fiber matrix by the producing of additional tensile resistant from the fiber, which led to increasing the residual strength of the composite.

4.3.3 Influence of glass fiber on failure strain

As observed in Fig.4.19 and Fig.4.20, the increase in failure strain due to fiber reinforcement was not consistent, indicating an improvement in the ductility was not significantly altered of the composite under saturated condition. However, the failure strain of the composite was improved gradually with the increase in fiber concentration, confining pressure, and fiber aspect ratio. For example, the failure strain of SB10 composite was 8.23% under a confining pressure of 150 kPa. Under the same confining pressure, the failure strain was decreased from 8.25% to 4.12% at 0.5% fiber content of aspect ratio 40. With the same aspect ratio, the failure strain was increased from 4.12% to 5.54 and 6.32% with a further increase in the fiber content from 1 and 1.5% under the same confining pressure. With the increase the aspect ratio from 40 to 80, the failure strain was relatively improved from 8.23% to 5.91% at 0.5% fiber concentration. With increase the fiber concentration from 0.5% to 1 and 1.5%, failure strain was improved from 5.91% to 6.25 and 7.04% under the same aspect ratio. With increase the aspect ratio from 80 to 120, the failure strain was comparatively improved from 8.32% to 6.02% at 0.5% fiber concentration, however, it was increased from 7.02% to 7.7 and 8.32% with the presence of 1 and 1.5% fiber concentration.

In a similar manner, the failure strain of the SB20 was found to be 9.94 % under the confining pressure of 150 kPa (Fig.4.20a). Under the same configuration, failure strain was reduced from 9.94% to 6.15% at

0.5% fiber concentration of aspect ratio of 40. However, failure strain was improved from 6.15% to 6.60 and 6.71 % at 1% and 1.5% fiber concentration with an aspect ratio of 40, respectively. With increase the aspect ratio from 40 to 80, the failure strain was increased to be 6.21%, 6.76 and 7.61% at 0.5, 1 and 1.5% of fiber content, respectively. With further increase in the aspect ratio from 80 to 120, the failure strain was improved to 6.57%, 8.24, and 9.69% at 0.5%, 1 and 1.5% fiber content, respectively.

The glass fiber offered only small deformations and thereafter, the stress concentration initiated in the fiber-matrix interface. Once adhesion strength is achieved, reinforcement tends to be pulled out quickly (Fig.4.21). As a result, the failure strain decreases with the inclusion of glass fiber but this trend was changed as the fiber aspect ratio increased.

4.3.4 Stress-strain behavior of SB30 composite

It can be noticed that with fiber reinforcement the stress-strain response of SB30 has shown a strain hardening behavior with large strength improvement. Stress-strain behavior of SB30 composite was significantly different from SB20 and SB10 composite. From the earlier analysis, it was observed that SB10 and SB20 composite exhibited strain-softening behavior, but peak behavior was clearly absent for SB30 composite due to predominant clay behavior of the composite and presented in Fig.4.22. However, stress-strain behavior was again altered by the inclusion of glass fiber. The deviatoric stress was found to increase significantly with fiber content up to 1%, thereafter, it starts to decrease with 1.5% fiber content. This pattern was observed for all the fiber aspect ratio. For example, under a confining pressure of 150 kPa, the deviatoric stress (at 20% strain level) was enhanced from 184.43 kPa to 247.68 and 305.17 kPa at 0.5% and 1% fiber concentration with an aspect ratio of 40, respectively. However, the deviatoric stress was decreased from 305.17 kPa to 287.92 kPa at 1.5% fiber concentration of an aspect ratio of 40. With an increase in the aspect ratio from 40 to 80, the deviatoric stress was increased from 184.43 kPa to 318.44 to 370.2 kPa at 0.5% and 1% of aspect ratio 80; thereafter, it was reduced from 370.2 kPa to 332.82 kPa at 1.5% fiber content. Further, increasing the aspect ratio from 80 to 120, the deviatoric stress was

increased from 184.43 kPa to 383.68 and 446.92 kPa and then decreased from 446.92 kPa to 395.2 kPa. As the fiber content increases, the quantity of fibres within the specimen increases and provides more soil-fibre surficial friction, and thus the mobilization of additional fiber tensile strength ultimately increases the specimen strength. However, for higher fiber content (i.e.1.5%), the bonding strength between soil and fiber was not sufficient to improve the deviatoric stress under hydrostatic loading.

4.3.5 Impact of glass fiber on excess pore water pressure (EPP)

Influence of glass fiber on pore water pressure under a confining pressure of 150 kPa has been depicted in Fig.4.19 and Fig.4.20. It was noticed that the EPP was positive at the beginning and finally became negative at higher strain levels for both unreinforced and reinforced samples. This pattern was strongly followed by SB10 and SB20 composite; however, SB30 composite showed a very different pattern in comparison to SB10 and SB20 composite. The result shows that for SB10 and SB20 composite, the EPP increased as the confining pressure increased and decreased as the fiber content and fiber aspect ratio increases. Composite with a dilative tendency exhibited a negative pore water pressure under undrained condition. The negative pore water pressure, which is strongly susceptible to sudden failure (Budhu 2008), decreased continuously due to the inclusion of fiber at a higher level of strain.

This tendency can be explained in terms of change in pore pressure with respect to peak (i.e. peak pore water pressure ratio = $\Delta R/\Delta UR$) (Özkul and Baykal 2007). For example, peak pore water pressure (PPR) of SB10 increased to 1.13, 1.3, and 1.44 at 0.5%, 1 and 1.5% for an aspect ratio of 40, respectively. However, with the increase the aspect ratio from 40 to 80, the PPR reduced to 0.46, 0.38 and 0.27 at 0.5%, 1 and 1.5% fiber content under the confining pressure of 150 kPa. Under the same configuration, PPR reduced to 0.44, 0.31, and 0.25 with the increase in the aspect ratio from 80 to 120. This trend indicates that small aspect ratio forcefully increased the composite stiffness or composite responsible for sudden failure; however, sudden failure might be controlled by the larger aspect ratio of the fiber.

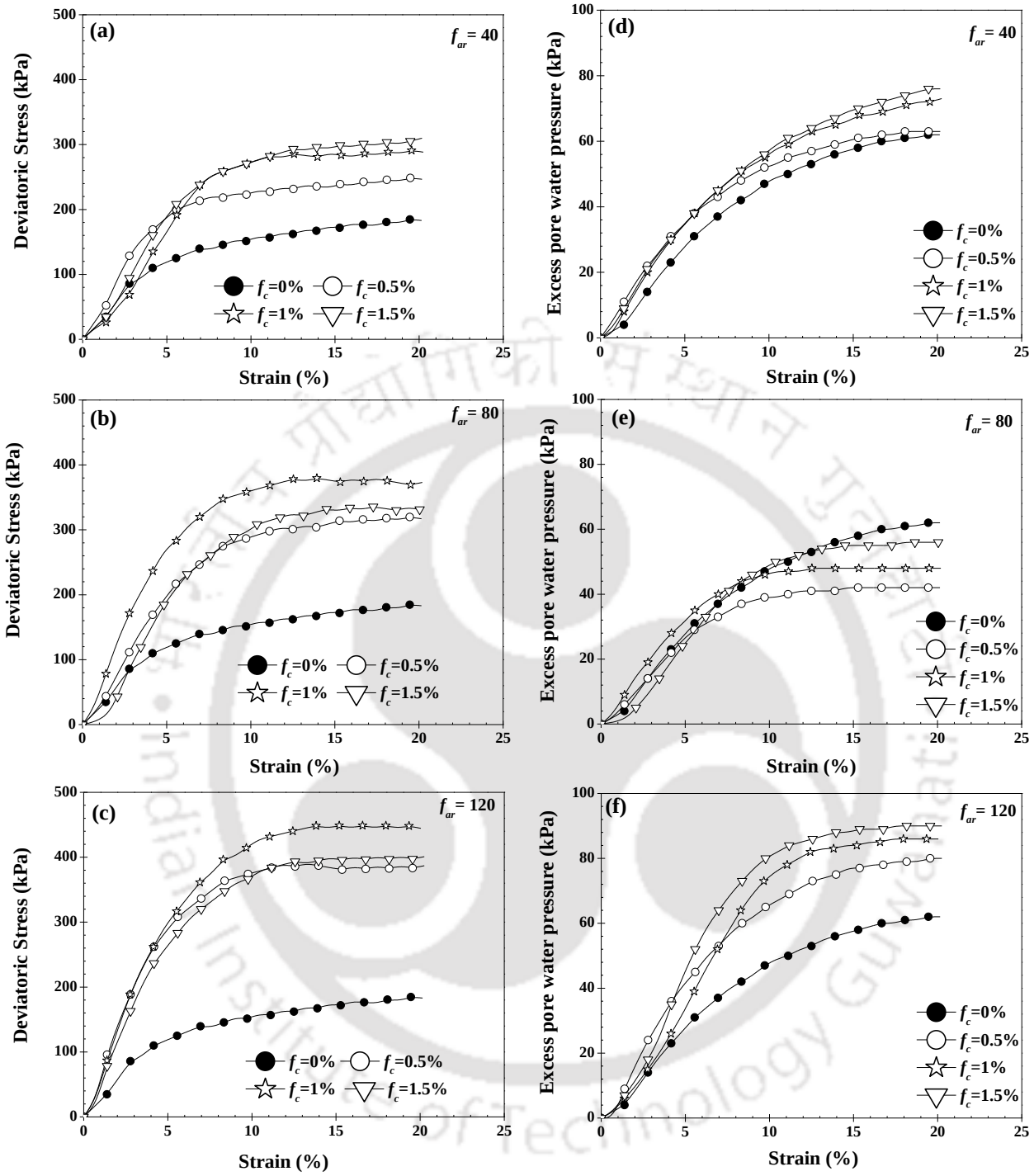

Figure 4.22 Deviatoric stress-strain response of different fiber content under a confining pressure of 150 kPa (a) SB30 composite with an aspect ratio of 40; (b) SB30 composite with an aspect ratio of 80; (c) SB30 composite with an aspect ratio of 120; Excess pore water pressure of different fiber content under a confining pressure of 150 kPa; (d) SB30 composite with an aspect ratio of 40; (e) SB30 composite with an aspect ratio of 80; (f) SB30 composite with an aspect ratio of 120

For SB20 composite, PPR was found to be 0.6, 0.64, and 0.76 at 0.5, 1 and 1.5% fiber concentration of aspect ratio 40, respectively. However, with increase the aspect ratio from 40 to 80, the PPR reduced to 0.33, 0.22 and 0.13 at 0.5, 1 and 1.5%, under the confining pressure of 150 kPa, respectively. Under the same configuration, with the increase in the aspect ratio from 80 to 120, PPR was further reduced from 0.18, 0.15, and 0.11 at 0.5%, 1, and 1.5% fiber concentration, respectively. Hence, it may be concluded that PPR was also affected by the bentonite fraction. As bentonite fraction increased the negative pore-water pressure was continuously reduced when it compared between SB10 and SB20 composite.

The plot also exhibited that maximum positive pore water pressure (PWP) was higher for unreinforced soil in comparison to reinforced soil up to some extent for SB10 and SB20 composite. After that, PWP was continuously increased as the fiber content and fiber aspect ratio increases. For example, for SB10 composite under a confining pressure of 150 kPa, the maximum PWP was found to be 35 kPa; however, it decreased to 8 kPa and then increased to 10 kPa and 15 kPa with the inclusion of 0.5, 1 and 1.5% of fiber content of aspect ratio of 40, respectively. Similarly, with increase the aspect ratio from 40 to 80, the PWP was found to be 11, 15 and 23 kPa at 0.5%, 1 and 1.5% fiber content, respectively. Finally, with a further increase in the aspect ratio from 80 to 120, the PWP again increased gradually from 35 kPa to 36, 41 and 46 kPa at 0.5%, 1 and 1.5%, respectively. A similar pattern was also observed for SB20 composite. Since glass fiber is very stiff in nature, glass fibre-reinforced specimen reaches maximum strength with a small deformation in comparison with unreinforced soil indicating less positive pore water pressure as compared to unreinforced soil under an undrained condition. However, a reverse trend was observed with a higher percentage of glass fiber. Therefore, it can be concluded that the tendency of the positive pore water pressure increases with fiber content and confining pressure indicating an enhancement of the elastic resistance of the composite.

For excess pore pressure, generation of SB30 was very different in comparison to SB20 and SB10. It can be observed that EPP induced only positive pore water pressure during undrained shearing and it was

affected significantly by the inclusion of glass fiber. Comparing to the unreinforced mixture, it was noticed that the EPP of SB30 composite was increased with an aspect ratio of 40 and 120 but decreased with an aspect ratio of 80 for all fiber concentration. For example, EPP was found to increase from 58 kPa to 61, 65 and 71 kPa at 0.5%, 1 and 1.5% fiber concentration with an aspect ratio of 40, respectively. Hence, it can be concluded that more positive excess pore water pressure was accumulated with confining pressure and the elastic resistance of the composite was enhancing due to better bonding between soil -fiber matrix. However, with the increase in the aspect ratio from 40 to 80, the EPP was reduced from 58 kPa to 42, 49 and 54 kPa at 0.5%, 1 and 1.5% fiber concentration of an aspect ratio of 80. The EPP further increased from 58 kPa to 76, 84 and 89 kPa at 0.5% to 1 and 1.5% fiber concentration with an aspect ratio of 120, respectively. From the above analysis, it can be concluded that EPP increases with increase in fiber percentage but reduces with for the aspect ratio 80. Hence, fiber aspect ratio (i.e. 80) played a crucial role to reduce the positive excess pore water pressure, and it led to an increase in the effective stress of the composite.

4.3.6 Normalized response

The undrained strength of compacted fiber composite is normalized by dividing the maximum shear stress (q) by the mean effective consolidating stress (σ'_0) and named as stress ratio. The normalized response has been exhibited in Fig.4.23 to Fig. 4.25 for the composite of SB10, SB20, and SB30. From the figure, it has been observed that stress ratio was decreased as the confining pressure increased and this consistent test result was followed by all the composite. Stress ratio of the unreinforced SB10 was found to be 1.4, 1.65, and 2.28 under an effective confining pressure of 150, 100 and 50 kPa. However, for SB10 reinforced with 0.5% concentration the stress ratio was increased to 2.1, 2.56 and 3.02 kPa under an effective confining pressure of 150, 100 and 50 kPa, respectively. This pattern was followed by other SB10 composites also. Similarly, the stress ratio of SB20 was found to be 0.94, 1.23 and 1.52 under a confining pressure of 150,100 and 50 kPa, respectively. At the same configuration, the stress ratio of SB20

reinforced with fiber concentration of 0.5% was found to be 1.49, 1.67 and 2.0 under an effective confining pressure of 150,100 and 50 kPa, respectively. Similar kind of response was observed for SB20 with another composite also. In a similar pattern, the stress ratio of the SB30 was calculated to be 0.57, 0.64, and 0.75 under an effective confining pressure of 150,100 and 50 kPa, respectively. Under the same confining pressure, stress ratio for reinforced SB30 was found to be 0.72, 0.78, and 1.03 in comparison to unreinforced SB30 mixture. The excess pore water pressure response of compacted–fiber soil composite is normalized by dividing the pore water pressure (Δu_{excess}) by the mean effective consolidating stress and defined as pore water pressure ratio (P_r) as shown in Fig.4.23 and Fig.4.25.

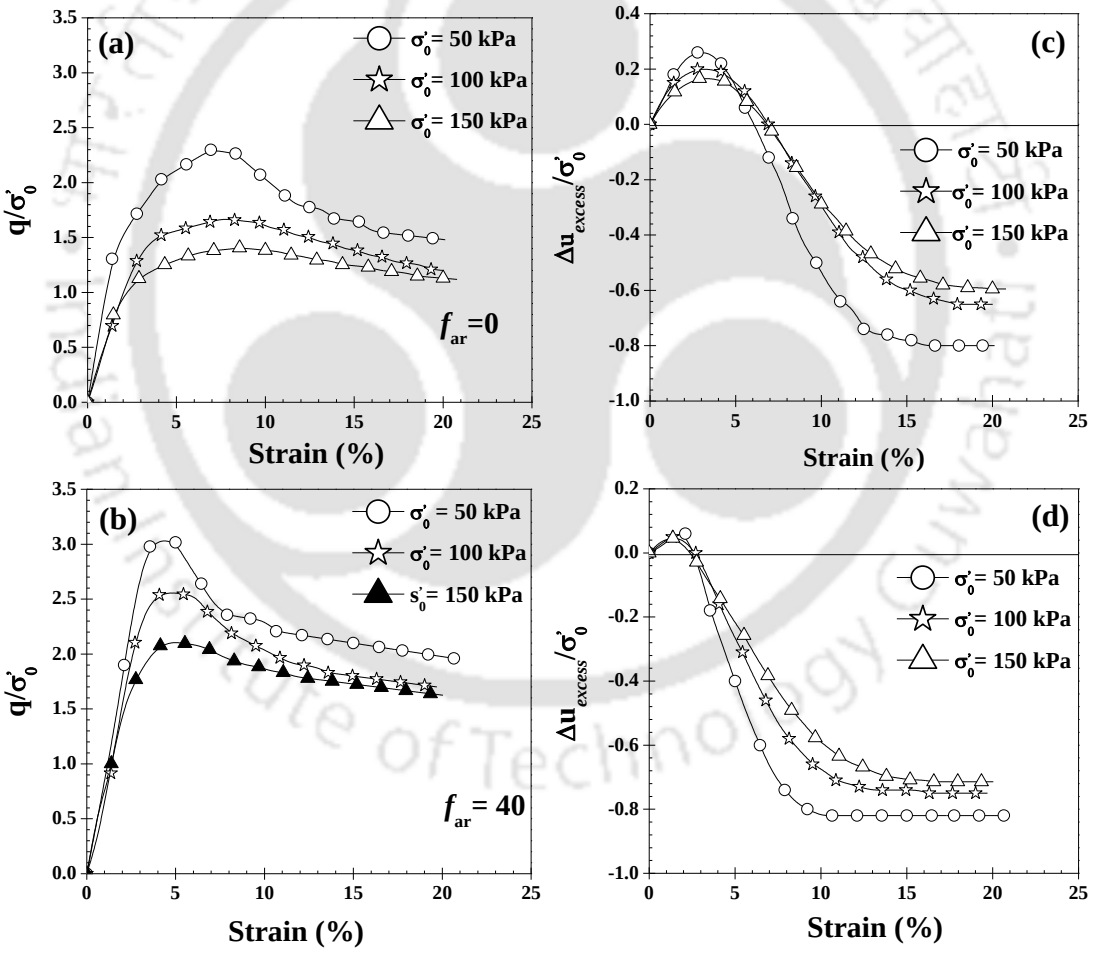

Figure 4.23 Stress ratio-strain with different confining pressure (a) unreinforced SB10; (b) SB10 reinforced with 0.5% fiber concentration with an aspect ratio of 40; Pore water pressure ratio-strain; (c) unreinforced SB10; (d) SB10 reinforced with 0.5% fiber concentration with an aspect ratio of 40

From the figure, it was observed that P_r was continuously decreased as the confining pressure increased. For example, P_r for SB10 composite decreased from 0.24, 0.18, 0.15 under the effective consolidating pressure of 50, 100 and 150 kPa at 2.25% of strain. An identical trend was followed by all composite of SB10. Comparing with SB10, P_r for SB20 composite decreased from 0.08, 0.17, 0.25 under the same effective consolidating pressure at 2.25% of strain and this ratio was less in comparison to SB10 composite.

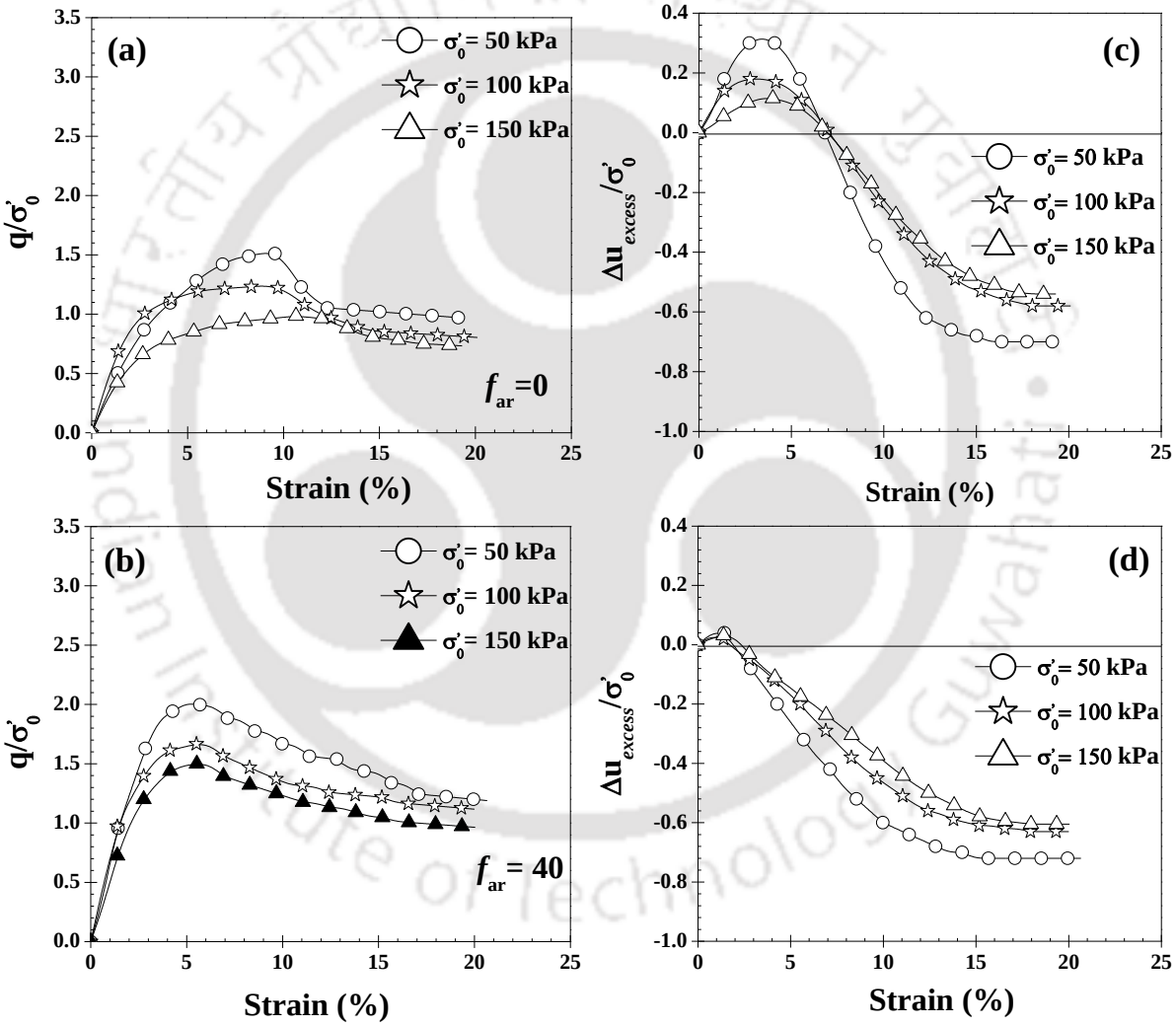

Figure 4.24 Stress ratio-strain with different confining pressure (a) unreinforced SB20; (b) SB20 reinforced with 0.5% fiber concentration with an aspect ratio of 40; Pore water pressure ratio-strain; (c) unreinforced SB20; (d) SB20 reinforced with 0.5% fiber concentration with an aspect ratio of 40

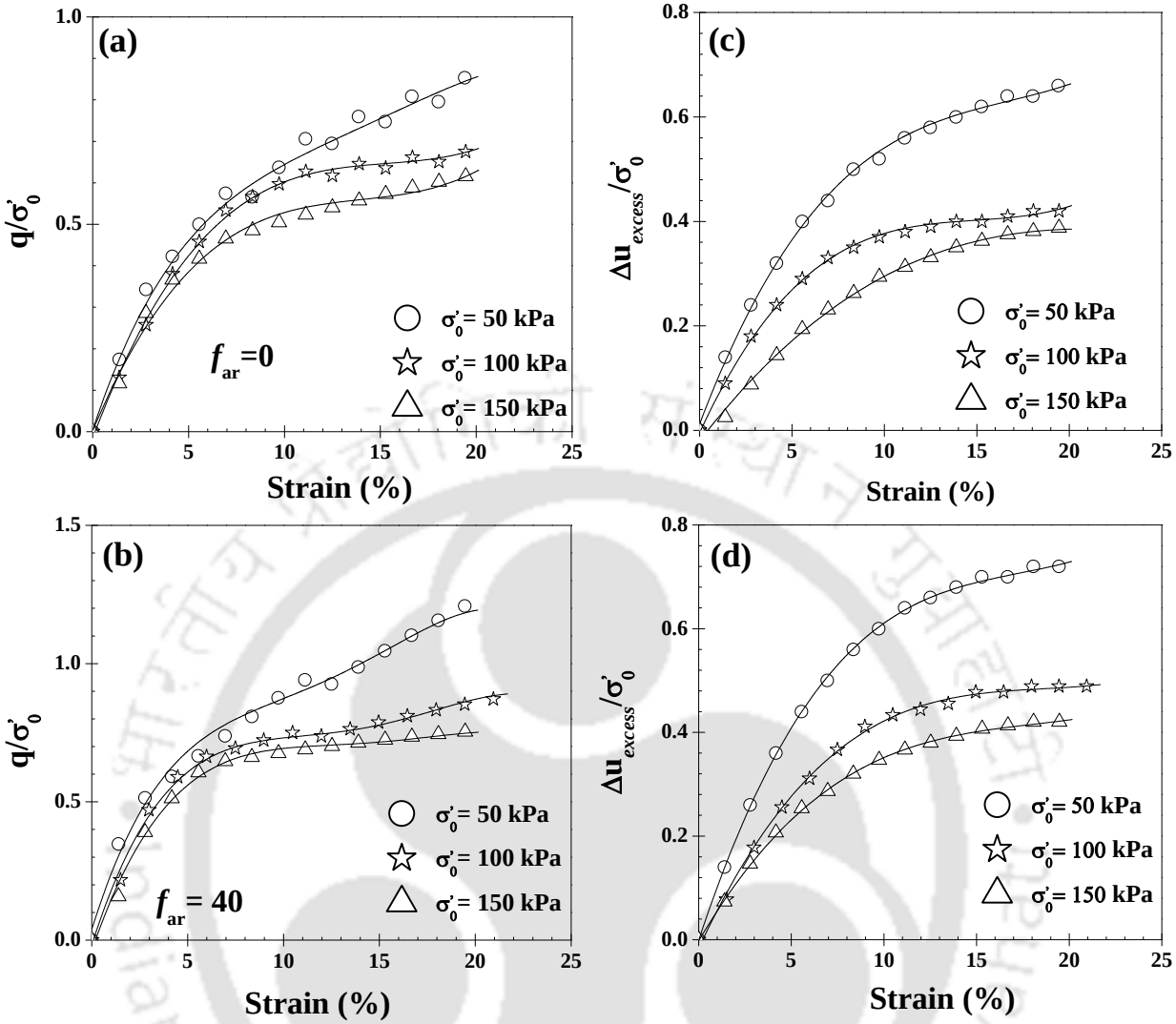

Figure 4.25 Stress ratio-strain with different confining pressure (a) unreinforced SB20; (b) SB20 reinforced with 0.5% fiber concentration with an aspect ratio of 40; Pore water pressure ratio-strain; (c) unreinforced SB20; (d) SB20 reinforced with 0.5% fiber concentration with an aspect ratio of 40

Overall, all the composite exhibited a similar pattern for all SB20 composite. Comparing with SB20, SB30 showed a totally different pore water response during the shearing process. According to their response, P_r was continuously decreased as the confining pressure increased; indicating volume expansion is prevented by the confining pressure. For example, Pr was decreased from 0.19, 0.14 and 0.07 under the effective consolidating pressure of 150, 100 and 50 kPa at 2.25% of strain. Hence, It has indicated that P_r was also affected by the bentonite fraction.

4.3.7 Impact of fiber on moduli of compacted sand-bentonite –fiber composite

The slope of the tangent to the initial section of the curve, a measure of the material's stiffness designated as initial tangent modulus (E_i), was also found out from the stress-strain behavior of the compacted sand-bentonite composite and shown in Fig.4.26 and Fig.4.28. Initial tangent modulus of composite significantly alters with the confining pressure as reported by Rao and Dutta (2006). E_i of the composite was enhanced linearly with the confining pressure and this sharp pattern was followed by all the composite. For example, E_i of the SB10 composite was found out to be 12.93 MPa under a confining pressure of 150 kPa. Under the same confining pressure, E_i increased from 12.93 MPa to 14.73 and 21.92 MPa at 0.5% and 1% and then decreased to 19.61 MPa at 1.5% fiber concentration with an aspect ratio of 40, respectively. Similar kind of pattern was observed for SB10 reinforced with glass fiber (i.e. same amount of fiber content) with an aspect ratio of 80 and 120 and presented in Fig.4.26.

In a similar pattern, E_i of the SB20 was calculated to be 11.25 MPa, however, it was enhanced from 11.25 MPa to 13.82 MPa and 18.18 MPa, at 0.5% and 1% fiber content, thereafter, it dropped from 11.25 MPa to 15.87 MPa at 1.5% with an aspect ratio of 40. At the same configuration, a similar trend was observed with an aspect ratio of 80 and 120 and presented in Fig.4.27.

SB30 composite was also followed the similar trend with different fiber content with an aspect ratio of 40. For example, under the confining pressure of 150kPa, E_i increased from 8.87 MPa, to 9.48 and 13.78 MPa due to increase in the fiber concentration from 0 to 0.5 and 1%, respectively; however, it reduced from 13.78 MPa to 12.55 MPa with a further increase in fiber concentration to 1.5%. SB30 reinforced with glass fiber with an aspect ratio of 80 and 120 exhibited the same trend and presented in Fig.4.28. Hence, it can be concluded that E_i reduced with 1.5% fiber content at any aspect ratio for all the mixtures. It was also noticed that E_i increased when bentonite fraction in the mixture decreases.

According to field condition, the actual applied stress can be at any strain level. Therefore, it is more suitable to specify the stiffness modulus at different strain levels. For any point on the stress-strain curve, the stiffness modulus is the ratio of deviator stress level to the corresponding strain level. Under a confining pressure of 150 kPa, the secant modulus (E_{sec}) was calculated at four different axial strain values (i.e.1.5, 2.5, 5, 10 and 20%) and depicted in Fig.4.26 and Fig.4.28. The result shows that the E_{sec} was increased (corresponding to 2.5% strain level) as the aspect ratio of the fiber increased.

At 0.5% fiber concentration, E_{sec} of the SB10 composite was increased from 17.22 MPa to 19.59, 21.64, 30.37 MPa with an aspect ratio of 40, 80 and 120, respectively. Comparing with SB10, at same fiber concentration, E_{sec} was increased from 16.84 MPa to 18.22, 20.79, and 24.41MPa with an aspect ratio of 40, 80, and 120 for the mixture of SB20 composite, respectively. In case of SB30 composite, at the same configuration, E_{sec} was enhanced from 10.2 MPa to 12.48, 14.78, 18.75 MPa with an aspect ratio of 40, 80 and 120. Hence, it was observed that E_{sec} was significantly enhanced with a different aspect ratio of the fiber and this pattern was followed by the all composite.

It was noticed that E_{sec} gets significantly changed with the addition of fiber concentration. The aspect ratio of 80 used for the comparison of the different composite. From the figure, it was observed that the E_{sec} decreased progressively with increasing axial strain. However, E_{sec} of the composite was increased up to 1% fiber content and then decreased. At 2.5% strain level, E_{sec} of SB10 was increased from 17.22 MPa to 21.84, 24.15 MPa at 0.5 and 1% fiber content; and decreased from 24.15 to 19.53 MPa at 1.5% fiber content under a confining pressure of 150 kPa. However, at the higher strain level, i.e.20%, E_{sec} was increased from 1.44 MPa to 3.49, 5.55 and 6.57 MPa at 0.5, 1 and 1.5% fiber content, respectively. Hence, it is noted that at 1.5% fiber content, reduction tendency of E_{sec} was comparatively less in comparison to 0.5% and 1%, for a relatively high strain level. It is indicating that material property was improved significantly at the high strain level for comparatively soft and compressible soil. An identical trend was followed by the SB20 and SB30 composite and exhibited in Fig.4.27 and Fig. 4.28.

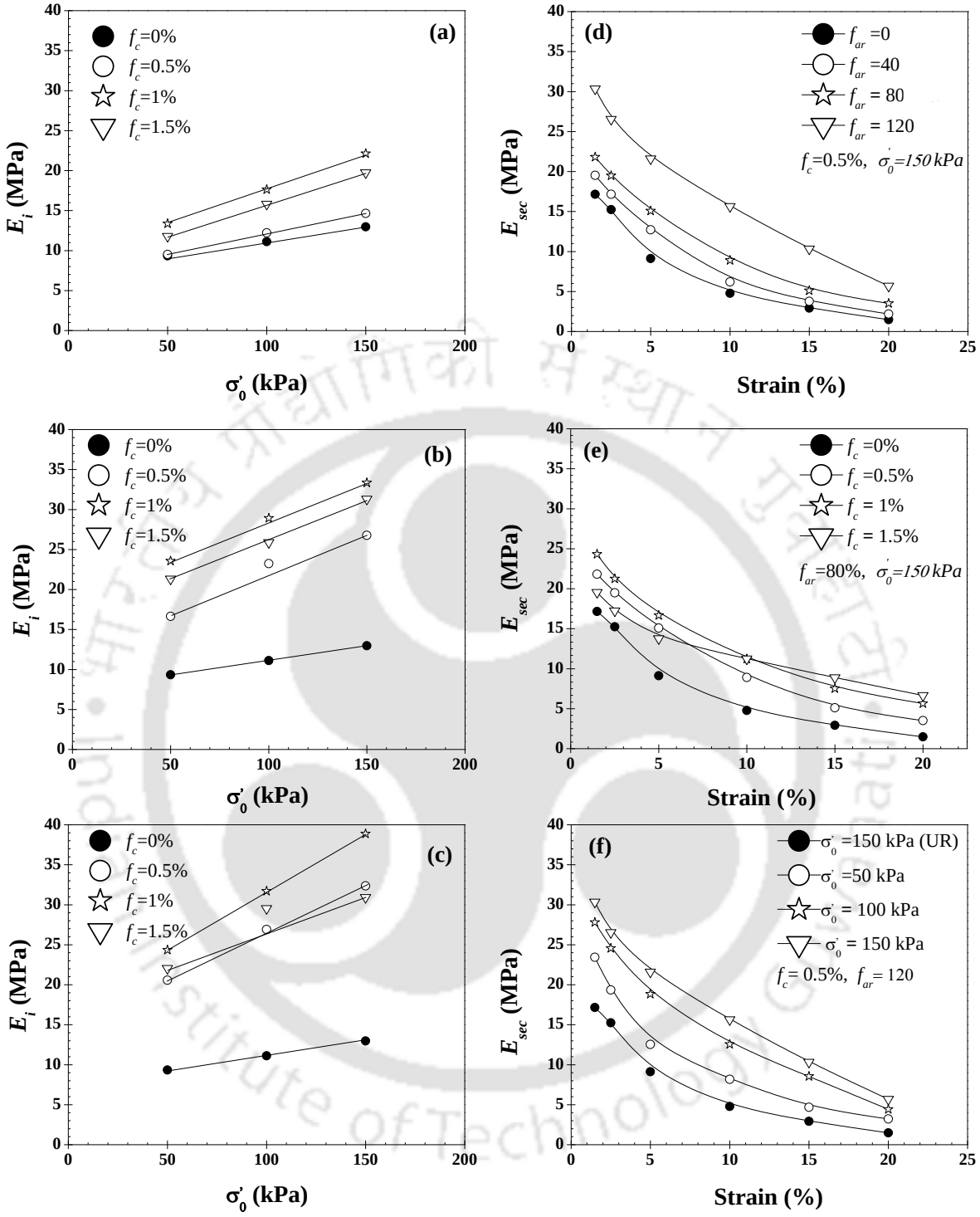

Figure 4.26 E_i-effective consolidating stress with different fiber content (a) SB10 with an aspect ratio of 40; (b) SB10 with an aspect ratio of 80; (c) SB10 with an aspect ratio of 120; E_{sec} –strain response of the composite (d) SB10 with different aspect ratio; (e) SB10 with different fiber content; (f) SB10 with different confining pressure

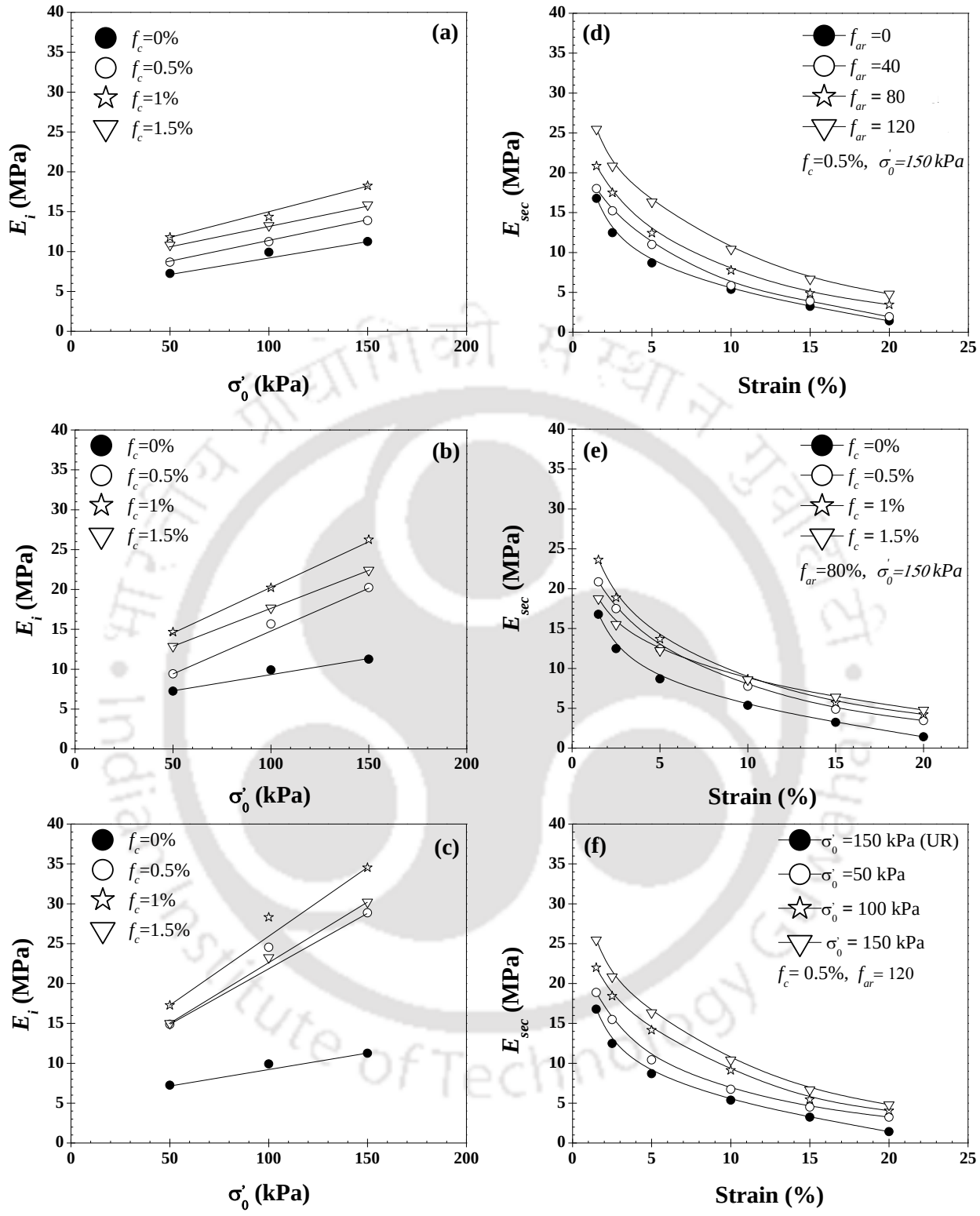

Figure 4.27 Ei-effective consolidating stress with different fiber content (a) SB20 with an aspect ratio of 40; (b) SB20 with an aspect ratio of 80; (c) SB20 with an aspect ratio of 120; Esec –strain response of the composite (d) SB20 with different aspect ratio; (e) SB20 with different fiber content; (f) SB20 with different confining pressure

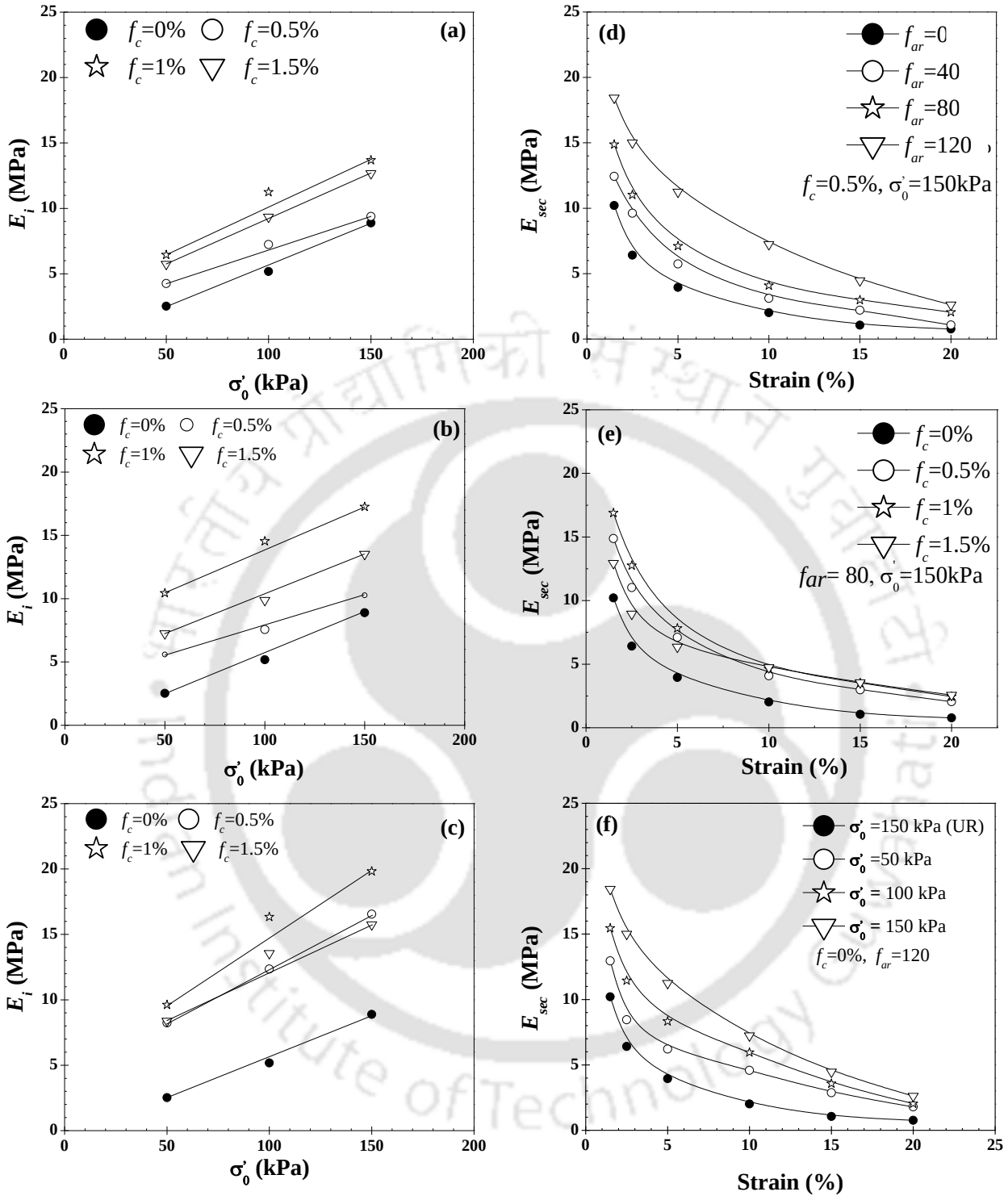

Figure 4.28 E_i-effective consolidating stress with different fiber content (a) SB30 with an aspect ratio of 40; (b) SB30 with an aspect ratio of 80; (c) SB30 with an aspect ratio of 120; E_{sec} –strain response of the composite (d) SB30 with different aspect ratio; (e) SB30 with different fiber content; (f) SB30 with different confining pressure

4.4 Shear strength behaviour of fiber reinforced compacted sand bentonite – glass fiber soil composite

Shear strength parameters of unreinforced and reinforced specimen have been obtained by plotting Mohr's circle and presented in Fig.4.29 to Fig.4.31. The effective stress strength parameter (c' and ϕ') derived from Mohr-Columb theory are widely used in geotechnical practice to quantify the strength of the soil. To avoid a cluster of data, Mohr's circle was depicted in the form of two aspect ratios (i.e. 40 and 80) and two different concentrations (0.5% and 1%) for individual composite. Figure 4.29 indicates that the load-carrying capacity of fiber-reinforced soil is much higher in comparison to unreinforced soil. The failure envelopes specify a general trend of shear strength improvement with fiber reinforcement, with a noticeable increase in both cohesion intercept and friction angle.

In the case of SB10 composite (Fig.4.30), the effective internal frictional angle was increased from 27.3˚ to 31.3˚, 33.6˚ and 35.2˚ due to the addition of 0.5, 1 and 1.5% of the fiber of aspect ratio of 40. Similarly, with increase the aspect ratio from 40 to 80, the effective internal frictional angle was increased from 27.3˚ to 33.7˚, 35.7˚, and 37.1˚ at 0.5%, 1 and 1.5% fiber content. At same fiber content, a similar trend was found for SB10 with an aspect ratio of 120.

The plot in Fig.4.29 and Fig.4.30 exhibited a typical residual strength envelop for both reinforced and unreinforced composite. The residual strength envelops for reinforced and unreinforced specimen were drawn by taking at constant pore water pressure and constant stress-strain data at higher strain level (Console et al.1998). For SB10 composite, ϕ'_{res} was found to increase from 25.3˚ to 26.4˚, 29.8˚ and 37.87˚ at 0.5%, 1 and 1.5% fiber content with an aspect ratio of 40. At same fiber content, ϕ'_{res} was further increased from 25.3˚ to 30.2˚, 32.4˚ and 34.2˚ with increase the aspect ratio from 40 to 80. At same configuration, SB10 composite with an aspect ratio of 120 followed the same pattern.

Based on the peak stress response (Fig.4.30), cohesion component (c') of SB10 was altered by the inclusion of glass fiber. For example, c' for unreinforced specimen was found to be 28.43 kPa, thereafter,

it marginally changed to 26.71, 29.41, 27.42 kPa at due to the inclusion of 0.5, 1 and 1.5% of fiber of aspect ratio 40, respectively indicating that c' was almost constant at smaller aspect ratio with different fiber concentration. However, at same fiber content c' was further increased from 28.43 kPa to 33.7, 35.7 and 37.1 kPa with an increase in the aspect ratio from 40 to 80. With a further increase in the aspect ratio from 80 to 120, the c' further increased from 28.43 kPa to 36kPa at 0.5% fiber content and then reached to a constant value and exhibited in Fig.4.30.

Based on the residual stress response, the effect of glass fiber on c'_{res} was significant and presented in Fig.4.29. From the figure, it was observed that c'_{res} was increased up to some level and thereafter, no improvement was observed with the addition of fiber inclusion. For example, at the fiber content of 0.5% to 1 and 1.5%, c'_{res} was increased from 7 kPa to 10.74 and 16.22 and 18.33 kPa with an aspect ratio of 40, respectively. However, at same fiber content, c'_{res} was further increased from 7 kPa to 22.3, 25.07 and 28.11 kPa with an increase in the aspect ratio from 40 to 80. At the same configuration, it was observed that c'_{res} increased from 7 kPa to 26.22 kPa at 0.5% fiber content and then it moved towards an asymptotic value as shown in Fig.4.30.

The shear stress-effective normal stress relationships of SB20 is shown in Fig.4.31. From the figure, it can be observed that failure line (i.e. k_f = common tangent of the Mohr's circle) of SB20 composite exhibiting a lower shear strength in comparison to SB10. The failure line of SB20 composite exhibiting the shear strength of fiber-reinforced composite was improved significantly. It led to indicate that the effective internal frictional angle was increased continuously with different fiber content and fiber aspect ratio. Based on peak strength envelop (Fig.4.32), ϕ'_p was increased from 24.8˚ to 27.1˚, 30.7˚ and 32.0˚ at 0.5%, 1 and 1.5% fiber content of the aspect ratio of 40, respectively. In a similar way, ϕ'_p was further increased from 24.8˚ to 32.4˚, 34.1˚and 35.8˚ at 0.5%, 1 and 1.5% fiber content with an aspect ratio of 80. Moreover, ϕ'_p was maximally improved from 24.8 ˚to 35.9 ˚at 1.5% fiber content with an aspect ratio of 120.

However, based on residual strength envelop (Fig.4.32), ϕ'_r was also enhanced from 18.2˚ to 20.7˚, 25.7˚ and 27.1˚ at 0.5%, 1 and 1.5% fiber content with an aspect ratio of 40. In a similar fashion, ϕ'_r was increased from 18.2˚ to 28.6˚,30.5˚33.3˚ at 0.5% 1 and 1.5% fiber content of aspect ratio of 80 and ϕ'_r was enhanced maximally from 18.2˚ to 33.5˚ at 1.5% fiber concentration with an aspect ratio of 120.

From the peak strength envelop, c'_p was increased gradually from 15.2 kPa to 22.8, 26.6 and 29.0 kPa at 0.5, 1 and 1.5% fiber content with an aspect ratio 40, respectively. Similarly, the SB20 composite with an aspect ratio of 80 followed a similar trend as discussed earlier. It was noticed that c'_p increased maximally from 15.2 kPa to 30.2 kPa at 1.5% fiber content with an aspect ratio of 120; thereafter, it moved towards an asymptotic value.

From residual strength envelop, the cohesion component was increased from 2.9 kPa to 9.2, 9.9 and 11.5 kPa at 0.5, 1 and 1.5% fiber content of aspect ratio of 40, respectively. At same configuration, c'_r was further enhanced from 2.9 kPa to 14.5, 19.4 and 25.5 kPa at 0.5%, 1 and 1.5% fiber content with an aspect ratio of 80, respectively. The c'_r was found to improve maximally from 2.9 kPa to 25.5 kPa at 1.5% fiber content and then it moved towards an asymptotic value and exhibited in Fig.4.32.

The stress-strain response of the SB30 composite was discussed in earlier section i.e. Fig.4.25. From the stress-strain behavior, it has been observed that SB30 composite is showing strain hardening behavior and it has been also noticed that excess pore water was almost getting towards an asymptotic value but some cases, it did not reach towards asymptotic value. Hence, for simplicity, residual strength was not discussed yet, however, all the required data has been considered up to 15% strain level.

The shear stress-normal stress relationships have been presented in Fig.4.33. From the figure, it has been observed that the diameter of the Mohr's circle was much smaller in comparison to SB20 composite. However, the k_f line of the fiber-reinforced composite was significantly improved up to 1% fiber content for all aspect ratio and then it started to decrease with 1.5% fiber content. However, the improvement of the shear strength (i.e.1.5% of glass fiber content) was always higher in comparison to unreinforced soil.

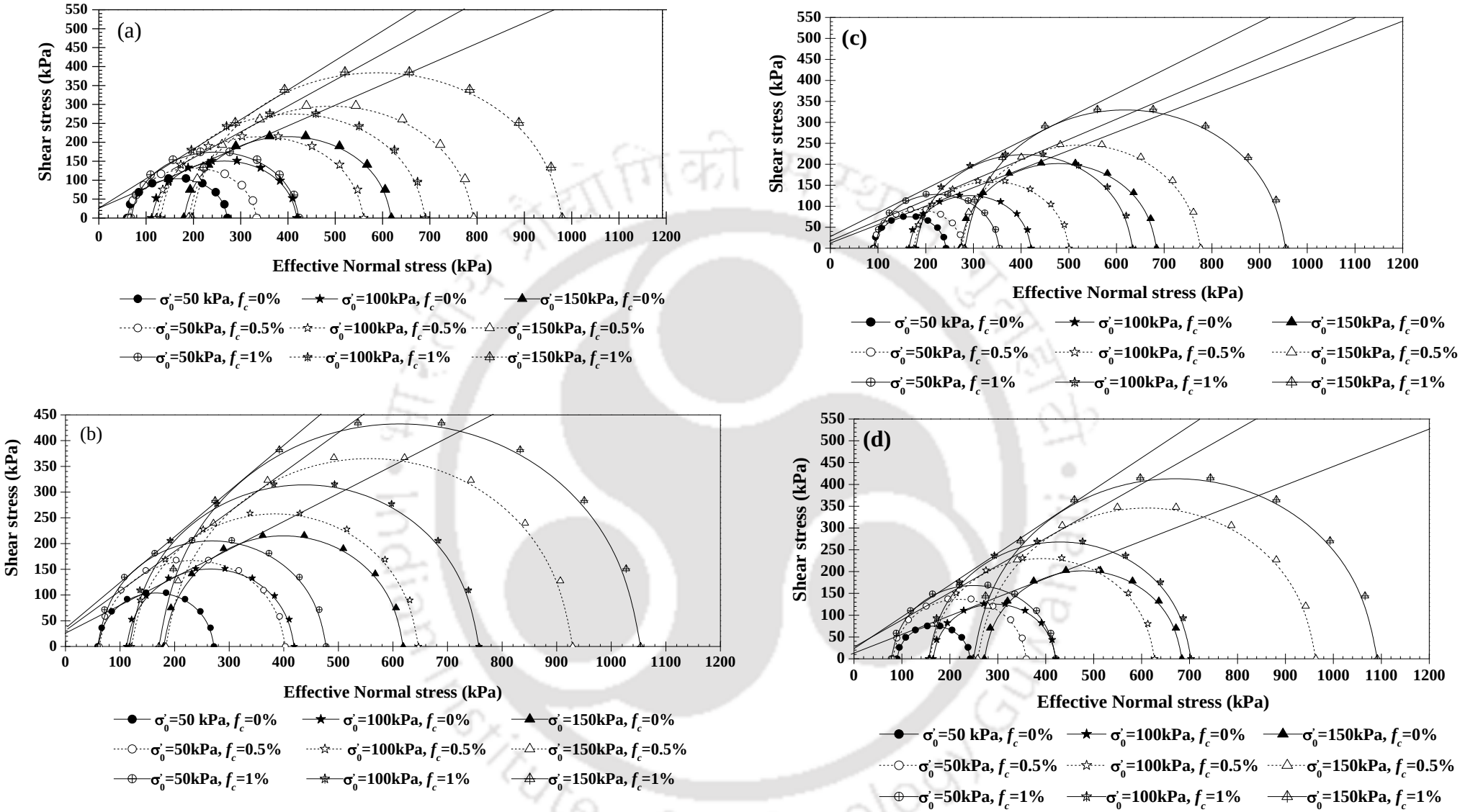

Figure 4.29 Mohr's circle of SB10 composite at concentration of 0.5% and 1%; (a) Peak strength envelop with an aspect ratio of 40; (b) Peak strength envelop with an aspect ratio of 80; (c) Residual strength envelop with an aspect ratio of 40;(d) Residual strength envelop with an aspect ratio of 80

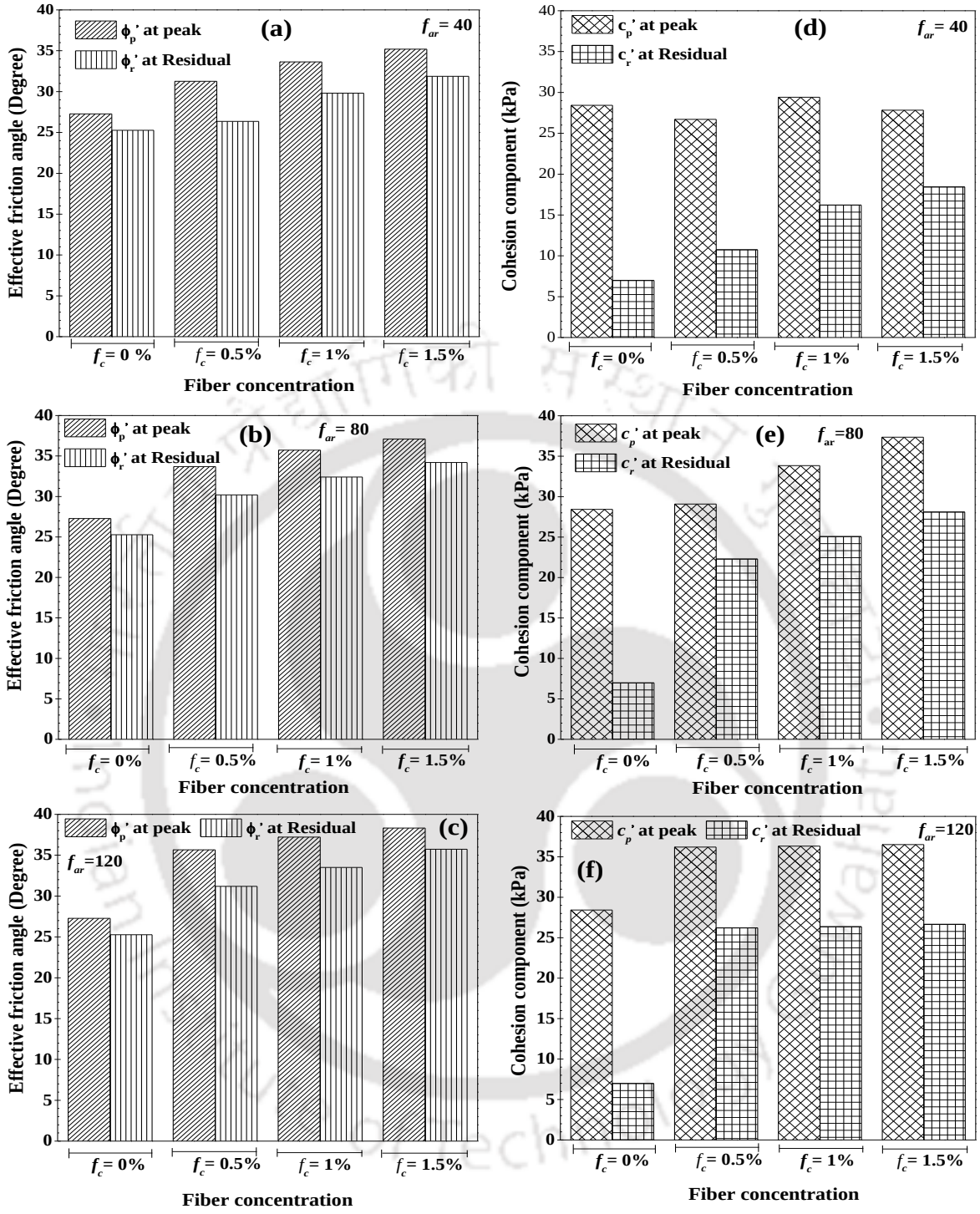

Figure 4.30: Shear strength parameter of SB10 composite; (a) Effective frictional angle of peak and residual with an aspect ratio of 40; (b) Effective frictional angle of peak and residual with an aspect ratio of 80;(c) Effective frictional angle of peak and residual with an aspect ratio of 120;(d) Effective cohesion component of peak and residual an aspect ratio of 40;(e) Effective cohesion component of peak and residual an aspect ratio of 80;(f) Effective cohesion component of peak and residual an aspect ratio of 120

For example (Fig.4.34), ϕ' was found to increase from 21.1˚ to 24.8˚, 28.0˚ at 0.5 and 1% fiber content and then it started to decrease from 28.0˚ to 27.1˚ at 1.5% fiber content with an aspect ratio of 40. Similarly, it was also noticed that ϕ' was further increased from 21.1˚ to 28.7˚ and 30.6˚ at 0.5 and 1% fiber content and then it moved to reduce from 21.1˚ to 28.8˚ at 1.5% fiber content with an aspect ratio of 80. An identical trend was followed by SB30 reinforced with glass fiber with an aspect ratio of 120 and exhibited in Fig.4.34. On the other hand, cohesion component (*c'*) was found to increase from 14.9 kPa to 18.8 kPa 26.2 and 26.2 kPa at 0.5%, 1 and 1.5% with an aspect ratio of 40. Hence, it is indicating that *c'* was increased up to 1% thereafter, no significant change was observed with the inclusion of high fiber concentration. However, with increase the aspect ratio from 40 to 80, *c'* was found to increase from 14.9 kPa to 21.8 kPa, 25.7 kPa and 19.57 kPa at 0.5%, 1 and 1.5% fiber content, respectively. With increase the aspect ratio of 80 to 120, the *c'* was increased from 14.9 kPa to 26.26, 20.68 and 20.84 kPa at 0.5, 1 and 1.5% fiber concentration, respectively.

From the above analysis, it was found that the shear strength parameters of the reinforced composite were improved significantly. However, the effective internal angle was enhanced more in comparison to the cohesion component at high fiber content as well as the high aspect ratio. Hence, reinforcing action is developed primarily by local stitching in between fiber and their adjacent soil particle; as a result, tensile stress developed to the mobilization of friction and interlocking resistance was increased over its surface. To some extent, fiber overcomes this limited resistance and thereby suffers pullout failure else undergoes breakage leading to rupture the fiber. This complex geometry was accountable for the surface rupture of the fibre. The surface rupture of the fibre was recorded by FESEM (with1000 times magnifications) and presented in Fig.4.35 comparing the fibre after (Fig.4.35a) and before shear (Fig.4.35b).

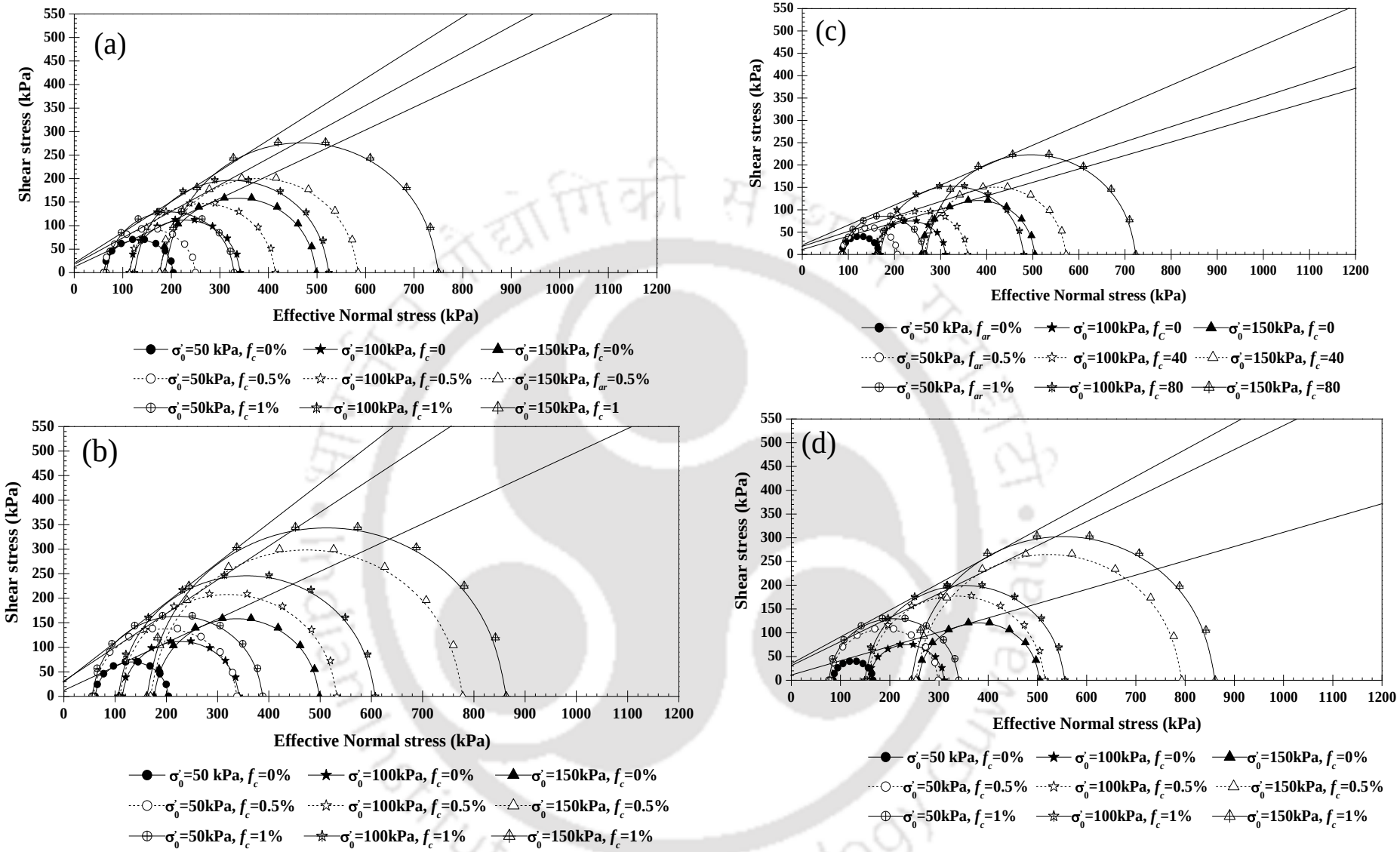

Figure 4.31 Mohr's circle of SB20 composite at concentration of 0.5% and 1%; (a) Peak strength envelop with an aspect ratio of 40;(b) Peak strength envelop with an aspect ratio of 80;(c) Residual strength envelop with an aspect ratio of 40;(d) Residual strength envelop with an aspect ratio of 80

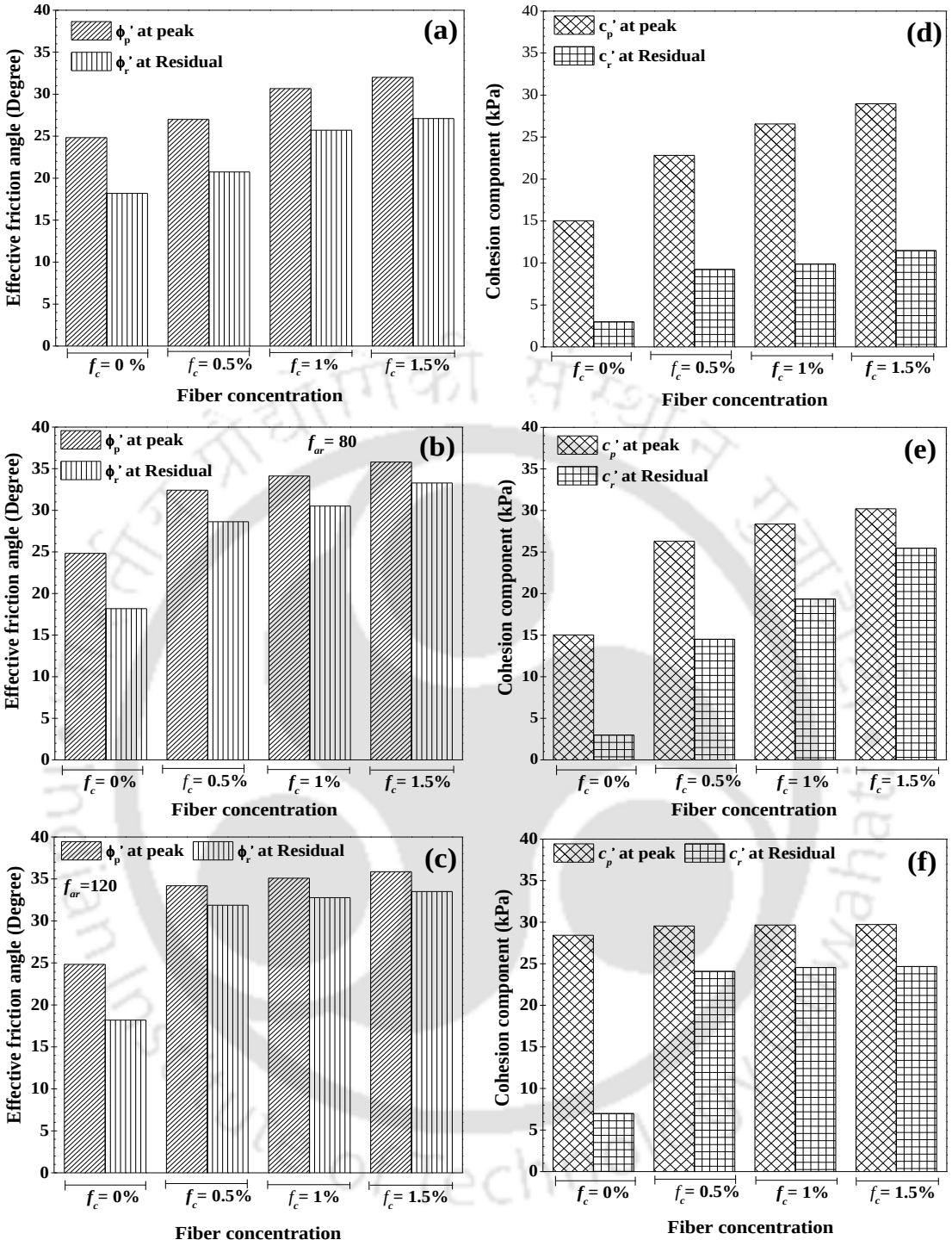

Figure 4.32 Shear strength parameter of SB20 composite; (a) Effective frictional angle of peak and residual with an aspect ratio of 40; (b) Effective frictional angle of peak and residual with an aspect ratio of 80;(c) Effective frictional angle of peak and residual with an aspect ratio of 120;(d) Effective cohesion component of peak and residual an aspect ratio of 40;(e) Effective cohesion component of peak and residual an aspect ratio of 80;(f) Effective cohesion component of peak and residual an aspect ratio of 120

It has been also seen that the cohesion component was altered due to increasing the bonding strength of fiber soil matrix and confining effect. Another interesting observation was found that the shear strength parameter was strongly governed by the bentonite fraction. As bentonite fraction is increased, the shear strength was decreased drastically. Since the saturated bentonite does not act as binder agent and it helps to reduce the overall bonding strength of the matrix (i.e. soil-fiber) due to the highly plastic nature of the bentonite under a saturated condition.

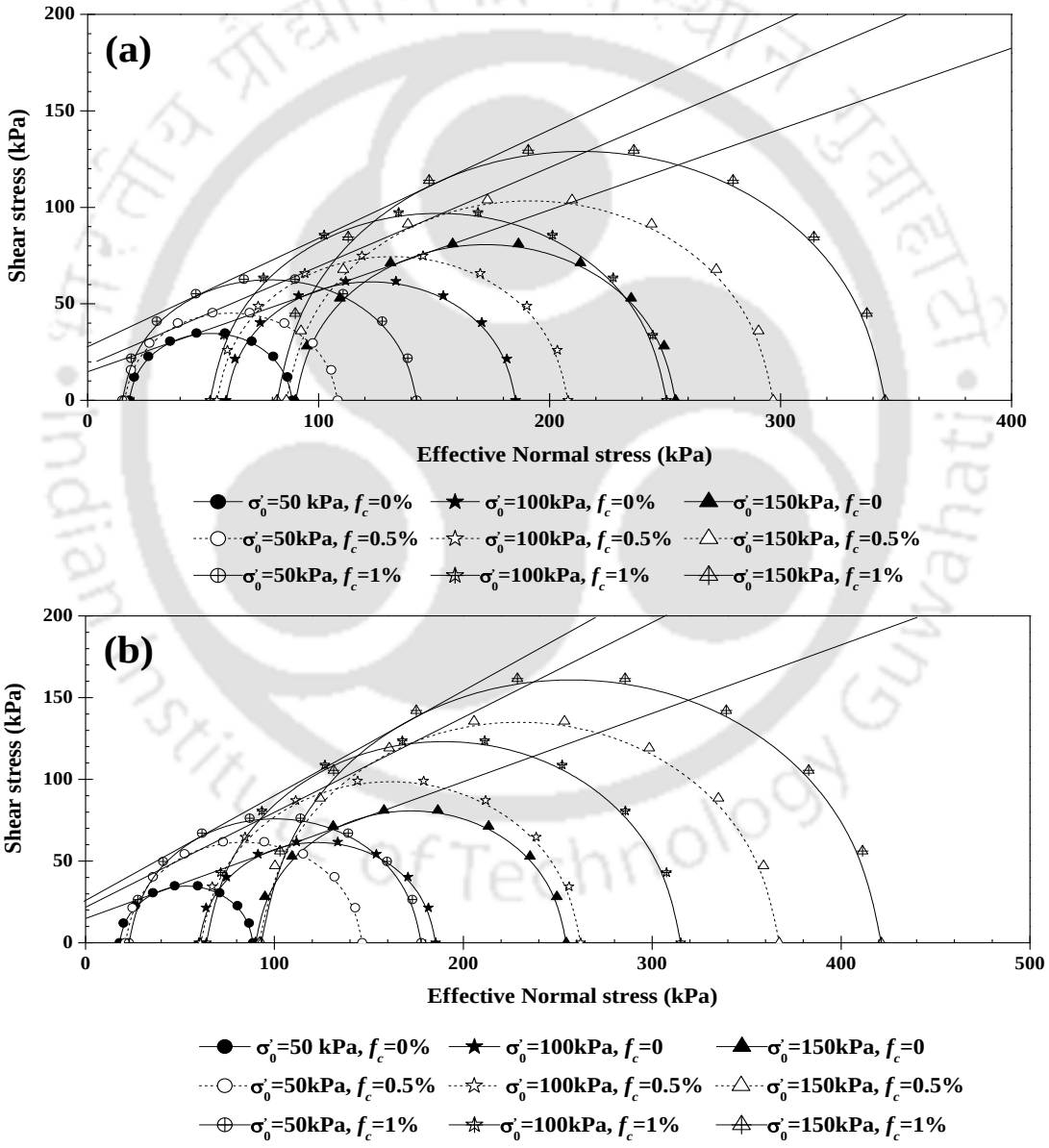

Figure 4.33:Mohr's circle of SB30 composite at concentration of 0.5% and 1%; (a) Strength envelop with an aspect ratio of 40; (b) Strength envelop with an aspect ratio of 80

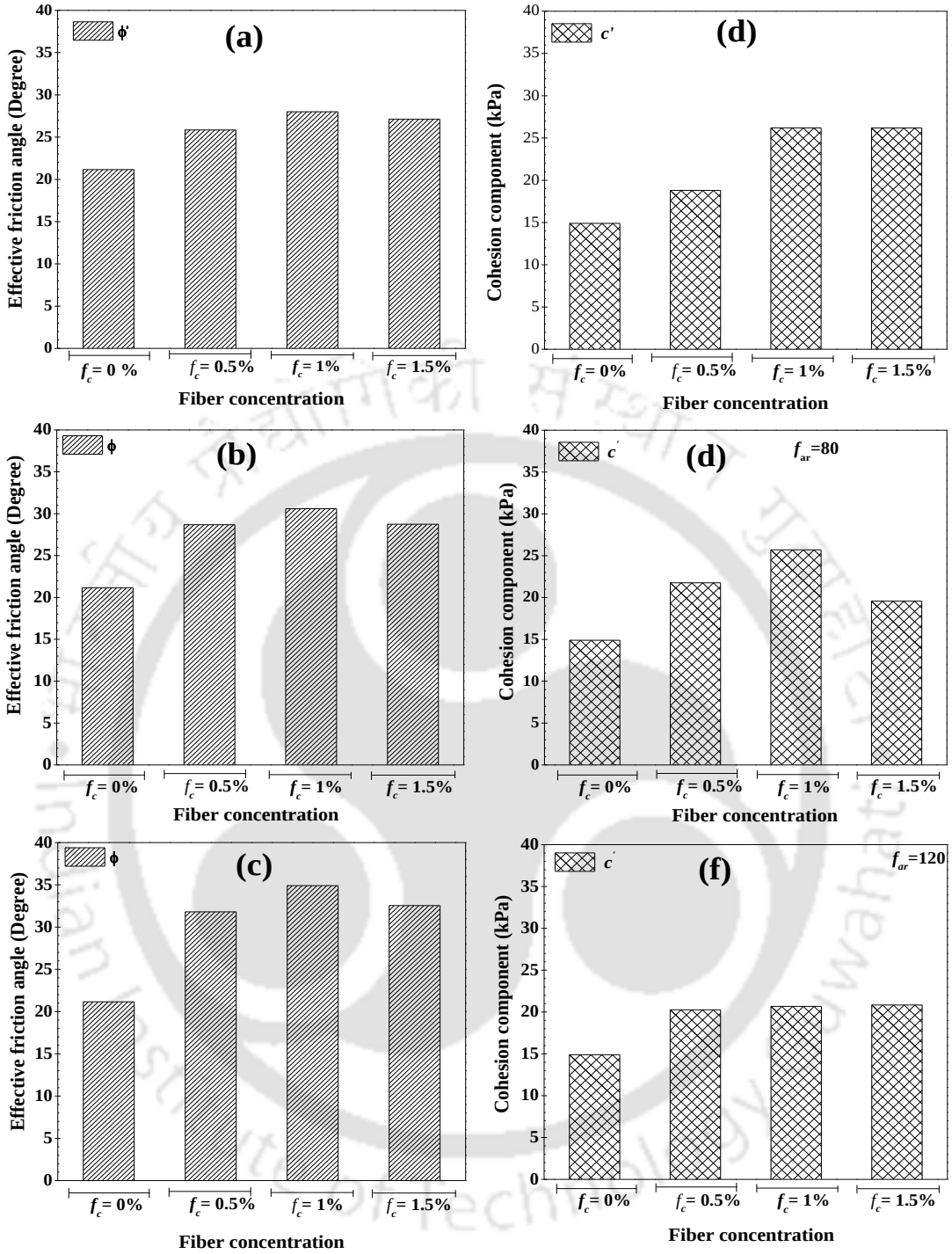

Figure 4.34 Shear strength parameter of SB30 composite; (a) Effective frictional angle of peak and residual with an aspect ratio of 40; (b) Effective frictional angle of peak and residual with an aspect ratio of 80;(c) Effective frictional angle of peak and residual with an aspect ratio of 120;(d) Effective cohesion component of peak and residual an aspect ratio of 40;(e) Effective cohesion component of peak and residual an aspect ratio of 80;(f) Effective cohesion component of peak and residual an aspect ratio of 120

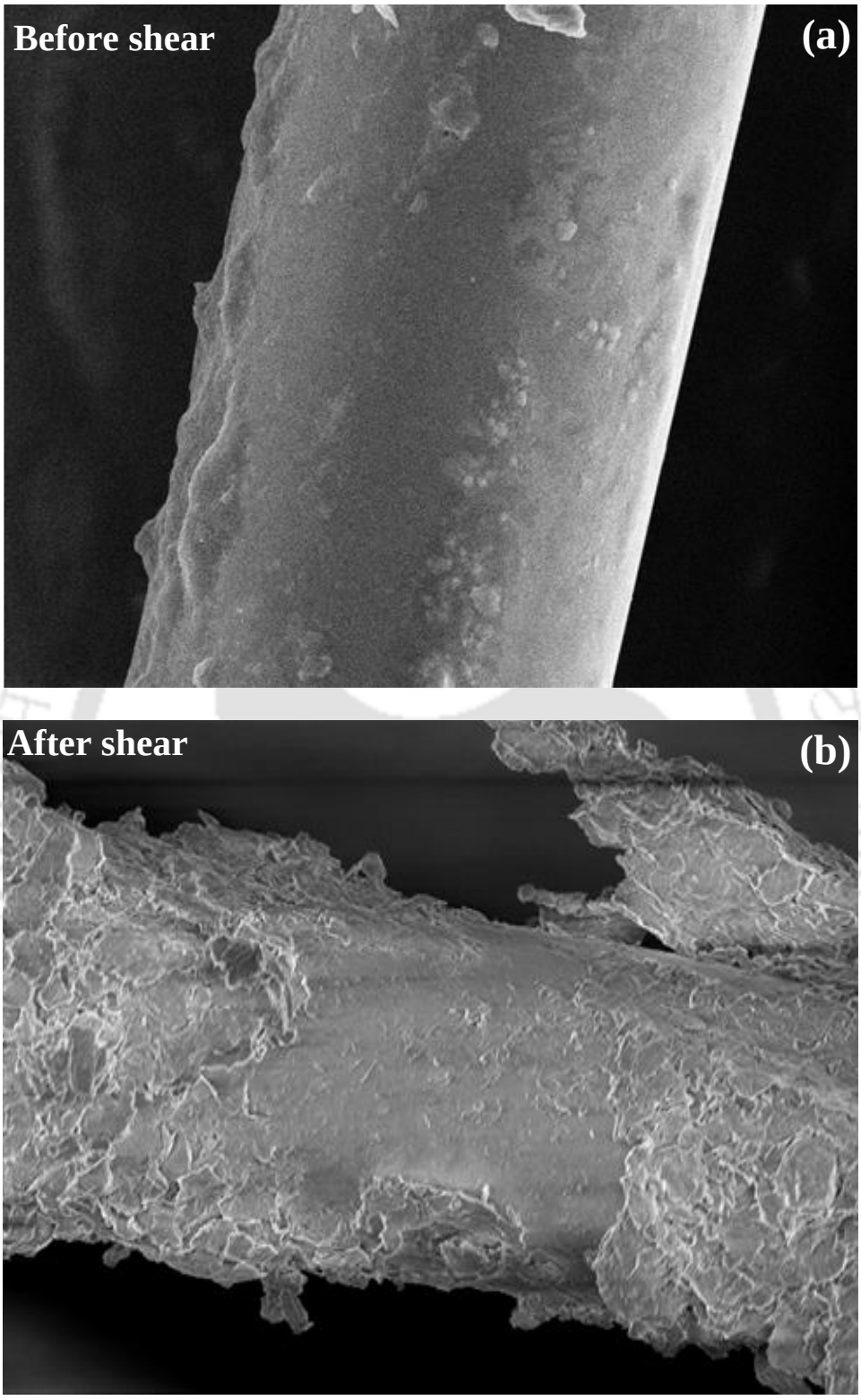

Figure 4.35 Surface behavior of the single glass fiber; (a) fiber surface before shear; (b) fiber surface after shear

4.5 Failure mode and Energy absorption capacity of the compacted sand bentonite –fiber soil composite

Failure mode of the SB10 and SB20 composites were considered at the end of the test when the composite was in the residual state, much beyond the peak deviatoric stress. While failure mode of the SB 30 composite ware taken at the end of the test corresponding to 20% axial stress. The failure mode of the individual composite was discussed, under the confining pressure of 150 kPa.

For SB10 composite, the modes of failure vary from shear failure to entirely distinct shear bond in the various specimens. Referring to the shape of the SB10 composite after the tests, it could be observed that the specimen undergoes shear failure with development of rupture in the presence of fiber and presented in Fig.4.36. As seen in Fig.4.36 (a and e), the failure plane of unreinforced soil was developed from the bottom and undergoes shear failure. With the inclusion of 0.5% of fiber, the shear failure occurs (Fig.4.36 b) more progressively toward the central region but further addition of 1% and 1.5% of fiber [Fig.4.36 (c and d)], shear failure was more clear within the central zone. It was clear that SB10 with a higher content of fiber exhibits a well-defined failure plane, indicating that randomly distributed fiber was stitched up by a potential rupture within the soil mass. It can be noticed that the fiber was pulled out when loading was exceeded. This complex geometry was accountable for the surface rupture of the fiber. The surface rupture of the fiber was recorded by FESEM and presented in Fig.4.35 comparing the fiber after and before shear.

At fixed fiber content, the failure mode of the SB10 composite was slightly different when the aspect ratio of the fiber was increased from smaller to higher. For example, at 0.5% fiber content, the SB10 failure mode was not changed significantly with increasing the aspect ratio of 40 and 80, in comparison to unreinforced soil composite (Fig.4.36e). In this scenario [Fig.4.36 (f and g)], it has been observed the shear zone has been expanded and mild shear failure took place. However, with the increase in the aspect ratio from 80 to 120, the failure mode has been shifted drastically. In this case, mild shear failure was disappeared and the specimen was slightly tilted diagonally under an undrained condition (Fig.4.36h).

This is indicating that the bulging tendency of the composite was developed, because, long aspect ratio held the soil piratical for excessive volume change.

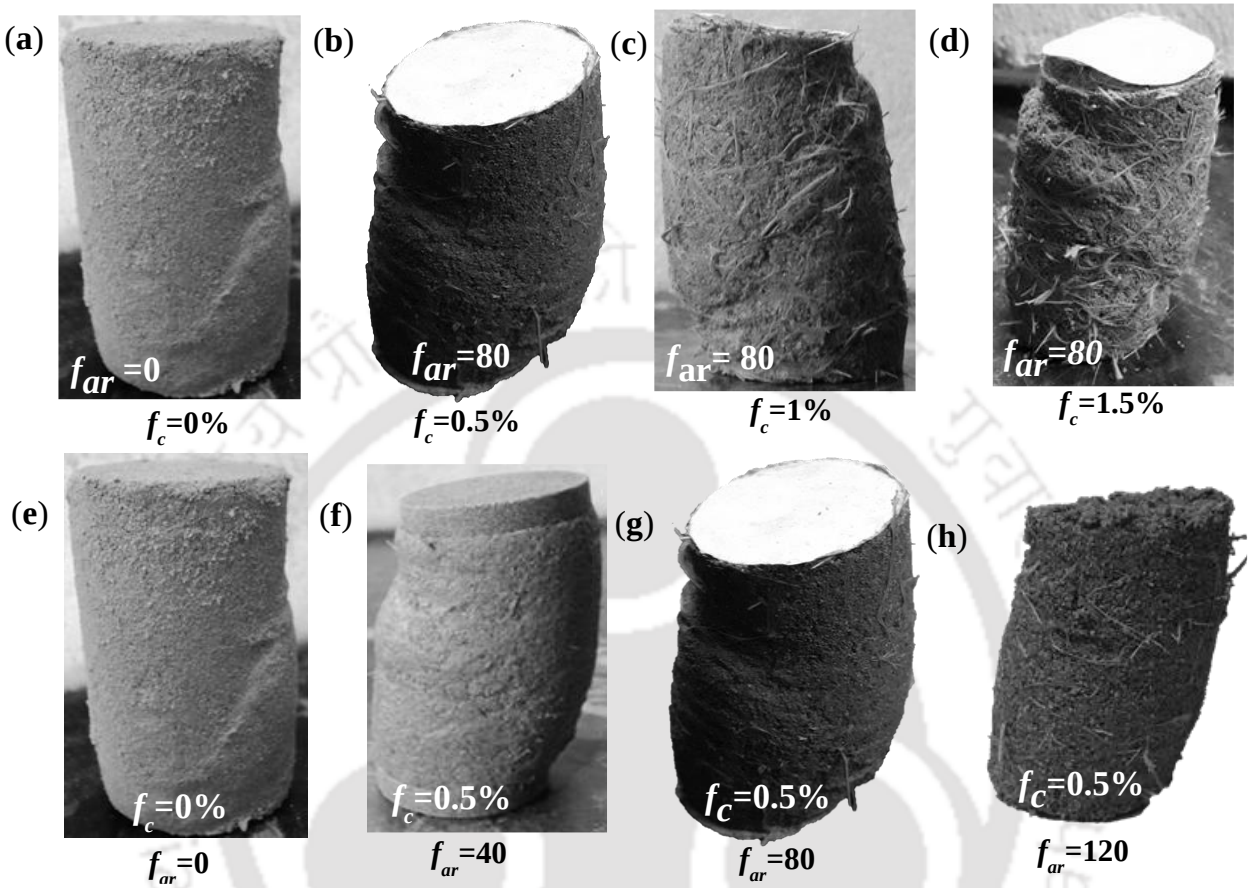

Figure 4.36 Failure mode of the SB10 composite

Almost similar behavior of failure mode was found for SB20 composite but, 20% bentonite fraction played a crucial role in this case. As observed in the Fig.4.37a, unreinforced soil is showing mild shear failure and their shear zone is horizontally buldged due to the presence of 20% bentonite clay (Fig.4.37a). However, as the fiber concentration increased, the specimen shows a gradually well-defined failure plane and their shear zone was slightly expanded towards center [Fig.4.37(b, c and d). In this case, fiber and bentonite, both were played a very crucial role. The combination of glass fiber with sand tends to brittle failure, while bentonite clay prevents from brittle failure and bentonite clay forcefully tried to fail the specimen towards bulging. Hence, the mild shear failure and expanded shear zone occurred.

At fixed fiber concentration, the failure mode of SB20 was altered significantly, as the aspect ratio of the fiber was increased. As seen in the Fig.4.37(e), the failure mode of the specimen was shown slightly tilting towards left in comparison to unreinforced soil (Fig.4.37f). However, with increase the aspect ratio from 80 and 120, the specimen looks to stand like a column, indicating the high resistance has been generated against large deformation as presented in the Fig.4.37 (g & h).

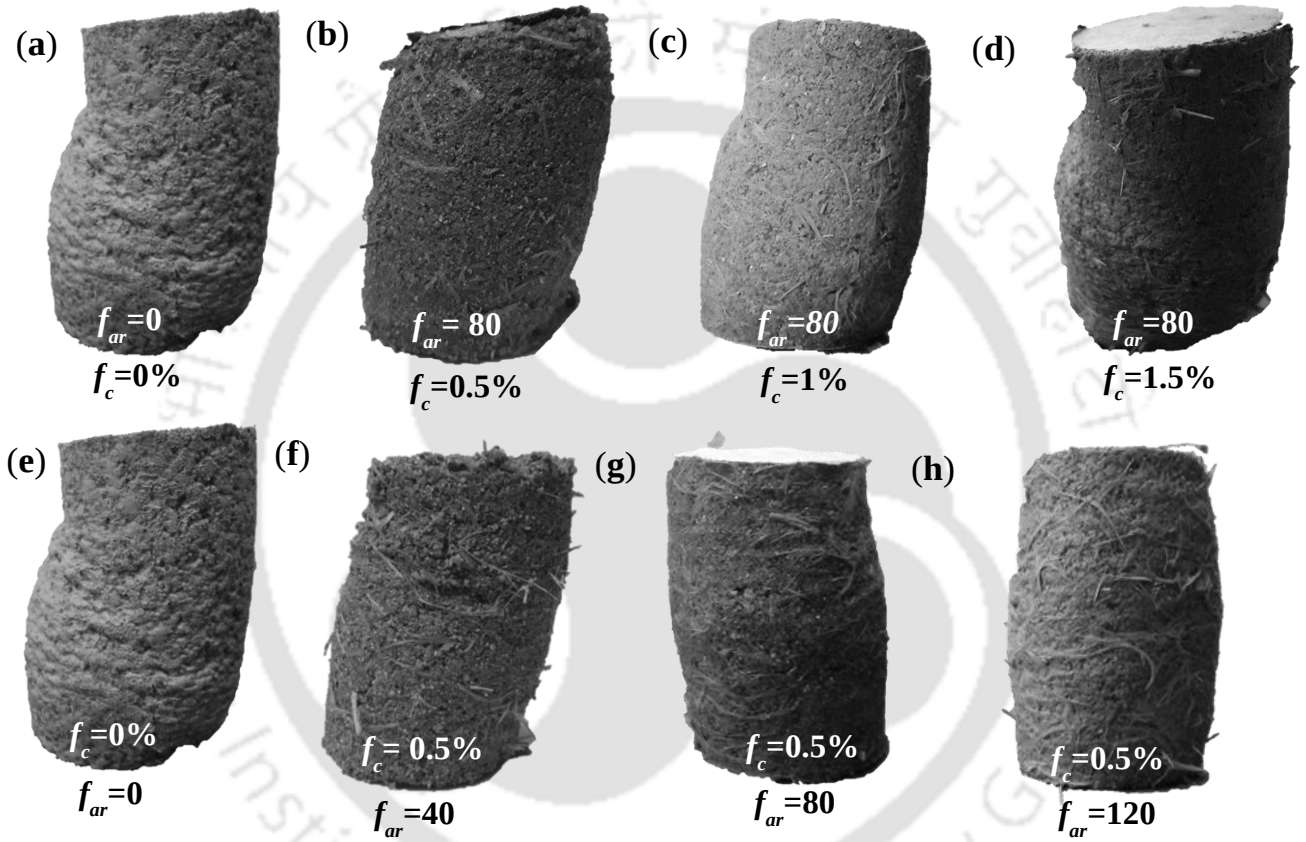

Figure 4.37 Failure mode of SB20 composite

The plot in Fig.4.38 exhibits typical failure modes of the unreinforced and reinforced specimens of SB30 composite. From the figure, a sharp horizontal wrinkle was observed (Fig.4.38a) for unreinforced soil during shearing and it was well indicated that specimen had undergone large deformation with poor effective stress (i.e. Fig.4.38b). However, at 0.5% fiber content, the specimen has shown barrel failure (Fig.4.38c) under an undrained condition, indicating that partial development was noticed under an

undrained condition (Ozkul and Bykal 2007). However, with increasing the fiber concentration from 0.5% to 1 and 1.5%, specimen exhibited mild barrel failure i.e. intensity of the centroidal bulb was gradually decreased [Fig.4.38 (c and d)], specifying that induced shear resistance was being developed against shear failure under rapid loading.

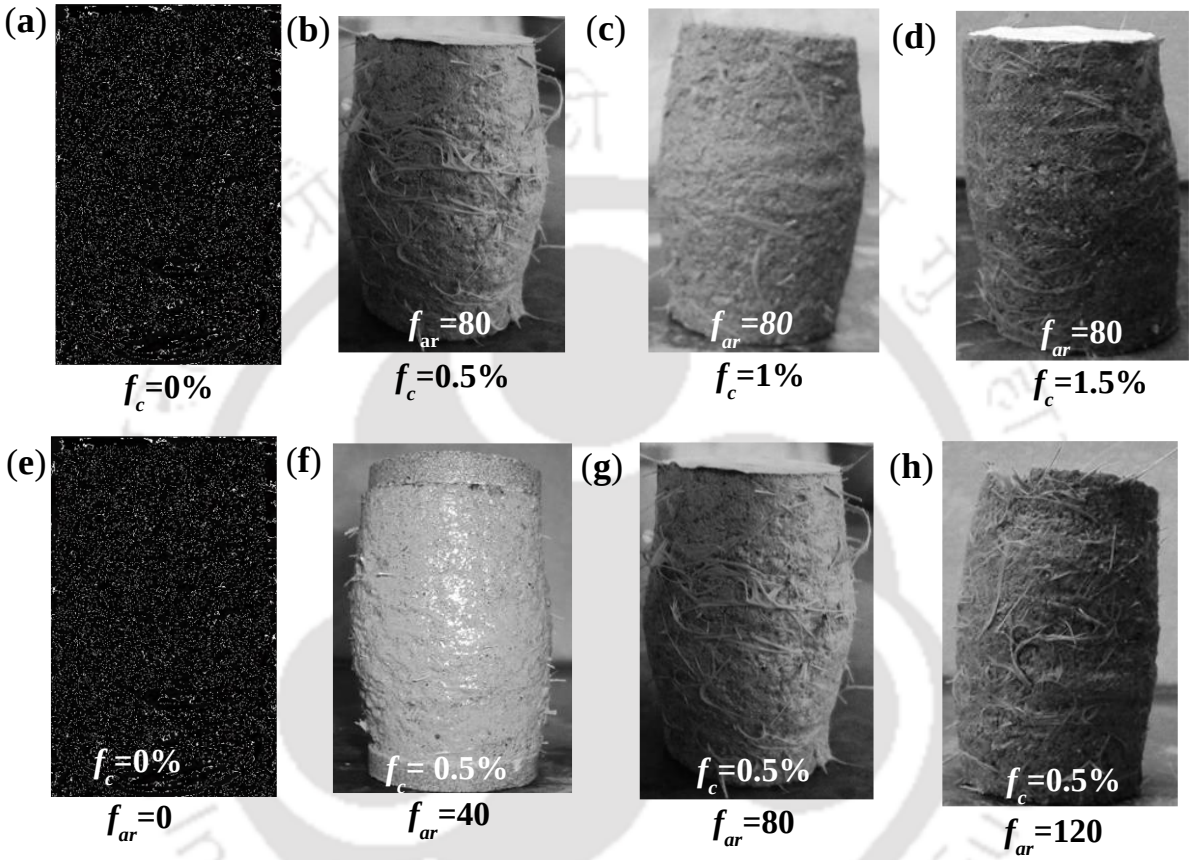

Figure 4.38 Failure mode of the SB30 composite

Reinforced specimen (i.e. f_{ar}=40) exhibited mixed-mode (Fig.4.38f) and showed a slight bulging with mild rupture in comparison to Fig.4.38e. With the increase in aspect ratio (i.e. f_{ar}=80), specimen exhibited bulging failure (Fig.4.38g), indicating that the resistance of the composite was improving against volume expansion. However, at large aspect ratio (i.e. f_{ar}=120), specimen depicted like a vertical column (Fig.4.38h), showing a strong resistance against volume expansion. Hence, fiber with increasing aspect

ratio exhibited that strength of the composite increased against pull out, and it held the soil mass against high volume expansion due to rapid loading.

4.5.1 Impact of fiber on energy absorption capacity (EAC)

In the current study, the energy absorption capacity and failure modes were examined for the different sand-bentonite mixture at different fiber content, fiber aspect ratio and confining pressure. Overall improvement of the composite was also explained in terms of energy absorption capacity (EAC) and measures the toughness of a soil sample (ASTM C1609/C1609M 2012). The absolute values of energy absorption are obtained by calculating the area under the stress–strain curve of unreinforced and reinforced specimens up to 20% of strain (Babu and Vasudevan 2008) with a confining pressure of 50, 100 and 150 kPa and presented in Fig.4.39, under the confining pressure of 150kPa.

The absolute values of energy absorption are obtained by calculating the area under the stress–strain curve of unreinforced and reinforced specimens up to 20% of strain. Numerical integration has been used to analysis the stress-strain data of the individual SB composite and the programed was performed by MATLAB (R2014a). The composite trapezoidal rule has been chosen for numerical integration and the suitable number of the segment (i.e. integration interval) has been taken under consideration to improve the accuracy of the result.

The typical result of EAC under the confining pressure of 150 has been shown in Fig.4.39. From the figure, it has been observed that EAC of the composite was increased with fiber content and fiber aspect ratio. In case of SB10, EAC was increased from 8.63×10^3 kJ/m^3 to 1.44×10^4 kJ/m^3,1.81×10^4 kJ/m^3 and 2.18×10^4 kJ/m^3 at 0.5%, 1 and 1.5% fiber content as the aspect ratio of 80. However, at same fiber content, EAC of the SB10 composite was further enhanced from 8.63×10^3 kJ/m^3 to 1.80×10^4 kJ/m^3, 2.09×10^4 and 2.46×10^4 kJ/m^3 with an increase in the aspect ratio from 80 and 120 (Fig.39b) and SB10 reinforced with glass fiber followed the same trend with an aspect ratio of 40. An identical trend was followed by the

SB20 composite also and exhibited in Fig.4.39. However, it was found that EAC of the SB20 was lower than SB10 composite for all aspect due to the presence of a higher amount of bentonite clay.

From the earlier study, it has been observed that compacted SB30 mixture is very different from SB20 and SB10 composite in every aspect. Here, it has been noticed that EAC was increased up to 1% fiber content for all aspect ratio [Fig.4.39 (e and f)]. For example, EAC was found to increase from 2.77×10^3 kJ/m^3 to 4.01×10^3 kJ/m^3, 4.66×10^3 kJ/m3 at 0.5% and 1% fiber content, thereafter, EAC was slightly dropped from 4.66×10^3 kJ/m^3 to 4.43×10^3 kJ/m^3 for the aspect ratio of 80. At same fiber content, EAC was increased from 2.77×10^3 kJ/m^3 to 6.45×10^3 kJ/m^3, 7.09×10^3, 6.37×10^3 kJ/m^3 for the aspect ratio of 120. A similar pattern was followed by the other SB30 composite as well. Hence, EAC of the fiber-reinforced soil was much more than unreinforced soil, indicating that toughness of the composite was increased. Indirectly, composite has increased its ability to resist failure against rapid loading.

4.6 Critical state and yielding behavior of SB-glass fiber composite

Generally, soils have a highly nonlinear stress-strain response, which is strongly dependent on recent stress history. To make dependable predictions of field performance, the stress path method (Lambe 1967 and Lambe and Marr 1979) boosts engineers to derive soil parameters from laboratory data that follow, as closely as possible, the stress paths likely to occur in the field (Muir Wood et al. 1992). The modified Cam clay soil model (Roscoe and Burland 1968) is generally used in soil mechanics. The model describes three important aspects of soil behavior, strength, compression or dilatancy (the volume change that occurs with shearing), and critical State at which soil elements can experience unlimited distortion without any changes in stress or volume. The primary assumption of this current study is that $\phi_{rs}' = \phi_{cs}'$ and it has been used to determine the yield surface from the individual composite. The critical state is an idealization of the observed behavior of saturated soils in a triaxial compression test. It described that soil sheared continuously up to a well –defined critical state. At this state, shear distortions (q') occur without any further changes in mean effective stress (p'), deviatoric stress-specific volume v;

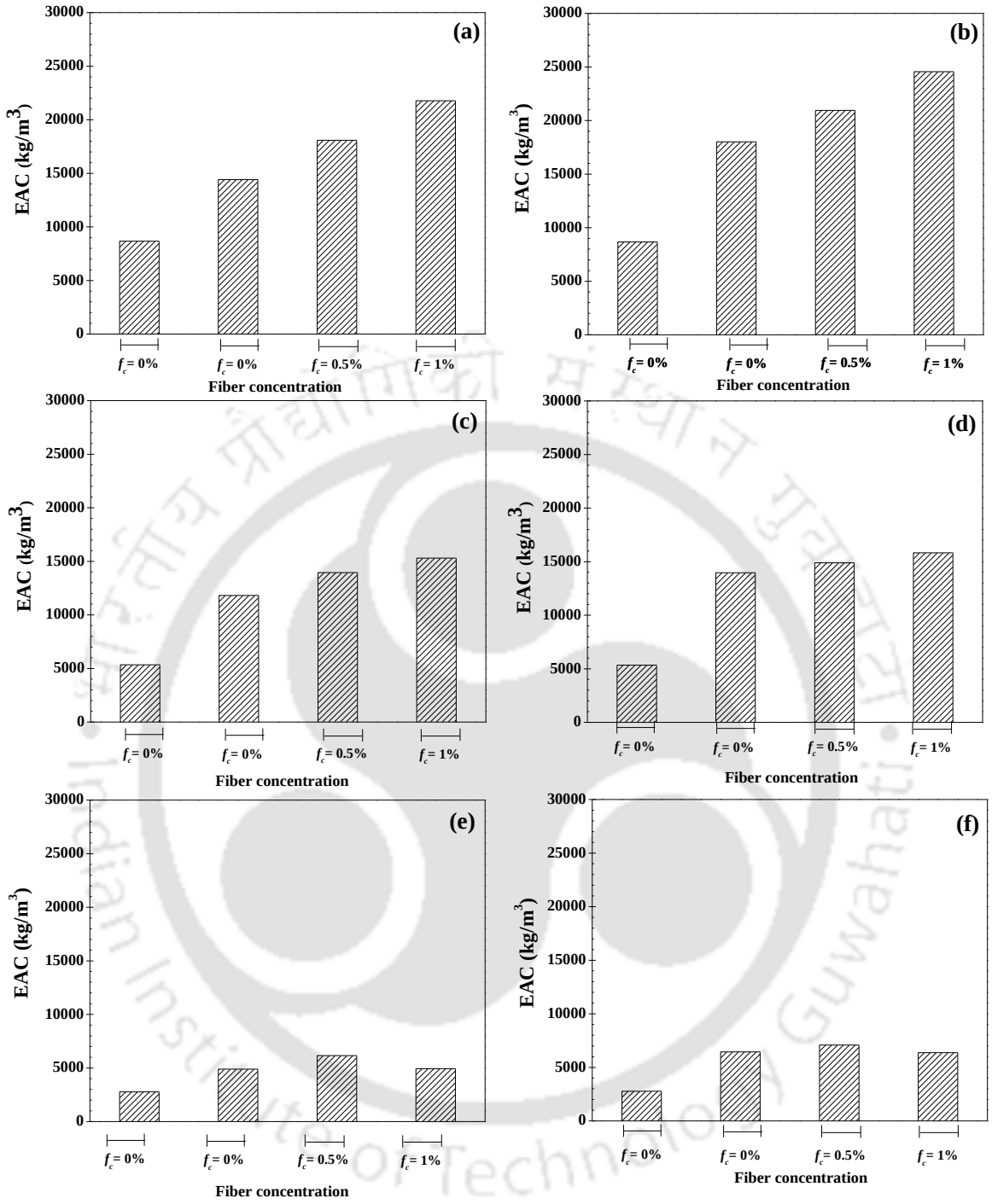

Figure 4.39 EAC of SB-Glass fiber composite ;(a) SB10 with an aspect ratio of 80; (b) SB10 with an aspect ratio of 120;(c) SB20 with an aspect ratio of 80; (d) SB20 with an aspect ratio of 120;(e) SB30 with an aspect ratio of 80;(f) SB30 with an aspect ratio of 120

$$\frac{\delta p'}{\delta \varepsilon_s} = \frac{\delta q'}{\delta \varepsilon_s} = \frac{\delta v'}{\delta \varepsilon_s} = 0 \quad (4.4)$$

where,

$v = 1 + e$

$$p' = \frac{1}{3}(\sigma_1' + \sigma_2' + \sigma_3')$$

$$q = \sqrt{\frac{(\sigma_1' - \sigma_2')^2 + (\sigma_2' - \sigma_3')^2 + (\sigma_1' - \sigma_3')^2}{2}} \quad (4.5)$$

Due to axisymmetric condation,

$$p' = \frac{1}{3}(\sigma_1' + 2\sigma_3')$$

$$q = (\sigma_1' - \sigma_3')$$

All critical states, for a given soil, form a unique line called the Critical State Line (CSL) defined by the following equations in the space (p', q, v);

$$q = M_c p' \quad (4.6)$$

$$v = \Gamma - \lambda \mathrm{In}(p') \quad (4.7)$$

In $p' - q$ plane, the CSL is a straight line passing through the origin with the slope equal to M_c, one of the characteristics of the material that is the main parameter in the definition of yield surface. λ is the slope of the normal compression (virgin consolidation) line on υ− In p' plane, while κ is the slope of swelling line. All the model parameters were found out from triaxial and oedometer test are reported in Table 4-2. Test result suggested that critical state frictional angle (M_c) was drastically changed with the inclusion of glass fiber. Such as, M_c of the SB10 composite was increased from 0.996 to 1.04, 1.19,1.28 at 0.5%, 1 and 1.5% with an aspect ratio of 40. At same fiber content, M_c was found to increase again from 0.996 to 1.21, 1.31 and 1.38 with increase the aspect ratio from 40 to 80. However, with increase the aspect ratio from 80 to 120, M_c was further improved from 0.996 to 1.25, 1.35 and 1.45 at the same fiber content. An identical trend was found for SB20 composite also.

However, improvement of M_c was observed up to 1% fiber content (for any aspect ratio) for the mixture SB30 reinforced with glass fiber, thereafter, it was reduced slightly with the further addition of glass fiber.

For example, M_c was improved from 0.82 to 1.02, and 1.11 at 0.5 and 1% fiber content, thereafter, M_c was reduced from 1.11 to 1.08 at 1.5% fiber concentration with an aspect ratio of 40. A similar pattern was also noticed with an aspect ratio of 80 and 120 (for any fiber concentration) as presented in Table 4-2.The λ of the SB-tire fiber composite was decreased up to 1% fiber content and then it started to degrade with the further addition of fiber content. This pattern was captured for the SB-glass fiber composite throughout. For example, λ of the SB30 composite was calculated to be 0.143, but it was reduced from 0.143 to 0.117 and 0.099 at 0.5% and 1% fiber content, respectively. However, λ was increased slightly from 0.143 to 0.11 at 1.5% fiber content with an aspect ratio of 40. With increase the aspect ratio from 40 to 80, λ was decreased from 0.143 to 0.087 and 0.082 at 0.5% and 1% respectively, thereafter, it was decreased from 0.082 to 0.104 with the addition of 1.5% at the same fiber content. The same trend was obtained for SB30 reinforced with glass fiber for the aspect ratio of 120 and presented in Table 4-2. A similar tendency was captured for SB10 and SB20 composite also and shown in Table 4-2.

The κ of the composite increased sharply with fiber concentration and the effect of aspect ratio on the κ was marginal. For example, κ of the SB10 composite was found out to be 0.001, 0.007, 0.009 and 0.009 at 0%, 0.5%,1 and 1.5% fiber content with an aspect ratio of 40. With increase the aspect ratio from 40 to 80, κ was increased from 0.001 to 0.011 and 0.012 at 0.5% and 1% fiber content and then it kept the similar value i.e.0.012 at 1.5% fiber content. A similar result was found for the aspect ratio of 120 as well and presented in Table 4.2. Therefore, change in λ and κ value was strongly depended for compressibility and swelling index for the composite.

A state that defines the limit of elastic and the start of plastic deformation under any possible combination of stresses is known as the yield condition or yield criterion. The locus of the stress at which a soil yield is called a yield surface. Stress below the yield stress cause the soil to respond elastically; stress beyond the yield stress causes the soil to respond elastoplastically. An elastic material recovers its original configuration on unloading; an elastoplastic material undergoes both elastic (recoverable) and plastic

(permanent) deformation during loading. The yield surface is assumed to be an ellipse, and its initial size or major axis is determined by the preconsolidation stress, p_c.

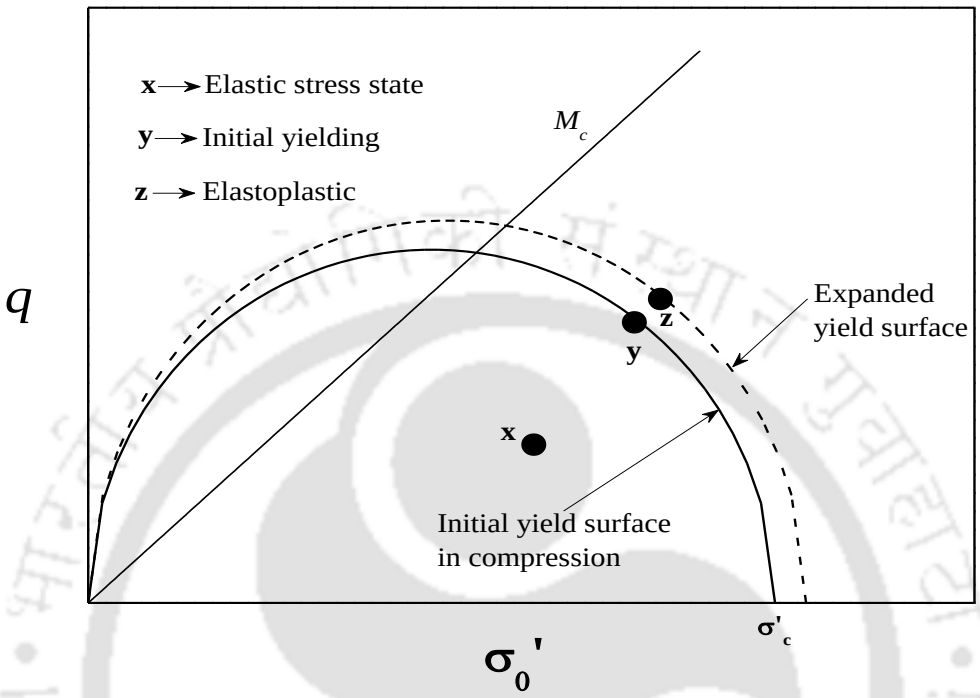

Figure 4.40 Conceptual framework of yielding surface

Experimental evidence indicated that an elliptical yield surface is a reasonable approximation for soils (Wong and Mitchel 1975). The higher the preconsolidation stress, the larger the initial ellipse. Budhu (2008) described the theoretical critical state framework and yield surface of the soil. All the combination of q and p, that is within the yield surface, for example, the point "x" in Fig.4.40

Fig.4.40, will cause the soil to respond elastically. If a combination of *q* and *p*' lies on the initial yield surface (point y, Fig.4.40), the soil yields in a similar fashion to the yielding of a steel bar. Any tendency of a stress combination to move outside the current yield surface is accompanied by an expansion of the current yield surface, such that during plastic loading the stress point (*p*', *q*) lies on the expanded yield surface and not outside, as depicted by "z". Effective stress paths such as YZ (Fig.4.40) cause the soil to behave elastoplastically.

Table 4-2 summaries of the CSP of SB-glass fiber composite

Table summary of the	M_c	λ	κ
SB10, f_c=,f_{ar}=0	0.996	0.014	0.001
SB10, f_c=0.5,% f_{ar}=40	1.04	0.011	0.007
SB10, f_c=1%, f_{ar}=40	1.19	0.013	0.009
SB10, f_c=1.5%, f_{ar}=40	1.28	0.012	0.009
SB10, f_c=0.5%, f_{ar}=80	1.21	0.012	0.011
SB10, f_c=1%, f_{ar}=80	1.31	0.011	0.012
SB10, f_c=1.5%, f_{ar}=80	1.38	0.011	0.012
SB10, f_c=0.5%, f_{ar}=120	1.25	0.008	0.013
SB10, f_c=1%, f_{ar}=120	1.35	0.007	0.013
SB10, f_c=1.5%, f_{ar}=120	1.45	0.039	0.013
SB30, f_c=0, f_{ar}=0	0.82	0.143	0.008
SB30, f_c=0.5, f_{ar}=40	1.02	0.117	0.013
SB30, f_c=1, f_{ar}=40	1.11	0.099	0.018
SB30, f_c=1.5%, f_{ar}=40	1.08	0.11	0.022
SB30, f_c=0.5%, f_{ar}=80	1.14	0.087	0.013
SB30, f_c=1%, f_{ar}=80	1.23	0.082	0.017
SB30, f_c=1.5%, f_{ar}=80	1.15	0.104	0.022
SB30, f_c=0.5%, f_{ar}=120	1.28	0.078	0.013
SB30, f_c=1%, f_{ar}=120	1.41	0.061	0.018
SB30, f_c=1.5%, f_{ar}=120	1.31	0.087	0.022

From the [Fig.4.41 (a to f)], it can be observed that yield surface was expanded by the inclusion of fiber concentration and fiber aspect ratio. This pattern was captured for all the composite. However, it can be seen that yield surface was strongly depended with bentonite fraction. As the bentonite fraction is

increased, the yield surface was decreased drastically. The yield surface was maximum for SB10 composite [Fig.4.41 (a and b)] and it was minimum for SB30 composite. For SB30 composite, yield surface was expanded up to 1% fiber content (for any fiber concentration) [Fig.4.41(e and f)]. However, it was reduced slightly with the further addition of glass fiber. Hence, it concluded that the elastic zone of the composite was increased with the inclusion of glass fiber. The higher percentage of bentonite content is highly susceptible for high settlement and poor strength and it is always dangerous for landfill construction material, in the end, fiber inclusion is capable to enhance the performance of the landfill material.

4.7 Fiber –reinforced proposed model

Generally, regression analysis is one of the most widely used statistical tools because it provides a simple method for establishing a functional relationship among variable. It is interesting because it delivers a theoretically simple process for exploring functional interactions among variables. The standard method in regression analysis is to take the data, fit a model and then evaluate the fit using statistics such as t, F and R^2 (Maliakal and Thiyyakkandi 2013; Chatterjee and Hadi 2015;)

Based on the experimental result, multiple-regression statistical analysis was performed to develop models for predicting the effective major principal stress at failure ($\boldsymbol{\sigma}_1'$). The model developed to explore the effects of unreinforced liquid limit (LL) fiber percentage (f_c), fiber aspect ratio (f_{ar}) and confining pressure (σ_0') of fiber reinforced composite on major principal stress at failure.

It has been designated that the response variable by y and set of predictor variables by x_1, x_2, x_3 … x_p. Where p signifies the number of the predictor variable. The true relationships between " y " and x_1, x_2, x_3 … x_p can be approximated by the regression model

$$y = f(x_1, x_2, ..., x_p) \qquad (4.8)$$

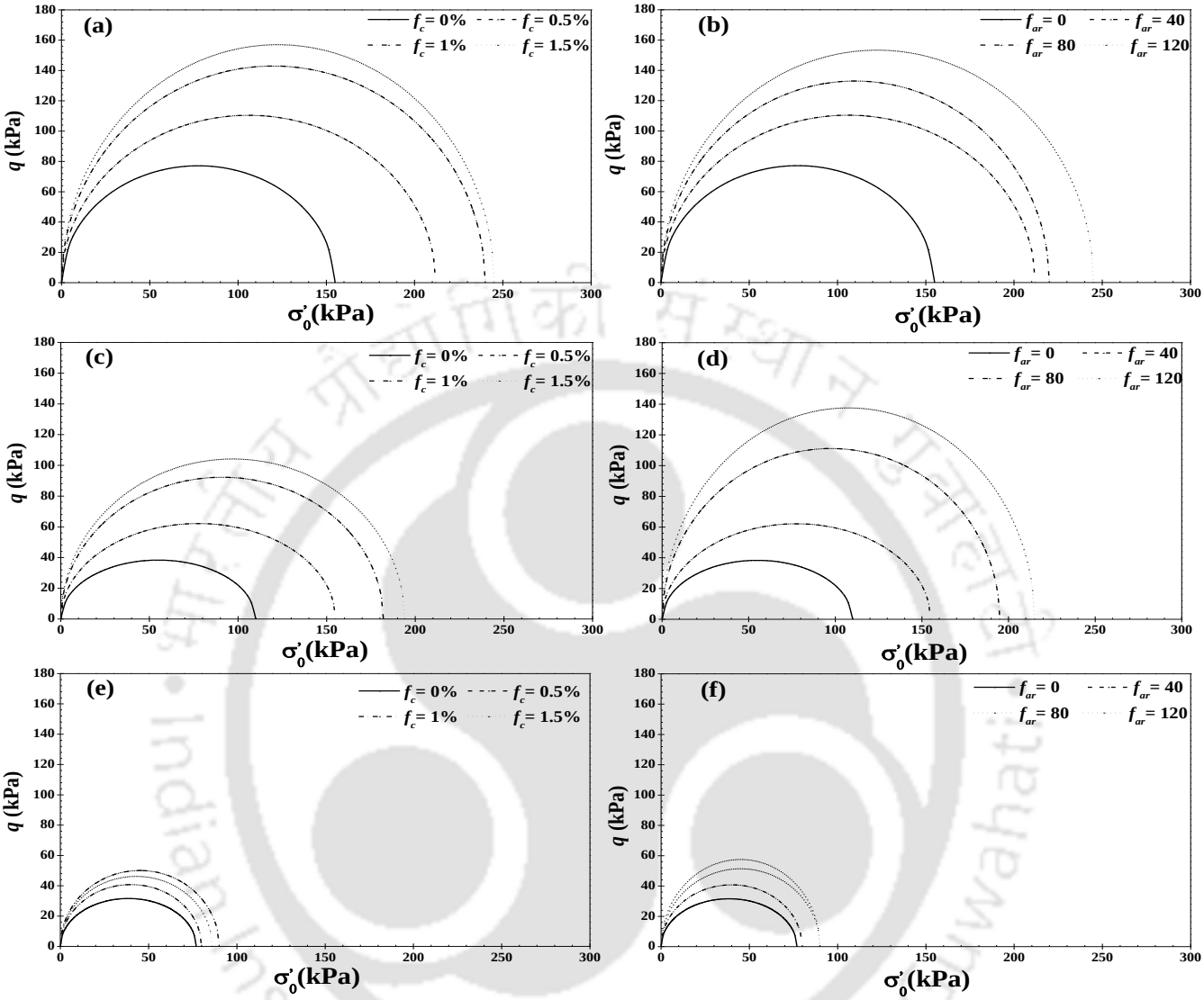

Figure 4.41 Yield surface of SB-glass fiber composite; (a) SB10 with an aspect ratio of 40;(b) SB10 with fiber concentration of 0.5%; (c) SB20 with an aspect ratio of 40;(d) SB20 with fiber concentration of 0.5%;(e) SB30 with an aspect ratio of 40 (f) SB30 with fiber concentration of 0.5%

The function $f(x_1, x_2, ..., x_p)$ defines the relationships between y and x_1, x_2, x_3 … x_p. The estimated

Using the equation number 4.8, it can compute n fitted values, one for each of the n observation from the data point. For example, the i[th] fitted value y_i is

$$y_i = \lambda_0 + \lambda_1 x_{i1} + \lambda_2 x_{i2} + \lambda_3 x_{i3} + \cdots\cdots + \lambda_p x_{ip}, \qquad i = 1, 2, 3, ...n \tag{4.10}$$

Where x_{i1}, x_{i2}, x_{i3} … x_{ip} are the values of the p predictor variable for the i[th] observation.

Based on the experimental output, the regression model was developed to investigate the impact of unreinforced liquid limit, effective confining pressure (σ_0'), tire fiber content (T_f) and liquid limit (LL) on effective major principle stress at failure (σ_1') and it has been given below:

$$\log(\sigma_1') = 3.245 + 0.751\log(\sigma_0') + 0.125\log(f_c) + 0.182\log(f_{ar}) + (-1.477)\log(LL) \quad (4.11)$$

$$\sigma_1' = 1757.92 \times \sigma_0'^{0.751} \times f_c^{0.125} \times f_{ar}^{0.182} \times LL^{-1.477} \quad (4.12)$$

For equation 4.12, it was found that regression coefficient is 0.95, indicating excellent superiority of the fit was noticed for this model. The suitability of the suggested model and importance of the coefficient of individually variable was tested by Fischer's F-test and student's t test respectively at 95 % confidence level as shown in Table 4-3 and Table 4-4. From the table, it was noticed that t_{value} was less than t_{crit} and F_{value} was less than F_{crit}. Therefore, the models with four independent variables were satisfactory to consistently the predict dependent variable (i.e. σ_1') at 95% confidence level. From the Table1, it was noticed that all the p value for all the coefficients were far below from 0.05, specifying that coefficient of all the variables were significant at 95% confidence level.

$$\text{RMSE} = \sqrt{\frac{1}{n}\sum_{i=1}^{n}(y_i^p - y_i^a)^2} \quad (4.13)$$

$$\text{NRMSE} = \frac{RMSE}{y_{\max}^a - y_{\min}^a} \times 100 \quad (4.14)$$

Normalized root-mean-square error (NRMSE) was calculated according to Soltani et al. (2018) and found out to 3.96%, which was less than 5% reference label. Finally, the experimental values and predicted values have been compared and presented in the Fig.4.42. From the figure, it was noticed that experimental and predicted value is showing a good agreement for effective major principle stress at failure and both values are very close to 1:1 line.

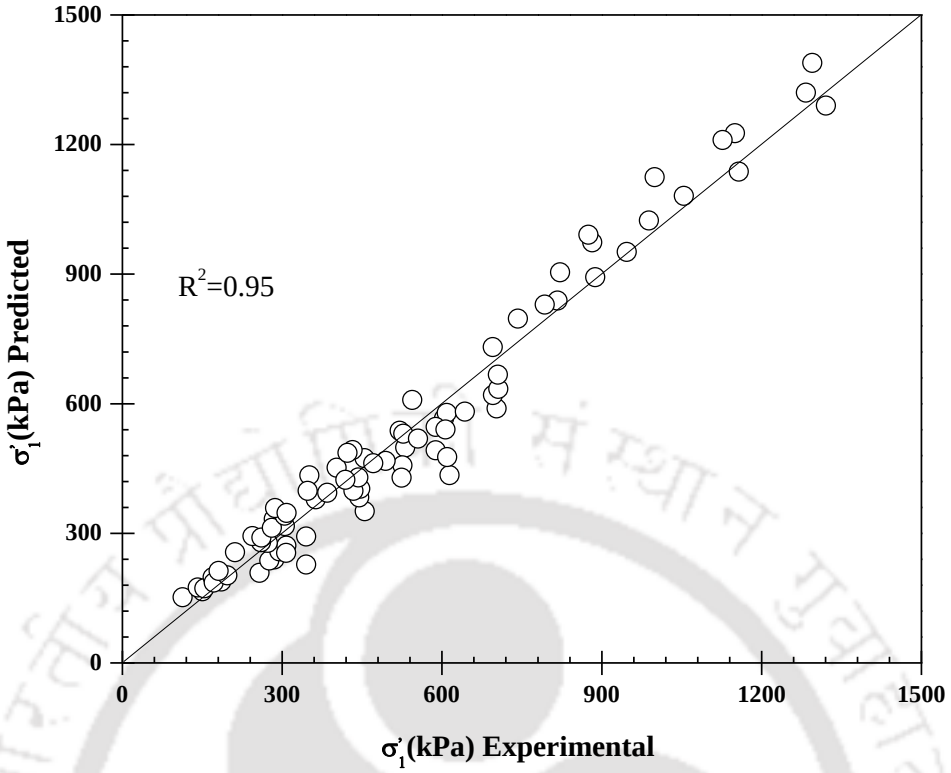

Figure 4.42 comparing the predicted and experimental result from the model

Table 4-3 Summary of the F-test result

F_{value} (F)	$F_{critical}$ (F_C)	Remark	NRSME≲5%
332.83	2.494	F>Fc	4.84 (accepted)

Table 4-4 Summary of the t-test result

Coefficients (λ)	t-stat (t_s)	P-value	$t_{critical}$ (t_c)	Remark
0.751	21.99	1.09×10^{-34}		$t_s > t_c$
0.125	3.66	4.57×10^{-4}	±1.992	P-value<0.05
0.182	5.32	9.8×10^{-7}		
-1.477	-28.39	3.37×10^{-42}		

4.8 Unconfined compression strength of compacted sand bentonite –glass fiber soil composite

A minimum unconfined compressive strength of 200 kPa was arbitrarily selected for liner and cover system as reported by (Daniel and Wu 1993). This strength is the lowest value for very stiff soils based on the terminology of peck et al. (1974). According to this fact, the unconfined compressive strength of different sand–bentonite mixture reinforced with glass fiber was determined. The typical stress-strain response of the different SB composites is exhibited in the Fig.4.43. From the figure, it can be observed that each SB composite behaved differently but in all the cases, it could be observed that fiber reinforced composite reaches to a higher peak in comparison to unreinforced soil.

For example, UCS of the SB 10 was increased from 12 kPa to 25, 35 and 40 kPa at 0.5, 1 and 1.5% fiber concentration with an aspect ratio of 40, respectively. At same fiber content, UCS was further increased from 12 kPa to 34, 42 and 46 kPa with an aspect ratio of 80. However, at the same configuration, UCS was again increased from 12 kPa to 48, 56, and 63 kPa with an increase in aspect ratio of 80 to 120. UCS was found to increase maximally from 12 kPa to 63 kPa at 1.5% fiber content with an aspect ratio of 120. An identical pattern was followed by SB20 composite also. However, UCS was found to increase maximally from 42 kPa to 117 kPa at 1.5% fiber concentration with an aspect ratio of 120 and presented in Fig.4.43.

In case of SB30, UCS was increased up to 1% fiber content for all aspect ratio, thereafter it was found to reduce with increase the fiber content from 1 to 1.5%. For example, UCS was increased from 163 kPa to 186 kPa and 199 kPa at fiber content of 0.5 and 1%, and then it was dropped from 199 kPa to 195 kPa at 1.5% fiber content with an aspect ratio of 40. At same amount of fiber content, UCS was further enhanced from 163 kPa to 211 kPa and 247 kPa and it was further reduced from 247 kPa to 219 kPa with increase the aspect ratio from 40 to 80. Similarly, SB30 with an aspect ratio of 120 followed the same trend as it was discussed earlier. UCS of the SB30 was increased maximally from 162.45 kPa to 272 kPa at fiber

content of 1% with an aspect ratio of 120. Interestingly, it was also noticed that unconfined compression strength was increased with increase in bentonite content.

This phenomenon can be described that tensile stress was developed due to the stretching of fiber and rearrangement of soil particles within the weakest section of the fiber soil matrix. As strain continued, the rearrangement of the particle was also continued, thereafter, particle gradually mobilized the tensile stress of the fiber after a limited percentage of strain. At this time, particle-to-particle stress was converted on to the fibrous fiber. After attaining the peak stress, fiber was pulled out or fiber was broken by tangential stress (i.e. acting along the failure plane). This mechanism can increase the overall shear resistance of the fiber soil matrix against the shear stress produces from the weakest section. This shear resistance was increased with fiber aspect ratio as well as fiber content.

Compressive stress at the failure of the composite was increased with fiber aspect ratio as well as fiber content. This mechanism was predominant for the mixture of SB10 and SB20 mixture. However, it has also been noticed that as the bentonite content increased the UCS strength of the composite also increased. Under an unsaturated condition, bentonite fraction acts as a purely binding agent. Therefore, a strong cohesive force was developed between bentonite clay (i.e. producing cementation property), sand particle, and fibrous fiber; as a result, cementations property of the bentonite gave the intact packing to the fiber – soil composite. Hence, unconfined strength was increased maximally with bentonite fraction. At one stage, as the fiber concentration increased, the slippage failure was taken in between fiber and higher amount of bentonite clay. Hence, SB30 with 1.5% fiber exhibited lower compressive strength in comparison with SB30 reinforced with 1% glass fiber for all range of aspect ratio.

4.8.1 Effect of fiber on post peak stress

The impact of fiber on post-peak stress was portrayed in Fig.4.43. The stress–strain behavior of SB composite is depicted by an increase in stress up to peak stress, tracked by a sharp drop in stress on further straining. This stress reduction is associating to failure along the shear plane, as specified by the specimen in Fig.4.43. From the figure, it was observed that post peak drop was considerably less in comparison to

unreinforced soil. For example, post peaks stress (PPS) of SB10 was found to be 6 kPa. However, the PPS was further increased from 6 kPa to 14, 19 and 28 kPa at 0.5,1 and 1.5% fiber content with an aspect ratio of 40. Similarly, at same fiber content, the PPS was further enhanced from 6 kPa to 25, 35 and 44 kPa with an aspect ratio of 80. However, at the same configuration, the PPS was found to increase from 6 kPa to 35 to 45 and 56 kPa with increase the aspect ratio from 80 to 120. An identical trend was observed for the mixture of SB20 and SB30 composite also.

4.8.2 Effect of fiber on improvement factor (I_F) and displacement ratio

The improvement of the composite further defined in terms of improvement factor (I_F), which was calculated as the ratio of peak compressive strength of reinforced soil and peak compressive strength of unreinforced soil (i.e. UCS_r/UCS_{ur}). This ratio is described as improvement factor for reinforced soil, with values larger than 1 specifying that an improvement of compressive strength has been taken place due to reinforcement effect, under unconfined condition with respect to unreinforced soil. For example, I_F of the SB10 was found to be 2.11, 2.92 and 3.37 at 0.5,1 and 1.5% fiber content with an aspect ratio of 40, respectively. The maximum I_F was found to be 5.22 for the mixture of SB10 reinforced with 1.5% fiber content with an aspect ratio of 120. The details of the improvement factor are given in Table 4-5.With the inclusion of glass fiber, ductility of the compacted sand bentonite mixture was improved and is defined by displacement ratio, which is defined as the ratio of failure strain of reinforced soil to failure strain of unreinforced soil ($\varepsilon_r/\varepsilon_{ur}$). The value of D_r was considered more than one, indicating that improvement of the ductility was observed due to the reinforcement effect and it has been compared to the unreinforced soil. For example, D_r of the SB10 mixture was found to be 1.06, 1.09 and 1.24 at 0.5, 1 and 1.5% fiber content with an aspect ratio of 40, respectively. The details of the displacement ratio have been tabulated in Table 4-5.

4.8.3 Effect of failure pattern

It has been noticed that different failure crack has been developed in the specimen after the test. The pictures of the failed specimens are shown in Fig.4.43 to understand the crack pattern of the fiber-reinforced soil. From the figure, it has been observed that all unreinforced soil (i.e. SB10, SB20 and SB30) has undergone clear shear failure, indicating the upper half of the specimen slid over the lower half. For mixture with low bentonite content (i.e.SB10 and SB20), the failure behavior was gradually shifted from ductile to brittle. At low percentage of fiber content (i.e. 0.5%), the specimen exhibits multiple cracks on the shear plane, indicating the tensile strength was not fully mobilized in between adjacent soil particle and fiber of smaller aspect ratio. The failure pattern for a specimen with higher fiber content (i.e.1 or 1.5%), as depicted in Fig.4.43, exhibits barreling type failure under an undrained loading, akin to ductile failure. This pattern was mostly followed by the low amount of bentonite clay i.e. SB10 and SB20 composite.

However, SB30 composite with 0.5% fiber content of an aspect ratio of 40 showed multiple cracks in the shear zone. At higher fiber content of 1% and 1.5%, specimen produces predominantly bulging with the formation of smaller fissures. The shear stress along the failure plane was overcome by the tensile strength of the fiber due to stretching of the fiber, as a result, stress was distributed within the specimen under the rapid loading. Hence, predominant bulging occurs at greater axial strain indicating the inducement of ductility.

4.9 Volumetric shrinkage and cracking behavior of compacted sand bentonite–fiber soil composite

Volume changes in compacted sand-bentonite mixtures develop in several ways. Many researchers have reported that the pore water was dissipated from the voids upon static surcharge and this mechanism is well-known as consolidation.

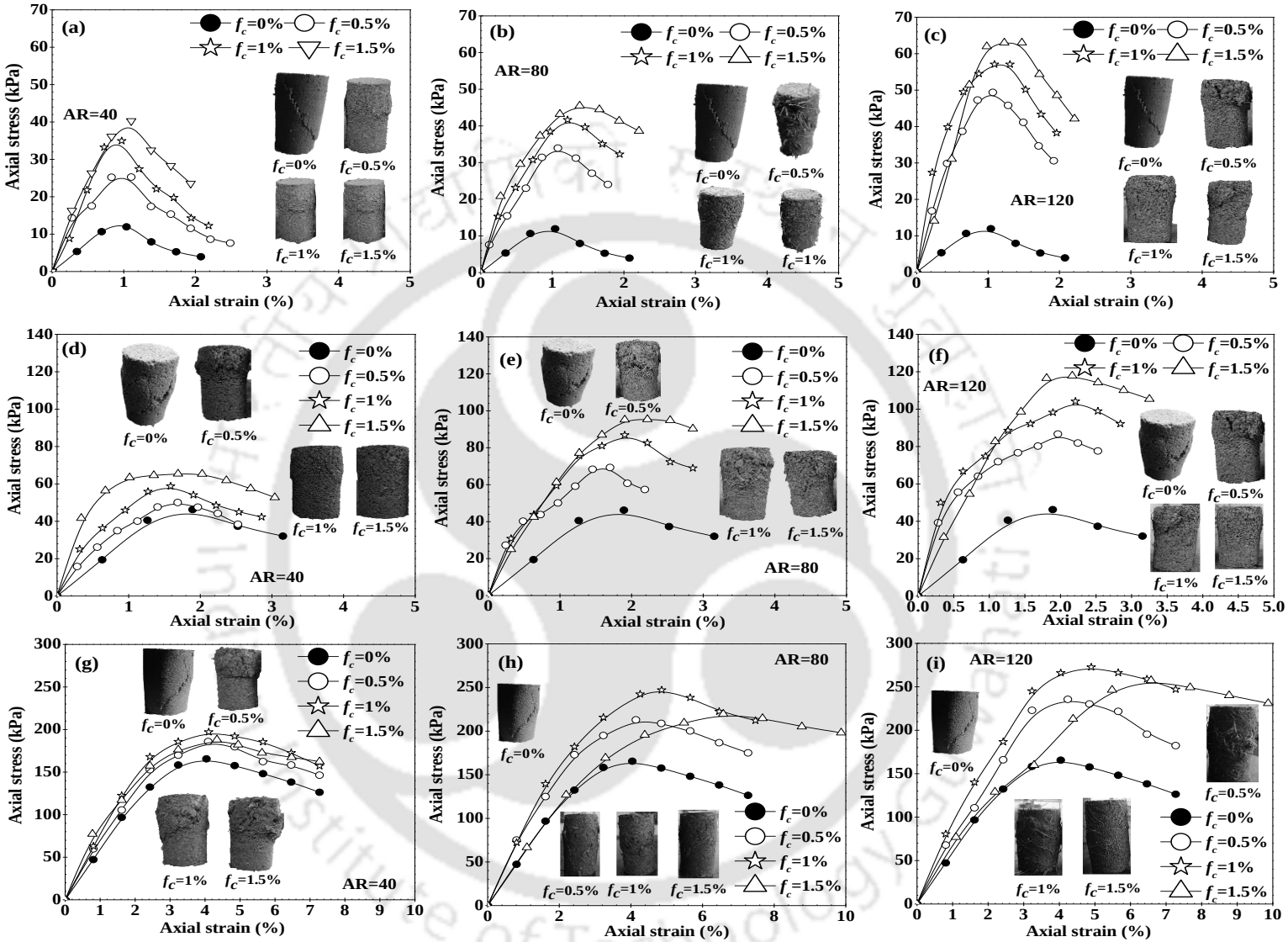

Figure 4.43 Stress-strain response of Sand bentonite mixture with different fiber concentration ;(a) SB10 with an aspect ratio of 40;(b) SB10 with an aspect ratio of 80;(c) SB10 with an aspect ratio of 120;(d) SB20 with an aspect ratio of 40;(e) SB20 with an aspect ratio of 80; (f) SB20 with an aspect ratio of 120;(g) SB30 with an aspect ratio of 40; (h) SB30 with an aspect ratio of 80;(i) SB30 with an aspect ratio of 120

Table 4-5 Summary of the improvement factor and displacement ratio of the compacted SB mixes

Fiber content and aspect ratio	SB10 composite		SB20 composite		SB30 composite	
Composite Name	Improvement factor	Displacement Ratio	Improvement Factor	Displacement Ratio	Improvement Factor	Displacement Ratio
f_c=0.5%, f_{ar}=40	2.11	1.06	1.17	1.02	1.12	1.01
f_c=1%, f_{ar}=40	2.92	1.09	1.37	1.04	1.2	1.03
f_c=1.5%, f_{ar}=**40**	3.37	1.24	1.62	1.11	1.18	1.09
f_c=0.5%, f_{ar}=80	2.87	1.21	1.62	1.07	1.26	1.06
f_c=1%, f_{ar}=80	3.49	1.36	2.01	1.31	1.49	1.22
f_c=1.5%, f_{ar}=**80**	3.81	1.53	2.26	1.47	1.32	1.68
f_c=0.5%, f_{ar}=120	4.04	1.24	2.05	1.29	1.42	1.09
f_c=1%, f_{ar}=120	4.69	1.45	2.47	1.48	1.64	1.23
f_c=1.5%, f_{ar}=**120**	5.22	1.62	2.78	1.50	1.55	1.72

f_c=fiber concentration; f_{ar}= fiber aspect ratio

Another phenomenon is due to the shrinkage of soil because of temperature variation. Desiccation is the continuous method of loss of pore water from soil exposed to a warm environment. During the process of drying, soil water volume decreases and soil shrinks. If the shrinkage of the soil was restrained, still it could be desiccated, when the tensile stress of the soil matrix exceeded the tensile strength of the soil. The shrinkage and cracking of SB mixture have a significant impact on the performance of SB mixtures in various geotechnical and environmental applications. Compressibility of the mixture, time rate of consolidation and shear strength of the mixture were significantly affected by the cracking behavior of the mixture. The compacted sand-bentonite mixture is one of the essential components of the municipal landfills and their design has usually been based on the basis of hydraulic conductivity criteria for landfill liner. However, desiccation induced cracks directly affect the hydraulic conductivity of the landfill liner material. Desiccation leads to the development of shrinkage cracks, which deliver the pathways for moisture migration into the landfill cell; as a result, this fact increases the generation of waste leachate, and ultimately increases the potential for soil and groundwater contamination. Another problem associated with desiccation cracks in soils includes expansion of the soils upon wetting and softening of the soils as a result of water entering the soil structure (Mitchell 1993). Expansion creates uplift forces in the soil and associated structures. Softening reduces soil strength as a result of water entry and may affect the stability of slopes (Miller et al. 1998). Therefore, the attention of using fibers has risen to improve the compacted sand bentonite performance as hydraulic barriers to make the crack less composite for the application of landfill. In this subsection was to investigate the impact of different glass fiber concentrations with three different aspect ratios (l/d) on the volumetric and cracking behavior of different sand–bentonite mixture. SB composite reinforced with different fiber content with an aspect ratio of 40 and 80 have been discussed below.

4.9.1 Impact of fiber on volumetric shrinkage (VS) and cracking behavior of compacted sand bentonite fiber soil composite

Volumetric shrinkage (VS) of the soil is one of the most important factors, which must be considered in order it to be used as a liner and cover material at the landfill. Daniel and Wu (1993) considered that 4% VS of the soil (under MDD and OMC condition) had been taken for the acceptable limit of the landfill liner and cover material. All the compacted specimen has been prepared to their respective MDD and OMC condition. In this condition, volumetric shrinkage has been measured and discussed below.

VS was evaluated for the unreinforced as well as reinforced specimen and exhibited in Fig.4.44 and Fig.4.49. From the figure, it has been noticed that volumetric shrinkage of the composite was gradually decreased with the inclusion of glass fiber concentration and different fiber aspect ratio. This flat trend was followed by the all SB composite. In the case of SB30 composite, the VS of the unreinforced specimen was measured to be 6.46%. However, with an aspect ratio of 40, the VS was reduced from 6.46% to 4.86, 3.66 and 2.94% at 0.5, 1 and 1.5% of fiber content. At same fiber content, VS was again decreased from 6.46% to 3.67, 2.91 and 1.59% with an increase the aspect ratio from 40 to 80. Similar kind of observation was noticed for SB30 composite with an aspect ratio of 120.

The another composite i.e. SB20, VS was found to decrease from 3.96% from 2.81%,2.42 and 1.88% at 0.5%, 1 and 1.5% fiber content with an aspect ratio of 40. However, at same fiber content, VS of the SB20 composite was further reduced from 3.96% to 2.32%, 1.84 and 1.37% with increase the aspect ratio from 40 to 80. SB20 composite with an aspect ratio of 120 followed the same trend as earlier it has been reported.

It was found that VS of the SB10 composite was decreased from 1.4% to 1.1, 0.74% at 0.5%, 1 and 1.5% fiber content with an aspect ratio of 40. However, no change in VS was observed for the SB10 composite reinforced with different content of the glass fiber of an aspect ratio of 80 and 120. As the concentration increased, the glass fiber was resisted against the volume change. With increase the fiber aspect ratio, the overall tensile stress of the fiber soil matrix was increased; as a result, the VS of the composite was continuously decreased with fiber aspect ratio. This finding suggests the fiber additives would minimize the volumetric shrinkage of landfill liner as well as landfill cover barrier when desiccation exists.

The cracking features of a composite have been estimated in terms of the crack intensity factor (CIF) and crack density factor (CDF) and both the factors were significantly altered by the inclusion of glass fiber. All the cracking parameters were measured at the end of equilibrium moisture content and reported with their standard deviation, which was below the 5% error level. CDF and CIF are exhibited in Fig.4.44 and Fig.4.49. From the figure, it was observed that CDF of the unreinforced soil was considerably high and it was measured to be 15.25. However, with an aspect ratio of 40, CDF was gradually reduced from 15.25 to 12.86, 10.41, and 8.35 at 0.5, 1, and 1.5% fiber content. From another observation, with an increase the aspect ratio from 40 to 80, the CDF was further reduced from 15.25 to 8.41, 8.85 and 5.23 at the same amount of fiber content and similar kind of trend was captured for SB30 composite with an aspect ratio of 120. All the CDF was obtained from the binary image of the composite and it was depicted in Fig.4.50 and Fig.4.51. The fiber inclusion was able to improve the desiccation-induced cracking. A typical hair type cracking was noticed on the unreinforced soil under the MDD-OMC condition and this crack divides the soil mass in to a series of small cells, however, fiber-reinforced soil presented a larger

cell with relatively small crack as a result CDF of the fiber-reinforced composite was found to reduce continuously due to the inclusion of glass fiber.

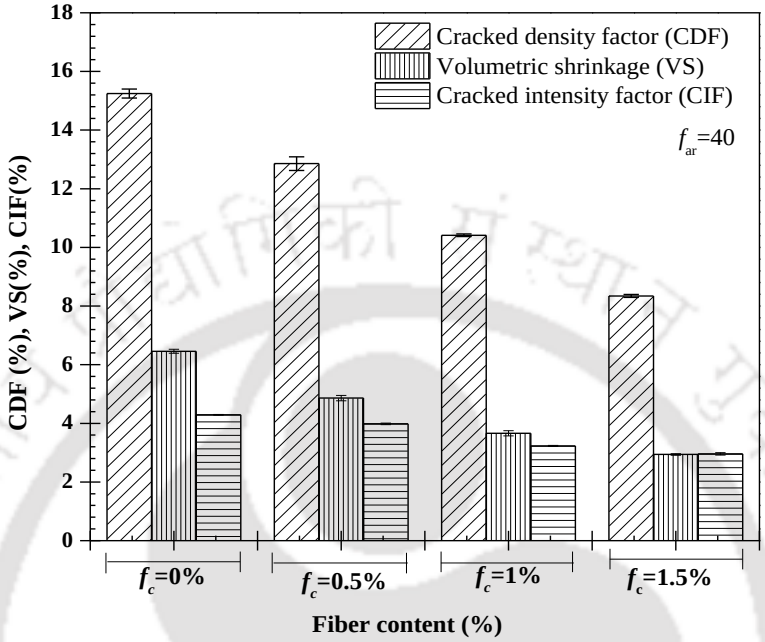

Figure 4.44. CDF, VS and CIF of the SB30 composite with an aspect ratio of 40

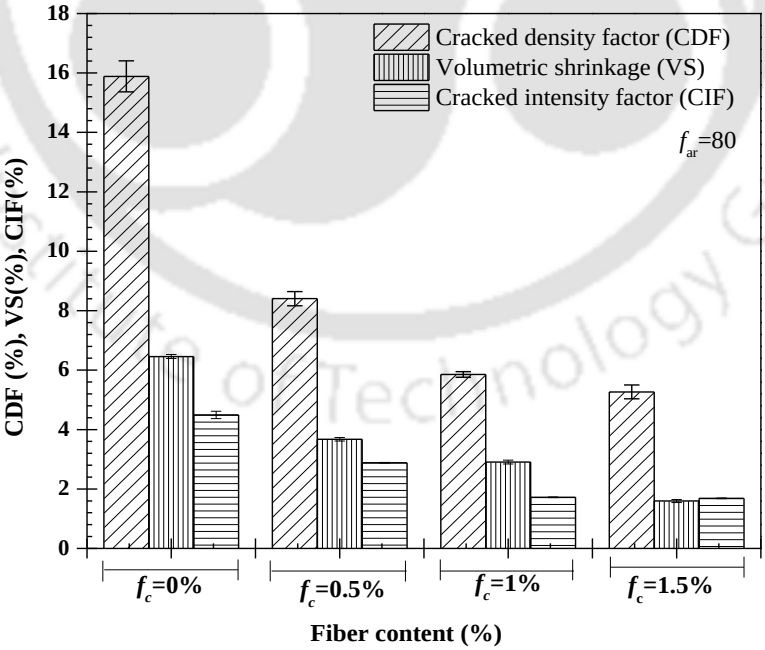

Figure 4.45 CDF, VS and CIF of the SB30 composite with an aspect ratio of 80

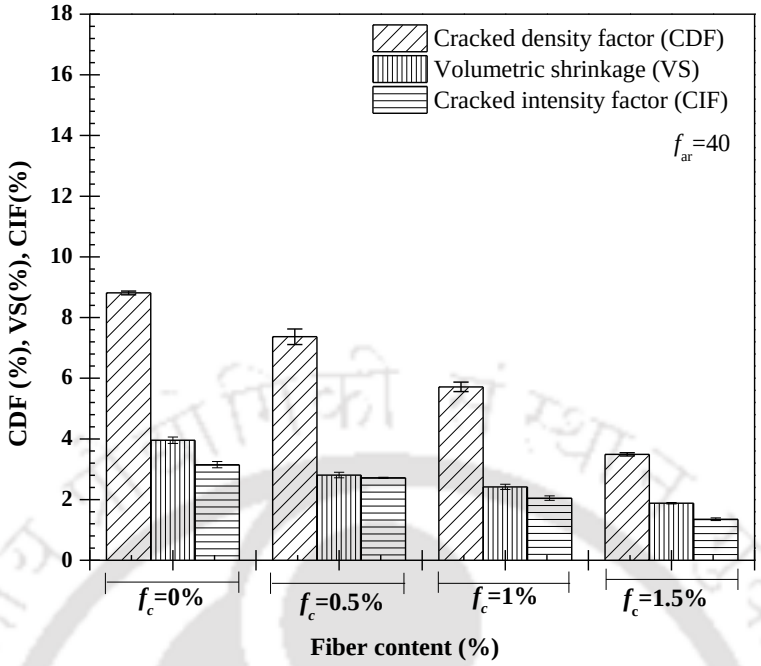

Figure 4.46 CDF, VS and CIF of the SB20 composite with an aspect ratio of 40

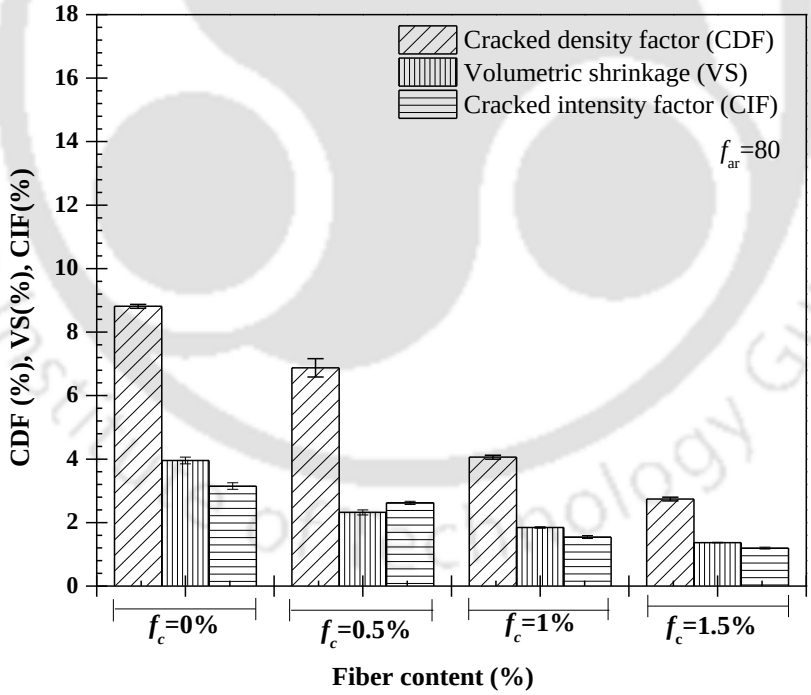

Figure 4.47 CDF, VS and CIF of the SB20 composite with an aspect ratio of 80

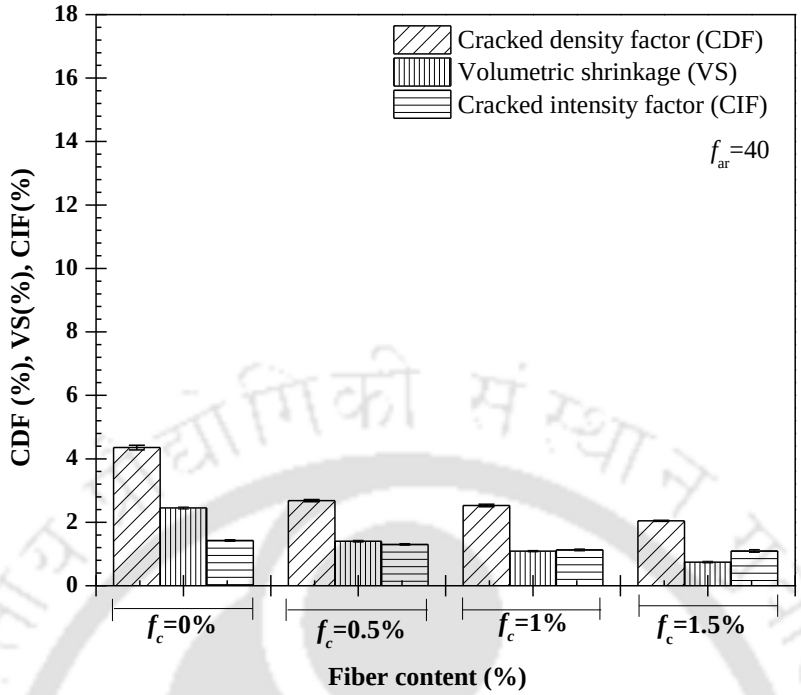

Figure 4.48 CDF, VS and CIF of the SB10 composite with an aspect ratio of 40

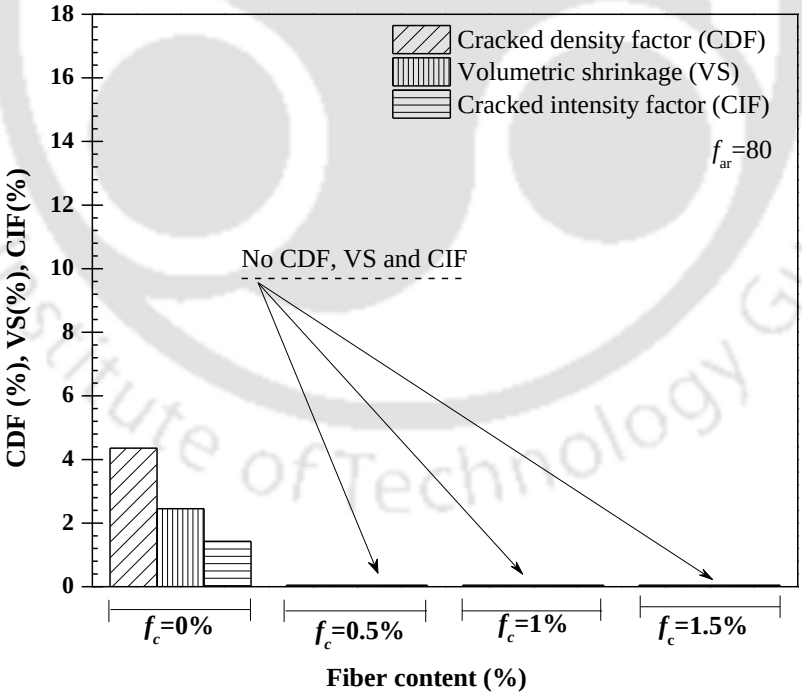

Figure 4.49 CDF, VS and CIF of the SB10 composite with an aspect ratio of 80

Similarly, in the case of SB20, the CDF was reduced from 8.87 to 7.37, 5.72 and 3.49 at 0.5, 1 and 1.5% fiber content with an aspect ratio of 40, respectively. With an increase in the aspect ratio from 40 to 80, CDF was further decreased from 8.81 to 6.87, 4.06, and 2.74 at the same fiber content. An identical trend was followed by SB20 reinforced with glass fiber with an aspect ratio of 120. A similar trend was followed by the SB10 with an aspect ratio of 40, but no crack was observed in the specimen; as a result, CDF was found to be negligible for SB10 with an aspect ratio of 80 and 120. Since a higher bentonite content is more susceptible for desiccation crack, the CDF was considered high for SB30 in comparison to SB20 composite. Hence, CDF was strongly dependent on the fiber content, fiber aspect ratio, and bentonite content.

The impact of fiber reinforcement on desiccation cracking was determined as a function of fiber content and aspect ratio of the fiber and expressed in the form of CIF. CIF was found out for unreinforced soil to use as baseline data for comparison with the different reinforced mixture. The progress and propagation of cracks are mostly a function of active bentonite fraction, specifying that the higher the bentonite fraction, the greater the intensity of crack (Mitchell and Soga 2005). Highest CIF value was observed for SB30 composite and it gradually decreased with decrees in bentonite content and an increase in fiber content and their aspect ratio and presented in Fig.4.44 and Fig.4.49.

The relationships between CIF and fiber content and fiber aspect ratio exhibited that CIF was significantly reduced with fiber content and fiber aspect ratio. For example, CIF was found to be 4.29 for unreinforced SB30. However, CDF was reduced from 4.29 to 3.98, 3.23, and 2.96 at 0.5%, 1 and 1.5% fiber content with an aspect ratio of 40. With increase the aspect ratio from 40 to 80, CDF was decreased from 4.29 to 2.88, 1.72, and 1.69 at the same fiber content.

From another observation i.e., for SB20 composite, CIF was gradually decreased from 3.15 to 2.71, 2.05 and 1.35 at 0.5%, 1 and 1.5% fiber content with an aspect ratio of 40. However, at same fiber content, CIF was also reduced from 3.15 to 2.62, 1.55 and 1.19 with an aspect ratio of 80 and similar behavior were observed for SB20 reinforced with glass fiber with an aspect ratio of 120. An identical pattern was followed by SB10 composite also.

Costa et al. (2013) reported that tensile stresses produced within the soil could exceed the soil's tensile strength, thus resulting in the development and propagation of cracks during drying and wetting process. However, this tensile strength is governed by the fiber content and fiber aspect ratio; as a result, CIF (i.e. crack area) of the composite was decreased by the addition of fiber.

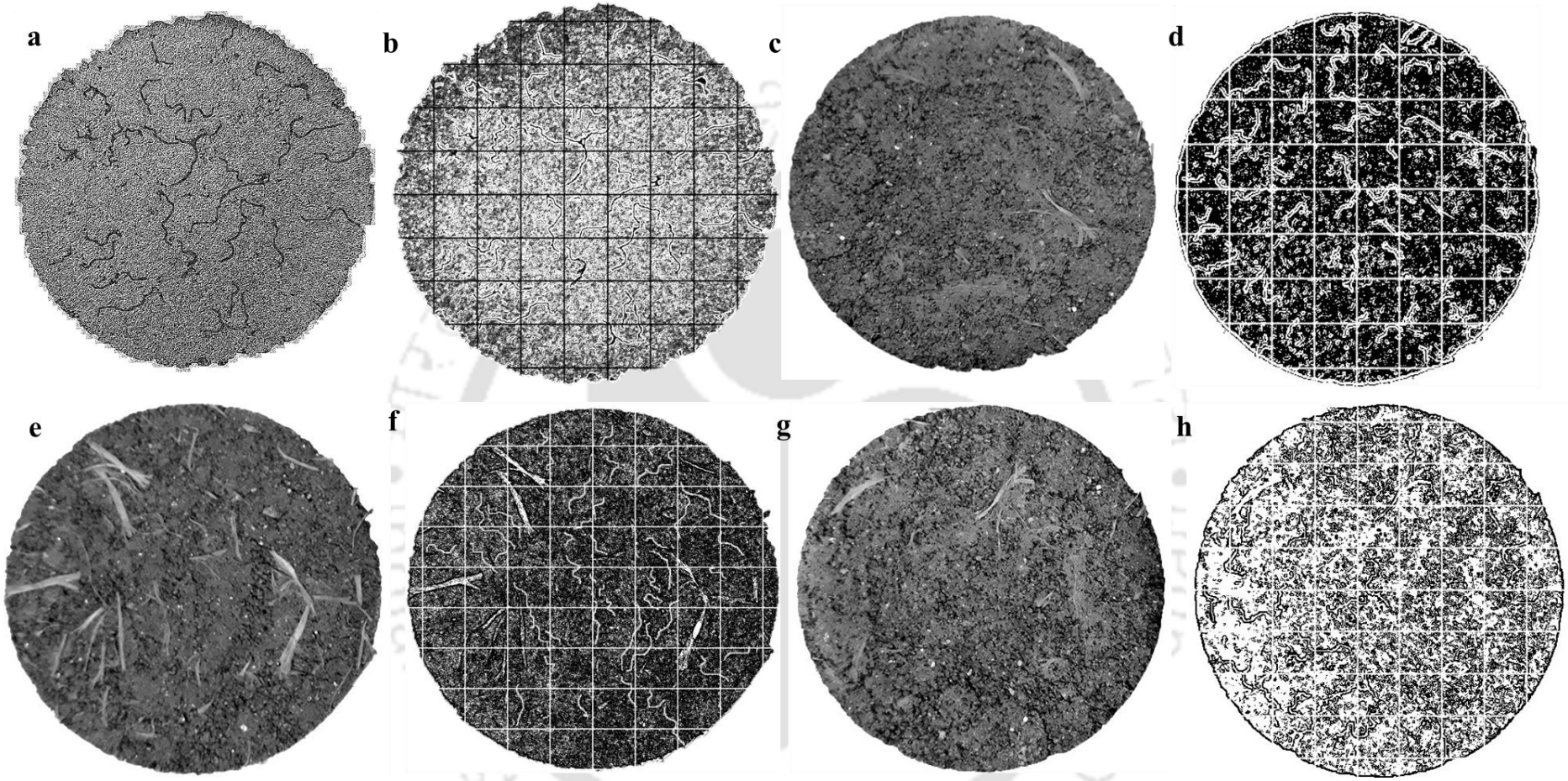

Figure 4.50 Noticeable crack pattern of SB30 composite;(a and b) SB30 gray scale and binary ;(c and d) gray scale and binary image of SB30 at 0.5% fiber content with an aspect ratio of 40;(e and f) gray scale and binary image of SB30 at 0.5% fiber content with an aspect ratio of 80; (g and f) gray scale and binary image of SB30 at 0.5% fiber content with an aspect ratio of 120

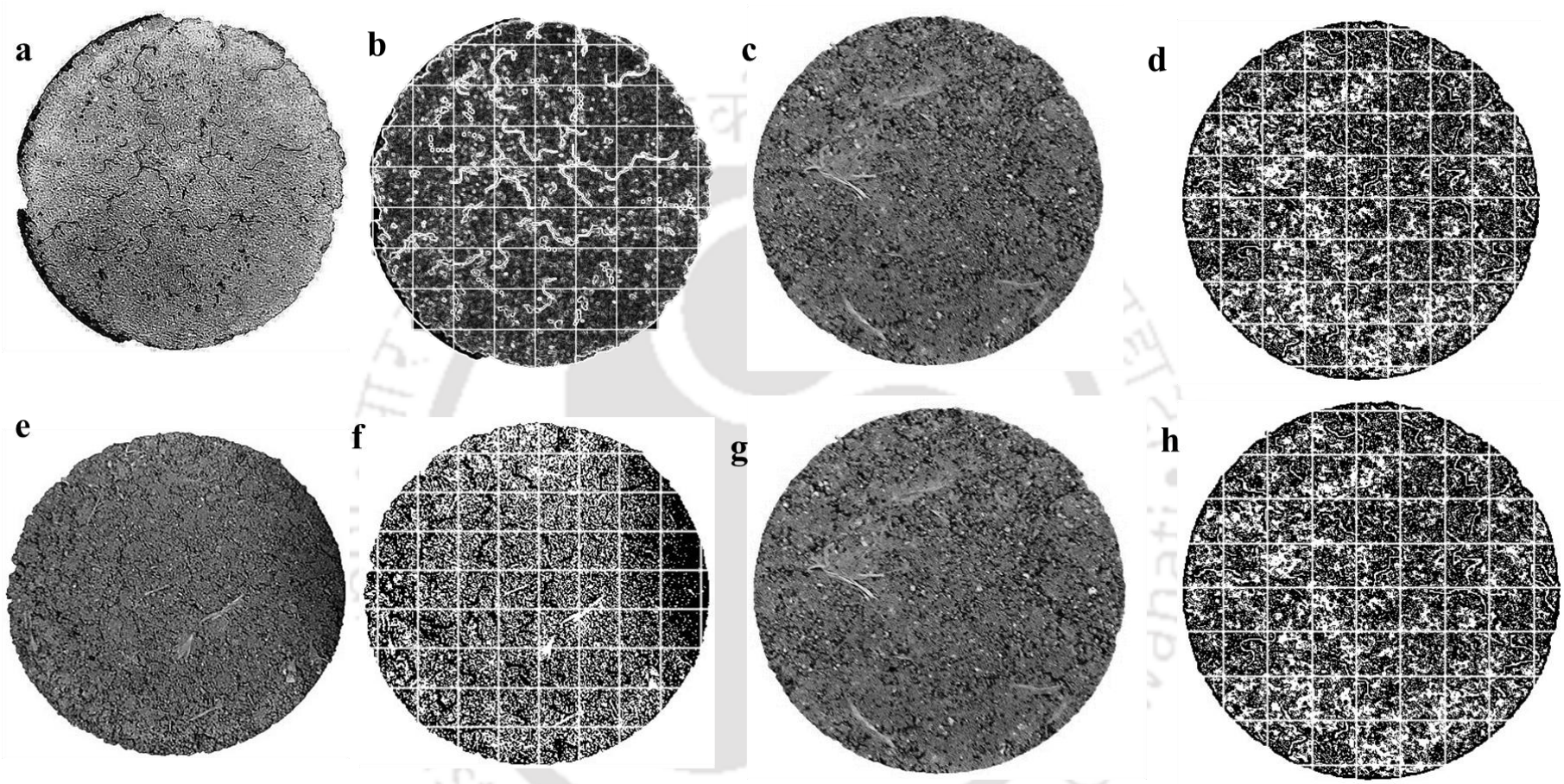

Figure 4.51 Noticeable crack pattern of SB20 composite;(a and b) SB20 gray scale and binary ;(c and d) gray scale and binary image of SB20 at 0.5% fiber content with an aspect ratio of 40;(e and f) gray scale and binary image of SB20 at 0.5% fiber content with an aspect ratio of 80; (g and f) gray scale and binary image of SB20 at 0.5% fiber content with an aspect ratio of 120

Chapter 5
Result and Discussion
(SB-Tire fiber Composite)

5.1 Compaction behavior

Stability and settlement of a landfill structure such as a liner and cover depend on how well the fill material is compacted. If the fill material, for example, is dumped or otherwise placed at random in a fill, the result will be a landfill structure undergoes with low stability and high settlement (Holtz and Kovacs 1981; Cetin et al.2006). Standard proctor (compaction) tests were performed to determine the compaction characteristics of both reinforced and unreinforced sand-bentonite mixture. The mixture of bentonite and sand mixed in a proportion of 90:10, 20:80, 30:70 by their dry weight were prepared and named as SB10, SB20, and SB30 in the further discussion. Different percentages of tire fiber (i.e. 0, 5, 10 and 15%) by their dry weight were then added to SB mixture. Maximum dry density (MDD) and optimum moisture content (OMC) were determined from the compaction test carried out as per ASTM D698 (2012).

5.1.1 Compaction behavior of various sand bentonite –tire fiber composites

The moisture-density relationships for unreinforced and reinforced specimens have been shown in Fig.5.1 and Fig.5.3. The addition of tire fiber caused an alteration in the moisture-density relationships. As the content of tire fiber increased, the OMC was reduced continuously but the MDD remained almost constant. In case of SB10 composite, the MDD decreased gradually from 1.76 g/cm^3 to 1.74, 1.71 and 1.69 g/cm^3 due to the addition of 5, 10 and 15% of tire fiber,

respectively. Similarly, for SB20 the MDD reduced from 1.727 g/cm^3 to 1.69, 1.655 and 1.57 g/cm^3 with the addition of 10 and 15% tire fiber, respectively.

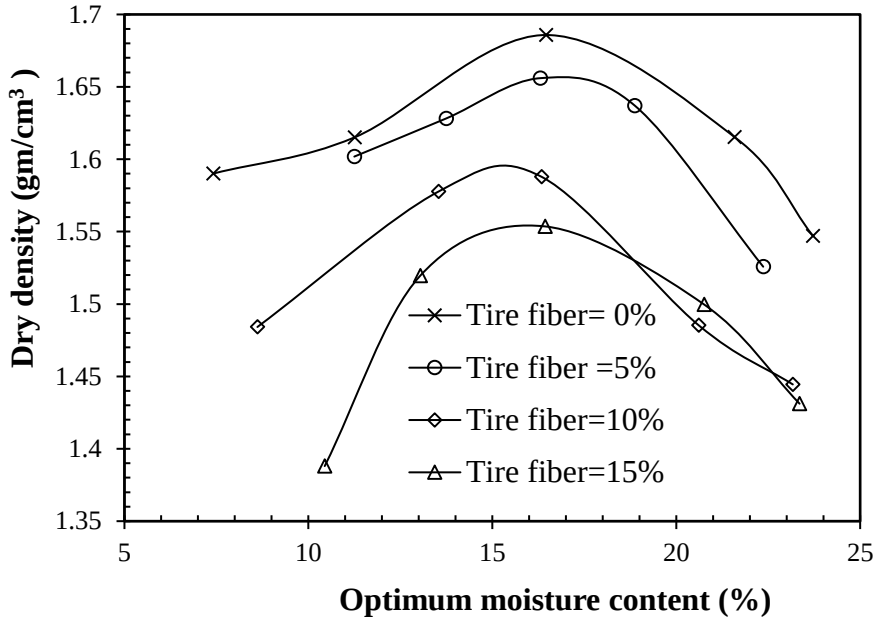

Figure 5.1 MDD and OMC relationships of SB30 composite

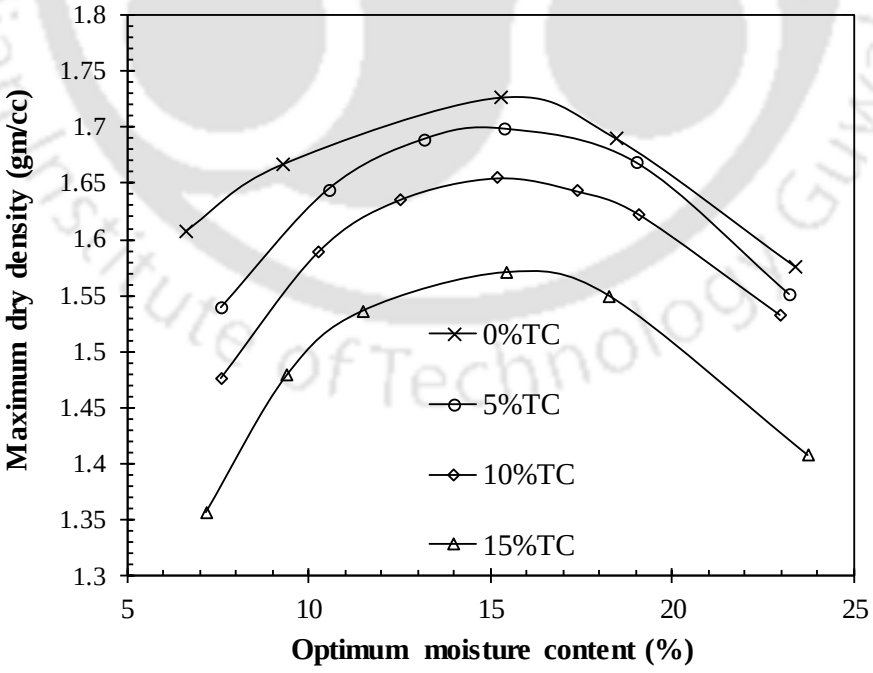

Figure 5.2 MDD and OMC relationships of SB20 composite

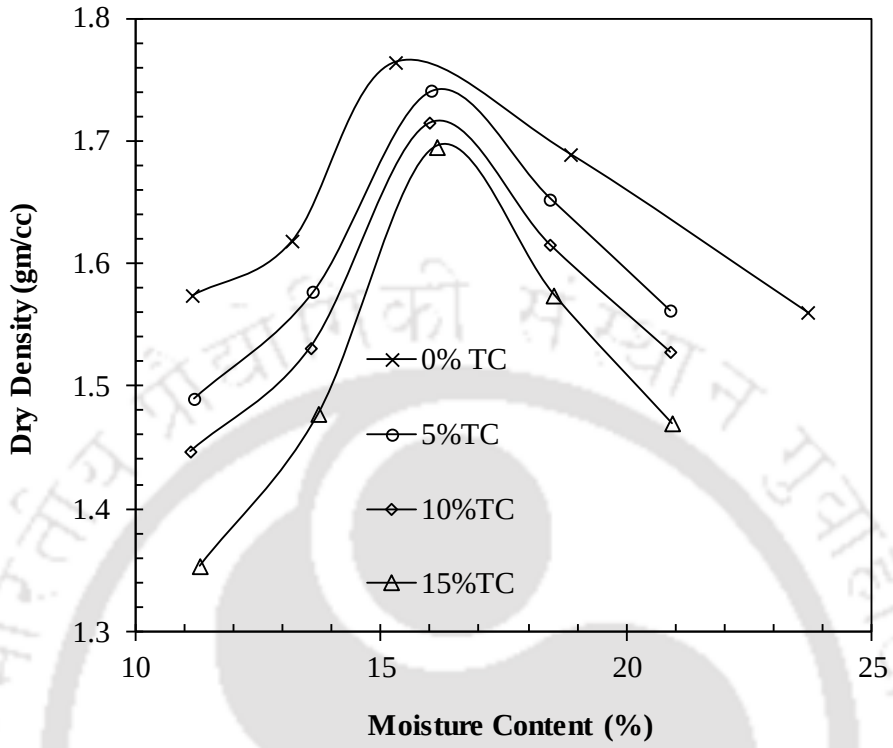

Figure 5.3 MDD and OMC relationships of SB20 composite

From SB30 composite, test result suggested that MDD was reduced from 1.686 g/cc to 1.656 g/cc, 1.587, and 1.55 g/cc with increase the tire fiber content from 5%, 10 and 15%. This is attributed to the lower specific gravity of the tire fiber. This combined effect was directly responsible to reduce the initial degree of saturation (IDS). For example, IDS of the SB20 composite was slightly reduced from 74.21% to 73.86%, 71.01 and 68.57% with the presence of 5, 10 and 15% of tire fiber, respectively. From another observation, IDS of the SB30 composite was reduced from 73.86% to 72.44, 70.71 and 69.43% with the addition of 5, 10 and 15% tire fiber, respectively. A similar pattern was observed for the mixture of SB10 composite as well.

5.2 Swelling behavior of SB-tire fiber composite

The influences of tire fiber on the swelling behavior of SB30 and SB20 are shown in Fig.5.4. From the figure, it can be observed that the swelling tendency of the tire fiber gets significantly affected by the addition of tire fiber. For the SB30 mixture, it was noticed that the increase in swelling height with time started rapidly, and then moved towards an asymptotic value. However, this pattern of swelling significantly changed with the addition of tire fiber to the mixture. In the case of the SB30 mixture reinforced with tire fiber, the increase in swelling height was slow initially and then increased sharply to reach a constant value. It was observed that the swelling height decreased with the addition of tire fiber to the mixture. Under vertical stress of 5 kPa, a swelling height of 1.44 mm was observed for the SB30 mixture. However, under the same vertical stress, the swelling height decreased from 1.44 mm to 0.98, 0.64, and 0.49 mm with the addition of 5, 10, and 15% of tire fiber, respectively. For SB20 composite, under the same vertical stress, swelling height was reduced from 0.58 mm to 0.44, 0.29, and 0.24 mm with the addition of 5, 10 and 15% tire fiber, respectively. A similar trend was also observed by Trouzine et al. (2012) for expansive clay reinforced with tire fiber. Additionally, the highest variances in the time-swelling pressure curve were noticed with the inclusion of 15% tire fiber. Due to the irregular and rough surface of tire fiber, as shown in (Fig.3.1) the surface area of the fiber produced a larger interaction surface with soil particles (Baykal 2008), which led to an additional interaction among fibers and soil particles. This increased the tensile forces between tire fibers and decreased the swelling tendency of the SB30 and SB20. On the other hand, the maximum swelling height for the SB10 mixture was 0.04 mm, which was considerably low due to the presence of a higher amount of sand. No swelling tendency was observed for SB10 mixtures reinforced with tire fiber.

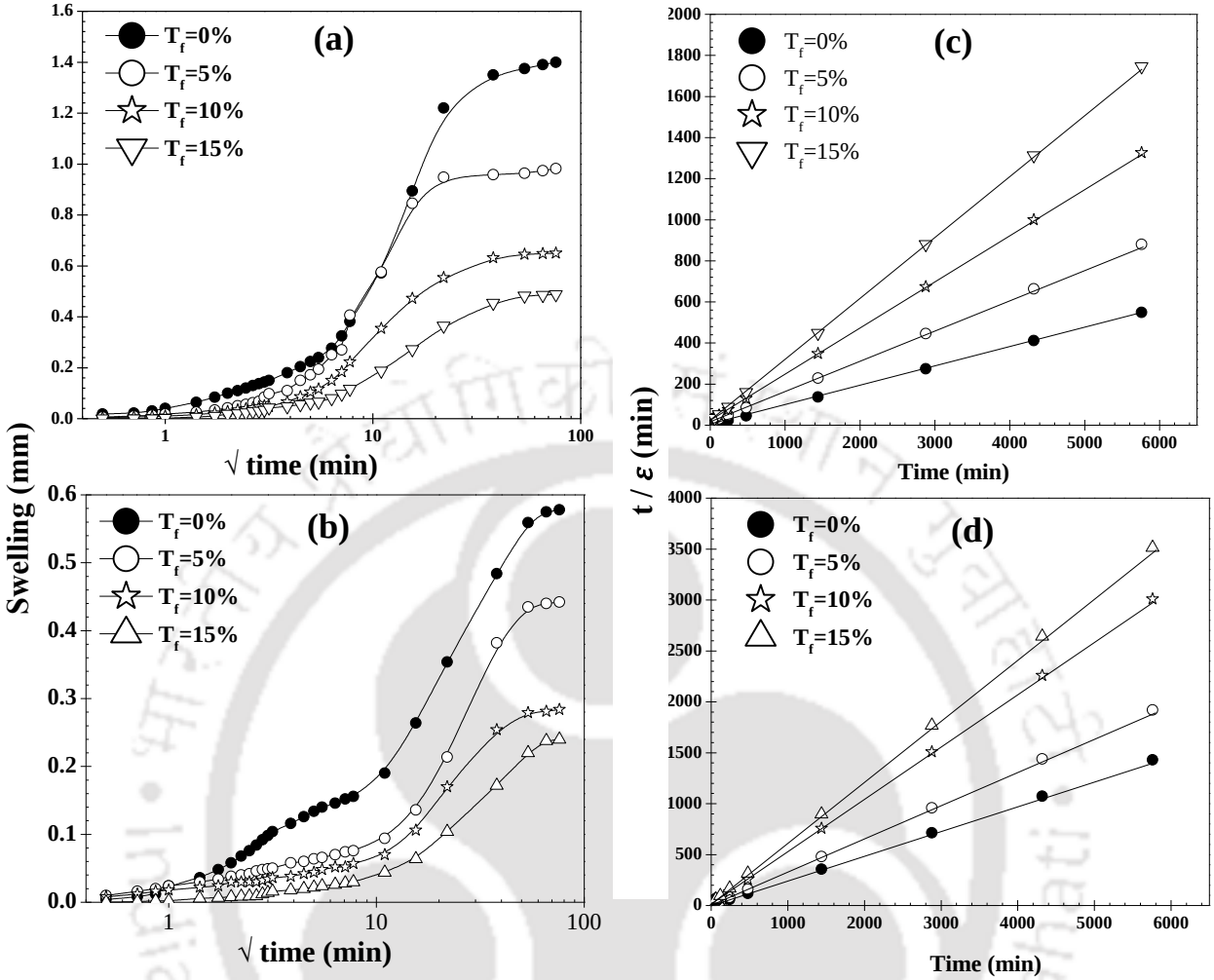

Figure 5.4 Swell-time relationships for; (a) SB30-tire fiber composite; (b) SB20-tire fiber composite; (c) linearized illustration of swelling data for SB30-tire fiber composite; (d) linearized illustration of swelling data for SB20-tire fiber composite

The swelling potentially was reduced gradually as the percentage of tire fiber increased. For SB30, swelling potentially was reduced significantly from 9.53% to 6.55, 4.33 and 3.25% at 5%, 10 and 15% tire fiber content, respectively. Similarly, for SB20 the swelling potential decreased from 3.85% to 2.95,1.89 and 1.6% with the presence of 5%, 10 and 15% of tire fiber, respectively. As the tire fiber content increased in the mixture, the overall expansion strain was restrained by the tensile strength, which developed by the tire fiber and adjacent soil piratical during the swelling

process of the composite. The maximum swelling was predicted using hyperbolic model as discussed in section 4.2.3and value listed in Table 5-1. From the table, it can be seen that the observed value was almost identical with the predicted value. The figure indicates that of the slope of the SB-tire fiber composite gradually increased in comparison to unreinforced composite, indicating that residual swelling potential was decreased by the inclusion of tire fiber.

Table 5-1Comparison of measured and predicted maximum swelling potential for SB20 and SB30 at the different tire fiber content

Composite Name	**a**	b	Measured swell (%)	Max. Swell Predicted (%)
SB20, T_f = 0%	0.248	0.071	3.85	4.03
SB20, T_f = 5%	0.333	0.150	2.95	3.00
SB20, T_f = 10%	0.521	7.221	1.89	1.92
SB20, T_f = 15%	0.606	24.521	1.61	1.65
SB30, T_f = 0%	0.0953	0.0239	9.53	10.46
SB20, T_f = 5%	0.151	12.631	6.55	6.64
SB20, T_f = 10%	0.226	21.856	4.33	4.42
SB20, T_f = 15%	0.301	16.235	3.25	3.33

T_f= Tire fiber content

The swelling pressure for the SB30 composite was reduced with the increase in the tire fiber content. Swelling pressure of the SB30 composite was reduced from 46 kPa to 35, 28 and 22 kPa with the presence of 5%, 10 and 15% tire fiber content, respectively as exhibited in Fig.5.5. In case of SB20 mixture, the swelling pressure decreased continuously from 32 kPa to 26, 17, and 11 kPa with the addition of 5%, 10%, and 15% of tire fiber, respectively. The addition of tire fiber decreased the swelling pressure of mixtures due to the reinforcement effect induced by the tensile strength of tire fiber against the swelling of the mixture, and this mechanism blocked the movement

of adjacent clay particles attached to the tire fiber. A similar trend was observed by Yadav and Tiwari (2017) for expansive soil mixed with crumb rubber.

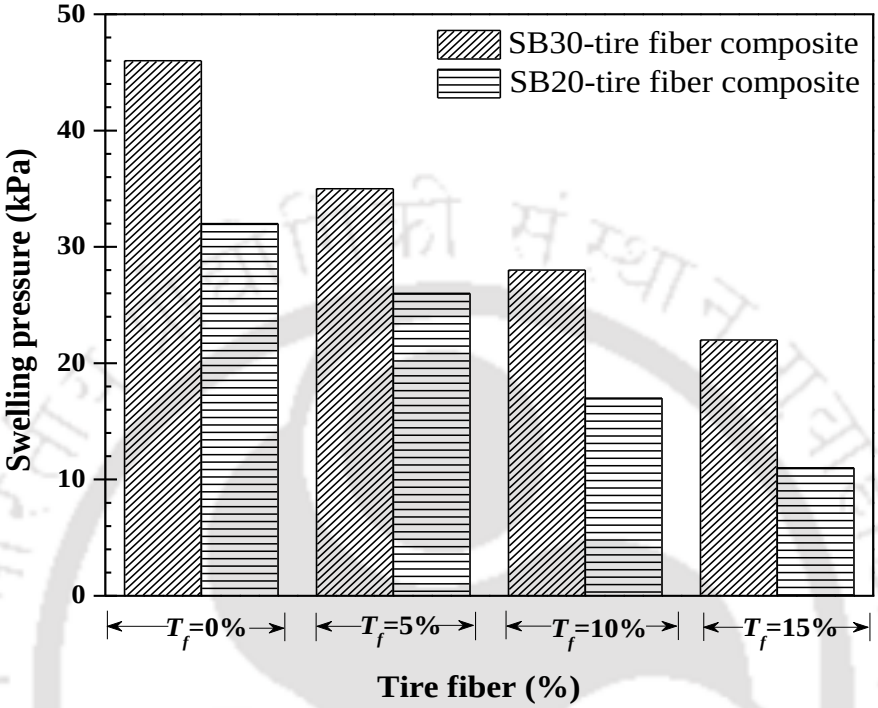

Figure 5.5 Relationships between swelling pressure and tire fiber content

5.2.1 Volume change behavior of SB-tire fiber composite

Void ratio– pressure response for the reinforced and unreinforced samples is exhibited in Fig.5.6 and Fig.5.8 for SB30 composite to SB10 composite. From the plots, it has been observed that tire fiber additions changed the compressibility behavior, promoting a noticeable downward shift over the curve, thereby reducing the swelling pressure as well. It was also noticed that reduction in void ratio is the function of tire fiber content. For example, under the consolidating pressure of 200 kPa, the void ratio of the SB30 composite was measured to be 0.54. However, the void ratio of the composite was reduced from 0.54 to 0.49, 0.42 and 0.40 at 5%, 10 and 15% tire fiber content, respectively. For SB20 composite, at same consolidating pressure, the void ratio was reduced from

0.48 to 0.44, 0.41 and 0.38 at 5, 10 and 15% of tire fiber content, respectively. A similar trend was followed by SB10 composite also. For SB20 and SB30 composite, the compression index (C_c) was reduced up to 5% tire fiber, thereafter, it increased sharply with further addition of tire fiber. For example, C_c of SB30 was decreased from 0.33 to 0.284, due to 5% tire fiber inclusion; however, C_c was increased from 0.284 to 0.352 and 0.387 with a further increase the tire fiber from 5 to 10 and 15%, respectively. An identical trend was followed by SB20 composite also. At the high percentage of tire fiber content, the compressibility of the SB30 and SB20 composite increased drastically due to tire-to-tire interaction and it was increased more in comparison to tire to soil interaction.

However, the behavior of SB10 composite has slightly diverged from the SB30 and SB20 composite. In this case, C_c was decreased up to 10% tire fiber content, after that, C_c was increased slightly with the further addition of tire fiber. For example, C_c was decreased from 0.033 to 0.013 and 0.009 at the presence of 5% and 10% tire fiber, however, with increase the tire fiber from 10% to 15%, C_c was increased from 0.009 to 0.11.

On the other hand, swelling index (C_s) was improved significantly as the tire fiber content increased. This sharp trend was observed for all the mixture. The swelling index of SB30 was increased from 0.018 to 0.044, 0.077and 0.104 with increase the tire fiber percentage from 5%, 10 and 15% respectively. For SB20 composite, the swelling index was increased from 0.103 to 0.192, 0.246, 0.286 with the inclusion of 5, 10 and 15% tire fiber, respectively. A similar pattern was observed for the composite of SB10. This rebound mechanism indicated that material property was improved due to the improvement of elasticity, which comes from the elastic nature of tire fiber.

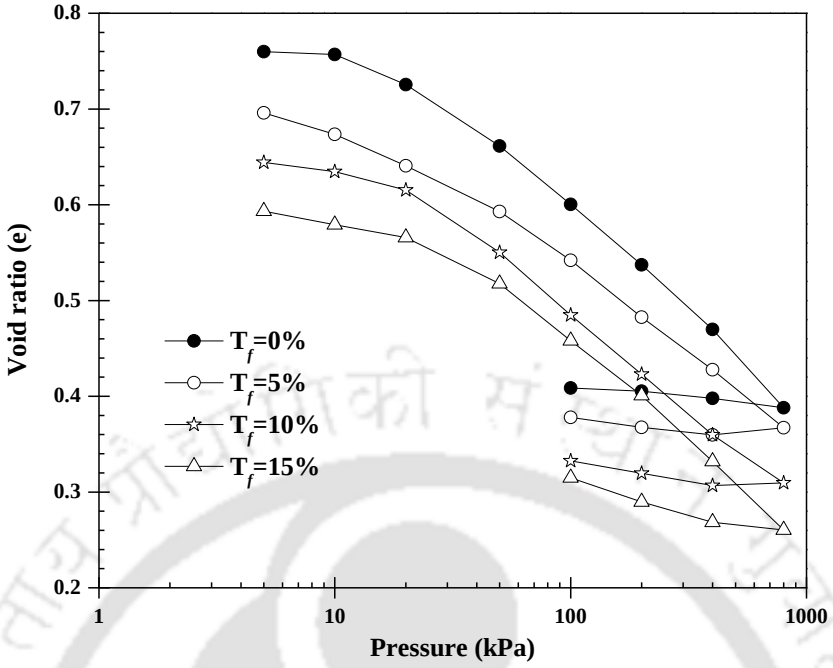

Figure 5.6 Void ratio vs pressure relationships for SB30 composite

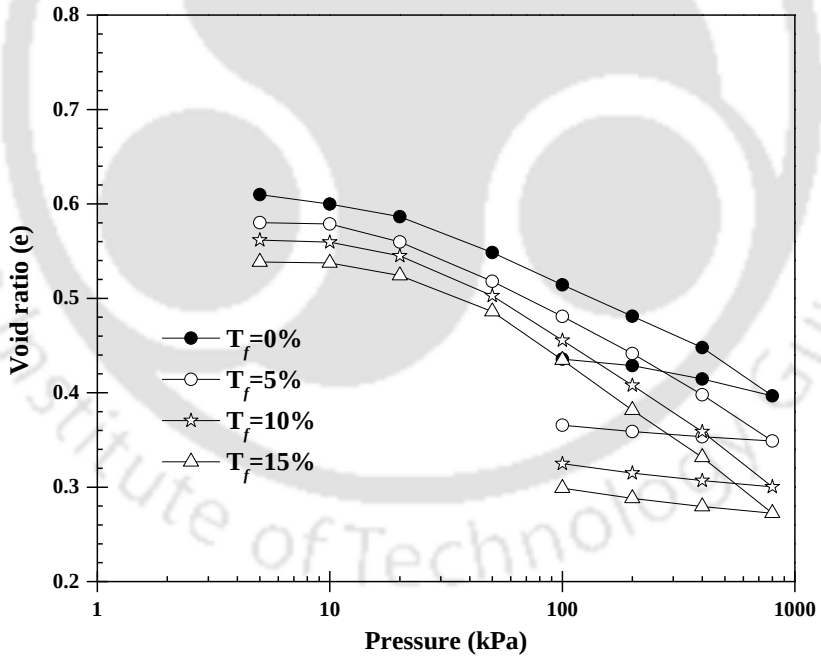

Figure 5.7 Void ratio vs pressure relationships for SB20 composite

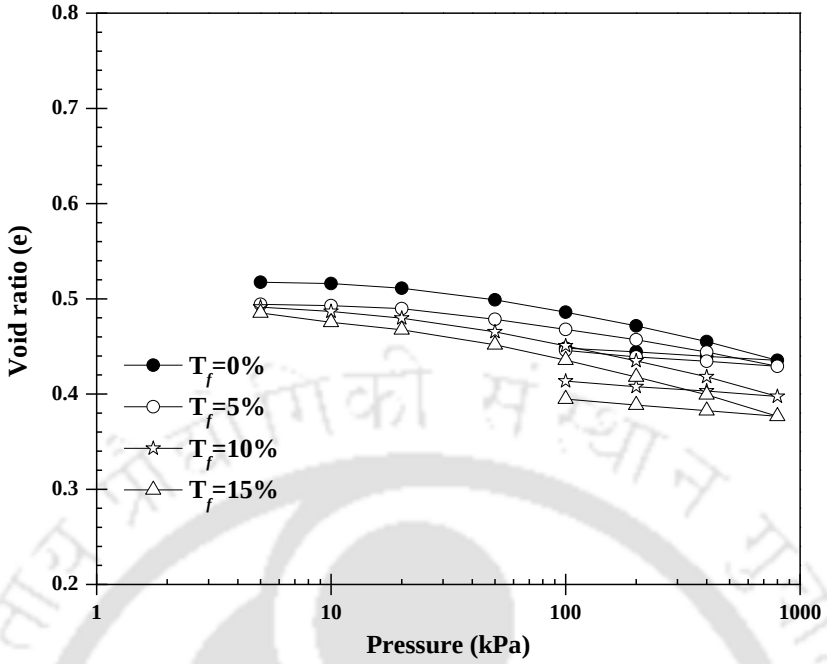

Figure 5.8 Void ratio vs pressure relationships for SB10 composite

5.3 Hydraulic behavior through composite soil

The behavior of landfill structure is utterly affected by the high compressible nature of the soil (i.e. sand-bentonite mixture or bentonite clay). In the current study, one-dimensional consolidation tests were performed on different sand-bentonite mixture reinforced with tire fiber to study the rate of consolidation and hydraulic conductivity of the composite. Coefficient of consolidation (c_v) is essentially an indicator of the rate of consolidation of soil composite and it dependents on the rate at which water can expelled out of the compacted sample for a given load increment. A higher value of c_v indicates a faster rate of consolidation. On the other important parameter, i.e. hydraulic conductivity of the soil is one of the most essential criteria that must be satisfied in order for it to be used as a liner and cover material at the landfill. Coefficient of consolidation and hydraulic conductivity behavior of the composite have been analyzed and discussed below.

5.3.1 Coefficient of consolidation of SB-tire fiber composite

Coefficient of consolidation (c_v) - Pressure relationship exhibited by various SB composite are represented in Fig.5.9 and Fig.5.11. With load increments, c_v values were found to be equally decreased in case of all SB composite. For example, c_v of the SB30 composite was measured to be 9.53×10^{-4} and 8.19×10^{-4} cm^2/sec, under the consolidating pressure of 50 and 100 kPa, respectively. At the same consolidating pressures, c_v was measured to be 7.8×10^{-3} cm^2/sec and 4.2×10^{-3} cm^2/sec with 5% tire fiber. With increase the fiber content from 5 to 10%, c_v was calculated to be 11×10^{-3} cm^2/sec and 6×10^{-3} cm^2/sec under the same consolidating pressure. At the same configuration, c_v was measured to be 35×10^{-3} cm^2/sec and 12×10^{-3} cm^2/sec with increase the tire fiber content from 10 to 15%.

A similar trend was obtained for the mixture of SB20 and SB10 composite and presented in Fig.5.10 and Fig.5.11. In case of an unreinforced mixture, when restricted by a surcharge pressure, bentonite particles in the sand-bentonite mixture swell upon access to water resulting in blocking or partial blocking of pathways, which would result in a reduced flow rate. However, in the case of fiber-reinforced soil, tire fiber developed an extra drainage path; therefore, hydraulic conductivity is increased with the addition of tire fiber.

For SB30 composite, c_v was accelerated from 8.19×10^{-4} cm^2/sec to 4.2×10^{-3}, 6×10^{-3} and 12×10^{-3} cm^2/sec at 5, 10 and 15% of tire fiber content, respectively. However, for SB20, it increased from 3.2×10^{-3} cm^2/sec to 7.97×10^{-3},1.53×10^{-2} and 2.56×10^{-2} cm^2/sec in the presence of 5, 10 and 15% of tire fiber contents, respectively. For SB10, c_v increased from 4.5×10^{-3} cm^2/sec to 8×10^{-3}, 9.8×10^{-3} and 1.05×10^{-2} cm^2/sec with the addition of 5, 10 and 15% tire fiber, respectively.

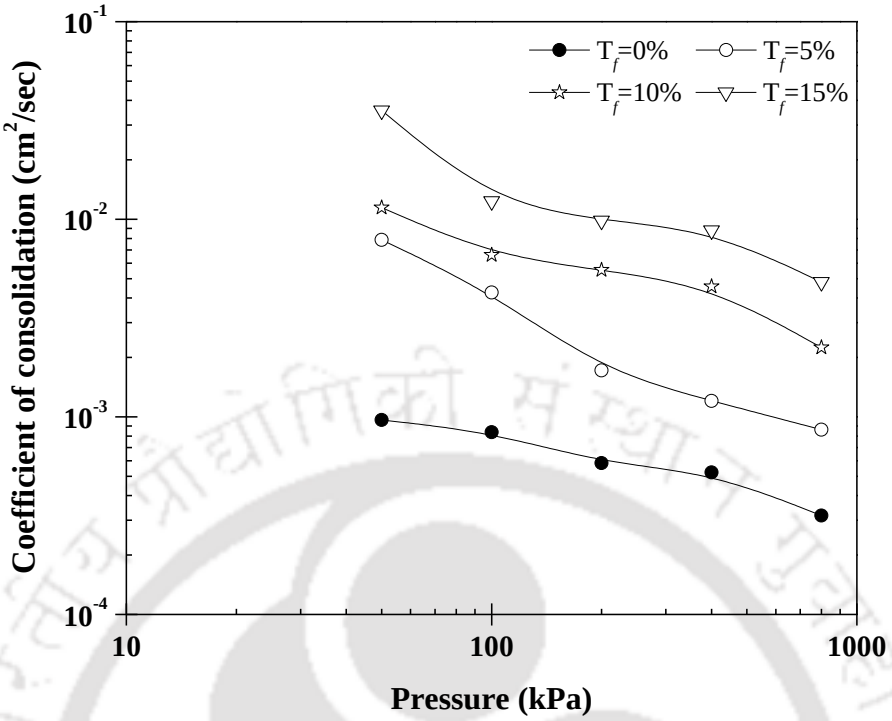

Figure 5.9 c_v vs pressure relationships for SB30 composite

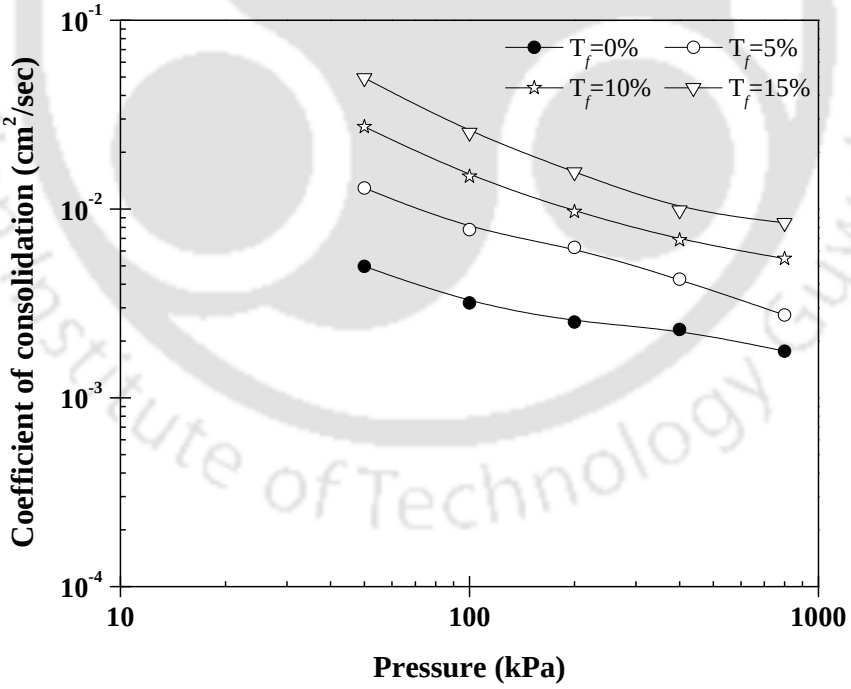

Figure 5.10 c_v vs pressure relationships for SB20 composite

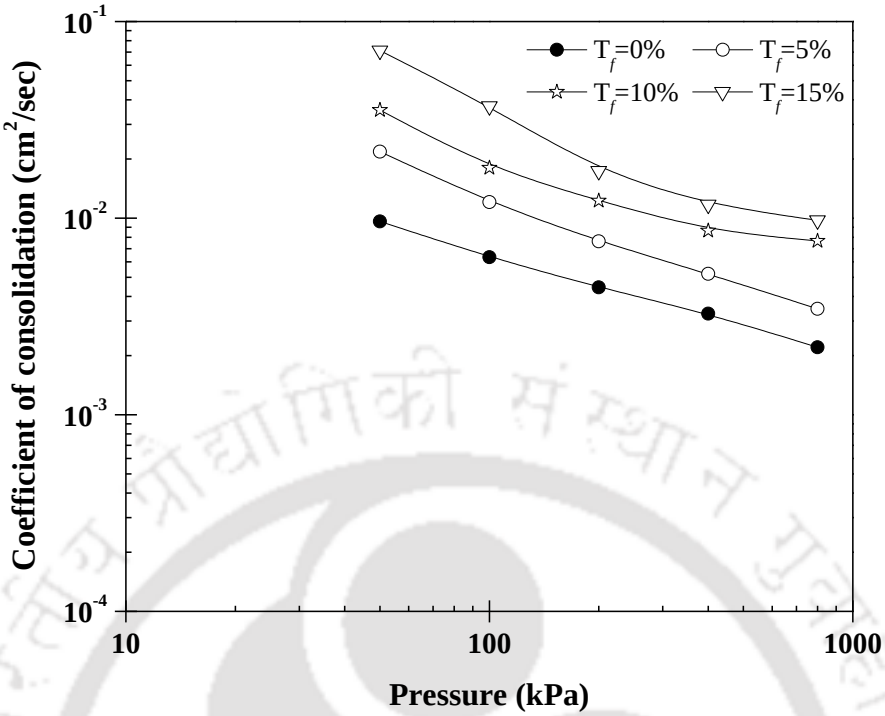

Figure 5.11 c_v vs pressure relationships for SB10 composite

5.3.2 Hydraulic conductivity of the SB-tire fiber composite

Hydraulic characteristics are perhaps the most sought after parameters while dealing with geotechnical barrier materials. Many environmental agencies and researchers (USEPA 1988; Koerner and Daniel 1997; Hauser et al. 2001) have suggested that landfill liner and cover material should have minimum hydraulic conductivity values of 10^{-7} and 10^{-5} cm/sec, respectively. The effect of tire fiber on the various sand bentonite mixture exhibited in the Fig.5.12 and Fig.5.14. For the unreinforced and reinforced sand-bentonite mixture, the hydraulic conductivity of the mixtures decreased with the decrease in the void ratio. In the case of an unreinforced sand-bentonite mixture, with decreased in the void ratio the space available for the flow of water reduced, the flow path becomes more tortuous and consequently, the hydraulic conductivity decreased. However, with the inclusion of tire fiber, hydraulic conductivity of SB30 composite

was increased drastically. For example, hydraulic conductivity was increased from 2.12×10^{-9} cm/sec to 1.07×10^{-8}, 3.86×10^{-8} and 7.29×10^{-8} cm/sec with the inclusion of 5, 10 and 15% of tire fiber, under the void ratio of 0.48. However, at the same void ratio, hydraulic conductivity of the SB20 composite was increased from 2.2×10^{-9} cm/sec to 6.8×10^{-8}, 3.6×10^{-7} and 9.1×10^{-7} cm/sec at the same fiber content. At the same configuration, hydraulic conductivity of SB10 composite increased from 2.7×10^{-8} cm/sec to 1.7×10^{-7}, 7.72×10^{-7} and 8.2×10^{-6} cm/sec with the inclusion of 5, 10 and 15% tire fiber, respectively. The increase in the hydraulic conductivity can be attributed to the development of an additional flow path due to the addition of the tire fiber into the sand-bentonite matrix.

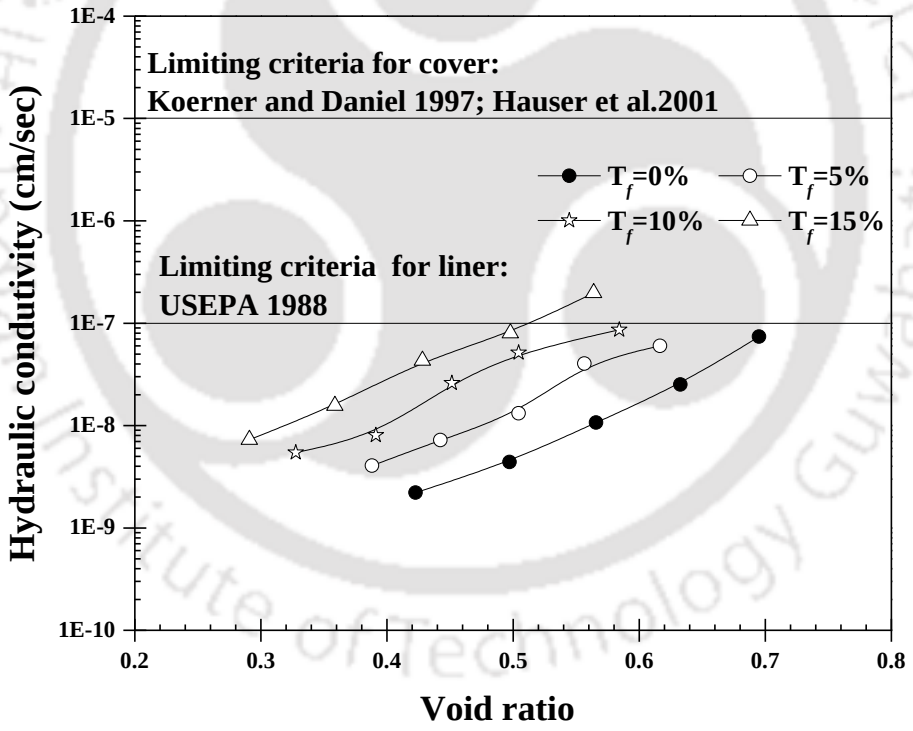

Figure 5.12 Hydraulic conductivity vs. void ratio of the SB30 composite

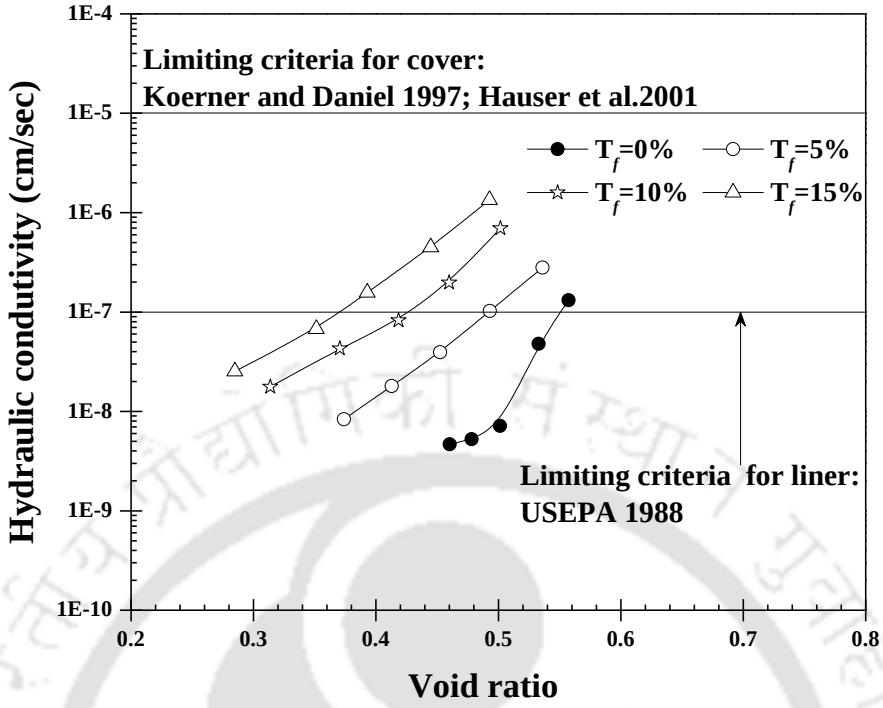

Figure 5.13 Hydraulic conductivity vs. void ratio of the SB20 composite

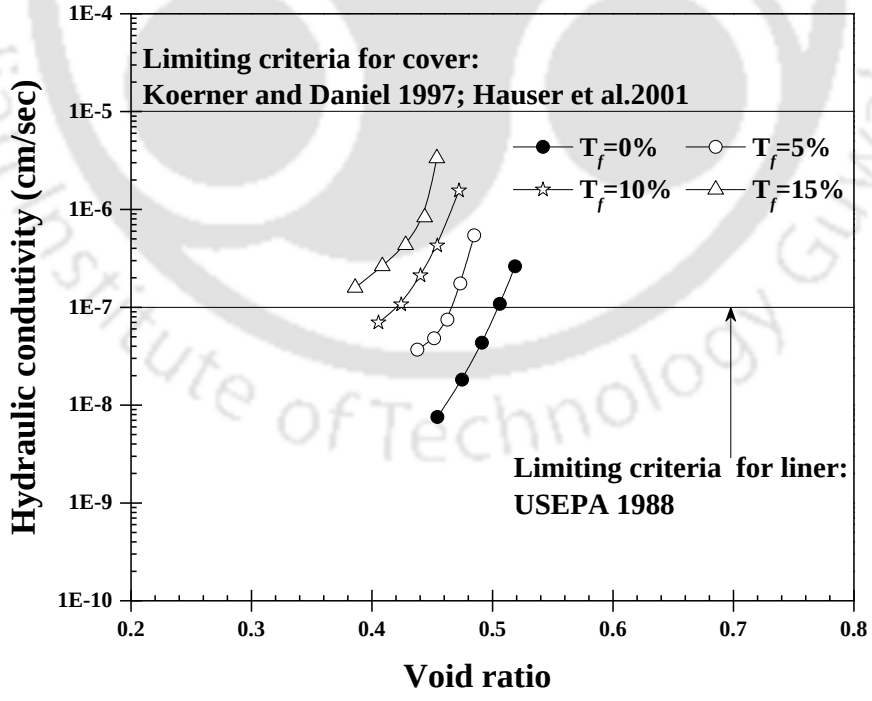

Figure 5.14 Hydraulic conductivity vs. void ratio of the SB10 composite

5.4 Undrained behavior of composite soil

Tensile and desiccation cracking poses major concerns for the proper functioning of clay liners and can threaten its function as a barrier as well as its stability on slopes. Bosscher and Connell (1988) stated that desiccated clay produces a significant effect on hydraulic conductivity, shear strength, compressibility, and slope stability. Benson and Othman (1993) stated that the hydraulic barrier should also be physically stable in order for it to be used as landfill material, and it should have acceptable shear strength to avoid sliding on the slope. Therefore, a series of consolidated undrained tests were performed in triaxial apparatus with the SB10, SB20 and SB30 mixtures with 5, 10, and 15% tire fiber content under confining pressures of 50, 100, and 150 kPa to study the strength behavior under undrained conditions for the material consistency of landfill material. The results of the stress-strain and pore water responses with different confining pressures are discussed subsequently.

5.5 Stress-strain behavior of sand bentonite –tire fiber mixture

The stress-strain performance of the SB-tire fiber composite exhibited in the Fig.5.15. and Fig.5.17. The plots show that the fiber-reinforced specimen exhibited a peak with large strength improvement for all ranges of confining pressure. This behavior was limited to SB10 and SB20 composite. The SB10 and SB20 exhibited strain-softening behavior for the unreinforced and reinforced specimen as shown in Fig.5.15 and Fig. 5.16. The deviatoric stress at failure was found to increase as the percentage of tire fiber increased. No optimum percentage of tire fiber was found for the composite of SB10 and SB20 composite. However, SB10 composite exhibited much more deviatoric stress at failure in contrast to SB20 composite due to the presence of higher sand fraction. For SB10 composite, deviatoric stress at failure was increased from 334 kPa to 405, 538 and 610 kPa with the addition of 5%, 10% and 15% tire fiber under the confining pressure of 100

kPa, respectively. Similarly, under the confining pressure of 150 kPa, the deviatoric stress at failure was increased from 490 kPa to 559, 741 and 875 kPa with the inclusion of 5%, 10 and 15% tire fiber, respectively. In comparison, the deviatoric stress at failure for SB20 composite was increased from 251 kPa to 305, 361 and 432 kPa, under the confining pressure of 100 kPa, respectively. However, under the confining pressure of 150 kPa, the deviatoric stress at failure was increased from 355 kPa to 414, 509 and 625 kPa with the inclusion of 5, 10 and 15% tire fiber, respectively. As the soil grains held tight against shearing by the tire fibers, the composite exhibited some additional increase in the strength, which developed when sufficient bonding between the soil and reinforcement existed.

The stress-strain behavior of SB30 composite exhibited strain hardening in comparison to SB10 and SB20 composite. The composite did not show any peak throughout the shearing. It was also observed that deviatoric stress at failure was low in comparison to SB10 and SB20 composite. At this stage, the effect of reinforcement was limited up to 10% tire fiber. With a further increase in the tire fiber, the deviatoric stress at failure was decreased. For example, the deviatoric stress was increased from 135 kPa to 171 and 202 kPa with an increase in the fiber content from 0 to 5 and 10%, respectively. However, a further increase in the fiber content from 10 to 15% under the confining pressure of 100 kPa the deviatoric stress decreased from 202 to 186 kPa. Under the confining pressure of 150 kPa, the deviatoric stress at failure increased again from 180 kPa to 217 and 254 kPa with the increase in the fiber content from 0 to 5 and 10%. Thereafter, it reduced from 254 to 239 kPa with a further increase in the tire fiber content from 10 to 15%. At high tire fiber content, deviatoric stress at failure was found to decrease due to inadequate bonding between tire fiber and soil within the fiber soil matrix.

5.5.1 Post peak performances of the sand bentonite-tire fiber soil composite

Stress-strain performance of the sand-bentonite and sand-bentonite tire fiber composite are shown in Fig.515 and Fig.5.16. Unreinforced soil has high the post-peak strength loss, whereas, composite improved the post-peak strength throughout the test. It can be seen that the post-failure deviatoric stress (at a strain level of 20%) of the fiber-reinforced composite was much higher than that of the unreinforced soil under confining pressures of 50, 100 and 150 kPa.

For example, under a confining pressure of 150 kPa, the deviatoric stress of the SB10 composite was approximately 354 kPa, whereas, for the fiber-reinforced soils it increased to 477, 658, and 796 kPa in the presence of 5%, 10%, and 15% of tire fiber, respectively. For SB20 composite, under a confining pressure of 150 kPa the deviatoric stress increased from 256 kPa to 331, 443, and 563 kPa with the addition of 5, 10, and 15% of tire fiber, respectively. Additionally, it was observed that the post-peak stress of both composites improved with the confining pressure and tire fiber content, indicating a significant increase in the residual stress of the composite due to the addition of the tire fiber.

5.5.2 Impact of tire fiber on Excess pore water pressure

The effect of tire fiber on excess pore water pressure (EPP) is shown in Fig.5.15 and Fig.5.16. for the SB10 and SB20 composites for a confining pressure of 150 kPa. The positive excess pore water pressure increased when the SB10 and SB20 composites were compressed during loading under undrained conditions. Similarly, during the expansion of the composite, the negative excess pore water pressure decreased. This trend was in agreement with the result reported by Budhu (2010) for highly over consolidated clay.

The test result showed that negative EPP increased with an increase in the confining pressure and decrease in the tire fiber content. For the SB10 composite under a confining pressure of 150 kPa,

the maximum negative EPP decreased from 122 kPa to 88, 73, and 66 kPa due to the inclusion of 5, 10, and 15% of tire fiber, respectively. For the SB20 composite under a confining pressure of 150 kPa, the maximum negative EPP dropped from 108 kPa to 74, 65, and 58 kPa due to the inclusion of 5, 10, and 15% of tire fiber, respectively. This pattern indicates that the tire fiber deformed (Kaneko et al. 2012) and stretched during shearing, and the fiber did not allow the soil particles to move over each other as the negative pore water pressure was reduced. This behavior of the tire fiber reduced the chances of a sudden failure of the composite material. This mechanism took place when the tire fiber was readily available in the shear zone.

It is clear that the impact of tire fiber on the positive pore water pressure of sand-bentonite composites was significant, and their outcome was noticed. For example, under a confining pressure of 150 kPa, the maximum positive EPP of the SB10 composite increased from 33 kPa to 37, 39, and 53 kPa with the inclusion of 5, 10, and 15% of tire fiber, respectively. Similarly, the maximum positive EPP was improved from 22 kPa to 24, 34, and 35 kPa in the presence of 5, 10, and 15% of tire fiber, respectively, for the SB20 composite under a confining pressure of 150 kPa.

Therefore, it can be concluded that the positive pore water pressure increases with confining pressure and tire fiber content indicating a sharp improvement in the elastic resistance of the composite. On the other hand, the SB30 composite showed that EPP was positive throughout the shearing process for both reinforced and unreinforced specimen. Interestingly, it was observed that EPP was reduced by the inclusion of tire fiber.

For example, under the confining pressure of 100 kPa, EPP was reduced from 40 kPa to 36, 30 and 27 kPa with the inclusion of 5, 10 and 15% of tire fiber, respectively. However, under the confining pressure of 150 kPa, the EPP was slightly increased initially, after that, it followed the similar behavior as in the case of 100 kPa confining pressure. For example, under the confining

pressure of 150 kPa, the EPP was reduced from 60 kPa to 51, 49 and 46 kPa with the inclusion of 5, 10 and 15% tire fiber, respectively.

5.5.3 Effect of tire fiber on elastic moduli

The slope of the tangent to the initial section of the stress-strain curve, a measure of the material's stiffness designated as initial tangent modulus (E_i), was determined for compacted sand-bentonite composite. Rao and Dutta (2006) reported that E_i of the soil changed with different confining pressure. E_i of the various SB-tire fiber composite was found out and presented in the Fig.5.18.

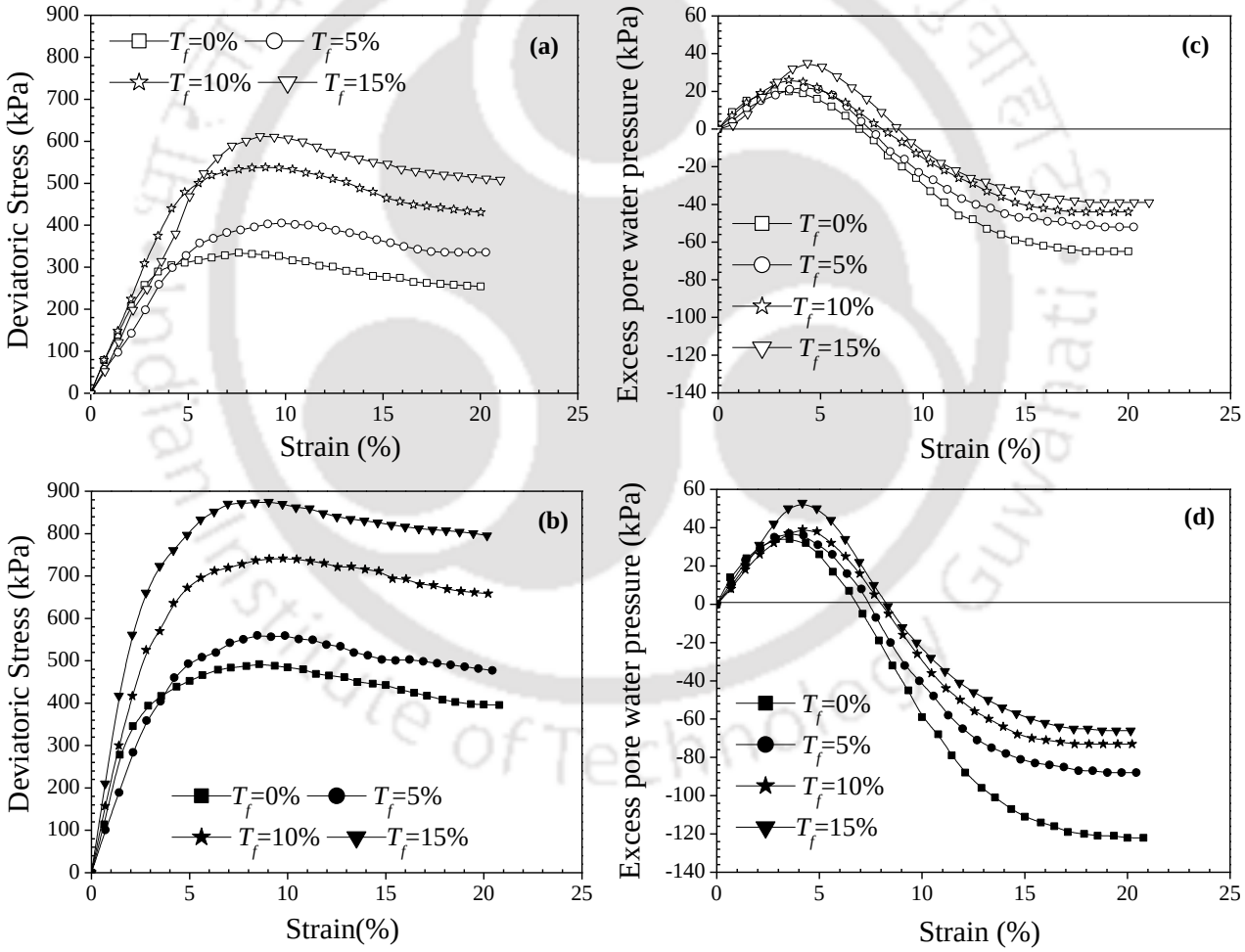

Figure 5.15 Stress-strain behavior of SB10 composite;(a) SB10 composite under the confining pressure of 100kPa;(b) SB10 composite under the confining pressure of 150kPa; Excess pore water pressure (EPP) behavior of SB10 composite;(c) EPP of the SB10 composite under the confining pressure of 100kPa; (d) EPP of the SB10 composite under the confining pressure of 150kPa

From the figure, it was observed that the E_i of the composite increases linearly as the percentage of the tire fiber increased. However, it was also noticed that E_i of the composite was improved up to 10% tire fiber for all the composite, thereafter, it moved down slightly with the further addition of tire fiber. For example, under the confining pressure of 150 kPa, E_i of the SB10 composite was enhanced from 12.93 MPa to 14.55 and 21.54 MPa at 5% and 10% tire fiber respectively, however, E_i was reduced from 21.54 MPa to 20.59 MPa with increase the tire fiber from 10 to 15%.

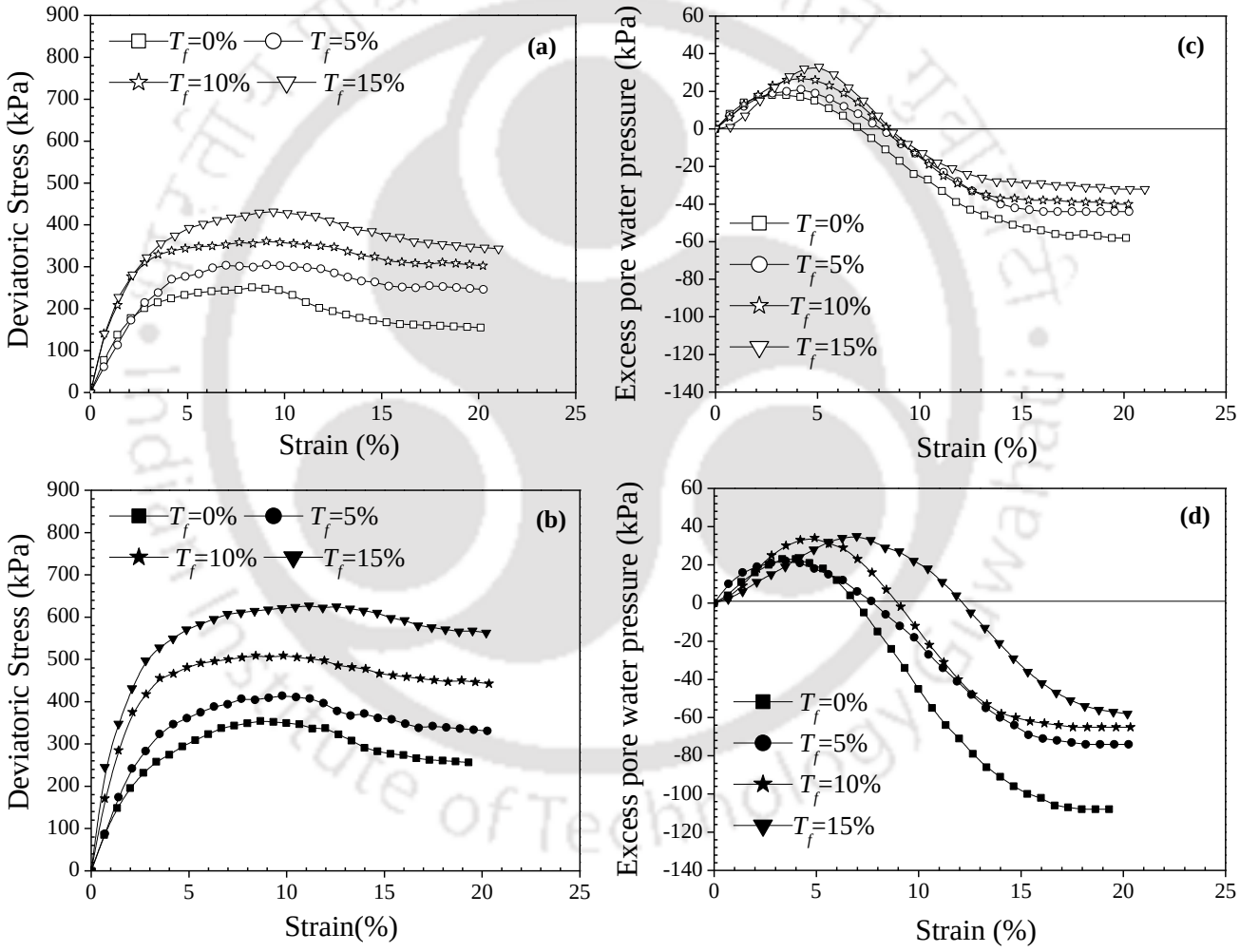

Figure 5.16 Stress-strain behavior of SB20 composite;(a) SB20 composite under the confining pressure of 100kPa;(b) SB20 composite under the confining pressure of 150kPa;(c) Excess pore water pressure (EPP) behavior of SB20 composite;(c) EPP of the SB20 composite under the confining pressure of 100kPa; (d) EPP of the SB20 composite under the confining pressure of 150kPa

An identical trend was observed for the composite of SB20. For SB20 composite E_i was measured as 11.25, 12.06, 16.98 and 15.76 MPa at 0%, 5%, 10 and 15% tire fiber, respectively. For SB30, E_i was increased from 8.87 MPa to 11.68 and 13.65 MPa at 5 and 10% tire fiber content, respectively; however, E_i was reduced from 13.65 MPa to 12.45 MPa with the increase in the tire fiber content from 10 to 15%.

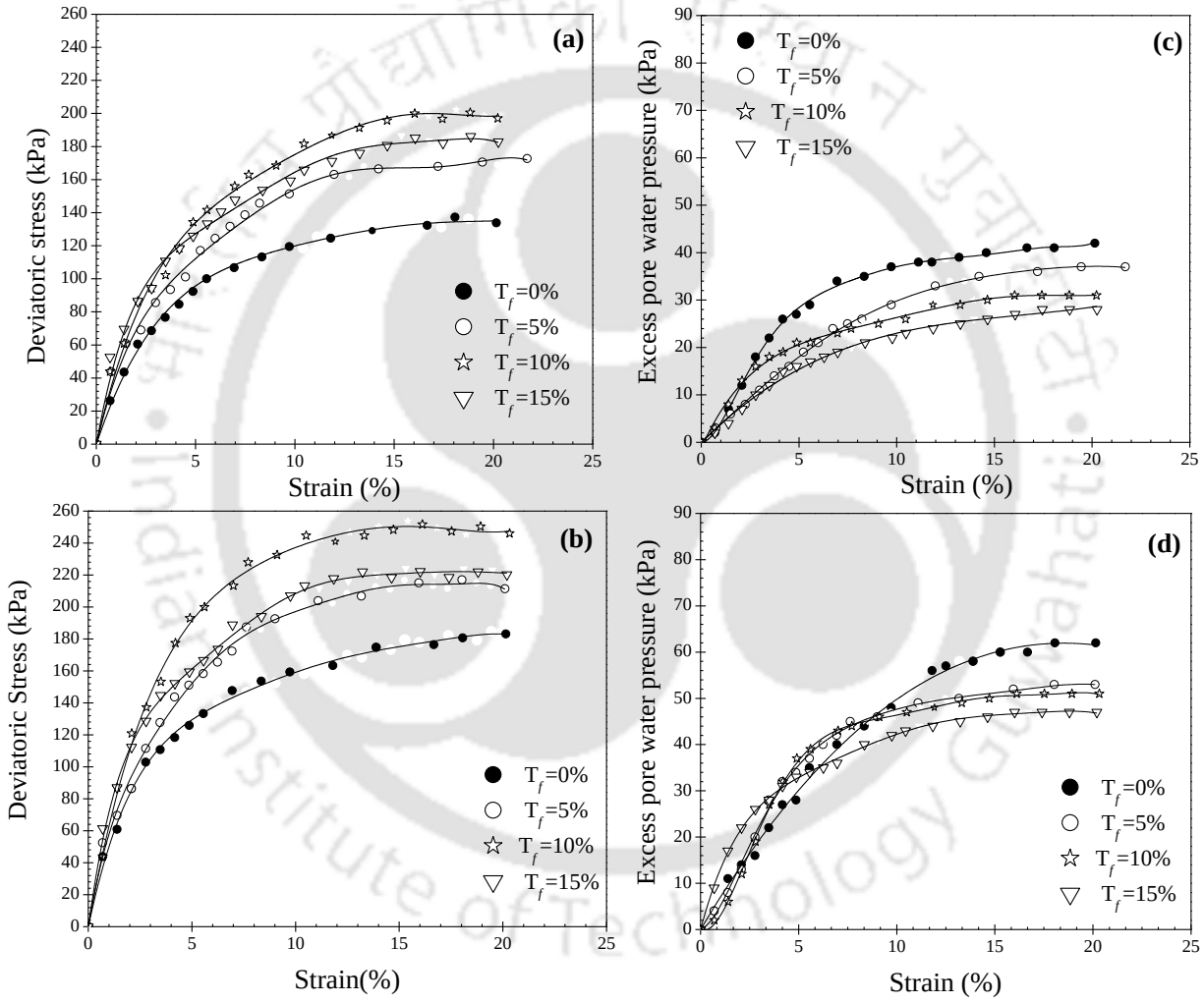

Figure 5.17 Stress-strain behavior of SB30 composite; (a) SB30 composite under the confining pressure of 100kPa;(b) SB30 composite under the confining pressure of 150kPa;(c) Excess pore water pressure (EPP) behavior of SB30 composite;(c) EPP of the SB30 composite under the confining pressure of 100kPa; (d) EPP of the SB30 composite under the confining pressure of 150kPa

For any point on the stress-strain curve, the E_{sec} is defined as the ratio of deviator stress to the corresponding strain level. Under a confining pressure of 150 kPa, E_{sec} was calculated at four different axial strain (i.e. 2.5, 5, 10 and 20%) and depicted in Fig.5.18. From the figure, it was noticed that the E_{sec} decreased progressively with increasing axial strain.

A comparison due to the effect of the addition of tire fiber on E_{sec} shows that it improved up to the addition of 10% tire fiber and reduced thereafter. For example, E_{sec} of the SB10 composite was improved from 5.95 MPa (at 10% strain) to 9.5 and 17.85 MPa at 5% and 10% tire fiber, respectively; however, it decreased from 17.85 MPa to 15.25 MPa with the increase in the tire fiber content from 10 to 15%. At the same fiber content, E_{sec} of the SB20 composite was measured to be 4.77, 10.02, 13.25 and 11.75 MPa at 5, 10 and 15% tire fiber under the 10% of strain level. Similarly, for SB30 composite it was improved from 4.04 MPa to 9.52 and 12.35 MPa at 5% and 10% tire fiber, respectively and reduced from 12.35 MPa to 10.86 MPa with increase in the tire fiber from 10 to 15% and shown in Fig.5.18.

5.5.4 Shear strength parameter of SB-tire fiber soil composite

To avoid a cluster of data, the Mohr circle has been presented by considering 5 and 10% fiber content for SB10, SB20, and SB30 composite. Mohr circle of composite has been drawn and presented based on their peak and residual stress and shown in Fig.5.19 and Fig.5.20. Under any confining pressure, diameter increased significantly as the percentage of the tire fiber increased.

For SB10 composite, peak frictional (ϕ_p') angle was improved from 27.3˚ to 28.4˚, 31.0˚ and 33.1˚ due to the increase in the tire fiber content from 0 to 5, 10 and 15%, respectively. Due to reinforcement action, the cohesion component (at peak) was increased from 28.4 kPa to 38.8, 49.1 and 45.5 kPa with 5%, 10 and 15% tire fiber, respectively and presented in Fig.5.21.

According to landfill liner design concern, the designer should be preferred the residual strength parameter rather than the peak strength parameter. However, residual strength parameter diverged significantly from the peak strength parameter of these composite. For SB10, residual frictional angle (ϕ_r') was increased from 25.3˚ to 26.1˚, 29.0˚ and 30.0˚ due to an increase in fiber content from 0 to 5, 10 and 15%, respectively.

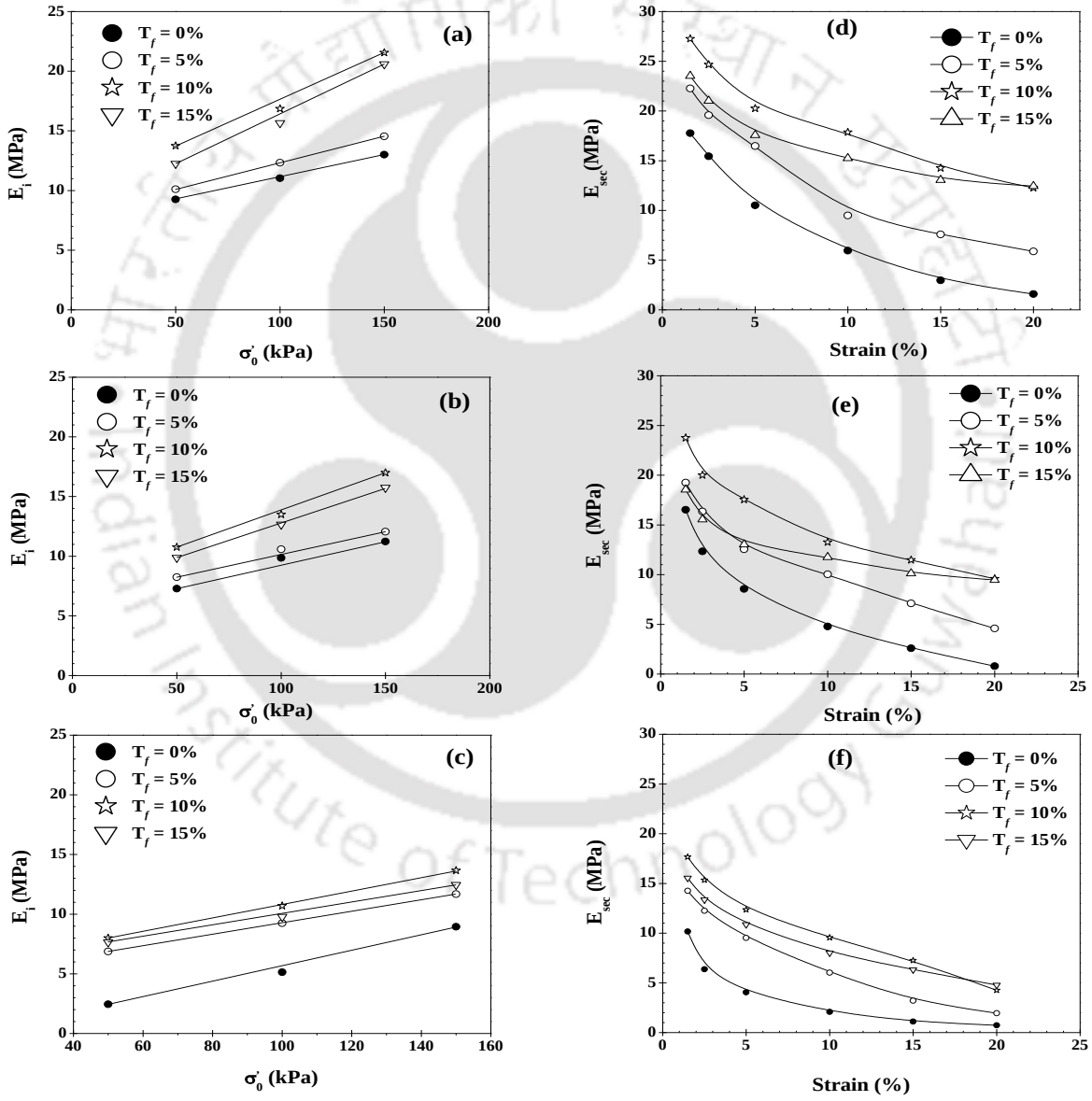

Figure 5.18 Elastic modulus for various SB-tire fiber mixes; (a) E_i for SB10 composite;(b) E_i for SB20 composite; (c) E_i for SB30 composite; (d) E_{sec} for SB10 composite;(e) E_{sec} for SB20 composite; (f) E_{sec} for SB30 composite

At the same time, residual cohesion component (c_r') was improved from 6.9 kPa to 29.3, 40.3 and 39.9 kPa at same amount of fiber content Fig.5.22. All most an identical trend was obtained for SB20 composite, where the ϕ_p' increased from 24.9˚ to 26.5˚, 28.6˚ and 30.5˚ with the increase in the fiber content from 0 to 5, 10 and 15% tire fiber, respectively. Cohesion component (at peak) of the SB20 composite was altered from 16.4 kPa to 23.2, 30.2 and 39.6 kPa with the increase in the fiber content from 0 to 5, 10 and 15%, respectively. Based on the residual strength envelop, ϕ_r' increased from 24.9˚ to 26.5˚, 28.6˚ and 30.5˚ due to a rise in concentration from 0 to 5, 10 and 15% of tire fiber, respectively. The corresponding increase in the c_r' was found from 2.9 kPa to 13.23, 21.61 and 32.22 kPa and shown in Figure 5.22. Hence, it can be concluded that the residual strength of the composite was improved significantly with tire fiber that would be beneficial for the design of landfill liner and cover.

The SB30 composite did not exhibit a peak throughout the shearing; therefore, MC was drawn by taking the data corresponding to 15% strain and presented in Fig.5.23. From the figure, it was observed that MC diameter was increased maximally up to 10% tire fiber inclusion, and then reduced slightly with the addition of 15% tire fiber. For example, the internal frictional angle was increased from 22.4˚ to 23.8˚, 24.9˚ with the inclusion of 5 and 10% tire fiber, respectively, thereafter, it reduced from 24.9˚ to 24.2˚ with the inclusion of 15% tire fiber due to inadequate bonding between soil and tire fiber inside the matrix (Fig.5.24a). Cohesion component was increased maximally from 15.02 kPa to 21.97 kPa with the inclusion of 10% tire fiber in to the mixture and presented in Fig.5.24.

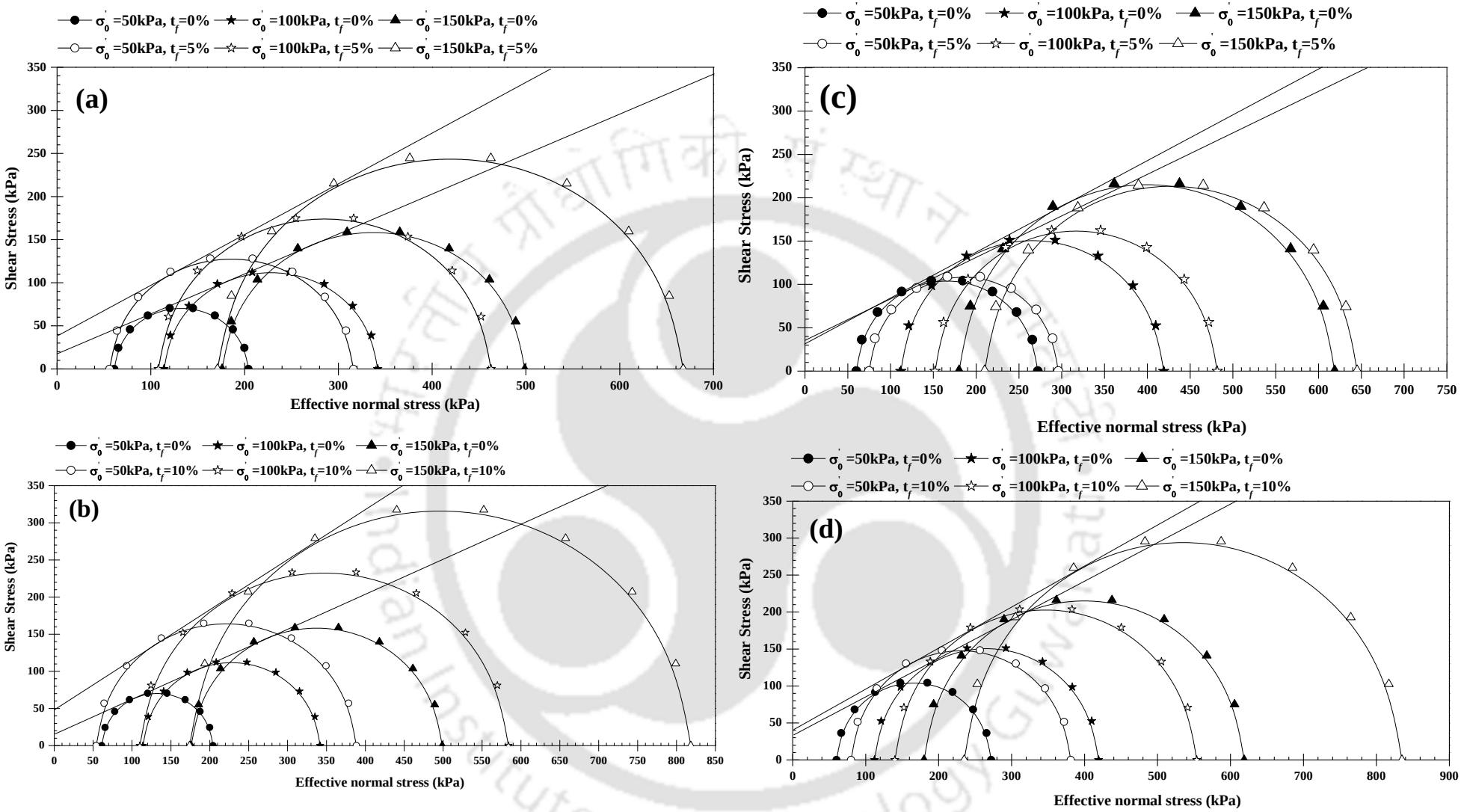

Figure 5.19 Mohr circle and their envelop of SB10 composite;(a) Peak strength envelop with 5% tire fiber;(b) Peak strength envelop with 10% tire fiber;(c) Residual strength envelop with 5% tire fiber;(d) Peak strength envelop with 10% tire fiber

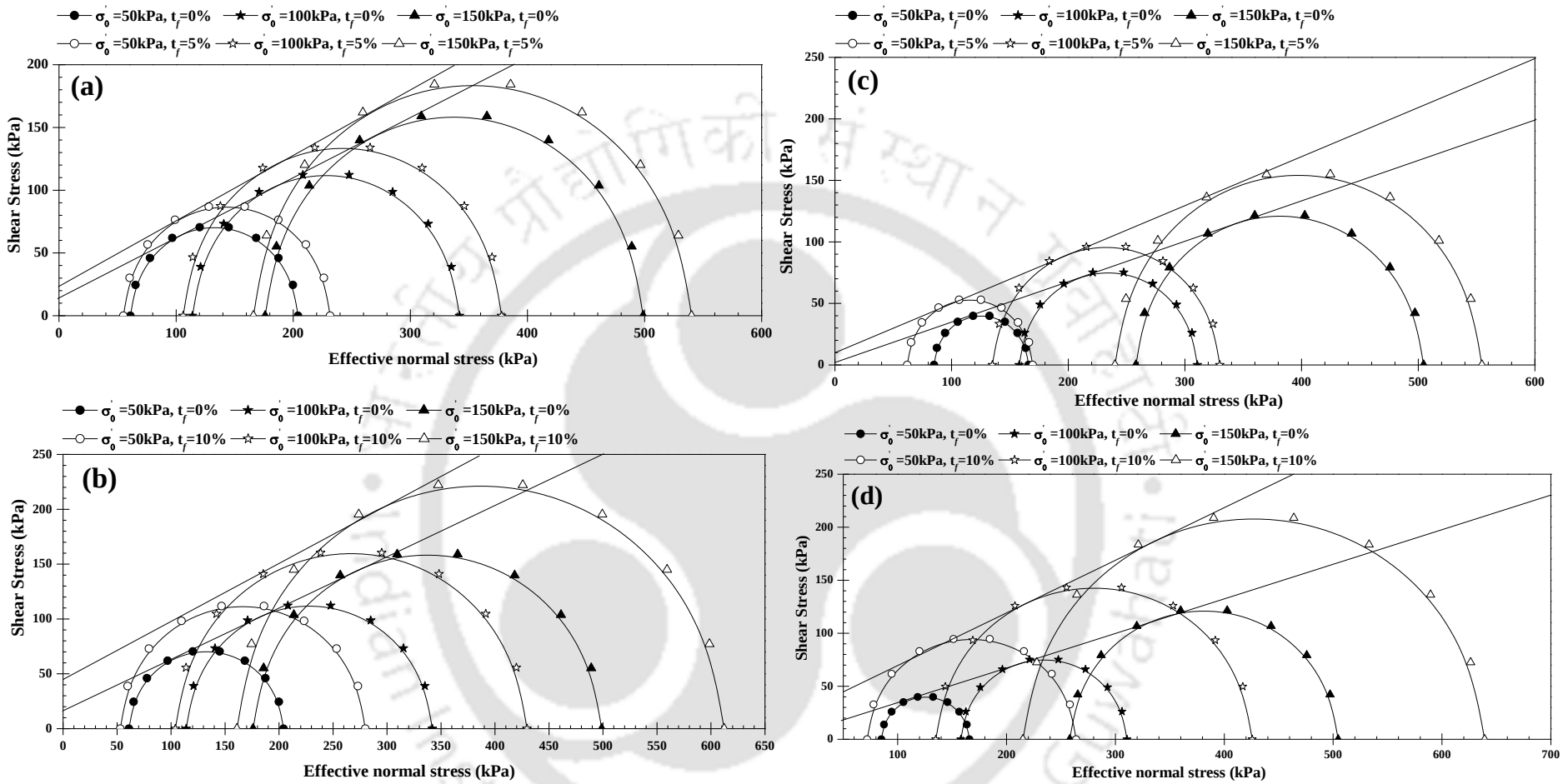

Figure 5.20 Mohr circle and their envelop of SB20 composite;(a) Peak strength envelop with 5% tire fiber;(b) Peak strength envelop with 10% tire fiber;(c) Residual strength envelop with 5% tire fiber;(d) Peak strength envelop with 10% tire fiber

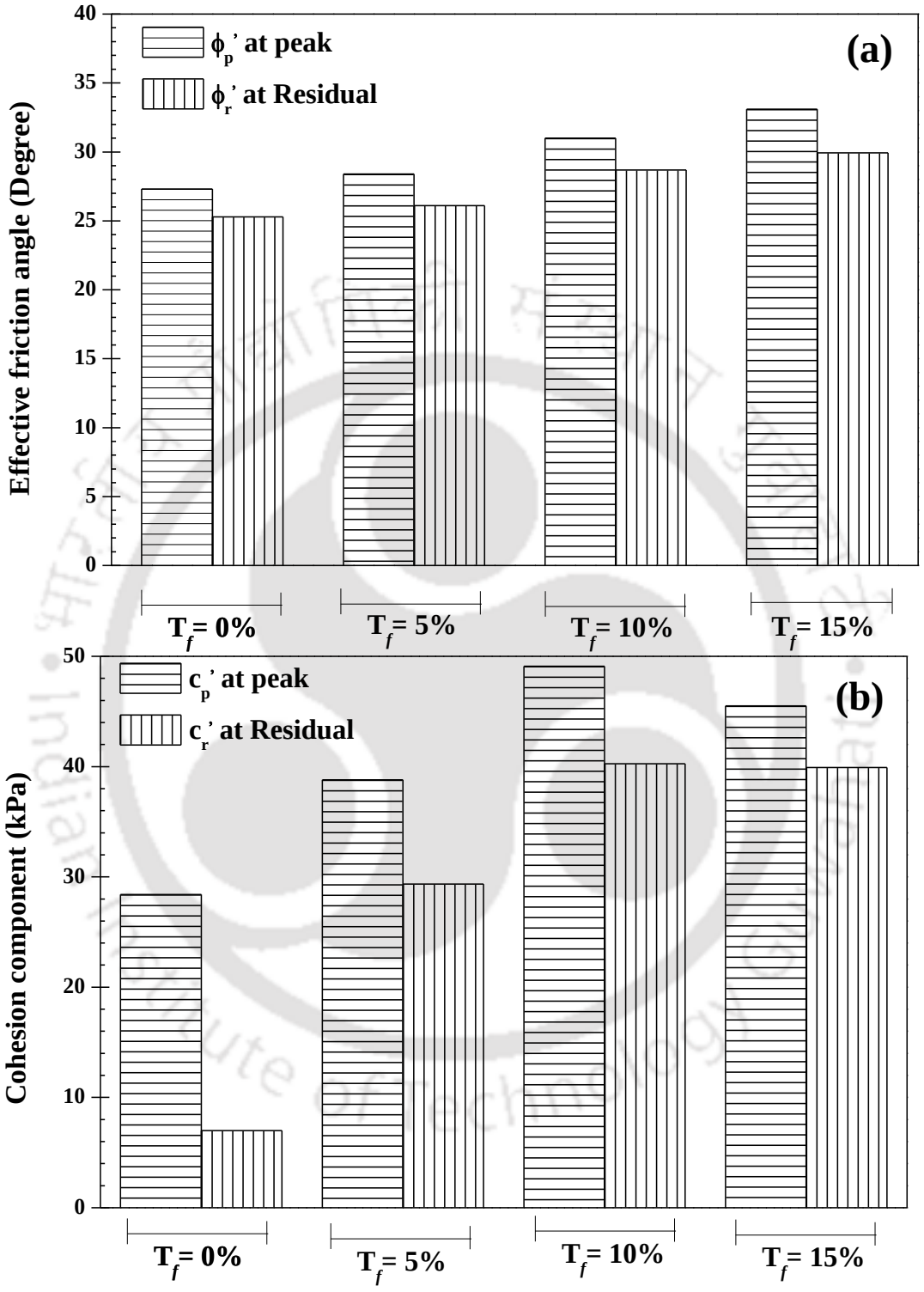

Figure 5.21 Effective shear strength parameter of SB10 composite

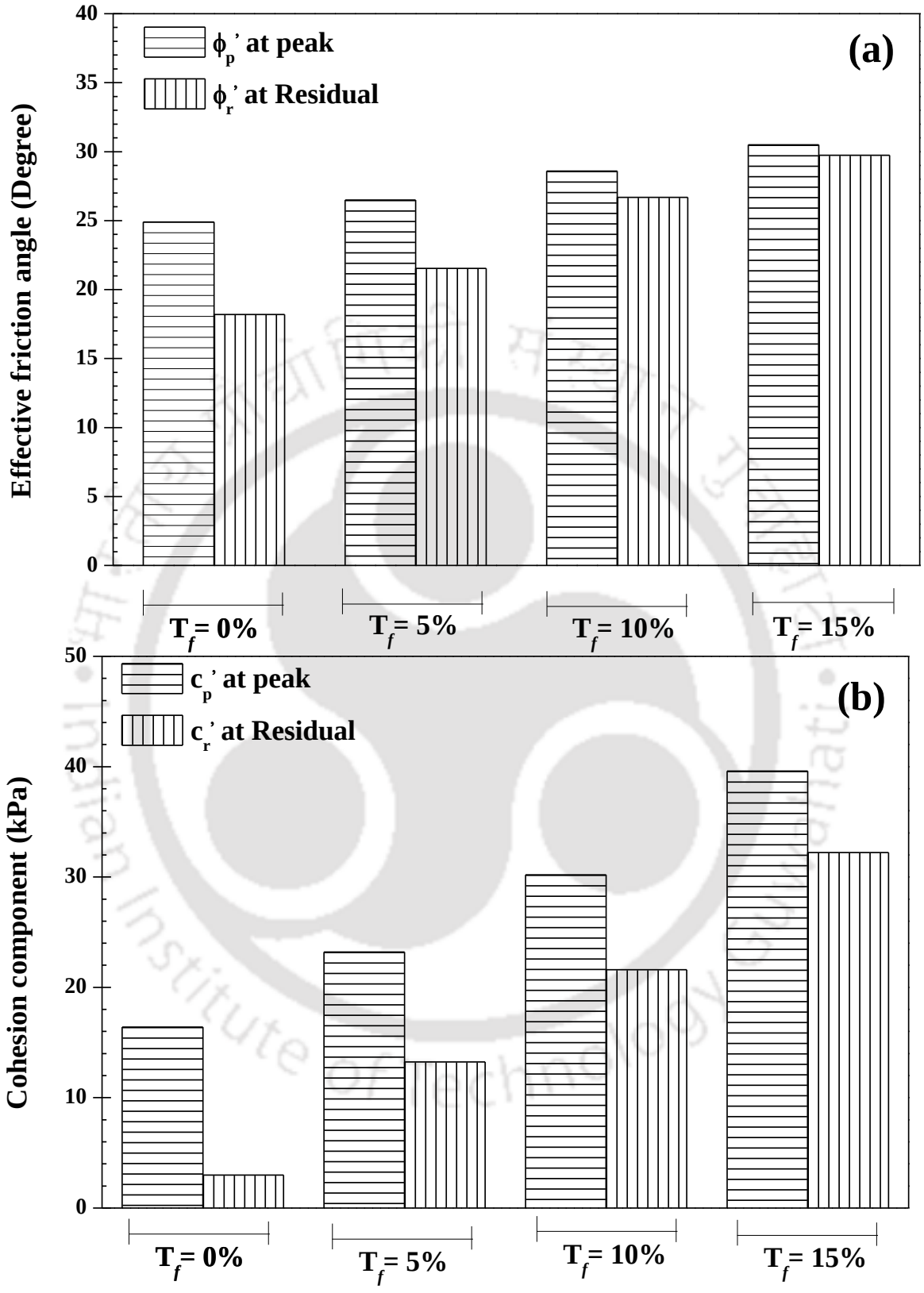

Figure 5.22 Effective shear strength parameter of SB20 composite

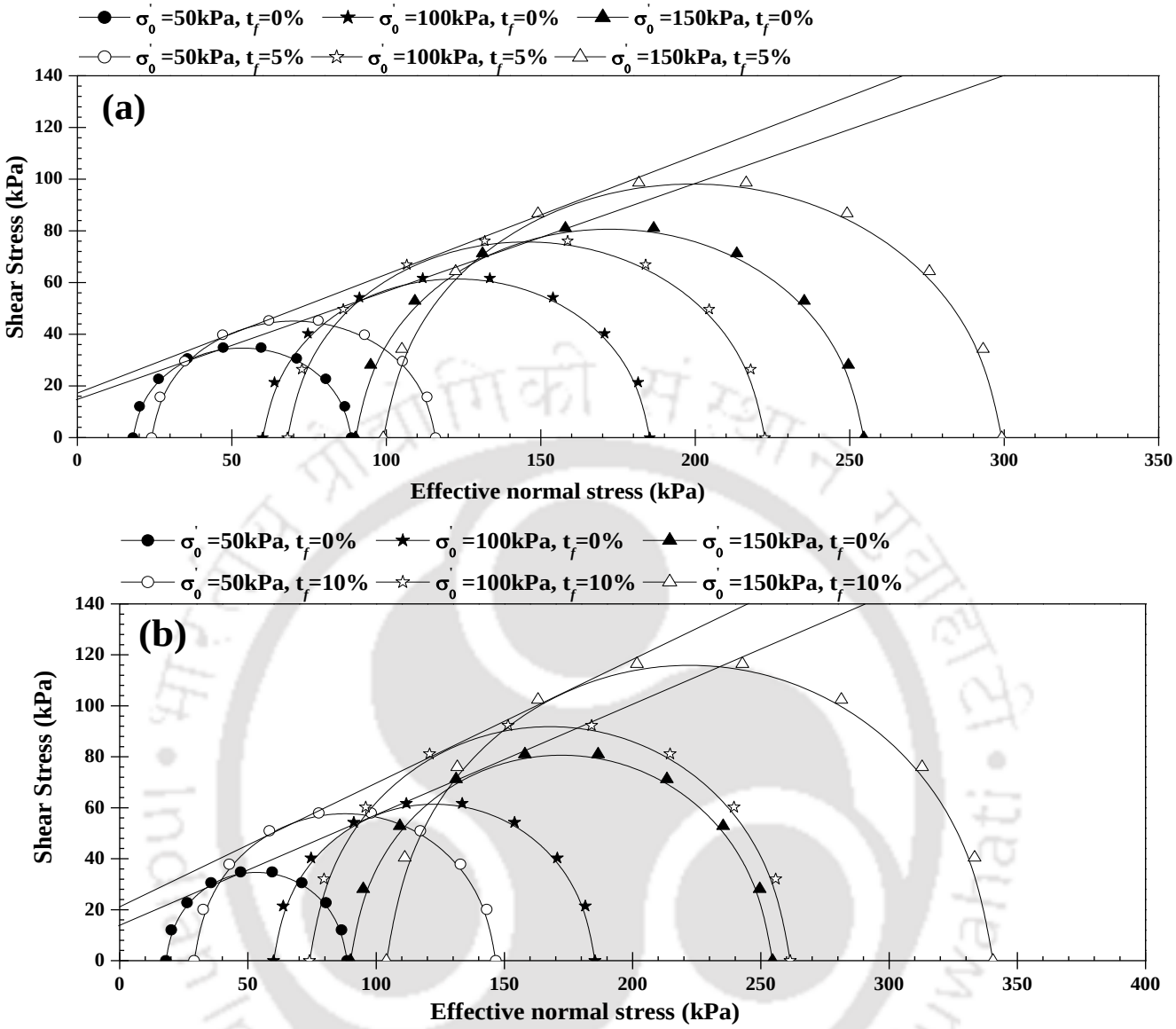

Figure 5.23 Mohr's Circle and strength envelop of SB30 composite;(a) SB30 with 5% tire fiber;(b) SB30 with 10% tire fiber

5.5.5 Influence of tire fiber on energy absorption capacity (EAC)

Overall improvement of the composite was also specified in terms of energy absorption capacity (EAC). The absolute values of energy absorption were obtained by calculating the area under the stress-strain curve (i.e., unreinforced and reinforced specimens) up to 20% of strain (Babu and Vasudevan 2008) and are presented in Fig.5.25. From Figure, it is clear that EAC increased with tire fiber content and confining pressure, indicating an increase in the toughness of the composite. For example, under a confining pressure

of 150 kPa, the EAC of SB10 increased from 8,629 kJ/m^3 to 9,206, 11,930, and 15,067kJ/m^3 due to the inclusion of 5%, 10%, and 15% of tire fiber, respectively. In the case of SB20, under confining pressure of 150 kPa, the EAC increased from 5,437 kJ/m^3 to 6,846, 9,084, and 11,238 kJ/m^3 with the inclusion of 5%, 10%, and 15% of tire fiber, respectively. A similar pattern was obtained by Dutta and Rao (2009) for sand reinforced with tire chips. A comparison between the two composites indicated that the EAC of SB10 was always higher in comparison to SB20 due to its relatively lower shear strength. An identical trend was followed by the SB30 composite.

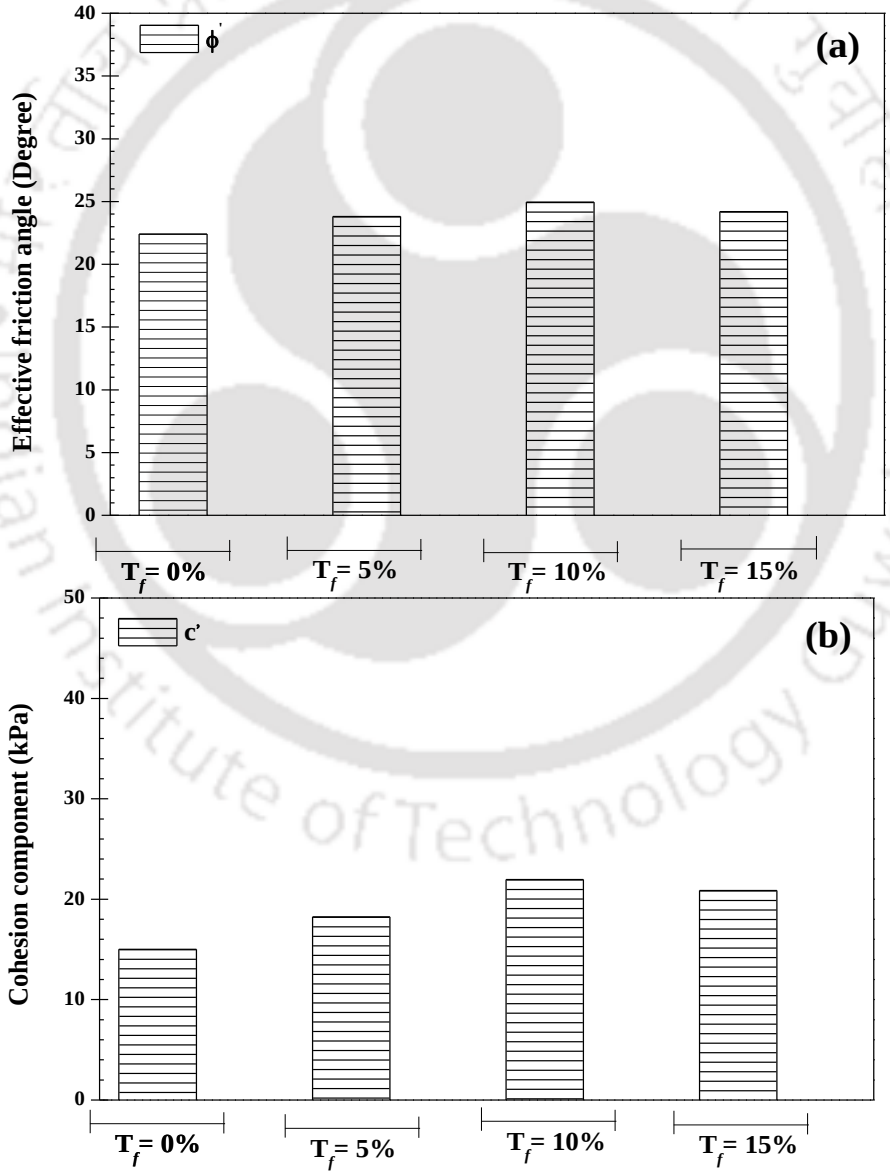

Figure 5.24 Effective shear strength parameter of SB30 composite

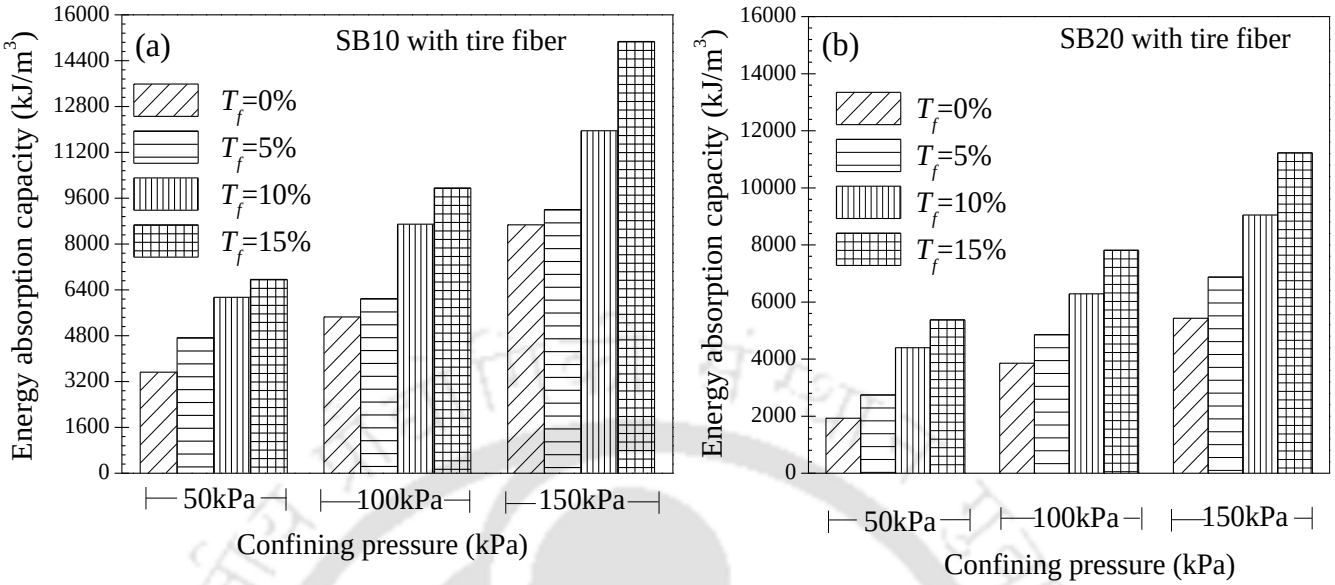

Figure 5.25 EAC of the SB-tire fiber ;(a) SB10 composite;(b) SB20 composite

5.5.6 Influence of tire fiber on failure mode

The failure pattern of the soil specimens was taken corresponding to 20% axial strain under a confining pressure of 150 kPa and presented in Fig.5.26 to Fig.5.28. For SB10 composite, it can be seen that the specimen undergoes shear failure with development of clear rupture in the presence of fiber. As seen in Fig.5.26 (a), the failure plane of unreinforced soil was developed from the bottom and undergoes shear failure. However, this failure behavior was changed significantly with the inclusion of tire fiber. With the addition of 5% tire fiber, failure plain progressively appeared in the central region and strain localization was observed within the shear zone (Fig.5.26 b), which became narrow and converged towards the center of the specimen. With increase the tire fiber from 5 to 10%, shear zone became wider, specifying that composite introduced resistance against the weakest section of the soil-fiber matrix and preventing the catastrophic failure of composite (Fig.5.26c). With the inclusion of 15% tire fiber, the shear zone was expanded significantly, and specimen exhibited approximately barrel type failure (Fig.5.26d).

In the case of SB20, similar kind of observation was followed but the failure trend slightly diverged from SB10 composite. The failure pattern of SB20 composite showed a shear failure with horizontal expansion (Fig.5.27a). With the inclusion of 5% tire fiber, the specimen underwent sliding failure with the presence of tiny crack (Fig.5.27b). However, due to the addition of 10% tire fiber, the shear zone expanded horizontally with the network of tiny cracks (Fig.5.27c). After that, the specimen exhibited predominantly barrel failure and strain localization was restricted with the presence of 15% tire fiber (Fig.5.27d). However, the failure mechanism of the SB30 composite was significantly different from the SB10 and SB20 composite. The unreinforced SB30 specimen depicted sharp horizontal wrinkle, indicating the specimen underwent a large settlement with poor effective stress (Fig.5.28a). With 5% tire fiber, specimen exhibited pure bulging with random crack (Fig.5.28b), but specimen reinforced with 10% showed barrel failure with diagonal crack (Fig.5.28c). With the increase the tire fiber from 10% to 15%, specimen exhibited like a vertical column (Fig.5.28d), showing a strong resistance against volume expansion.

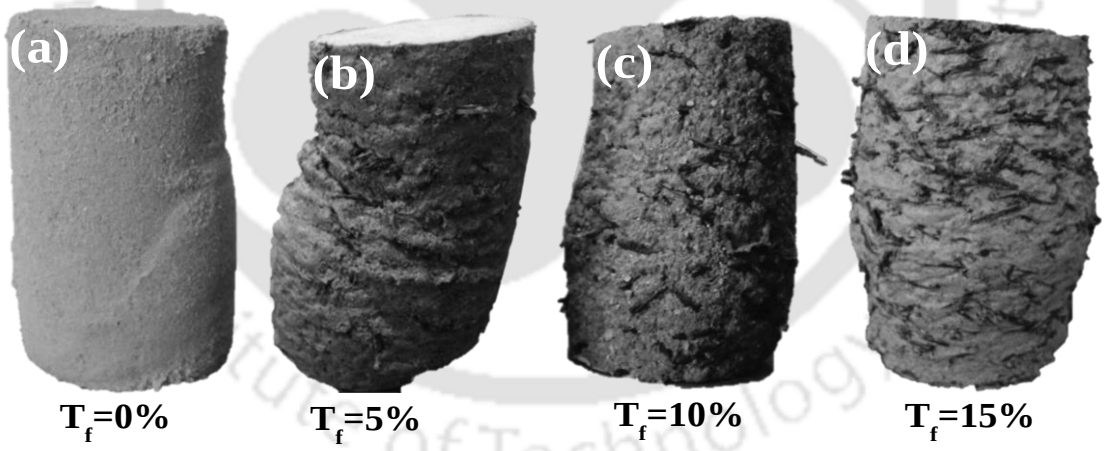

Figure 5.26 Failure mode of SB10 composite

5.6 Yielding behavior of fiber-reinforced soil and critical state model parameter

The modified Cam clay soil model (Roscoe and Burland 1968) is well defined and broadly used in soil mechanics. This model is based on critical state theory and the basic assumption that there is a logarithmic relationship between the mean stress and the void ratio. The model describes three important aspects of

soil behavior, strength, compression or dilatancy (the volume change that occurs with shearing), and critical state at which soil elements can experience unlimited distortion without any changes in stress or volume. The primary assumption of this current study is that $\phi_{rs}' = \phi_{cs}'$ and it has been used to determine the yield surface of the individual composite. The governing equation and basic definition has been discussed in section 4.6. All the model parameters were found out from triaxial and oedometer test are reported in Table 5-2.

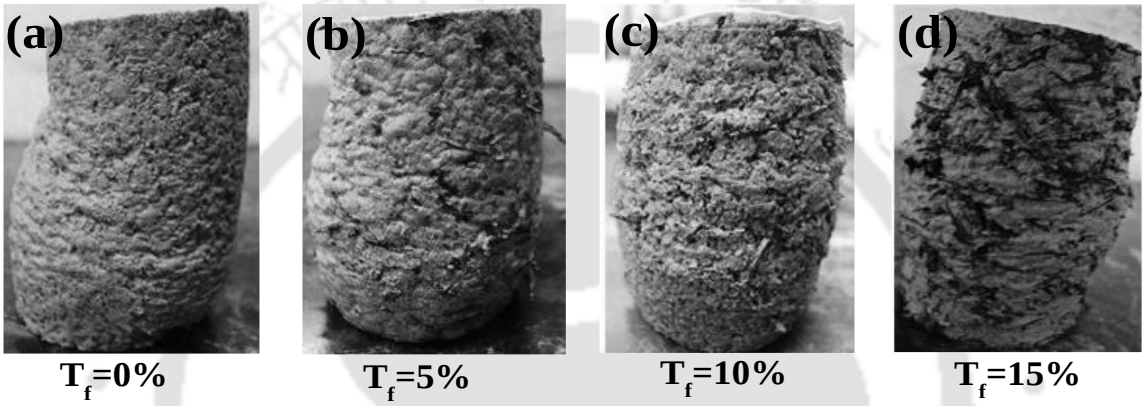

Figure 5.27 Failure mode of the SB20 composite

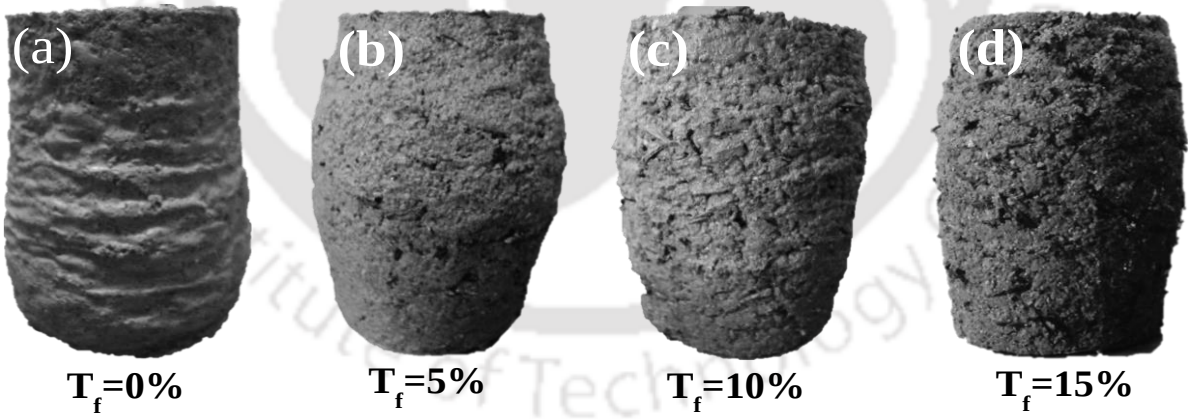

Figure 5.28 Failure mode of SB30 composite

Test result indicated that λ was decreased up to 10% tire fiber for the composite of SB10, but it was increased slightly with 15% tire fiber. This pattern was not consistent and it diverged significantly for SB20 and SB30 composite. The λ was reduced due to the 5% tire fiber addition for the SB20 and SB30

composite; however, it increased significantly with the addition of 10 and 15% tire fiber. However, λ was reduced up to 10% tire fiber for the composite of SB10 and then increased with further addition of tire fiber.

For SB30, λ was reduced from 0.143 to 0.123 due to increasing in fiber content from 0 to 5% and increased thereafter 0.123 to 0.153 and 0.168 with a further increase in tire fiber content to 10 and 15%. An identical trend was observed for the composite of SB20. In the case of SB10, λ was decreased from 0.014 to 0.006, 0.004 due to the increase in the tire fiber content from 0 to 5 and 10%, respectively. However, λ increased from 0.004 to 0.048 with a further increase in tire fiber from 10 to 15%.

The κ of the composite behaved significantly different in comparison to λ. The κ was increased as the tire fiber increased in to the mixture. In the case of SB10 composite, the κ increased from 0.01 to 0.022, 0.039 and 0.052 at 5, 10 and 15% tire fiber, respectively. Similar behavior was followed by the SB20 and SB30 mixture. It was also found that κ improved with an increase in the sand content in the mixture.

The critical state frictional angle (M_c) was altered significantly with the inclusion of tire fiber. For SB10 composite, M_c was enhanced from 0.996 to 1.031, 1.143 and 1.197 at due to the addition of fiber content from 0 to 5, 10 and 15%, respectively. An identical trend was obtained for the composites of SB20 and SB30 composite exhibited a similar pattern.

A state that defines the limit of elastic and the start of plastic deformation under any possible combination of stresses is known as the yield condition or yield criterion. The locus of the stress at which a soil yield is called a yield surface. Stress below the yield stress cause the soil to respond elastically; stress beyond the yield stress causes the soil to respond elasto-plastically. An elastic material recovers its original configuration on unloading; an elastoplastic material undergoes both elastic (recoverable) and plastic (permanent) deformation during loading. The yield surface is assumed to be an ellipse and its initial size or major axis is determined by the pre-consolidation stress (σ_0'). The conceptual soil yielding was

described by Budhu (2010) as presented in Fig.4.40. Yield surface of the composite is presented in the Fig.5.29 and Fig.5.31. From the plot, it can be observed that yield surface was expanded continuously with tire fiber. As the tire fiber increased, the overall zone of elastic resistance was improved significantly indicating that the composite is less susceptible for a higher settlement. Moreover, it was also found that yield surface reduced with bentonite fraction and SB30 composite exhibited poor yielding stress in comparison to SB20 and SB10. In the case of SB30 composite, yield surface was expanded up to 10% tire fiber, however, reduced with further addition of tire fiber.

Table 5-2 Summary of the critical state parameter of the different SB-tire fiber composite

Composite Name	M_c	λ	κ
SB10	0.996	0.014	0.001
SB10,T_f=5%	1.031	0.006	0.022
SB10,T_f=10%	1.143	0.004	0.039
SB10,T_f=15%	1.197	0.048	0.052
SB30	0.82	0.143	0.008
SB30,T_f=5%	0.933	0.123	0.019
SB30,T_f=10%	0.982	0.153	0.033
SB30,T_f=15%	0.950	0.168	0.045

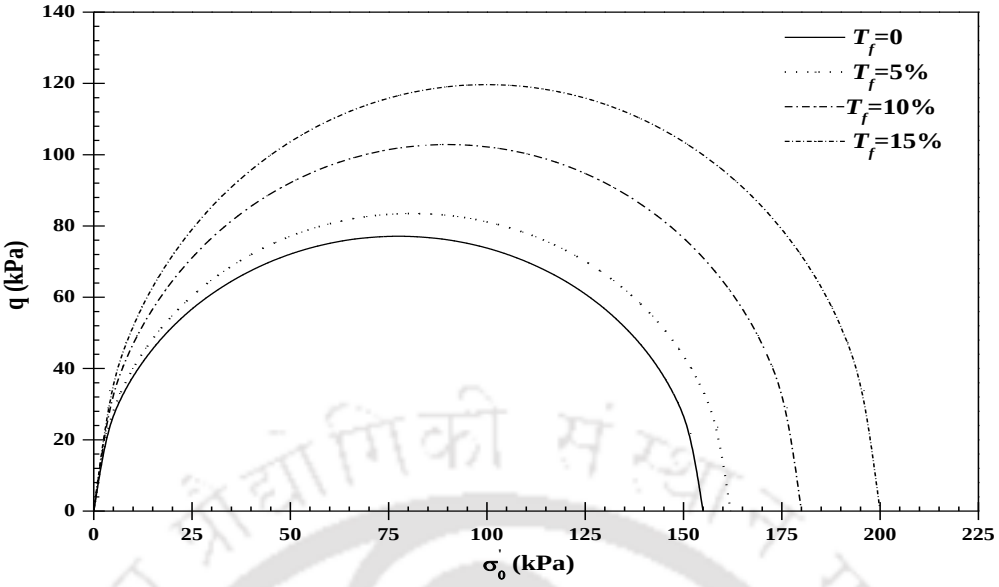

Figure 5.29 Yield surface of the SB10 composite

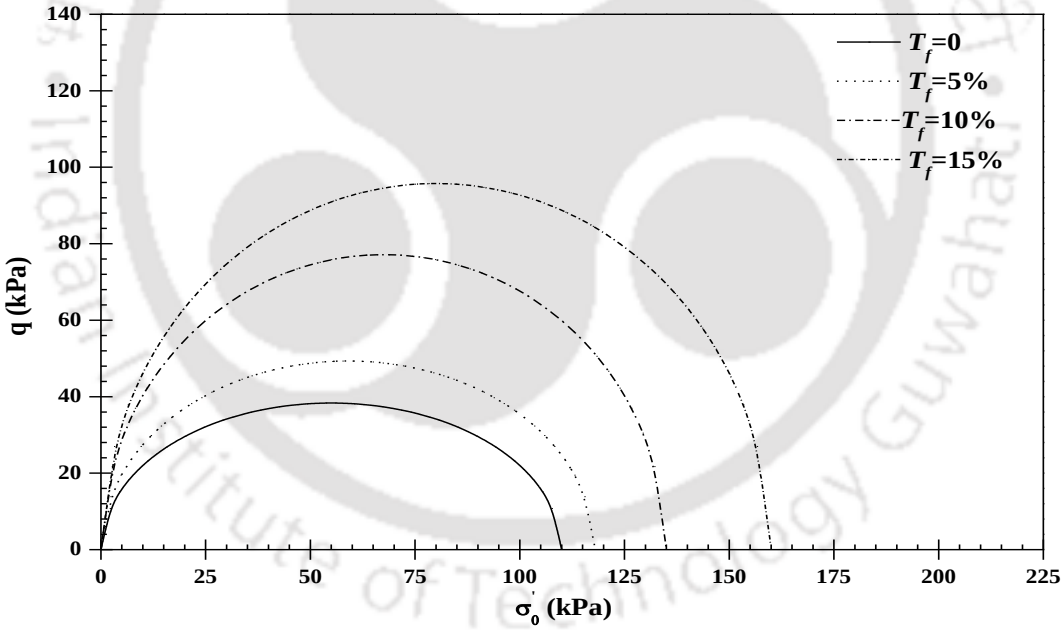

Figure 5.30 Yield surface of the SB20 composite

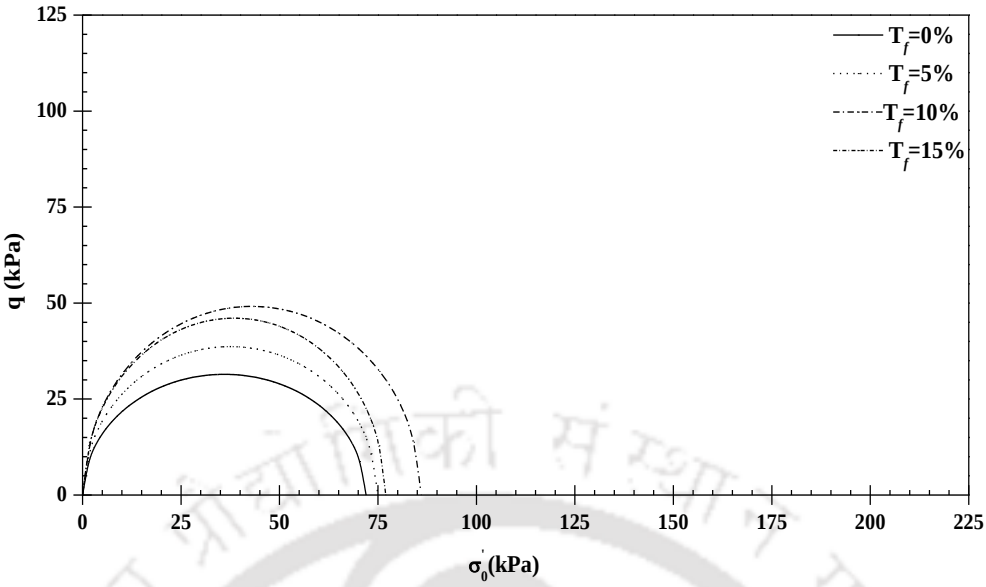

Figure 5.31 Yield surface of the SB30 composite

5.6.1 Fiber-reinforced regression model

Regression analysis is one of the most broadly used statistical tools for investigating multifactor data and it delivers a theoretically simple process for exploring functional interactions among variables. The standard method in regression analysis is to take the data, fit a model and then evaluate the fit using statistics such as t, F and R^2 (Maliakal and Thiyyakkandi 2013; Chatterjee and Hadi 2015)

Based on the experimental outcomes, multiple-regression statistical analysis was performed to develop models for predicting the effective major principal stress at failure. The model developed to explore the effects of fiber percentage, fiber aspect ratio and confining pressure of fiber-reinforced composite on major principal stress at failure. It has been designated that the response variable by y and set of predictor variables by x_1, x_2, x_3 … x_p. Where p signifies the number of the predictor variable. The true relationships between "y" and x_1, x_2, x_3 … x_p can be approximated by the regression model

$$y = f(x_1, x_2, ..., x_p) \qquad (5.8)$$

The function $f(x_1, x_2, ..., x_p)$ defines the relationships between y and x_1, x_2, x_3 … x_p. The estimated regression equation then becomes

$$y = \lambda_0 + \lambda_1 x_1 + \lambda_2 x_2 + \lambda_3 x_3 + \cdots\cdots\cdots + \lambda_p x_p \qquad (5.9)$$

Where, λ_0, λ_1, λ_2,… λ_p called the regression parameters or coefficients are unknown constants to be determined (estimated) from the data point.

Using the equation number 5.9, it can compute n fitted values, one for each of the n observation from the data point. For example, the ith fitted value y_i is

$$y_i = \lambda_0 + \lambda_1 x_{i1} + \lambda_2 x_{i2} + \lambda_3 x_{i3} + \cdots\cdots\cdots + \lambda_p x_{ip}, \qquad i = 1, 2, 3, ...n \qquad (5.10)$$

Where x_{i1}, x_{i2}, x_{i3} … x_{ip} are the values of the p predictor variable for the ith observation.

Based on the experimental output, the regression model was developed to investigate the impact of effective confining pressure (σ_0'), tire fiber content (T_f) and liquid limit (LL) on effective major principle stress at failure (σ_1') and it has been given below:

$$\log(\sigma_1') = 2.975 + 0.712\log(\sigma_0') + 0.216\log(T_f) + (-1.23)\log(LL) \qquad (5.11)$$

$$\sigma_1' = 933.25 \times \sigma_0'^{0.712} \times T_f^{0.216} \times LL^{-1.23} \qquad (5.12)$$

For equation 5.12, it was found that regression coefficient is 0.95, indicating that excellent superiority of the fit was noticed for this model. The suitability of the suggested model and importance of the coefficient of individually variable was tested by Fischer's F-test and student's t test respectively at 95 % confidence level as shown in Table 5-3 and Table 5-4. From the table, it was noticed that t_{value} was less than t_{crit} and F_{value} was less than F_{crit}. Therefore, the models with three independent variables were satisfactory to consistently the predict dependent variable (i.e. σ_1') at 95% confidence level. From the, it was noticed that

all the p value for all the coefficients were far below from 0.05, specifying that coefficient of all the variables were significant at 95% confidence level.

$$\text{RMSE}=\sqrt{\frac{1}{n}\sum_{i=1}^{n}(y_i^p - y_i^a)^2} \quad (5.13)$$

$$\text{NRMSE} = \frac{RMSE}{y_{\max}^a - y_{\min}^a}\times 100 \quad (5.14)$$

Normalized root-mean-square error (NRMSE) was calculated according to Soltani et al. (2018) and found out to 3.96%, which was less than 5% reference label. Finally, the experimental values and predicted values were compared and presented in the Fig.5.32. From the figure, it was noticed that experimental and predicted value shows a good agreement for effective major principle stress at failure and both values are very close to 1:1 line.

Table 5-3 Summary of the F-test result

F_{value} (F)	$F_{critical}$ (F_C)	Remark	NRSME≤5%
100.935	2.78	F>Fc	4.72 (accepted)

Table 5-4 Summary of the t-test result

Coefficients (λ)	t-stat (t_s)	P-value	$t_{critical}$(t_c)	Remark
0.712	11.51	6.49×10^{-16}		$t_s > t_c$
0.216	3.45	0.001	±2.01	P-value<0.05
-1.23	-13.03	5.3×10^{-18}		

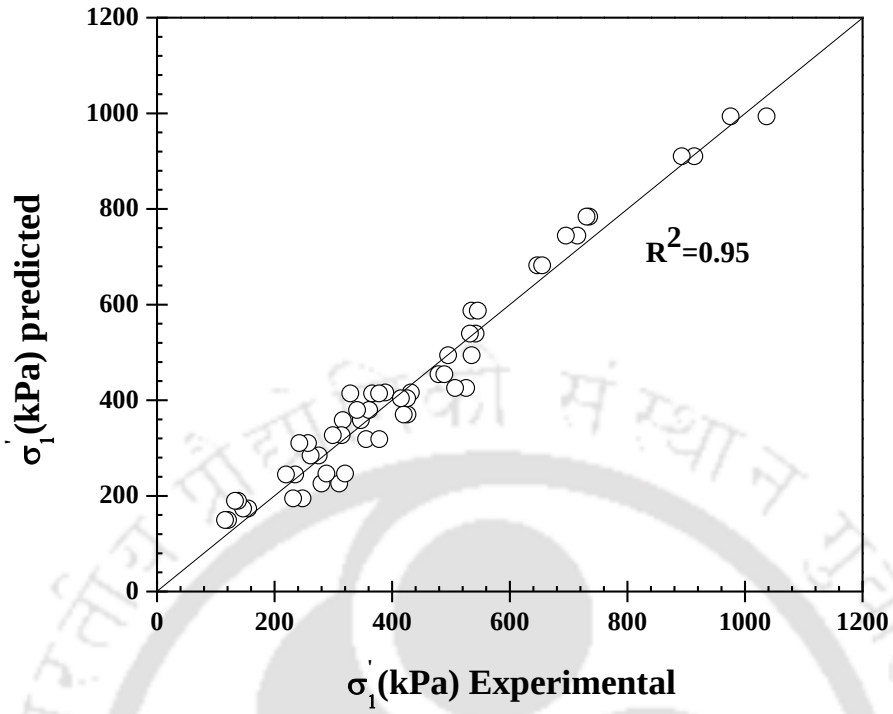

Figure 5.32 Comparing the model of experimental and predicted values of major principal stress at failure

5.7 Compressive strength of the composite under an unconfined condition

Lining structures founded on weak soils are prone to bearing capacity failure and large settlement owing to their poor strength and highly compressible nature. The problem is more severe in case of a sand-bentonite mixture, which undergoes a further reduction in shear strength upon an increase in void ratio due to swelling. To analyze this problem, the compressive strength of sand-bentonite mixture reinforced with waste fiber is an important parameter in evaluating its suitability for use as a landfill construction material. Unreinforced and reinforced mixture have been analyzed for their unconfined compressive strength and presented below.

5.7.1 Unconfined compression strength of SB-tire fiber composite

Stress-strain behavior of the SB-tire fiber composite exhibited in the Fig.5.33. From the figure, it can be observed that axial stress at failure was increased as the percentage of tire fiber increased, and this trend was followed up to 10% tire fiber for the SB30 composite. With the further addition of tire fiber, axial

stress at failure was reduced. The improvement of the composite further defined in terms of improvement factor (I_f), which was calculated as the ratio of peak compressive strength of reinforced soil to the unreinforced soil (UCS_r/UCS_{ur}). The I_f of the SB20 composite was determined to be 1.3, 1.71 and 1.97 at 5, 10 and 15% of tire fiber, respectively. As the tire fiber content increased, the bonding between fiber to soil increases which results in the increase in the overall resistance.

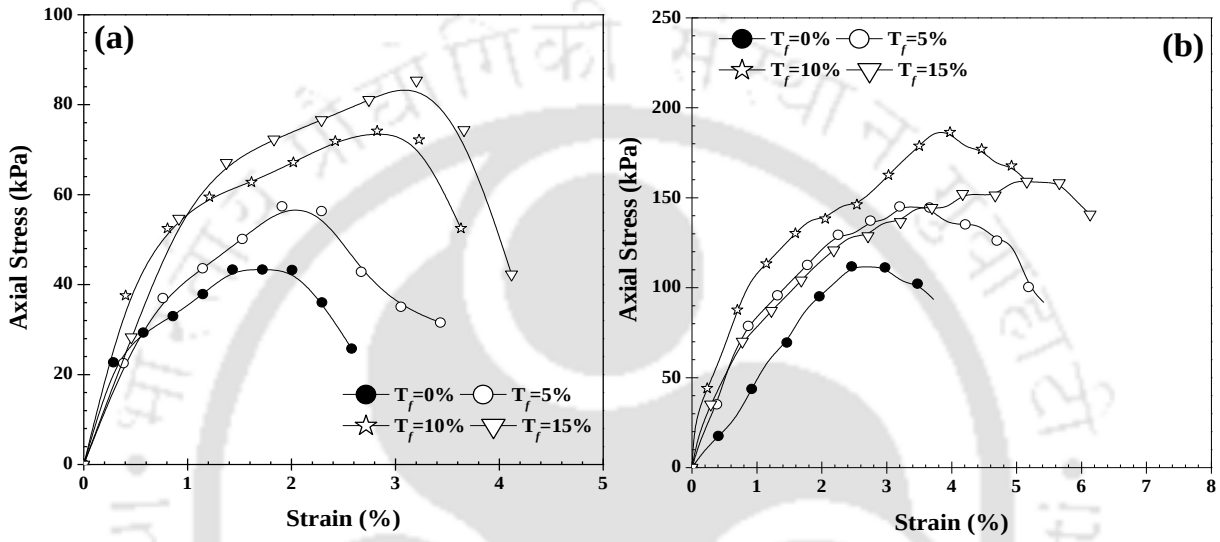

Figure 5.33 Stress-strain response of the composite;(a) SB20 composite;(b) SB30 composite

I_f for the SB30 composite was found to be 1.29 and 1.67 at 5 and 10% tire fiber content, respectively. With a further increase in the tire fiber from 10 to 15%, I_f was reduced from 1.67 to 1.42 due to increase in the tire to tire interaction. The improvement of failure strain was calculated according to displacement ratio (D_r) which is defined as the ratio of failure strain of reinforced soil to unreinforced soil ($\varepsilon_r/\varepsilon_{ur}$). The displacement ratio of the SB20 composite was increased continuously with the increase in tire fiber. For example, D_r was increased from 1.33 to 1.64 and 1.86 with an increase in the fiber content from 5% to 10 and 15%; whereas, for a similar increase in the fiber content the D_r increased sharply from 1.29 to 1.51 and 2.01 for SB30 composite. Daniel and Wu (1993) stated that compacted soils used for liner and cover systems must have satisfactory shear strength. A minimum unconfined compressive strength of 200 kPa

was arbitrarily selected. This strength is the lowest value for very stiff soils based on the terminology of Peck et al. (1974). From the above criteria, it was noticed that SB composite did not satisfy the criteria of stiff clay and their maximum unconfined compressive strength was found out to be 189 kPa for SB30 reinforced with 10% tire fiber.

From the failure pattern, it can be concluded that the unreinforced specimen of SB10 underwent shear failure (Fig.5.34a). SB10 with 5% tire fiber showed a well–defined failure plane with vertical crack. Multiple fractures was observed near the weakest failure plane of composite (Fig.5.34b). With increase the tire fiber from 5 to 10%, specimen exhibited a diagonal shear failure with smaller cracks adjacent to the failure plane (Fig.5.34c). However, with increase the tire fiber content from 10 to 15%, the shear failure mode was changed and the failure was limited within the middle of the specimen indicating an increase in the ductile tendency of the composite the tire fiber (Fig.5.34d). Failure plane of SB30 was developed from the top with multiple rupture as presented Figure 5.35a.

The failure behavior of SB30 reinforced with 5% tire fiber shifted towards shear failure as shown in Fig.5.35b. With the inclusion of 10% tire fiber, specimen exhibited mix-mode failure pattern i.e. mild shear failure with horizontal bulging (Fig.5.35c). The bulging failure was fully observed for SB30 specimen reinforced with 15% tire fiber, indicating a significant increase in strain at failure under an undrained loading (Fig.5.35d).

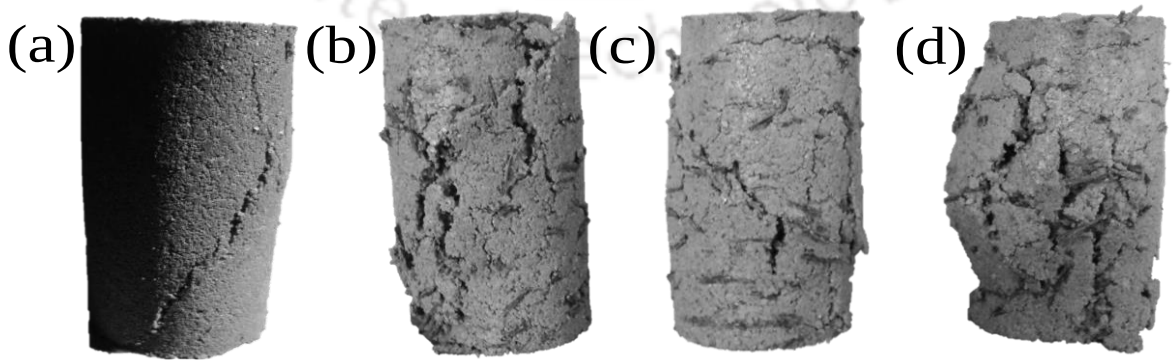

Figure 5.34 Failure mode of SB20 composite

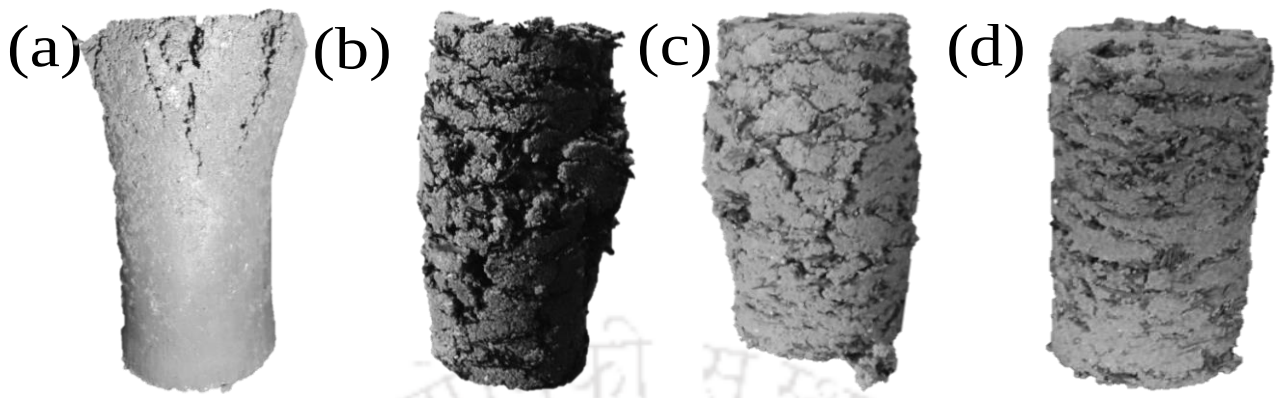

Figure 5.35 Failure mode of SB30 composite

5.8 Shrinkage and Desiccation crack

Cracking can badly affect the barrier material. Cracks produce zones of weakness in a barrier material and cause reductions in the overall strength, stability, and increases in the compressibility of the soil. Lining structures constructed over barrier material can be affected by mechanical changes caused by cracking. Cracks can also produce pathways for the transport of fluids, which can significantly increase the hydraulic conductivity of the barrier material. Development of cracks can be due to various processes including desiccation and shrinkage, freezing and thawing and differential settlement. Volumetric shrinkage and desiccation cracking of compacted sand-bentonite mixture may be controlled with the inclusion of waste tire fiber. For this current study, the shrinkage behavior of SB10, SB20 and SB30 mixtures reinforced with tire fiber are analyzed and reported below.

5.8.1 Shrinkage behavior of the SB-tire fiber composite

Daniel and Wu (1993) suggested that 4% volumetric shrinkage of compacted clay upon drying should be the maximum allowable value for landfill liner. They also reported that soils with minimal volumetric shrinkage upon drying were minimal potential to crack upon drying. Volumetric shrinkage of the SB-tire fiber composite exhibited in the Fig.5.36 to Fig.5.39. From the plots, it can be observed that volumetric

shrinkage was higher for the unreinforced specimen in comparison to the reinforced specimen. The volumetric shrinkage was controlled significantly as the percentage of tire fiber increased. For example, volumetric shrinkage for SB30 was reduced from 6.46% to 4.57, 2.66 and 1.50% due to the increase in the fiber content from 0 to 5, 10 and 15%, respectively. The corresponding reduction for SB20 was from 3.96% to 2.04, 1.26 and 0.98%. A similar observation was also noticed for SB10 composite.

For unreinforced soil, the particle bond may get broken upon drying resulting in a weakening of the soil matrix. Cracking mainly occurred at the weakest section of the soil structure and at the location where the cohesion is low (Youg and Warkentin 1975). The broken bonds get developed by drying which attracts water and becomes preferential zones of cracking. The results showed that the volumetric shrinkage was reduced significantly at higher tire fiber content as shown in Fig.5.36. On the other hand, the SB–tire fiber composite exhibited a high effective shear strength. The cohesion component and the frictional angle of the composite was improved; hence, the volumetric shrinkage was reduced as the percentage of tire fiber increased.

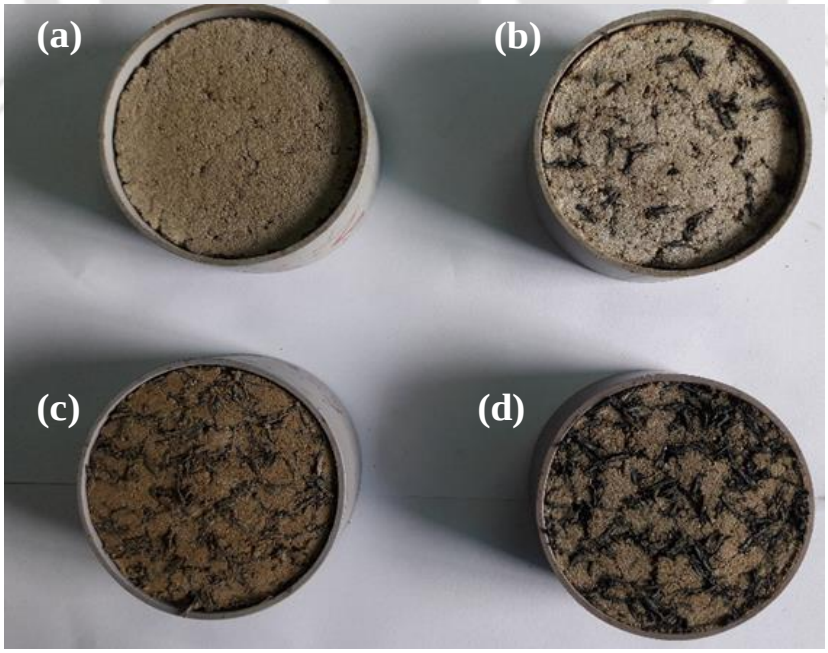

Figure 5.36 Volumetric shrinkage of SB30 composite

5.8.2 Effect of tire fiber on cracked density factor (CDF) and cracked intensity factor (CIF)

Crack density factor (CDF) and crack intensity factor (CIF) are presented in Fig. 5.37 to Fig.5.39 for various SB-tire fiber composite. The inclusion of the tire fiber was able to control the desiccation induced cracking. For the unreinforced soil compacted at MDD-OMC typical hairline types of cracking pattern was observed which caused a series of rather small cells with crack openings. However, the SB-tire fiber composite illustrated relatively small crack opening. For example, CDF of the SB30 reduced from 15.25 to 9.77, 7.23 and 6.34 at due to the addition of 5, 10 and 15% tire fiber, respectively. Similarly, for SB20 the CDF was reduced from 8.81 to 6.35, 4.73, 3.74 due to the addition of 5, 10 and 15% tire fiber, respectively. This results indicated that the total cracked area was reduced as the percentage of tire fiber increased.

Mitchell and Soga (2005) described that the development and propagation of cracks were primarily a function of clay content, specifying that higher the clay content higher will be the intensity of cracks. As a result, the maximum crack intensity was observed for SB30 composite due to the presence of the higher amount of bentonite fraction. The results showed that the intensity of the crack can be controlled by the inclusion of tire fiber. As the percentage of tire fiber increased, crack intensity was found to be decreased sharply. For example, CIF of SB30 was reduced from 4.29 to 3.68, 2.35 and 1.79 due to the addition of 5, 10 and 15% tire fiber to the mixture, respectively. Similarly, for SB20 the CIF was decreased from 3.15 to 2.06, 1.73 and 1.17 for the corresponding increase in fiber.

Due to the irregular and rough surface of tire fiber, as shown in Fig.3.1, the surface area of the fiber produced a larger interaction surface with soil particles (Baykal 2008), which led to an additional interaction among fibers and soil particles. This, in turn, increases the tensile strength of the soil-tire fiber matrix resulting in a decrease in CIF of the composite. In another mechanism, an increase in the friction due to the inclusion of the tire fiber the composite exhibited less crack susceptibility resulting in a

reduction in CIF. It was also observed that SB10 reinforced with tire fiber did not exhibit any crack activity upon drying and presented in Fig.5.39.

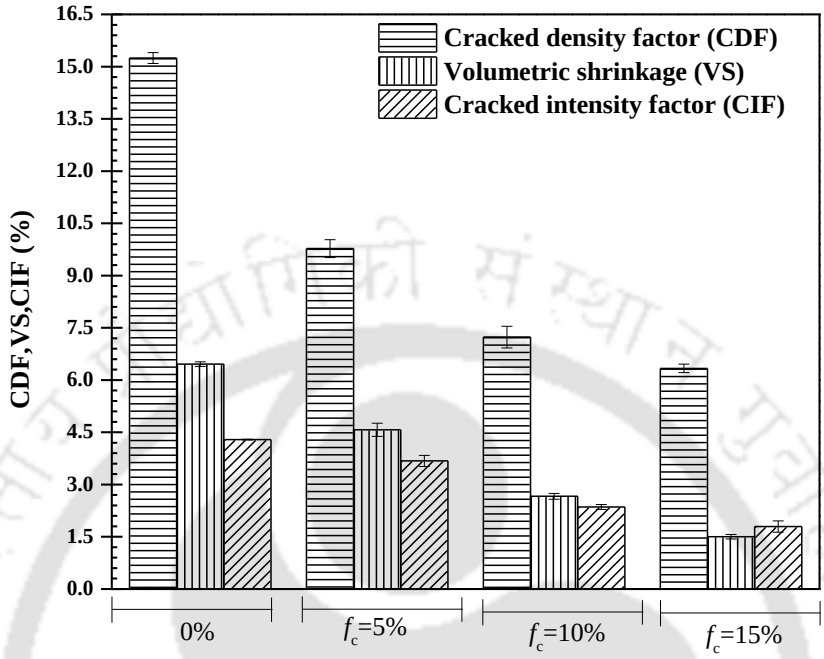

Figure 5.37 Shrinkage and cracking behavior of SB30 composite

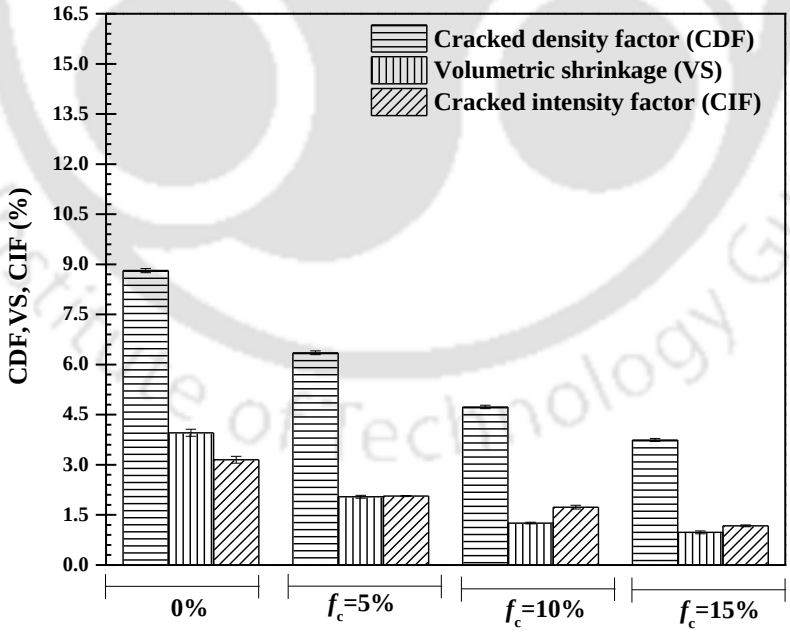

Figure 5.38 Shrinkage and cracking behavior of SB20 composite

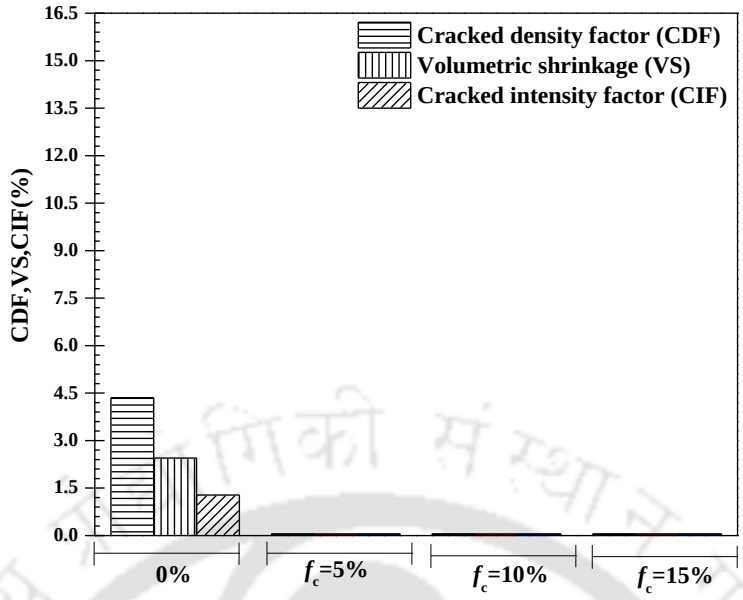

Figure 5.39 Shrinkage and cracking behavior of SB10 composite

CHAPTER 6

CONCLUSIONS AND SCOPE FOR THE FUTURE WORK

6.1 Conclusion

Sand-bentonite has been used as a landfill liner material due to its low hydraulic conductivity. However, bentonite present in the mixture may get desiccated and produce shrinkage crack resulting in a manifold increase in the hydraulic conductivity and differential settlement endangering the life of the liner. Fibers, obtained from the waste material such as tire and glass, can be effectively used as a reinforcement material to reduce the shrinkage. However, the addition of fiber to the sand-bentonite mixture may change the hydro-mechanical behavior of mixture. Therefore, the main objective of the present investigation was to study the effect of the addition of the fiber on the hydro-mechanical behavior of the sand-bentonite mixture. Glass (different aspect ratio), and tire fiber of different percentage were added to three sand-bentonite mixture added with a proportion of 90:10, 80:20 and 70:30 and studied for their change in the hydro-mechanical behavior.

The summary of the finding from this investigation has been summarized below;

- **SB-Glass fiber soil composite**

1. OMC of the compacted sand-bentonite mixture was reduced continuously with increasing the glass fiber content, whereas, the MDD remained constant. However, at the same fiber content with the increase in the aspect ratio the OMC did not change significantly. At 1.5% fiber content, OMC of the composite was reduced to 6.69, 4.36, and 2.74% for SB30, SB20 and SB10 with the aspect ratio of 120, respectively.

2. The swelling tendency of the compacted sand-bentonite composite was reduced with the increase in the fiber concentration in the mixture. At the same fiber concentration, the swelling tendency was reduced with the increase in the aspect ratio.
3. The reduction of the swelling pressure was found to be the function of fiber content and fiber aspect ratio. At the same fiber concentration, the swelling pressure was reduced with the increase in the aspect ratio.
4. The result suggested that compression index was reduced up to 1% fiber content (for all aspect ratio), indicating a reduction in the consolidation settlement due to the inclusion of glass fiber. However, the compression index was slightly increased with the inclusion of 1.5% glass fiber. Swelling index of the composite was increased with an increase in fiber concentration, but no effect was observed with increase in the aspect ratio.
5. The result indicated that the coefficient of consolidation (c_v) increase due to the addition of fiber indicating specimens consolidated at a faster rate due to the inclusion of fiber.
6. A comparison among the reinforced specimens of same sand-bentonite composition indicated that with the increase in fiber concentration and aspect ratio the c_v reduces.
7. The hydraulic conductivity (k) for the composite also followed a similar trend as observed for the c_v.
8. With the inclusion of glass fiber the hydraulic conductivity obtained was higher than the limiting value for a landfill liner (i.e.10^{-7} cm/sec), however, lower than the limiting value that for a landfill cover (i.e. 10^{-5} cm/sec) and the composite could be recommended for the use as a landfill liner and cover material.
9. Analysis of the test data indicated that fiber reinforcement substantially improved material property. SB10 and SB20 composite exhibited strain-softening behavior with well-defined peak, whereas, SB30 composite exhibited strain hardening behavior. No optimum fiber percentage was

found for SB10 and SB20 composite. For SB30 composite, 1% fiber content was considered as optimum for the strength improvement.

10. Post-peak drop of the SB10 and SB20 composite improved with fiber content and fiber aspect ratio. The FESEM study indicated that the fiber was pulled out from adjacent soil particle during the shearing process.
11. Negative EPP increased as the percentage of fiber content increased for the aspect ratio of 40. A similar trend was observed by SB20 and SB10 composite as well. However, the negative EPP was gradually decreased due to the increase in fiber content of aspect ratio of 80 and 120.
12. Positive EPP increased as the fiber content increased and this identical trend was noticed for the aspect ratio of 40, 80, and 120.
13. SB30 exhibited only positive EPP throughout the shearing process and it increased for the composite with the aspect ratio of 40 and 120 at any fiber concentration, whereas, the positive EPP drastically reduced for the composite with the aspect ratio of 80 for any fiber concentration.
14. Stress ratio (SR) of the unreinforced and reinforced specimen decreased with the increase in the confining pressure. The pore water pressure ratio (P_r) reduced with increase in confining pressure.
15. Initial tangent modulus (E_i) increased with confining pressure for reinforced-unreinforced soil composite. However, E_i of the composite increased up to 1% fiber content and reduced with a further increase in fiber content.
16. E_{sec} of the composites reduced with increase in strain. Overall improvement of E_{sec} was noticed up to 1% fiber content for all aspect ratio and reduced thereafter. However, at the higher strain level, i.e. 20%, E_{sec} improved more with 1.5 % of fiber content in comparison to 0.5 and 1%.
17. The peak frictional angle of SB10 improved maximally from 27.3˚ to 38.3˚ at 1.5% fiber content with an aspect ratio of 120, whereas, peak frictional angle of SB20 was found to increase

maximally from 24.9˚ to 35.9˚. Cohesion component was improved maximally from 28.43 kPa to 37.4 kPa at 1.5% fiber content with an aspect ratio of 80 among all the composites.

18. In comparison to SB30, frictional angle improved from 22.4˚ to 34.9˚ at 1% fiber content with an aspect ratio of 120 and reduced thereafter.
19. Residual strength parameter of reinforced specimen improved significantly in comparison to unreinforced ones. Residual frictional angle of SB10 was improved maximally from 25.3˚ to 35.7˚ at 1.5% fiber content with an aspect ratio of 120 among all the composites. When composite subjected to an undrained loading, specimen exhibited a well-defined failure plane with an increase in fiber content. However, for any fiber concentration, with increase in the aspect ratio the specimen undergoes barrel type of failure.
20. Based on the experimental result, multiple regression model was developed, which uses, fiber content, aspect ratio and confining pressure as an input parameter for predicting the effective major principle stress at failure. This regression model could be beneficial in the design phase for selecting the suitable combination of glass fiber content and fiber aspect ratio to find the required principle stress at the failure of compacted sand bentonite–fiber soil composite.
21. M_c of the composites increased with the fiber content and aspect ratio for SB10 and SB20 composite. The κ increased with fiber concentration and remained almost unchanged with increase the aspect ratio. With an increase in fiber concentration and aspect ratio, λ decreased. Yield surface of the composite improved with fiber concentration and fiber aspect ratio.
22. Volumetric shrinkage and desiccation–induced cracking reduced with inclusion of glass fiber. Desiccation–induced crack described in the form of CDF and CIF, however, both decreased with increase in fiber concentration and aspect ratio for all composite.

23. UCS was increased with the fiber aspect ratio in comparison to fiber concentration. Improvement factor was higher for SB10 in comparison to SB20 and SB30 composite. Displacement factor increased continuously with the fiber aspect ratio for all composites.

- **SB-tire fiber composite**

1. Result suggested that MDD of the composite was reduced significantly by the inclusion tire fiber, whereas, OMC of the composite remained almost unchanged.
2. Fiber reinforced composite showed substantially lower vertical swell height in comparison to unreinforced ones. Swelling pressure of the composite was reduced significantly by the addition of tire fiber into the mixture. An identical trend was noticed for the composite of SB20 and SB30.
3. A rectangular hyperbola model was proposed to predicate the maximum swelling potential of the reinforced and unreinforced soil. Model suggested that slope of the t/ε-t was increased with the addition of tire fiber content indicating that the residual swelling tendency of the composite reduces with the inclusion of tire fiber.
4. Coefficient of consolidation of the composite was increased with increased in tire fiber content and hydraulic conductivity was followed the same pattern slimier to c_v.
5. The result indicated that stress-strain behavior of SB10 and SB20 composite improved significantly with the inclusion of tire fiber. However, no optimum fiber content was found for those composite. The material behavior of SB30 composite improved up to 10% tire fiber and reduced thereafter.
6. SB10 and SB20 composite exhibited a well-defined peak, whereas, SB30 composite showed a strain-hardening behavior indicating the role of bentonite clay. The strain at failure was found to improve as the percentage of tire fiber increased in the mixture.

7. The initial tangent modulus (E_i) increased due to the combined effect of tire fiber and confining pressure. However, E_i of the composite improved up to 10 % tire fiber content and reduced thereafter.
8. Negative EPP was found to reduce with an increase in tire fiber and bentonite content. With the inclusion of tire fiber, the negative EPP was reduced continuously for the composite of SB10 and SB20. Conversely, the positive EPP of the composite increased with increase in tire fiber content.
9. The positive EPP of the SB30 composite was reduced significantly with increase in tire fiber content in the mixture.
10. EAC of the composite increased with increase in tire fiber content and reduced with increase in bentonite fraction.
11. The result suggests that the undrained shear strength of the composite increased with the addition of tire fiber. The result pointed out that peak frictional angle was improved maximally from 27.3˚ to 33.1˚, whereas, residual frictional angle was improved from 25.3˚ to 29.9˚ with the addition of 15% tire fiber for the composite of SB10 composite, respectively. For the same composite, the cohesion component improved maximally from 28.4 to 49.1 kPa and residual cohesion component improved maximally from 6.99 to 39.92 kPa.
12. The frictional angle for the mixture of SB30 composite was improved from 22.4˚ to 24.9˚, whereas, the cohesion component was improved from 15.02 to 21.97 kPa. Mixture containing a higher amount of bentonite exhibited a lower undrained shear strength.
13. An identical failure mode was observed for SB10 and SB20 composite. Lower percentage of tire fiber was not able to prevent the strain localization, however, higher percentage of tire fiber exhibited barrel failure indicating that ductile tendency gradually buildup. The unreinforced SB30 specimen depicted sharp horizontal wrinkle indicating a large settlement at low effective stress.

However, specimen reinforced with a high percentage of tire fiber exhibited a vertical column type of failure showing a strong resistance against the volume expansion.

14. The λ of the SB10 composite was decreased up to 10% tire fiber, whereas, λ of the SB20 and SB30 composite reduced with the inclusion of 5% tire fiber and increased thereafter. The κ of the all composite was increased sharply with the inclusion of tire fiber. M_c of the SB10 and SB20 composite was improved continuously with the inclusion of tire fiber. However, the M_c of the SB30 composite improved up to 10% tire fiber and reduced with the addition of 15% tire fiber. SB-tire fiber composite exhibited higher yield surface in comparison to unreinforced soil.
15. A regression model based on experimental data set was developed and was reasonably good in predicting the principle stress at failure of sand bentonite -tire fiber composite.
16. The unreinforced SB30 exhibited a volumetric shrinkage more than 4%; however, it reduced significantly with the addition of tire fiber. Desiccation induced crack was examined in the form of CDF and CIF. The CDF and CIF both were decreased with the inclusion of tire fiber.
17. UCS was found to increase with the percentage of tire fiber due to an adequate bonding between sand and tire fiber. However, UCS of the SB30 composite was improved up to 10% tire fiber and reduced thereafter. Highest UCS was obtained with the inclusion of 10% tire fiber for the mixture of SB30.

6.2 Recommendation

There are a large number of applications of fiber-reinforced soils in civil and other related engineering areas. Major applications can be categorized as geotechnical applications, transportation applications and hydraulic and geoenvironmental applications. However, the impact of fibers on sand bentonite has been discussed below:

Tire fiber: In general, the presence of tire fiber, MDD of the composite decreases gradually, whereas the OMC of the composite remains constant. The swelling tendency of the composite decreases significantly

with the presence of tire fiber. In the presence of tire fiber, hydraulic conductivity increases significantly, and the compressibility of the composite increases. However, the swelling index of the composite improves considerably. In the presence of a high percentage of sand, strength improvement has been noticed; however, in the presence of a high percentage of bentonite clay, strength reduction has been observed in comparison to unreinforced soil. Failure strain of the composite has been improved significantly in the presence of tire fiber, which enhances the cohesion component more in comparison to the frictional angle for any composite. The excess pore water pressure of the composite has been reduced drastically by the inclusion of tire fiber.

Glass fiber: Generally, the presence of glass fiber, OMC of the composite reduces, whereas MDD changes marginally. The swelling tendency of the composite reduces more in comparison to tire fiber for the same mixture. The compressibility of the composite decreases with the inclusion of the glass fiber, whereas the swelling index improves with the inclusion of glass fiber concentration, not by the aspect ratio. It has a more positive impact on the compatibility of the reinforced composite in comparison to tire fiber. Hydraulic conductivity of the composite increases with glass fiber, but it has been decreased drastically with an increase in fiber concentration and aspect ratio. Therefore, hydraulic conductivity affects less in comparison with the presence of glass fiber in comparison to tire fiber. In the presence of glass fiber, strength improves more in comparison to tire fiber. Cohesion component improves up to a specific limit, but the frictional angle improves significantly in the presence of glass fiber. Failure strain decreases with smaller aspect ratio; however, it has been improved with increasing the fiber concentration and aspect ratio. Negative pore water pressure has been increased with a smaller aspect ratio and decreased with increasing the aspect ratio.

Note: Reinforcing the composite with discrete flexible fiber can be a cost effective means of improving their performance in several applications. Additionally the use of fibers from the waste material can be reduce the disposal problem in an economically and environmentally beneficial way. Performance

evaluations of tire glass fiber are significant and their impacts on sand bentonite are considered substantially. Technically, these two types of fiber are not be compared to each other. However, from the material response, it can be compared from their output result. Generally, the output result has been discussed above. After considering all the facts, it has been recommended that glass fiber have a significant impact on the sand bentonite mixtures (especially on hydraulic and mechanical performance) in comparison to tire fiber. At the same configuration of the base material, glass fiber has been referred most suitable as a reinforcement element for landfill applications in comparison to tire fiber.

6.3 Scope for the future work

Any research is not complete and always has avenues for future development. In this regards, the following are some of the scope for the future work in the line of present research work.

- The hydraulic conductivity is the prime criteria for landfill barrier (liner) materials and it should be recommended for detailed further study using flexible–wall permeability testing. How the hydraulic conductivity changes with exposure to leachate is also important to study.
- Any practical issues in using the studies mixture in actual field application should also be recommended for further study.
- Contaminant transport through these barrier material and stability of these materials should also be critical concern for future research.

REFERENCES

Abdi, M.R., Parsapajouh, A. and Arjomand, M.A., (2008). Effects of random fiber inclusion on consolidation, hydraulic conductivity, swelling, shrinkage limit and desiccation cracking of clays. *International Journal of Civil Engineering*, *6*(4), pp.284-292.

Agarwal, B.D., Broutman, L.J. and Chandrashekhara, K., (2017). *Analysis and performance of fiber composites*. John Wiley & Sons.

Ahmad, F., Mujah, D., Hazarika, H. and Safari, A., (2012). Assessing the potential reuse of recycled glass fibre in problematic soil applications. *Journal of Cleaner Production*, *35*, pp.102-107.

Akgün, H., (2010). Geotechnical characterization and performance assessment of bentonite/sand mixtures for underground waste repository sealing. *Applied Clay Science*, 49(4), pp.394-399.

Allan, M.L. and Kukacka, L.E., (1995). Strength and durability of polypropylene fibre reinforced grouts. *Cement and Concrete Research*, *25*(3), pp.511-521.

Al-Refeai, T.O., (1991). Behavior of granular soils reinforced with discrete randomly oriented inclusions. *Geotextiles and Geomembranes*, *10*(4), pp.319-333.

Al-Tabbaa, A. and Aravinthan, T., (1998). Natural clay-shredded tire mixtures as landfill barrier materials. *Waste Management*, 18(1), pp.9-16.

Al-Tabbaa, A., Blackwell, O. and Porter, S.A., (1997). An investigation into the geotechnical properties of soil-tyre mixtures. *Environmental technology*, 18(8), pp.855-860.

Asadzadeh, M. and Ersizad, A., (2013). Effect of tire-chips on geotechnical properties of clayey soil. In International Symposium on Advances in Science and Technology, 3(2), pp. 117-120.

ASTM D2166 (2016). Standard Test Method for Unconfined Compressive Strength of Cohesive Soil, West Conshohocken, PA.

ASTM D2256 (2015). Standard Test Method for Tensile Properties of Yarns by the Single-Strand Method, West Conshohocken, PA.

ASTM D2435 (2011). Standard Test Methods for One-Dimensional Consolidation Properties of Soils Using Incremental Loading, West Conshohocken, PA.

ASTM D422 (2002). Standard Test Method for Particle-Size Analysis of Soils, West Conshohocken, PA.

ASTM D4318 (2000). Standard Test Methods for Liquid Limit, Plastic Limit, and Plasticity Index of Soils, West Conshohocken, PA.

ASTM D4767 (2002). Standard Test Method for Consolidated Undrained Triaxial Compression Test for Cohesive Soils, West Conshohocken, PA.

ASTM D578/D578M (2018). Standard Specification for Glass Fiber Strands. West Conshohocken, PA

ASTM D6270 (1998). Standard Practice for Use of Scrap Tires in Civil Engineering Applications, West Conshohocken, PA.

ASTM D6913 (2017). Standard Test Methods for Particle-Size Distribution (Gradation) of Soils Using Sieve Analysis, West Conshohocken, PA.

ASTM D698-(2012). Standard Test Methods for Laboratory Compaction Characteristics of Soil Using Standard Effort (12 400 ft-lbf/ft^3 (600 kN-m/m^3), West Conshohocken, PA.

ASTM D792 (2013). Standard Test Methods for Density and Specific Gravity (Relative Density) of Plastics by Displacement, West Conshohocken, PA.

Ateş, A., (2016). Mechanical properties of sandy soils reinforced with cement and randomly distributed glass fibers (GRC). *Composites Part B: Engineering*, *96*, pp.295-304.

Babu, G. L. S. (2012). Final project report: Laboratory shear strength studies of soil admixed with plastic waste. Bangalore, India: Department of Civil Engineering, Indian Institute of Science.

Baruah, H., (2015). Effect of glass fibers on red soil. *International journal of technology in engineering and science*, 3, pp.217-223.

Basnett, C.R. and Bruner, R.J., (1993). Clay desiccation of a single composite liner system. In Proc. Geosynthetics . 93, pp. 1329-1340.

Baykal, G. (2008). Tire buffings–soil liners against hydrocarbon contamination. In Scrap tire derived geomaterials—Opportunities and challenges, edited by H. Hazarika and K. Yasuhara, 329. London: Taylor & Francis Group

Benessalah, I., Arab, A., Villard, P., Sadek, M. and Kadri, A., (2016). Laboratory study on shear strength behaviour of reinforced sandy soil: Effect of glass-fibre content and other parameters. *Arabian Journal for Science and Engineering*, *41*(4), pp.1343-1353.

Benson, C. and Khire, M., (1997). Earthen materials in surface barriers. Barrier Technologies for Environmental Management, pp.79-89.

Benson, C.H. and Othman, M.A., (1993). Hydraulic and mechanical characteristics of a compacted municipal solid waste compost. *Waste Management & Research*, *11*(2), pp.127-142.

Benson, C.H., (1997). A review of alternative landfill cover demonstrations. Department of Civil and Environmental Engineering, University of Wisconsin-Madison.

Bishop, A. W., and D. J. Henkel. (1962). The measurement of soil properties in the triaxial test. Second edition. London: Edward Arnold.

Blatz, J.A., Graham, J. and Chandler, N.A., (2002). Influence of suction on the strength and stiffness of compacted sand bentonite. *Canadian Geotechnical Journal*, 39(5), pp.1005-1015.

Booth, A. R. (1976). Compaction and preparation of soil specimens for oedometer testing. Soil specimen preparation for laboratory testing. ASTM STP 599. West Conshohocken, PA.

Bosscher, P.J. and Connell, D.E., (1988). Measurement and analysis of jointing properties in fine-grained soils. *Journal of Geotechnical Engineering*, 114(7), pp.826-843.

Budhu, M. (2010). Soil mechanics and foundations. Third Edition. New York: Wiley.

Burger, W. and Burge, M.J., (2016). Digital image processing: an algorithmic introduction using Java. Second ed. London: Springer.

Cabalar, A.F., Karabash, Z. and Mustafa, W.S., (2014). Stabilising a clay using tyre buffings and lime. *Road Materials and Pavement Design*, 15(4), pp.872-891.

Cerato, A.B. and Lutenegger, A.J., (2002). Determination of surface area of fine-grained soils by the ethylene glycol monoethyl ether (EGME) method. *Geotechnical Testing Journal*, *25*(3), pp.315-321.

Cetin, H., Fener, M. and Gunaydin, O., (2006). Geotechnical properties of tire-cohesive clayey soil mixtures as a fill material. *Engineering geology*, 88(1-2), pp.110-120.

Chai, J.C. and Miura, N., (2002). Comparing the performance of landfill liner systems. *Journal of material cycles and waste management*, 4(2), pp.135-142.

Chalmin, P. and Gaillochet, C., (2009). From Waste to Resource, an Abstract of World Waste Survey 2009. CyclOpe and Veolia Environmental Services. <http:// www.veolia-environmentalservices.com/veolia/ressources/files/1/927,753,Abstract_2009_GB-1.pdf> (accessed 22.06.19).

Chatterjee, S. and Hadi, A.S., (2015). Regression analysis by example. John Wiley & Sons.

Chen, Y. and Meehan, C.L., (2011). Undrained strength characteristics of compacted bentonite/sand mixtures. In Geo-Frontiers 2011: Advances in Geotechnical Engineering, pp. 2699-2708.

Cokca, E. and Yilmaz, Z., (2004). Use of rubber and bentonite added fly ash as a liner material. *Waste management*, 24(2), pp.153-164.

Consoli, N.C., Prietto, P.D. and Ulbrich, L.A., (1998). Influence of fiber and cement addition on behavior of sandy soil. *Journal of Geotechnical and Geoenvironmental Engineering*, 124(12), pp.1211-1214.

Consoli, N.C., Vendruscolo, M.A. and Prietto, P.D.M., (2003). Behavior of plate load tests on soil layers improved with cement and fiber. *Journal of geotechnical and geoenvironmental engineering*, 129(1), pp.96-101.

Consoli, N.C., Vendruscolo, M.A., Fonini, A. and Dalla Rosa, F., (2009). Fiber reinforcement effects on sand considering a wide cementation range. *Geotextiles and Geomembranes*, *27*(3), pp.196-203.

Costa, S., Kodikara, J. & Shannon, B. (2013). Salient factors controlling desiccation cracking of clay in laboratory experiments. *Géotechnique*, 63(1), pp.18–29,

Dakshanamurthy (1978).V. Dakshanamurthy New method to predict swelling using a hyperbolic equation. *Geotechnical Engineering*, 9 (1), pp. 29-38.

Daniel, D.E. and Wu, Y.K., (1993). Compacted clay liners and covers for arid sites. Journal of Geotechnical Engineering, 119(2), pp.223-237.

Daniel, D.E., Koener, R.M., (1993). Cover systems. In: Geotechnical Practice for Waste Disposal. Chapmanand Hall, pp. 455-497.

Das, A. and Viswanadham, B.V.S., (2010). Experiments on the piping behavior of geofiber-reinforced soil. *Geosynthetics international*, 17(4), pp.171-182.

Daud, N., Yusoff, Z. and Muhammed, A., (2015). Ground improvement of problematic soft soils using shredded waste tyre. In The Sixth Jordanian International Civil Engineering Conference (JICEC06).

Dixon, N. and Jones, D.R.V., (2005). Engineering properties of municipal solid waste. *Geotextiles and Geomembranes*, *23*(3), pp.205-233.

Dunham-Friel, J. and Carraro, J.A.H., (2014). Effects of compaction effort, inclusion stiffness, and rubber size on the shear strength and stiffness of expansive soil-rubber (ESR) mixtures. In Geo-Congress 2014: Geo-characterization and Modeling for Sustainability (pp. 3635-3644).

Dutta, J. and Mishra, A.K., (2015). A study on the influence of inorganic salts on the behaviour of compacted bentonites. *Applied Clay Science*, 116, pp.85-92.

EPA (U.S. Environmental Protection Agency). (1995). Policy for Risk Characterization at the U.S. Environmental Protection Agency. Memorandum from Carol M. Browner, Office of the Administrator, U.S. Environmental Protection Agency, Washington, DC.

Estabragh, A.R., Parsaei, B. and Javadi, A.A., (2015). Laboratory investigation of the effect of cyclic wetting and drying on the behaviour of an expansive soil. *Soils and foundations*, *55*(2), pp.304-314.

European Tyre, and Rubber Manufacturers' Association. (2010). End of life tires: A valuable resource with growing potential, Brussels.

Fowmes, G.J., Dixon, N. and Jones, D.R.V., (2006). Use of randomly reinforced soils in barrier systems. In *5th ICEG Environmental Geotechnics: Opportunities, Challenges and Responsibilities for Environmental Geotechnics: Proceedings of the ISSMGE's fifth international congress organized by the Geoenvironmental Research Centre, Cardiff University and held at Cardiff City Hall on 26–30th June 2006*. Thomas Telford Publishing, pp. 709-716.

Gacke, S., Lee, M., and Boyd, N. (1997). Field performance and mitigation of shredded tire embankment. Transport. Res. Rec., 1577(1), pp. 81–89.

Genan Business, and Development A/S. (2010). "Comparative life cycle assessment of two options for scrap tire treatment: Material recycling versus tire-derived fuel combustion." Rep. Genan Business and Development A/S by Franklin Associates, a Division of ERG, Prairie Village, KS.

Giroud, J. P., and J. F. Beech. (1989). Stability of soil layers on geosynthetic lining systems. In proceedings., Geosynthetics'89, Sand Diego: IFAI, pp.35–46

Gosavi, M. and Patil, K., (2004). Improvement of properties of black cotton soil subgrade through synthetic reinforcement. *Journal of the Institution of Engineers(India), Part CV, Civil Engineering Division*, *84*, pp.257-262.

Graham, J., Saadat, F., Gray, M. N., Dixon, D. A., & Zhang, Q. Y. (1989). Strength and volume change behaviour of a sand–bentonite mixture. *Canadian Geotechnical Journal*, 26(2), pp.292–305.

Gray, D.H. and Al-Refeai, T., (1986). Behavior of fabric-versus fiber-reinforced sand. *Journal of Geotechnical Engineering*, *112*(8), pp.804-820.

Greve, H.-H., (2000). Rubber. 2. Natural. In: Ullmann's Encyclopaedia of IndustrialChemistry. Wiley-VCH, Weinheim. https://doi.org/10.1002/14356007.a23_225

Grim, R.E., Guven, N., (1978). Bentonites: Geology, Mineralogy, Properties, and Uses. Developments in sedimentology, 24. Elsevier, Amsterdam

Gupta, P.K., (1988). Glass fibers for composite materials. *Elsevier Science Publishers B. V., Fiber Reinforcements for Composite Materials.*, *2*, pp.19-71.

Hauser, V.L., Weand, B.L. and Gill, M.D., (2001). Natural covers for landfills and buried waste. *Journal of Environmental Engineering*, *127*(9), pp.768-775.

Ho MH, Chan CM, Bakar I (2010). One dimensional compressibility characteristics of clay stabilised with cement-rubber chips. International Journal of Sustainable Construction Engineering and Technology 1(2), pp.91–104.

Holtz, R.D., Kovacs, W.D., (1981). An Introduction to Geotechnical Engineering. Prentice-Hall, Eaglewood Cliffs, N.J.

Horn, R., Baumgartl, T., Gräsle, W., Bohne, K., Plagge, R., Schmidt, M. and Richards, B.G., (1997). Effects of overburden pressure and degree of drainage on the soil-water characteristics of earthen liners. In *Advanced landfill liner systems*. Thomas Telford Publishing. pp.302-309.

Hughes, K.L., Christy, A.D., Heimlich, J.E., (2007). Landfill Types and Liner Systems (Extension Fact Sheet CDFS-138). Cincinnati, Ohio: Ohio State University

Humphrey, D. N., et al. (1993). Shear strength and compressibility of the tyre chips for use as retaining wall backfill. Transportation Research Record No. 1422, Lightweight Artificial and Waste Materials for Embankments over Soft Soils, *Transportation Research Board*, Washington, DC, pp.29–35.

Isenberg R.H. (2003). Landfill and waste geotechnical stability. Presentation at US EPA Bioreactor Workshop, February 27– 28, 2003, Arlington-VA

Joseph Priestley." Science and Its Times: Understanding the Social Significance of Scientific Discovery.Encyclopedia.com. 8 Jul. 2019 <https://www.encyclopedia.com>. https://www.encyclopedia.com/people/science-and-technology/chemistry-biographies/joseph-priestley (DOA:10/05/2019)

Kalita, D.M., Mili, I., Baruah, H. and Islam, I., (2016). Comparative Study of Soil Reinforced with Natural Fiber, Synthetic Fiber and Waste Material. *International journal Latest Trends Engineering and Technology*, *7*, pp.284-90.

Kalkan, E., (2013). Preparation of scrap tire rubber fiber–silica fume mixtures for modification of clayey soils. *Applied Clay Science*, 80, pp.117-125.

Kaniraj, S.R. and Havanagi, V.G., (2001). Behavior of cement-stabilized fiber-reinforced fly ash-soil mixtures. *Journal of geotechnical and geoenvironmental engineering*, *127*(7), pp.574-584.

Kar, R.K., Pradhan, P.K. and Naik, A., (2014). Effect of randomly distributed coir fibers on strength characteristics of cohesive soil. *The Electronic Journal of Geotechnical Engineering*, *19*, pp.1567-1583.

Karg, C. and Haegeman, W., (2009). Elasto-plastic long-term behavior of granular soils: Experimental investigation. *Soil dynamics and earthquake engineering*, *29*(1), pp.155-172.

Khire, M.V., Benson, C.H. and Bosscher, P.J., (1997). Water balance modeling of earthen final covers. *Journal of Geotechnical and Geoenvironmental Engineering*, 123(8), pp.744-754.

Kim, Y.T. and Kang, H.S., (2013). Effects of rubber and bottom ash inclusion on geotechnical characteristics of composite geomaterial. *Marine Georesources & Geotechnology*, 31(1), pp.71-85.

Kittrick, J.A., (1969). Interlayer Forces in Montmorillonite and Vermiculite 1. *Soil Science Society of America Journal*, 33(2), pp.217-222.

Kocasoy, G. and Curi, K., (1995). The Ümraniye-Hekimbaşi open dump accident. *Waste Management & Research*, *13*(4), pp.305-314.

Koerner, R.M. and Daniel, D.E., (1997). Final covers for solid waste landfills and abandoned dumps. Thomas Telford.

Koerner, R.M. and Soong, T.Y., (2000). Stability assessment of ten large landfill failures. In *Advances in transportation and geoenvironmental systems using geosynthetics*, pp. 1-38.

Komine, H., (2004). Simplified evaluation on hydraulic conductivities of sand–bentonite mixture backfill. *Applied Clay Science*, *26*(1-4), pp.13-19.

Kondner, R.L. (1963). Hyperbolic stress-strain response: cohesive soils. Journal of the Soil Mechanics and Foundations Division, *89*(1), pp.115-144.

Kraehenbuehl, F., Stoeckli, H.F., Brunner, F., Kahr, G. and Müller-Vonmoos, M., (1987). Study of the water-bentonite system by vapour adsorption, immersion calorimetry and X-ray techniques: I. Micropore volumes and internal surface areas, following Dubinin's theory. *Clay Minerals*, 22(1), pp.1-9.

Kreith, F. (1994). Hand Book of Municipal Solid Waste Management, McGraw-Hill, Inc.,

Lachenbruch, A . H., Contraction theory of ice-wedge polygons (1963): A qualitative discussion, Proceedings Permafrost International Conference, , Natl. Acad. Sci., Natl. Res. Counc., Washington, D.C., Publ. 1287, pp. 63-71.

Laird, D.A. (1996). Model for crystalline swelling of 2: 1 phyllosilicates. Clays and Clay Minerals, 44(4), pp. 553-559.

Laird, D.A. (2006). Influence of layer charge on swelling of smectites. Applied Clay Science, 34, (1), pp. 74-87.

Lambe, T.W. (1967). Stress path method. Proceedings of the ASCE, 93(SM6), pp.309–331.

Lambe, T.W., and Marr, W.A. (1979). Stress path method: second edition. *Journal of the Geotechnical Engineering Division*, ASCE, 105(6), pp.727–738.

López, F.A., Martín, M.I., Alguacil, F.J., Rincón, J.M., Centeno, T.A. and Romero, M., (2012). Thermolysis of fibreglass polyester composite and reutilisation of the glass fibre residue to obtain a glass–ceramic material. *Journal of Analytical and Applied Pyrolysis*, 93, pp.104-112.

Maher, M.H. and Gray, D.H., (1990). Static response of sands reinforced with randomly distributed fibers. *Journal of Geotechnical Engineering*, *116*(11), pp.1661-1677.

Maher, M.H. and Ho, Y.C., (1994). Mechanical properties of kaolinite/fiber soil composite. *Journal of Geotechnical Engineering*, 120(8), pp.1381-1393.

Maliakal, T. and Thiyyakkandi, S., (2013). Influence of randomly distributed coir fibers on shear strength of clay. *Geotechnical and Geological Engineering*, *31*(2), pp.425-433.

McBean, E.A., Rovers, F.A. and Farquahar, G.J., (1995). Solid waste landfill; engineering and design. Prentice Hall.

Madsen, F.T. and Müller-Vonmoos, M., (1989). The swelling behaviour of clays. *Applied Clay Science*, *4*(2), pp.143-156.

McBride, M.B. (1994). Environmental chemistry of soils. Oxford University Press, NewYork.

Miller, C.J. and Mishra, M., (1989). Modeling of leakage through cracked clay liners-I: State of the art 1. *JAWRA Journal of the American Water Resources Association*, *25*(3), pp.551-556.

Miller, C.J. and Rifai, S., (2004). Fiber reinforcement for waste containment soil liners. *Journal of Environmental Engineering*, 130(8), pp.891-895.

Miller,W. P.,Willis, R. L. & Levy, G. J. (1998). Aggregate stabilization in kaolinitic soils by low rates of anionic polyacrylamide. Soil Use and Management, 14(2), pp.101–105, https://doi.org/10.1111/j.1475-2743.1998.tb00623.x.

Mitchell, J. K. & Soga, K. (2005). Fundamentals of Soil Behavior, 3rd edition. John Wiley & Sons, Hoboken, NJ, USA.

Mitchell, J.K. and Soga, K., (2005). Fundamentals of soil behavior (Vol. 3). Hoboken, NJ: John Wiley & Sons.

Mitchell, J.K., (1986). Personal Communications on Desiccation Cracks in a Hydraulic Fill Site at Terminal Island in Los Angeles Harbour.

Mokhtar, M. and Chan, C.M., (2007). Effect of using cement admixed with rubber chips on the undrained shear strength of soft soil. In National seminar on civil engineering research. Skudai: Universiti Teknologi Malaysia. http://eprints. uthm. edu. my/4150.

Mollins, L.H., Stewart, D.I. and Cousens, T.W., (1999). The drained strength of bentonite enhanced sand. Geotechnique, 49(4), pp.523-528.

Montgomery, R. and Parsons, L., (1989). The Omega Hills final cover test plot study: Three year data summary. In Annual Meeting of the National Solid Waste Management Association, Washington, DC.

Morris, P.H., Graham, J. and Williams, D.J., (1992). Cracking in drying soils. Canadian Geotechnical Journal, 29(2), pp.263-277.

Norrish, K. and Quirk, J.P., (1954). Crystalline swelling of montmorillonite: Use of electrolytes to control swelling. *Nature*, 173, pp.255-257.

Norrish, K., (1954). The swelling of montmorillonite. Discussions of the Faraday society, 18, pp.120-134.

Özkul, Z.H. and Baykal, G., (2006). Shear strength of clay with rubber fiber inclusions. Geosynthetics International, 13(5), pp.173-180.

Özkul, Z.H. and Baykal, G., (2007). Shear behavior of compacted rubber fiber-clay composite in drained and undrained loading. *Journal of geotechnical and Geoenvironmental engineering*, 133(7), pp.767-781.

Paladhi .R (2011). Engineering Chemistry, Second Edition, Mcgraw Hill Education.

Patel, S.K. and Singh, B., (2018). Shear Strength and Deformation Behaviour of Glass Fibre-Reinforced Cohesive Soil with Varying Dry Unit Weight. *Indian Geotechnical Journal*, pp.1-14. https://doi.org/10.1007/s40098-018-0323-5

Patel, S.K. and Singh, B., (2019). Shear strength and deformation behaviour of glass fibre-reinforced cohesive soil with varying dry unit weight. *Indian Geotechnical Journal*, *49*(3), pp.241-254.

Patel, S.K. and Singh, B., (2019). Shear strength response of glass fibre-reinforced sand with varying compacted relative density. *International Journal of Geotechnical Engineering*, 13(4), pp.339-351.

Patil, U., Valdes, J.R. and Evans, T.M., (2010). Swell mitigation with granulated tire rubber. Journal of materials in civil engineering, 23(5), pp.721-727.

Peck, R.B., Hanson, W.E. and Thornburn, T.H., (1974). *Foundation engineering* (Vol. 10). New York: Wiley.

Prasad, A.S., Ravichandran, P.T., Annadurai, R. and Rajkumar, P.R.K., (2014). Study on effect of crumb rubber on behavior of soil. *International Journal of Geomatics and Geosciences*, 4(3), pp.579-584.

Prost, R., Koutit, T., Benchara, A. and Huard, E. (1998). State and location of water adsorbed on clay minerals: consequences of the hydration and swelling-shrinkage phenomena. *Clays and clay minerals*, Vol.46, No.2, pp. 117-131.

Qian, X., R. Koerner, and D. Gray. (2002). Geotechnical aspects of landfill design and construction. 1st ed. Englewood Cliffs, NJ: Prentice Hall.

Quigley, R.M., 1993. Clay minerals against contaminant migration. *Geotechnical News*, 11(4), pp.44-46.

Rao, G.V. and Dutta, R.K., (2006). Compressibility and strength behaviour of sand–tyre chip mixtures. *Geotechnical & Geological Engineering*, 24(3), pp.711-724.

Ravichandran, P.T., Prasad, A.S., Krishnan, K.D. and Rajkumar, P.K., (2016). Effect of addition of waste tyre crumb rubber on weak soil stabilisation. Indian Journal of Science and Technology, 9(5), pp.1-5.

Rayhani, M.H.T., Yanful, E.K. and Fakher, A., (2008). Physical modeling of desiccation cracking in plastic soils. Engineering Geology, 97(1-2), pp.25-31.

Razali, N., Sa'don, M. N., & Karim, A. R. (2015). Strength and durability effect on stabilized soil. *Journal of Civil Engineering Science and Technology*, 7(1), pp.9–19.

Rodatz, W. and Oltmanns, W., (1997). Permeability and stress-strain behaviour of fibre-reinforced soils for landfill liner systems. In *Advanced landfill liner systems*, Thomas Telford Publishing, pp. 321-332.

Rodatz, W., & Oltmanns, W. (1997). Permeability and stress–strain behaviour of fibre-reinforced soils for landfill liner systems. In August, H., Holzlohner, U. and Meggyes, T. (Eds.) Advanced landfill liner systems, London: Thomas Telford Publishing. pp. 321–332.

Roscoe, K.H., and Burland, J.B. (1968). On the generalized stress–strain behaviour of 'wet' clay. *In* Engineering plasticity. *Edited by* J. Heyman and F.A. Leckie. Cambridge University Press, Cambridge, UK. pp. 535–609.

Rowe, R. K., R. M. Quigley, and J. R. Booker. (1997). Clayey barrier systems for waste disposal facilities. 1st ed. Boca Raton, FL: Taylor & Francis

Rubber Manufacturer Association. (2009). Scrap tire market in the United States. 9th Biennial Rep., Washington, DC.

Saberian, M. and Rahgozar, M.A., (2016). Geotechnical properties of peat soil stabilised with shredded waste tyre chips in combination with gypsum, lime or cement. Mires and Peat, 18(16), pp.1-16.

Sarvade, P.G. and Shet, P.R., (2012). Geotechnical properties of problem clay stabilized with crumb rubber powder. *Bonfring International Journal of Industrial Engineering and Management Science*, 2(4), pp.27-32.

Scalia, I. V., J., Benson, C. H., Albright, W. H., Smith, B. S., & Wang, X. (2017). Properties of barrier components in a composite cover after 14 years of service and differential settlement. *Journal of Geotechnical and Geoenvironmental Engineering*, 143(9), 04017055. doi:10.1061/(ASCE)GT.1943-5606.0001744)

Seda, J.H., Lee, J.C. and Carraro, J.A.H., (2007). Beneficial use of waste tire rubber for swelling potential mitigation in expansive soils. In Soil improvement, pp. 1-9.

Seed, R.B., Mitchell, J.K. and Seed, H.B., (1990). Kettleman hills waste landfill slope failure. II: stability analyses. Journal of Geotechnical Engineering, 116(4), pp.669-690.

Sellaf, H., Trouzine, H., Hamhami, M. and Asroun, A., (2014). Geotechnical properties of rubber tires and sediments mixtures. *Engineering, Technology & Applied Science Research*, 4(2), pp.618-624.
Shackelford, C.D., Benson, C.H., Katsumi, T., Edil, T.B. and Lin, L. (2000). Evaluating the hydraulic conductivity of GCLs permeated with non-standard liquids. *Geotextiles and Geomembranes*, 18 (2), pp. 133-161.

Sharma, M.R., Baxter, C.D., Hoffmann, W., Moran, K. and Vaziri, H., (2011). Characterization of weakly cemented sands using nonlinear failure envelopes. *International Journal of Rock Mechanics and Mining Sciences*, 1(48), pp.146-151.

Sharma, H.D. and Reddy, K.R., (2004). Geoenvironmental engineering: site remediation, waste containment, and emerging waste management technologies. John Wiley & Sons.

Signes, C.H., Garzón-Roca, J., Fernández, P.M., de la Torre, M.E.G. and Franco, R.I., (2016). Swelling potential reduction of Spanish argillaceous marlstone Facies Tap soil through the addition of crumb rubber particles from scrap tyres. *Applied Clay Science*, 132, pp.768-773.

Singh, S. and Sun, J.I., (1995). Seismic evaluation of municipal solid waste landfills. In *Geoenvironment 2000: Characterization, Containment, Remediation, and Performance in Environmental Geotechnics* ,ASCE, pp. 1081-1096.

Singh, S.P., Rout, S. and Tiwari, A., (2018). Quantification of desiccation cracks using image analysis technique. *International Journal of Geotechnical Engineering*, *12*(4), pp.383-388.

Sivakumar Babu, G.L. and Vasudevan, A.K., (2008). Strength and stiffness response of coir fiber-reinforced tropical soil. *Journal of Materials in Civil Engineering*, 20(9), pp.571-577.

Soltani, A., Deng, A., Taheri, A. and Mirzababaei, M., (2018). Rubber powder–polymer combined stabilization of South Australian expansive soils. *Geosynthetics International*, 25(3), pp.304-321.

Soltani, A., Deng, A., Taheri, A., Mirzababaei, M. and Vanapalli, S.K., (2019). Swell–Shrink Behavior of Rubberized Expansive Clays During Alternate Wetting and Drying. *Minerals*, 9(4), pp.224.

Soltani, A., Deng, A., Taheri, A., Sridharan, A., and Estabragh, A. R., (2018). A Framework for Interpretation of the Compressibility Behavior of Soils," *Geotechnical Testing Journal*, Vol. 41(1), pp. 1–16, https://doi.org/ 10.1520/GTJ20170088.

Sridharan, A. and Gurtug, Y., (2004). Swelling behaviour of compacted fine-grained soils. *Engineering geology*, *72*(1-2), pp.9-18.

Srivastava, A., Pandey, S. and Rana, J., (2014). Use of shredded tyre waste in improving the geotechnical properties of expansive black cotton soil. *Geomechanics and Geoengineering*, 9(4), pp.303-311.

Sun, W.J., Chen, C., Liu, S.Q., Sun, D.A., Liang, X.H., Tan, Y.Z. and Fatahi, B., (2016). Study on GMZ bentonite-sand mixture by undrained triaxial tests. In E3S Web of Conferences, 9, EDP Sciences.(http://hdl.handle.net/10453/88154)

Shukla, S.K., (2017). Fundamentals of fibre-reinforced soil engineering. Springer. DOI: 10.1007/978-981-10-3063-5

Tajdini, M., Nabizadeh, A., Taherkhani, H. and Zartaj, H., (2017). Effect of added waste rubber on the properties and failure mode of kaolinite clay. International Journal of Civil Engineering, 15(6), pp.949-958.

Tchobanoglous, G., 1993. Integrated solid waste management engineering principles and management issues (No. 628 T3).

Thomas, B.S. and Gupta, R.C., (2016). A comprehensive review on the applications of waste tire rubber in cement concrete. *Renewable and Sustainable Energy Reviews*, *54*, pp.1323-1333.

Toé Casagrande, M.D., Coop, M.R. and Consoli, N.C., (2006). Behavior of a fiber-reinforced bentonite at large shear displacements. *Journal of geotechnical and geoenvironmental engineering*, *132*(11), pp.1505-1508.

Trouzine, H., Bekhiti, M. and Asroun, A., (2012). Effects of scrap tyre rubber fibre on swelling behaviour of two clayey soils in Algeria. Geosynthetics International, 19(2), pp.124-132.

Trouzine, H., Bekhiti, M. and Asroun, A., 2012. Effects of scrap tyre rubber fibre on swelling behaviour of two clayey soils in Algeria. *Geosynthetics International*, *19*(2), pp.124-132.

United States Environmental Protection Agency (USEPA), (1988). Design, construction and evaluation on of clay liners for waste management facilities. Technical resource document, hazardous waste engineering research laboratory, Office of research and development, US Environmental protection agency, Cincinnati, Ohio, EPA/530-SW- 86-007F, NTIS PB 86-184496.

Van Olphen, H., (1965). Thermodynamics of interlayer adsorption of water in clays. I.—Sodium vermiculite. Journal of Colloid Science, 20(8), pp.822-837.

Vejmelková, E., Konvalinka, P., Padevět, P. and Černý, R., (2010). Thermophysical and mechanical properties of fiber-reinforced composite material subjected to high temperatures. *Journal of Civil Engineering and Management*, 16(3), pp.395-400.

Vipulanandan, C. and Leung, M., (1995). Treating contaminated, cracked and permeable field clay with grouts. In *Geoenvironment 2000: Characterization, Containment, Remediation, and Performance in Environmental Geotechnics*, PP.829-843

Wallenberger, F.T., (2000). Structural silicate and silica glass fibers. In *Advanced Inorganic Fibers* (pp. 129-168). Springer, Boston, MA.

Wan, A. W. L., Graham, J., & Gray, M. N. (1990). Influence of soil structure on the stress–strain behavior of sand–bentonite mixtures. *Geotechnical Testing Journal*, 13(3), pp.179–187

Wong, P.K.K. and Wong, P.K.K., (1975). Yielding and plastic flow of sensitive cemented clay. *Geotechnique*, *25*(4), pp.763-782.

Xin, L., He, J., Liu, H. and Shen, Y., (2015). Potential of using cemented soil-tire chips mixture as construction fill: a laboratory study. *Journal of Coastal Research*, 73(sp1), pp.564-572.

Yadav, J.S. and Tiwari, S.K., (2017). Effect of waste rubber fibres on the geotechnical properties of clay stabilized with cement. *Applied Clay Science*, 149, pp.97-110.

Yadav, J.S. and Tiwari, S.K., (2018). Evaluation of the strength characteristics of cement-stabilized clay–crumb rubber mixtures for its sustainable use in geotechnical applications. *Environment, development and sustainability*, 20(5), pp.1961-1985.

Yesiller, N., Miller, C.J., Inci, G. and Yaldo, K., (2000). Desiccation and cracking behavior of three compacted landfill liner soils. *Engineering Geology*, 57(1-2), pp.105-121.

Yong, R. N., and B. P. Warkentin, (1975). Soil Properties and Behavior. Amsterdam: Elsevier.

PUBLICATIONS

International Journals

1. **Mukherjee, K.** and Mishra, A. K**.** (2019). Hydro-mechanical properties of sand-bentonite-glass fiber composite for landfill application, KSCE Journal of Civil Engineering, 23, 4631-4640.

2. **Mukherjee, K.** and Mishra, A. K. (2020). Undrained performance of sustainable compacted sand-bentonite-glass fiber composite for landfill application, Journal of Cleaner Production, Elsevier, 244, 118662.

3. **Mukherjee, K.** and Mishra, A. K. (**Accepted and published online,2019**). Impact of glass fiber on hydro-mechanical behaviour of compacted sand-bentonite mixture for landfill application, European Journal of Environmental and Civil Engineering, Taylor and Francis. https://doi.org/10.1080/19648189.2019.1572541

4. **Mukherjee, K.** and Mishra, A. K. (2019). Evaluation of the hydraulic and strength characteristics of sand-bentonite mixtures added with tire fiber for landfill application, Journal of Environmental Engineering, ASCE, 145(6),04019026.

5. **Mukherjee, K.** and Mishra, A. K. (2018). Hydraulic and mechanical characteristics of compacted sand-bentonite-tyre chips mix for its landfill application, Environmental Development and Sustainability, 21(3), pp.1411-1428

6. **Mukherjee, K.** and Mishra, A. K. (2017). The impact of scrapped tyre chips on the mechanical properties of liner materials, Environmental Processes, Springer,4(1), 219-233.

7. **Mukherjee, K.** and Mishra, A. K. (2017). Performance Enhancement of sand-bentonite mixture due to addition of fiber and geosynthetic clay liner, International Journal of Geotechnical Engineering, Taylor and Francis, 11(2), 107-113.

Book Chapter

Mukherjee, K. and Mishra, A. K (**Proof Submitted 2019**). Experimental and numerical study on compacted sand bentonite -tire fiber composite for landfill application, IACMAG Symposium 2019, 5-7 March 2019, Gandhinagar, India

International conferences

1. **Mukherjee, K.** and Mishra, A. K. (2016). Hydro-mechanical behaviour of sand-bentonite mixture reinforced with scrap tyre, Recycle-2016, IIT Guwahati, India.

2. **Mukherjee K,** Mishra AK (2015). Behaviour of sand bentonite mixture by application of fiber and Geosynthetic clay liner (GCL), Discovery, 40(184), 267-273.

National Conferences:

1. **Mukherjee, K.** and Mishra, A. K. (2017). Influence of tyre chips on the behaviour of sand-bentonite mixture, Indian Geotechnical Conference, IIT Guwahati, India.

2. **Mukherjee, K.** and Mishra, A. K (2016). Influence of glass fiber on the behaviour of sand-bentonite mixture, Indian Geotechnical Conference, IIT Madras, India.

3. **Mukherjee, K.** and Mishra, A. K. and Balaji Mudaliyar, A. (2015). A review on consolidation and strength behaviour of fiber reinforced expansive soil, Indian Geotechnical Conference, Pune, India.

4. **Mukherjee, K.** and Mishra, A. K. (2014). Performance enhancement of sand-bentonite mixture due to addition of fiber and geo-synthetic clay liner, Indian Geotechnical Conference, Kakinada, India.